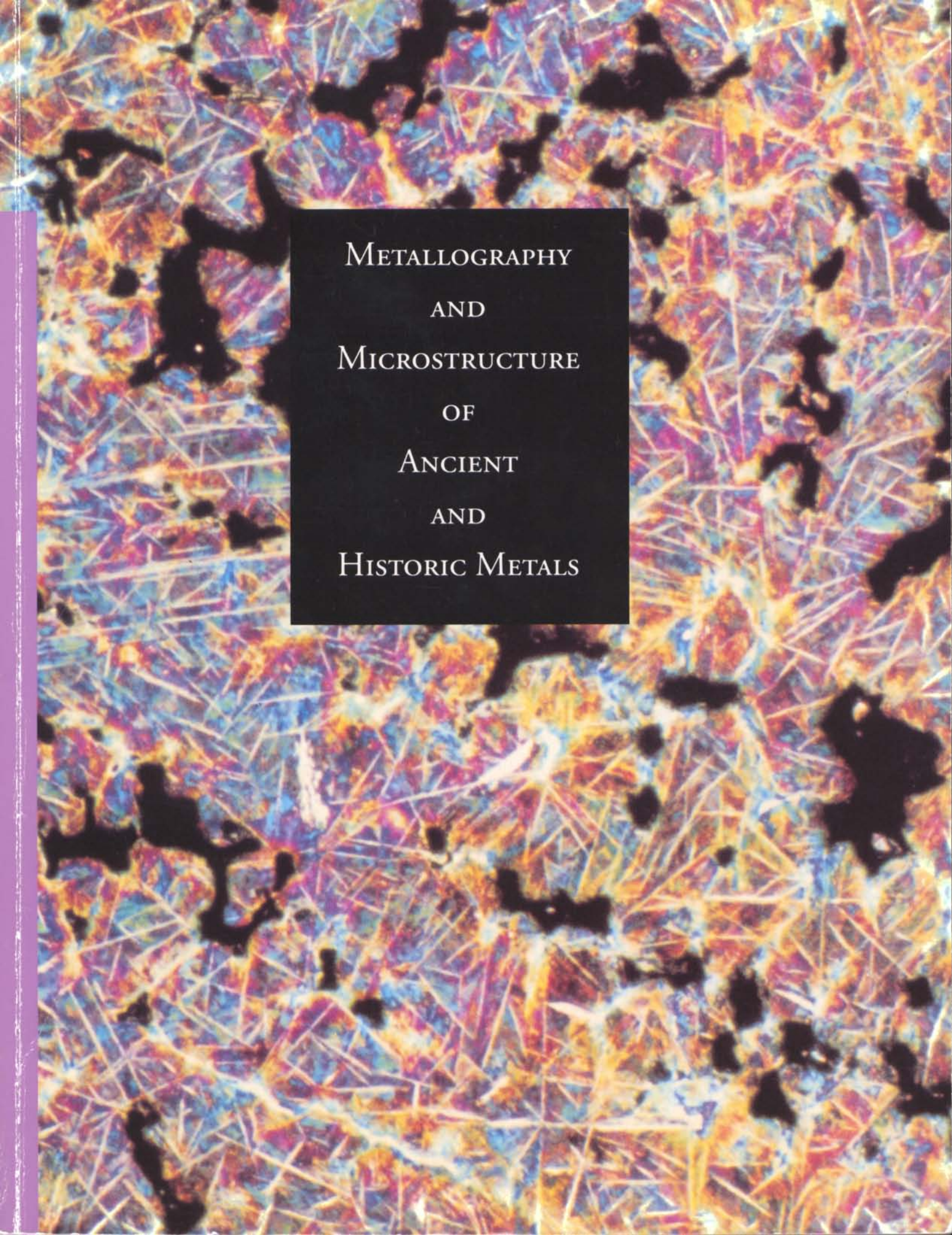

Metallography and Microstructure of Ancient and Historic Metals

Metallography and Microstructure of Ancient and Historic Metals

Metallography and Microstructure of Ancient and Historic Metals

David A. Scott

The Getty Conservation Institute
The J. Paul Getty Museum
in association with Archetype Books

Front and back cover: Photomicrograph of a Wootz steel prill from the Deccan region of India. The steel is hypereutectoid and cast, and was made in a crucible process. Voids appear dark. The pearlite appears in a variety of colors due to differences in spacing. The white needles are cementite; the occasional lighter patches are rich in phosphorus. This crucible steel is a high-quality product of ancient historic significance. Color interference tint etched in selenic acid. x420.

Credits: Figures 73–74: Courtesy of the American Society for Testing and Materials; Figures 106, 145, 148, 162: Peter Dorrell, Photography Department, Institute of Archaeology, London; Figures 1–8, 12–20, 26–40, 55, 198–212: redrawn by Janet Spehar Enriquez; Figures 198–212: Courtesy of the International Copper Research and Development Association; Figures 75–80: Dennis Keeley; Cover, Plates 1–20, Figures 9–11, 21–25, 41–54: David A. Scott.

Publications Coordinator: Irina Averkieff, GCI
Editor: Irina Averkieff
Technical Drawing: Janet Spehar Enriquez
Design: Marquita Stanfield Design, Los Angeles, California
Typography: FrameMaker / Adobe Garamond and Gill Sans
Printing: Tien Wah Press, Ltd.

Published in association with Archetype Books which acknowledge a grant from the Commission of European Communities

Printed in Singapore

Library of Congress Cataloguing-in-Publication Data
Scott, David A.
Metallography and microstructure of ancient and historic metals/
David A. Scott.
p. cm.
Includes bibliographical references and index.
ISBN 0-89236-195-6 (pbk.)
1. Metallography. 2. Alloys--Metallography. 3. Metallographic specimens. 4. Art objects--Conservation and restoration.
I. Title.
TN690.S34 1991
669'.95--dc20 91-19484
CIP

The Getty Conservation Institute

The Getty Conservation Institute, an operating program of the J. Paul Getty Trust, was created in 1982 to address the conservation needs of our cultural heritage. The Institute conducts worldwide, interdisciplinary professional programs in scientific research, training, and documentation. This is accomplished through a combination of in-house projects and collaborative ventures with other organizations in the USA and abroad. Special activities such as field projects, international conferences, and publications strengthen the role of the Institute.

Table of Contents

	Foreword	ix
	Preface	xi
	List of Color Plates and Figures	xiii
	Color Plates	xv
1	The Nature of Metals	1
2	The Microstructure of Ancient Metals	5
3	Two-phased Materials	11
4	The Microstructure of Tin Bronzes	25
5	Notes on the Structure of Carbon Steels	31
6	Martensite in Low-carbon Steels	33
7	The Tempering of Martensite	35
8	Structure and Properties of Cast Iron	37
9	Corroded Microstructures	43
10	Reflected Polarized Light Microscopy	49
11	Grain Sizes of Ancient Metals	51
12	Metallography and Ancient Metals	57
13	Metallographic Sampling of Metals	61
14	Mounting and Preparing Specimens	63
15	Recording Results	67
16	Etching and Etching Solutions	69
17	Mounting Resins	75
18	Microhardness Testing	77
A	Appendix: Common Microstructural Shapes	79
B	Appendix: Microstructure of Corroded Metals	81
C	Appendix: Microhardness Values for Different Alloys and Metals	82
D	Appendix: Alloys Used in Antiquity	84
E	Appendix: Terms and Techniques in Ancient Metalworking	85
F	Appendix: Metallographic Studies	86
G	Appendix: Phase Diagrams	121
	Glossary	137
	Bibliography	147
	Index	151

Foreword

Information about the structure of materials and technology of manufacture of ancient and historic objects and artifacts can provide insight into their date, place of origin, and probable use. Investigations of structure may also be very important for documentation, preservation strategy, or conservation treatment. For many decades objects from a variety of materials and dating from prehistory to the present have been scientifically studied, many of them by metallographic techniques. Most of the results are scattered throughout the international literature, are sometimes inaccessible, and often not published at all. Frequently the need has been expressed, in national and international meetings, to collect information on certain types of objects or classes of materials in one place and to make it available as a database or publication. This volume is an attempt to provide a measured amount of information regarding the techniques of metallography as they apply to ancient and historic metals. It is illustrated with many examples of different types of microstructure, drawn from David Scott's many years of experience in this field of study.

We hope that the present volume, developed with the guidance of Dr. Frank Preusser, Associate Director, Programs, GCI, will be a useful book for students, conservators, conservation scientists, and workers in the area of metallography, especially those seeking to understand the nature of microstructure as it applies to ancient materials. The book is the first in a series of reference works that the Getty Conservation Institute is publishing on materials used in conservation and technology. The Getty Conservation Institute and the J. Paul Getty Museum have been involved collaboratively with this work and present this volume as copublishers.

Miguel Angel Corzo
Director
The Getty Conservation Institute
Marina del Rey, California

Preface

This book began as a series of laboratory notes and the author hopes that in the process of rewriting and integrating, the original text has been rendered more accessible. There are many studies of ancient and historic metalwork published in the literature, but it is more difficult to find a general account of metallographic techniques and an interpretation of microstructure written primarily for the conservation scientist and conservator. This book attempts to fill this gap by providing a guide to the structure of metals. From the materials science perspective, it is also useful to explore the ways in which alloys have been used in ancient metalwork.

There are many reasons for studying the structure of metals. The proper conservation of objects requires or sometimes enables the conservator to observe microstructure. Investigative studies may be necessary in order to assess the degree of corrosion or embrittlement of an object. A new conservation treatment may have implications for the preservation of metallographic structure. Cyril Stanley Smith states that the hierarchy of structure can be examined at many different levels of aggregation and that the incorporation of empirical experience of materials into a theoretical framework has enabled materials science to appreciate the effects of structure on properties and even the artistic qualities of materials. It is certainly true that metallographic structures themselves are often visually compelling both in a scientific and an artistic sense. Metals are interesting materials since their properties can be manipulated in many ways. By combining metals, by heating and quenching, by making them liquid and casting them, or by working them to shape with a hammer or a lathe, they allow a plasticity of movement while being shaped and a finality of form when that process is completed.

The structure of the book should have a word of explanation here. The approach that has been taken is to describe briefly what metals are and to discuss phase diagrams and the kinds of structures to be found in different and relevant alloys, before proceeding to deal with the practical application of this knowledge: the sampling and preparation of samples for metallographic study. The quantitative interpretation of alloy phase diagrams has not been included here, and in general, mathematical content has been kept to a minimum. The practical information in the text also includes details on etching solutions and short accounts of microhardness and the grain size of metals. There is a lengthy appendix (F) in which examples of different types of alloys and microstructures are given, drawn from studies carried out by the author. This appendix is not comprehensive, but it is hoped that the reader will find it interesting and informative.

The analytical data that have been presented in the book are quoted without a discussion of how the results have been obtained. There are many accounts of analytical methods and techniques, such as electron microprobe analysis, atomic absorption spectrophotometry, inductively coupled plasma mass spectrometry, and X-ray fluorescence analysis, and one or more of these techniques are the principal methods by which the results quoted in the text have been obtained. It was not the aim of the present text to enter into detail concerning the chemical analysis of metals. Similarly, although corrosion and corrosion products are often essential components of ancient metals, there is no detailed discussion of the nature of corrosion products given, since to do so would add substantially to the length of the book. The smelting, casting, and working of metals is also not covered in detail by the text, although the glossary does provide some information and common terms used in describing metals and metalworking processes.

Acknowledgments

The author is very grateful to the staff of the Getty Conservation Institute Publications Department for seeing the manuscript through from editing to printing, in particular to Irina Averkieff for her thoughtful and dedicated editorial work. Janet Enriquez was responsible for redrawing the original figures, Dennis Keeley took the photographs in Chapter 11, and Marquita Stanfield directed the overall design. Nota-

bly, Frank Preusser, Associate Director for Programs, and Irina Averkieff, Publications Coordinator, must be thanked for their enthusiasm and support.

The author is also grateful to Summer Schools Press for assistance with the publication of the first version of the text.

Several of the photomicrographs taken by the author would not have been possible without the help and assistance provided by those who have generously devoted samples or time to the cause. In particular I would like to thank Dr. Nigel Seeley, former Head of the Department of Conservation and Materials Science, Institute of Archaeology, London, currently Surveyor of Conservation, National Trust, London; James Black, International Academic Projects, London; Dr. Rodney Clough, formerly Research Associate, Department of Conservation and Materials Science, London, and former students of the Department, Noël Siver, Heather Burns, Bob Haber, Dr. Warangkhana Rajpitak, Naylour Ghandour, Dr. Abdulrasool Vatandoost-Haghighi, and Jane Porter. I would like to give thanks to the following members of the staff at the Institute of Archaeology: Dr. Warwick Bray, Reader in South American Prehistory; Peter Dorrell, Head of the Photography Department; and Stuart Laidlaw, Senior Photographic Technician.

At the Getty Conservation Institute I would like to thank, in addition, my secretary Ruth Feldman, who has carried out many retyping and reformatting jobs in connection with the preparation of the manuscript; Dr. Neville Agnew, Director of Special Projects; and Michael Schilling, Associate Scientist. From the J. Paul Getty Museum I am most grateful to Jerry Podany, Head of the Department of Antiquities Conservation and Linda Strauss, Associate Conservator, Department of Decorative Arts and Sculpture Conservation.

Dr. David A. Scott
Head, Museum Services
The Getty Conservation Institute

Color Plates and Figures

Plate 1. Section from a Luristan dagger handle.
Plate 2. Fragment of corrosion crust from a Chinese cast iron lion.
Plate 3. Section from an outdoor bronze sculpture.
Plate 4. Fragment of a brass medallion from the La Perouse shipwreck off the coast of Australia.
Plate 5. Roman mirror from Canterbury.
Plate 6. Corroded section of a Roman incense burner.
Plate 7. Cast iron fragment from 19th-century scales.
Plate 8. Section from a high-tin bronze vessel from Thailand.
Plate 9. Section from a Greek Herm of about 120 B.C.
Plate 10. Iranian Iron Age dagger hilt.
Plate 11. Section of an Islamic inkwell.
Plate 12. Section of a corroded cast iron cannonball from the Tower of London.
Plate 13. Section of a cast iron cannonball from Sandal Castle.
Plate 14. Section of a high-tin bronze mirror from Java.
Plate 15. Section from a small Indian Wootz ingot.
Plate 16. Section from a Japanese sword blade.
Plate 17. Late Bronze Age sword from Palestine.
Plate 18. Polished and etched section of a late medieval Indian zinc coin.
Plate 19. Section of a small Luristan ceremonial axe from Iran.
Plate 20. Section from inside the base of a Greek Herm.
Fig. 1. Close-packed hexagonal unit cell structure.
Fig. 2. Face-centered cubic unit cell.
Fig. 3. Body-centered cubic unit cell.
Fig. 4. Graph of relationship between stress and strain.
Fig. 5a, b. Stress and strain relation for FCC, BCC, and CPH; stress and strain for interstitial materials.
Fig. 6. An edge dislocation.
Fig. 7. Progressive movement of an edge dislocation.
Fig. 8. Dendrite arms.
Fig. 9. Polished and unetched view of a section through a "Darien"-style pectoral from Ancient Colombia.
Fig. 10. Polished section of a small cast frog from the Tairona area of Colombia.
Fig. 11a–f. Some microstructural features in solid solution FCC metals.
Fig. 12. Relationship between single-phase structures in FCC metals.
Fig. 13. Section through copper alloy axe from Iran showing twinned grains.
Fig. 14. Twinned grains of gold-copper alloy sheet.
Fig. 15. Twin planes in Indian zinc coin.
Fig. 16. Twin planes in zinc.
Fig. 17. Twin planes in zinc.
Fig. 18. Phase diagram for the gold-silver system.
Fig. 19. Eutectic diagram of silver-copper alloy.
Fig. 20. Eutectic-type microstructures.
Fig. 21. Dendritic α in 60% Ag 40% Cu cast alloy.
Fig. 22. 60% Ag 40% Cu etched in potassium dichromate.
Fig. 23. 60% Ag 40% Cu cast alloy illustrating eutectic infill.
Fig. 24. Wootz steel ingot from India
Figs. 25a, b. α and β microstructures.
Fig. 26. Eutectic α and β.
Fig. 27. Eutectic and dendrites.
Fig. 28. Fibrous structure in worked two-phase alloy.
Fig. 29. α and δ eutectoid.
Fig. 30. Iron-carbon phase diagram.
Fig. 31a–d. Breakdown of δ grains.
Fig. 32. Cementite and pearlite.
Fig. 33. Copper-tin phase diagram.
Fig. 34. α + β peritectic.
Fig. 35. ε phase grains.
Fig. 36. Copper-zinc phase diagram.
Fig. 37. β grains in copper-zinc.
Fig. 38. Discontinuous precipitation in Ag-Cu.
Fig. 39. Cu-Au phase diagram.
Fig. 40. Cu-Pb phase diagram.
Fig. 41. Cast toggle pin from Iran.
Fig. 42. Chinese cast-bronze incense burner.
Fig. 43. A small mirror of beta-quenched bronze from Sumatra.
Fig. 44. High-tin bronze mirror from Java.
Fig. 45. Cast high-tin leaded bronze of 22% tin, 6% lead, and 72% copper.
Fig. 46. Laboratory quenched alloy of 24% tin, 76% copper.
Figs. 47–50. Japanese sword blade fragment.
Fig. 51. Partially Widmanstätten steel.
Fig. 52. Grain boundary structure with subgrain features.
Fig. 53. Grain size of knife edge.
Fig. 54. Banded structure of a quenched sword blade.
Fig. 55. Part of the Fe-Fe_3C phase diagram.
Fig. 56. Steel prill from lid of a Wootz crucible, Deccan area of India.
Fig. 57. Medieval knife blade from Ardingley, Sussex, England.
Fig. 58. Photomicrograph of kris from India.
Figs. 59, 60. French cut-steel bead.
Fig. 61. Part of the Fe-Fe_3C phase diagram for cast iron.
Fig. 62a–f. Flake graphite in cast iron.
Fig. 63. 18th-century cast iron scales.
Fig. 64. Cast iron cannonball from the Tower of London.
Fig. 65. Typical variations in the preservation of surface detail in ancient metallic artifacts.
Fig. 66. Mounted and polished section through a bronze rod fragment.
Fig. 67. Drawing of the cross section of a bronze rod fragment.
Fig. 68a–d. Examples of corrosion of gold-copper alloys.
Figs. 69, 70. Luristan ceremonial axe.
Fig. 71. Section of a corroded fragment from an Ecuadorian gilded copper ceremonial axe.
Fig. 72. Nomograph for grain size.
Fig. 73. Typical standard for estimating the (austenitic) grain size of steel.
Fig. 74. Typical standard for estimating the (austenitic) grain size of annealed nonferrous materials such as brass, bronze, and nickel silver.
Fig. 75. Mounting small specimens.
Fig. 76. Grinding mounted samples.
Fig. 77. Polishing mounted samples.
Fig. 78. Sample storage.
Fig. 79. Examination by polarized light microscopy.
Fig. 80. Use of inverted stage metallurgical microscope.
Fig. 81. Drawing of an axe showing ideal location of sample cuttings.
Fig. 82. Two samples of mounted wire or rod.
Fig. 83a–c. Holding small samples.
Fig. 84a–d. Embedding small samples.
Fig. 85. Shapes of ferrite in low-carbon steels.
Fig. 86. Common descriptive microstructural terms.
Figs. 87–89. Base silver-copper alloy coin from western India.
Figs. 90–93. Islamic inlaid inkwell cast in a copper-tin-zinc-lead alloy.
Figs. 94–96. Cast bronze arrowhead from Palestine.
Figs. 97–99. Palestine bronze sword.
Fig. 100. Roman wrought iron.
Figs. 101–103. Colombian gold-copper alloy sheet.
Figs. 104, 105. Ecuadorian copper-alloy nose ornament.
Figs. 106–108. Cast arsenical copper axe from Ecuador.
Figs. 109, 110. Chinese bronze incense burner.
Fig. 111. Thai bronze cast bell.
Figs. 112, 113. Luristan dagger handle.
Figs. 114, 115. Fragment of a Thai

bronze container.
Figs.116, 117. Columbian cast Sinú ear ornament.
Figs. 118–120. Cast iron cannonball from Sandal Castle.
Figs. 121, 122. Bronze Age copper ingot from Hampshire, England.
Figs. 123–125. Roman brass coin.
Figs. 126, 127. Thai bronze container fragment.
Figs. 128–130. Gold necklace bead from Colombia.
Figs. 131–133. Gold alloy nail and gold ear spool.
Figs. 134, 135. Tang and blade section.
Figs. 136, 137. Iron knife.
Fig. 138. Roman copper alloy coin.
Figs. 139, 140. Roman iron nail.
Figs. 141–144. Native copper from the Great Lakes region in North America.
Figs. 145–147. Head of a toggle pin from Iran.
Figs. 148–151. Javanese iron blade.
Figs. 152, 153. Bronze axe fragment from Iran.
Figs. 154, 155. Laboratory cast 60:40 brass.
Figs. 156–159. Gilded silver earring from Jordan.
Figs. 160, 161. Fragment of a brass medallion from Australian shipwreck.
Figs. 162–164. Fragment of a small Sinú ear ornament.
Fig. 165. Roman mirror fragment.
Fig. 166. Roman bronze figurine.
Fig. 167. Roman bronze microstructure.
Fig. 168. Renaissance silver basin from Genoa.
Fig. 169. Part of solder blob from a repair to the outer radial panel of the Renaissance silver basin.
Fig. 170. Section through the Renaissance silver basin.
Fig. 171. Overall view of a core drilled plug from the silver basin.
Fig. 172. Part of the silver sheet etched in acidified potassium dichromate.
Fig. 173. Section of a circular bracelet from Thailand.
Fig. 174. Structure of the circular bracelet from Thailand after etching in alcoholic ferric chloride.
Fig. 175. High magnification of circular bracelet from Thailand showing redeposited copper, copper sulfide inclusions, and bronze metal.
Fig. 176. Section through a Roman bronze bowl, lightly etched in alcoholic ferric chloride.
Fig. 177. Early medieval brass sheet etched in alcoholic ferric chloride and potassium dichromate.
Fig. 178. Recrystallized and heavily worked grain structure of brass stud.
Fig. 179. Microstructure of Romano-Greek iron arrowhead.
Fig. 180. Unusual corrosion pattern through Byzantine bronze blade.
Fig. 181. Heavily etched view of Byzantine leaf-shaped blade.
Fig. 182. Corroded iron knife blade from medieval Britain.
Fig. 183. Iron knife blade showing a weld where different pieces of iron have been joined together.
Fig. 184. Low-carbon steel area of medieval iron knife blade.
Fig. 185. Section of panpipes etched in cyanide/persulfate.
Fig. 186. Fragment of Byzantine iron dagger blade showing part of the edge.
Fig. 187. Overall view of the Roman coin of Victorenus etched in alcoholic ferric chloride.
Fig. 188. Grain structure of the Roman coin of Victorenus.
Fig. 189. Microstructure of grey cast iron of the early 20th century.
Fig. 190. Grey cast iron showing graphite flakes and pearlitic infill.
Fig. 191. Grey cast iron showing the cast structure of the iron-carbon alloy.
Fig. 192. Graphite flakes in a ferrite matrix with an infill of pearlite containing some steadite patches.
Fig. 193. White cast iron showing long cementite laths and small globular region of pearlite.
Fig. 194. White cast iron etched in Murakami's reagent and picral.
Figs. 195, 196. Tin ingot from Cornwall.
Fig. 197. Tensile properties, impact value, and hardness of wrought copper-tin alloys.
Fig. 198. Copper-tin system.
Fig. 199. Part of the copper-tin diagram under different conditions.
Fig. 200. Copper-arsenic system.
Fig. 201. Copper-lead binary system.
Fig. 202. Copper-iron binary system.
Fig. 203. Copper-gold binary system.
Fig. 204. Copper-antimony binary system.
Fig. 205. Copper-silver binary system.
Fig. 206. Copper-nickel binary system.
Fig. 207. Copper-zinc binary system.
Fig. 208. Iron-carbon system.
Fig. 209a. Lead-tin system (pewters). b. Gold-silver system.
Fig. 210. Copper-silver-gold ternary liquidus.
Fig. 211. Copper-silver-gold ternary solidus.
Fig. 212. Copper-tin-lead ternary system.

Color Plates

Plate 1, top left. Section from Luristan dagger handle. Etched in thiosulfate-acetate color tint reagent. The etchant reveals a few twinned crystals and equi-axed grains in the tang of the dagger which has become partially annealed as a result of the casting-on of the bronze dagger hilt. Grain boundaries are visible as are the copper sulfide inclusions (which appear light grey). Etching in ferric chloride does not reveal the coring that is still present in this annealed microstructure. x150 (see Figs. 112, 113).

Plate 2, top right. Fragment of corrosion crust from a Chinese cast iron lion. The iron oxide crust preserves some detail of the original metallic structure of the lion, with the polished section showing steadite and cementite remnants. x200.

Plate 3, bottom left. Section from the outdoor bronze sculpture of Pratt Hamilton showing the cast alloy which is a leaded brass. The orientation of the cast grain structure can be seen together with prominent coring in some clearly dendritic regions. The dark holes are interdendritic porosity. Etched in alcoholic ferric chloride and photographed under partially polarized reflected light. x65.

Plate 4, bottom right. Fragment of a brass medallion from the La Perouse shipwreck off the coast of Australia, which sank in 1726. The structure is lightly etched in alcoholic ferric chloride and shows the pronounced dendritic structure of this cast brass. Loss of both copper and zinc has occurred due to corrosion, which has penetrated to a remarkable depth into the metal. Often, dezincification occurs in brasses, but here it appears that copper has been lost from dendritic areas with zinc and copper corrosion products occupying interdendritic zones. x70.

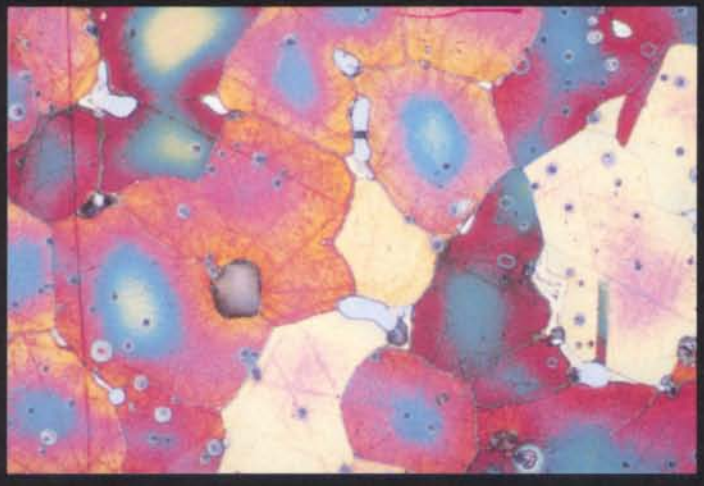

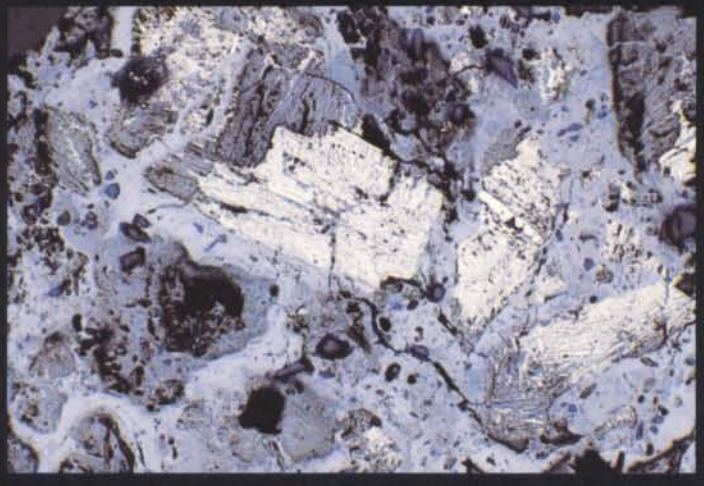

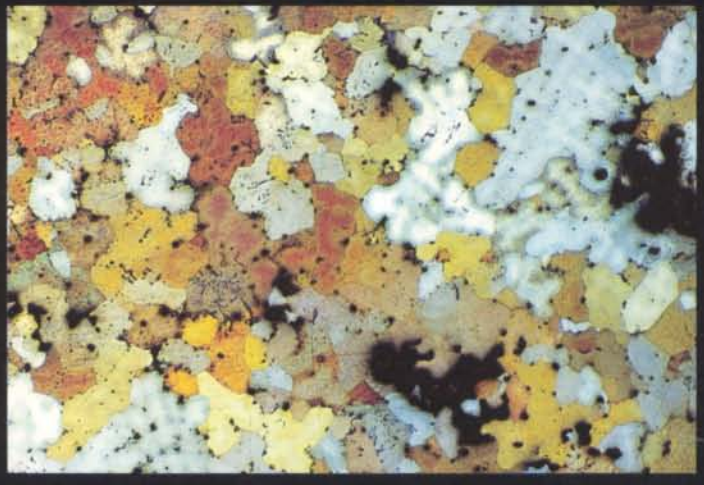

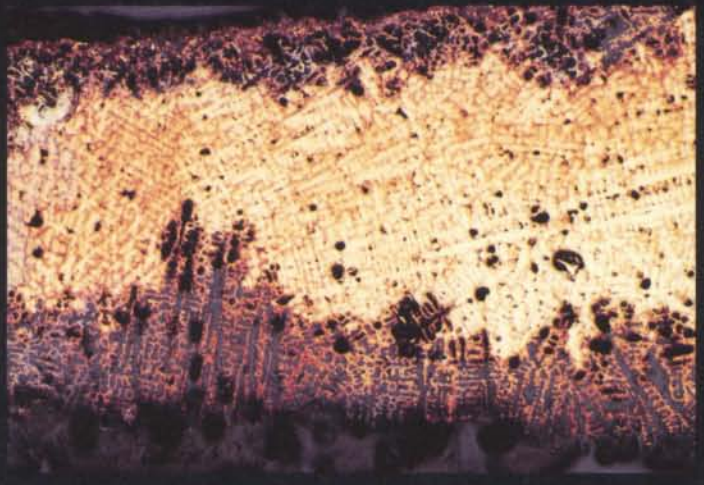

Plate 5, top left. Roman mirror from Canterbury. Some mirrors of the Roman period were made from high-tin leaded bronze and were cast and partially quenched to break up the $\alpha + \delta$ eutectoid. This mirror contains about 6% lead, 18% tin, and 76% copper and was cast into a shallow mold. The lead has begun to segregate to the bottom of the mold through gravity segregation. The section shows very large grains passing through the thickness of the mirror section. The fine structure within each grain is due to the δ phase which has a partially Widmanstätten structure due to rapid cooling. Etched in alcoholic ferric chloride. x64

Plate 6, top right. Corroded section of Roman incense burner from the first century A.D. Etched in thiosulfate-acetate. Copper-rich dendrites remain uncorroded with light blue centers and orange edges. The $\alpha + \delta$ eutectoid has mostly corroded and appears grey. Some redeposited copper remains unetched and looks bright metallic in this section. x350.

Plate 7, bottom left. Cast iron fragment from 19th-century scales. Etched in selenic acid color reagent. The cast morphology can clearly be seen and the graphite occurs in interdendritic spaces. The matrix of the cast iron consists of ferrite and pearlite. x150.

Plate 8, bottom right. Section from a high-tin bronze vessel from Thailand showing quenched β needles. The small yellow islands are remnant α phase showing that the bronze contained less than 24% tin; this was confirmed by analysis which found 21.6% of tin. These small blue-grey particles are sulfide inclusions. This is a fine example of the skill of ancient Thai metalsmiths in manipulating the properties of these high-tin bronze alloys, generally finished by quenching at about 700 °C. Etched in alcoholic ferric chloride. x450.

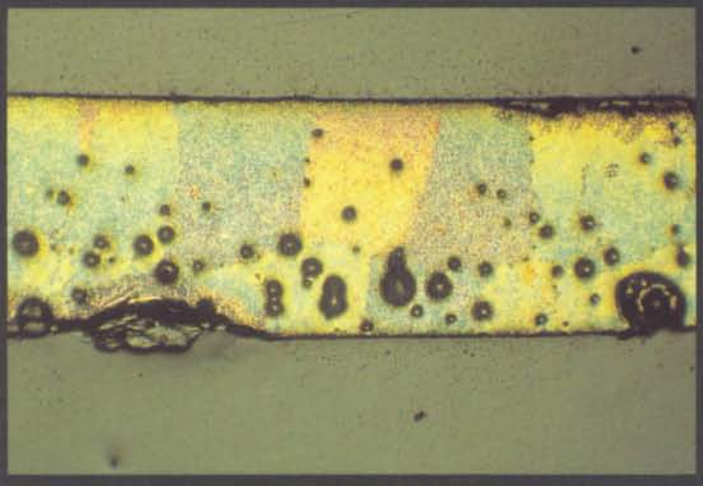

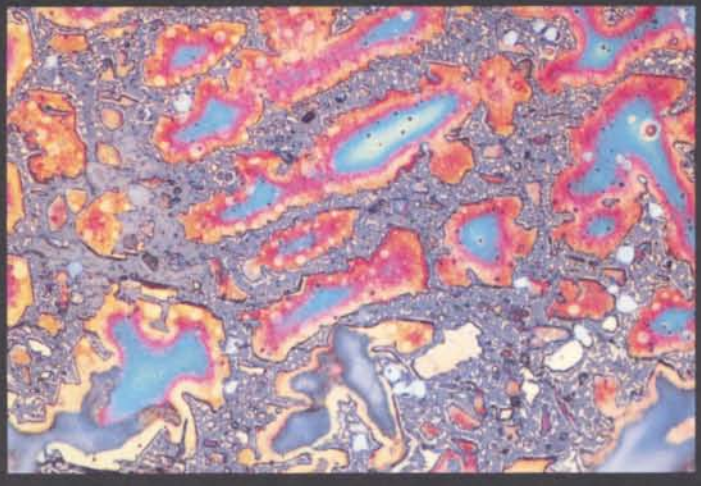

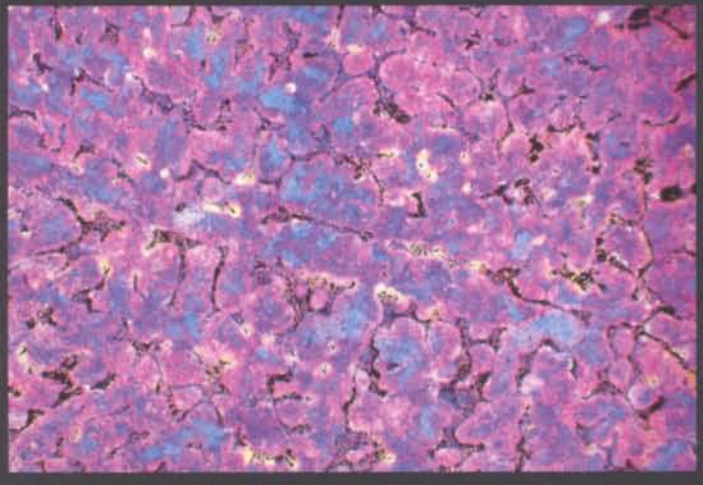

Plate 9, top left. Section from Greek Herm of about 120 B.C. cast in an alloy of about 68.5% copper, 11.5% tin, 18.5% lead. Etched in thiosulfate-acetate. $\alpha + \delta$ eutectoid areas are stained light purple, while the α phase is stained blue to purple. Lead globules are unaffected. Color variation, especially around the zones of the $\alpha + \delta$ eutectoid, reveals the segregation in the alloy. x240.

Plate 10, top right. Iranian Iron Age dagger hilt, about 13.5% tin, 83.6% copper. Etched in thiosulfate-acetate color reagent. The structure shows a cast bronze with dendritic segregation in which the arms of the dendrites are copper rich and cored. The $\alpha + \delta$ eutectoid is visible as blue-grey. The large twinned grains in the center are redeposited copper replacing the original $\alpha + \delta$ eutectoid that has been preferentially corroded. x420 (see Figs. 112, 113).

Plate 11, bottom left. Section of an Islamic inkwell made in the eastern Iranian province of Khurasan, late 12th to early 13th century A.D. The alloy has a composition of about 65% copper, 5% tin, 20% zinc, 10% lead. The structure is that of a cored casting. The rounded lead globules appear a mottled grey, while the lighter patches may represent the γ phase of the copper-tin-zinc system. x200 (see Figs. 90–93).

Plate 12, bottom right. Section of an 18th century corroded cast iron cannonball from the Tower of London. Areas of graphite nodules appear dark due to corrosion around the cathodic graphite flakes. The matrix is rich in phosphorus with large patches of the ternary eutectic steadite visible. Some cementite laths are also present in this grey cast iron. Unetched; x85.

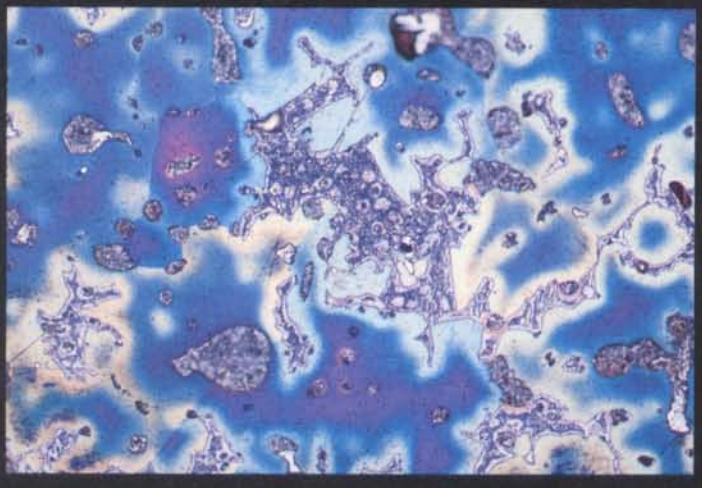

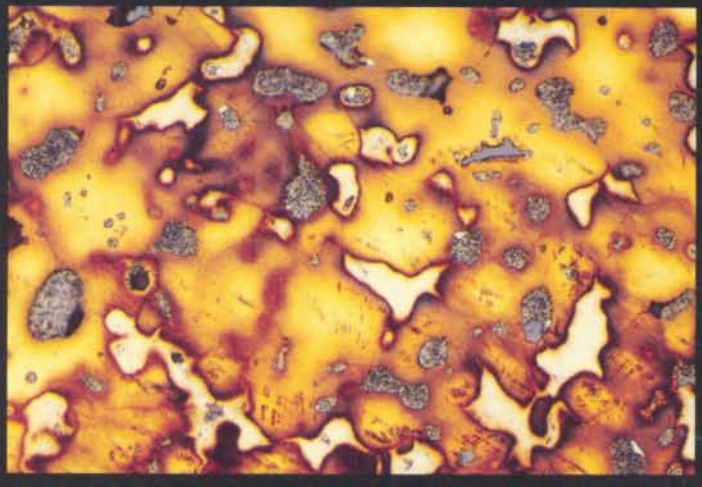

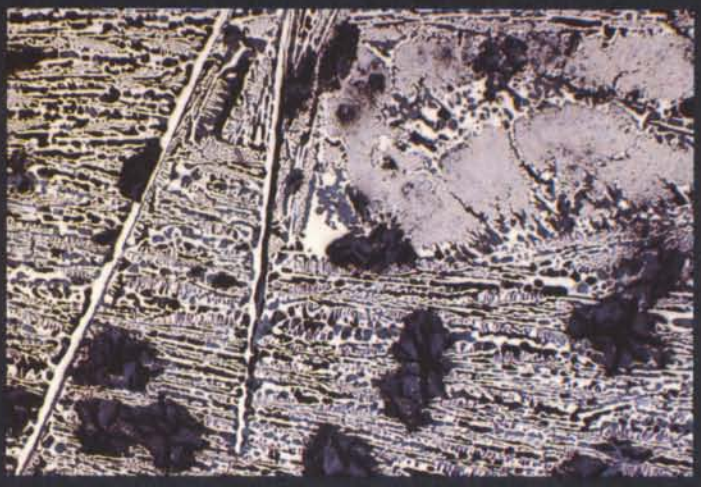

Plate 13, top left. Enlarged view of a cast iron cannonball from Sandal Castle showing the large graphite flakes and the pearlite matrix in which the ferrite and the cementite constituents can now be resolved. Etch: thiosulfate-acetate color reagent; x500 (see Figs. 118–120).

Plate 14, top right. Section of a high-tin bronze mirror from Java, probably dating to the early centuries B.C. Etched in alcoholic ferric chloride. The mirror has a tin content of about 22% and the microstructure shows that the bronze has been quenched, preserving the acicular structure of the β phase. The solid yellow phase is the remnant of the α phase. x150.

Plate 15, bottom left. Section taken from a small Indian Wootz ingot from the Deccan region of India and probably dating to the early historical period. The section was etched in picral followed by tint etching in potassium metabisulfite and sodium thiosulfate. The structure of the Wootz steel is that of a cast product consisting of long cementite needles in a pearlitic matrix. There is some phosphide present occurring as irregular particles that are white in color. The depth of etching of the pearlite is largely influenced by the orientation and spacing of the pearlite in this high-carbon (about 1–1.2%) quality steel. x200 (see Fig. 56).

Plate 16, bottom right. Section from a Japanese sword blade illustrating the principally pearlitic structure of the alloy, 3 or 4 mm back from the martensitic cutting edge. The microstructure consists of ferrite and pearlite. In this section, which has been etched by selenium tint deposition, the finely spaced pearlite is purple and the less finely spaced is yellow, while the ferrite grains are unetched. x230.

Plate 17, top left. Late Bronze Age sword from Palestine made in bronze with about 8.2% tin. This section was etched in alcoholic ferric chloride and shows the worked and annealed grain structure with some twinning visible, variable grain size, and some porosity seen as dark holes due to corrosion. Some inter-crystalline cracking has also occurred probably due to over-working of the bronze. x120.

Plate 18, top right. Polished and etched section of late Medieval Indian zinc coin. The coin section has been etched in Palmerton's reagent and is photographed under polarized reflected light. Twinning in the zinc grains is clearly revealed at a magnification of x60. From the structure it appears that the zinc coin was roughly cast into a blank and then struck.

Plate 19, bottom left. Section of a Luristan ceremonial axe from Iran. The axe section has been polished and etched in selenic acid etchant to produce color tinted deposition. The etchant not only reveals the recrystallized and twinned grain structure of the bronze, but the color variation is also very indicative of coring in the alloy. In this case, the unequal distribution of copper and tin is revealed by color variation. Some small sulfide inclusions appear unattacked by the etchant and are light grey in color. x110 (see Fig. 70).

Plate 20, bottom right. Section from inside the base of a Greek Herm dated to 125 B.C., cast in leaded bronze with about 18.5% lead, 11.5% tin, and 68.5% copper. The structure shows that this component of the Herm is in the as-cast condition. It is etched here by selenium tint deposition which clearly reveals the coring in the cast bronze. Areas richer in copper appear orange while the blue-grey zones are richer in tin. The extensive network of $\alpha + \delta$ eutectoid that appears white can be clearly seen and occupies a large area of the section due to the relatively high tin content. x220.

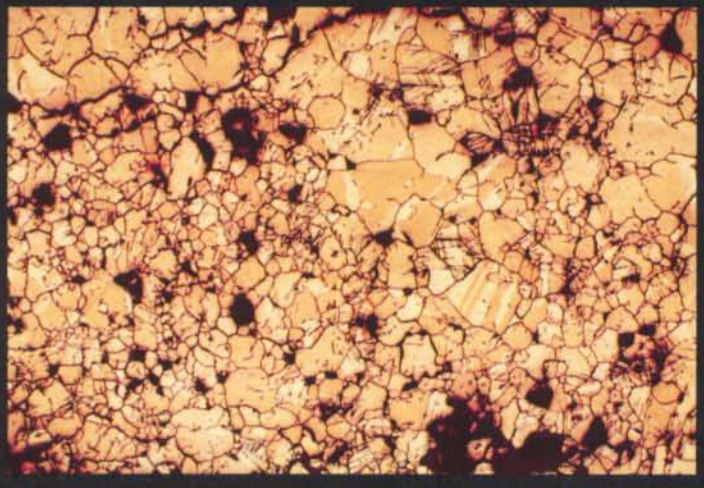

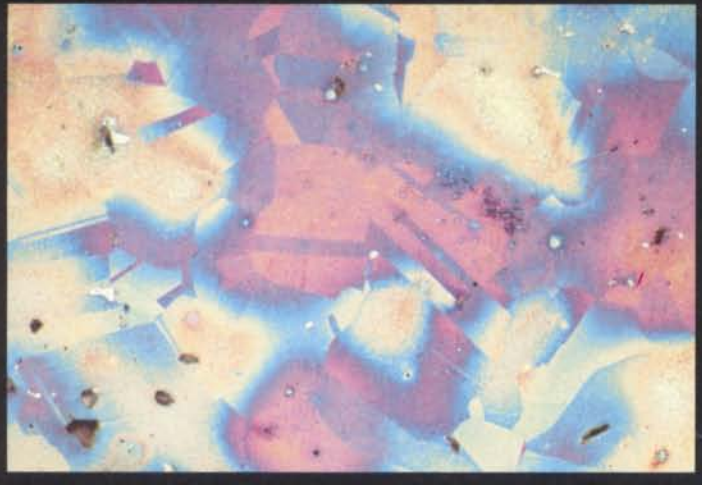

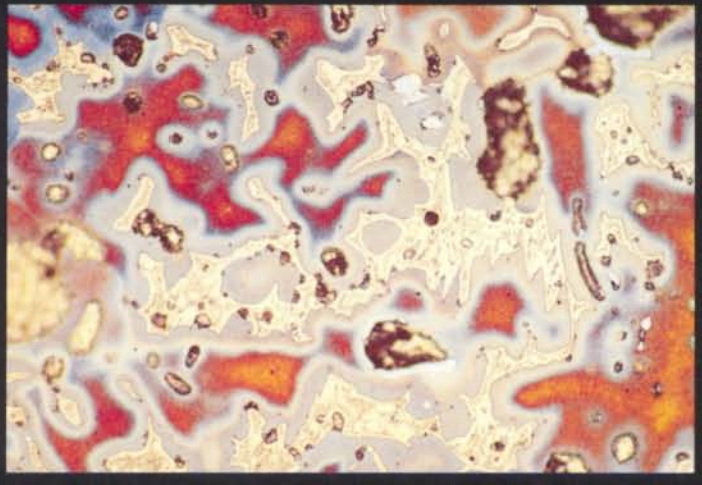

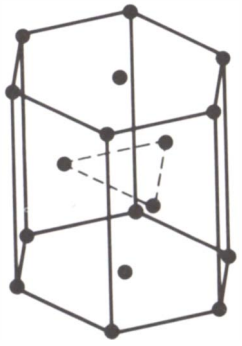

Figure 1. Close-packed hexagonal unit cell structure. Atomic packing factor of 0.74.[1]

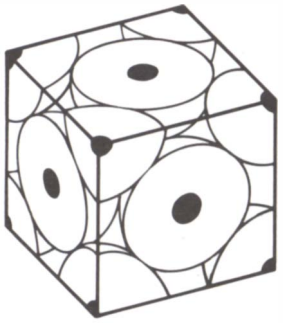

Figure 2. Face-centered unit. An FCC structure has four atoms per unit cell and an atomic packing factor of 0.74 in most elemental crystals.

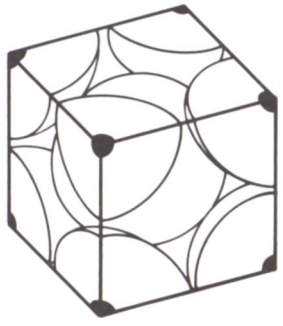

Figure 3. Body-centered cubic unit cell. A BCC metal has two atoms per unit cell and an atomic packing factor of 0.68 in elemental crystals. BCC metals are both ductile and strong (e.g., iron, chromium, tungsten, and molybdenum).

Metals are an aggregation of atoms that, apart from mercury, are solid at room temperature. These atoms are held together by "metallic bonds" that result from sharing available electrons. A negative electron bond pervades the structure, and heat and electricity can be conducted through the metal by the free movement of electrons. The negative electron bond surrounds the positive ions that make up the crystal structure of the metal. There are three common types of lattice structure that metals belong to: close-packed hexagonal, face-centered cubic, and body-centered cubic.

Close-Packed Hexagonal (CPH)

Models of crystal structures can be made up of spheres stacked in close-packed layers. Two arrangements are possible, one being hexagonal and the other cubic in basic structure. In the close-packed hexagonal system the spheres repeat the same position every second layer (ABABAB...; Fig. 1).

Face-Centered Cubic (FCC)

Layers can be built up so that the third layer of spheres does not occupy the same position as the spheres in the first row; the structure repeats every third layer (ABCABCABC...). FCC metals tend to be ductile[2] (i.e., can be mechanically deformed, drawn out into wire, or hammered into sheet). Examples are lead, aluminium, copper, silver, gold, and nickel (Fig. 2).

Body-Centered Cubic (BCC)

Another common type found in many metals, the body-centered cubic structure, is less closely packed than the FCC or CPH structures and has atoms at the corners and one atom at the center of the cube. The atoms at the corners are shared with each adjoining cube (Fig. 3).

Other metals important in antiquity have entirely different lattice structures; for example, arsenic, antimony, and bismuth are rhombohedral, and ordinary tin is body-centered tetragonal.

Metals are crystalline solids under normal conditions of working and melting. However, if a metal is cooled very rapidly, as in splat cooling, the normal crystalline structure can be suppressed. In splat cooling, metal droplets are cooled very quickly between chilled metal plates and the structure that develops is similar to glass—a random arrangement of atoms rather than a crystalline array. In the usual crystalline state, metal will consist of a number of discrete grains. The metal is then referred to as being polycrystalline. An important property of metals is that they undergo plastic deformation when stretched or hammered. This is illustrated by a stress-strain diagram using Young's Modulus (YM):

$$YM = \frac{stress}{strain} = \frac{\frac{load\ applied}{cross\text{-}sectional\ area}}{\frac{change\ in\ length}{original\ length}}$$

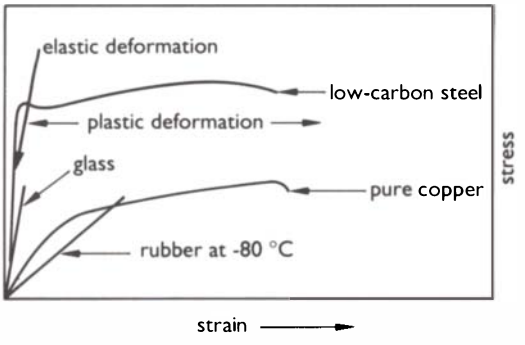

Figure 4. Relationship between stress and strain.

Before plastic deformation occurs, materials deform by the elastic movement of atoms that hold the structure together. This elastic deformation occurs in metals and in other materials, such as glass, which have no ability to deform at room temperature. Glass will stretch by elastic deformation and then break. Metals can deform plastically because planes of atoms can slip past each other to produce movement. This kind of movement cannot take place in a glassy structure. When metals such as pure copper or iron are stretched they will break or fracture, but only after a certain amount of plastic deformation has occurred (see Figs. 4, 5a, 5b).

Hardness

The hardness of a metal is measured by its resistance to indentation. The metal is indented under a known load using a small steel ball (as in the Brinell test) or a square-based diamond pyramid (as in the Vickers test). In the Vickers test the result is given as the Diamond Pyramid Number DPN (or H_V).

Dislocations

It is rare for crystals to have a perfect atomic structure; there are usually imperfections present. In metals, edge dislocations and screw dislocations are the most important faults (see Figs. 6, 7). These crystal faults enable deformation to take place at lower applied stress by slip than would be possible if the lattice structure was perfect. When

Figure 5a, right. Stress and strain relationship for FCC, BCC, and CPH metals compared with glass and a typical polymer. An increase in interatomic spacings is responsible for elastic behavior, while plastic movement results from dislocations giving rise to slip. When this plastic movement can no longer occur fracture will take place.

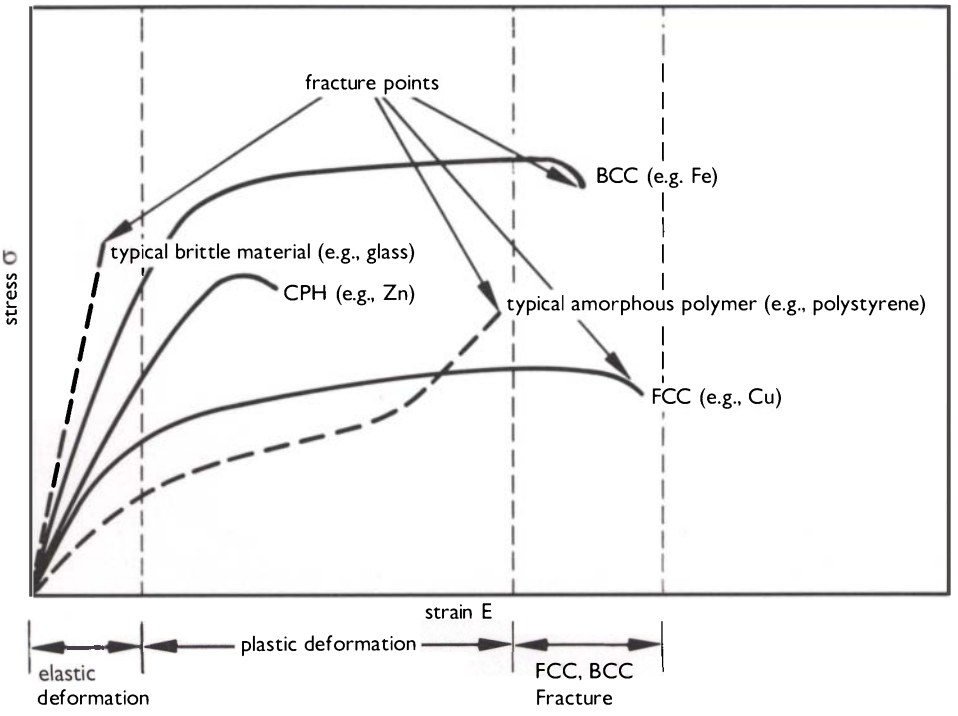

Figure 5b, below. Stress and strain for interstitial materials. Interstitial elements are small in size, such as carbon, and can be inserted into the lattice spacing of some metals, such as steel, which is an interstitial alloy of iron and carbon. Interstitials tend to reside at the base of dislocations and anchor them. When slip occurs, carbon is left behind and the dislocation is held until some higher stress is reached. When the stress factor is reached an enormous number of dislocations occur that can now move at a lower stress than originally required—hence the two yield points.

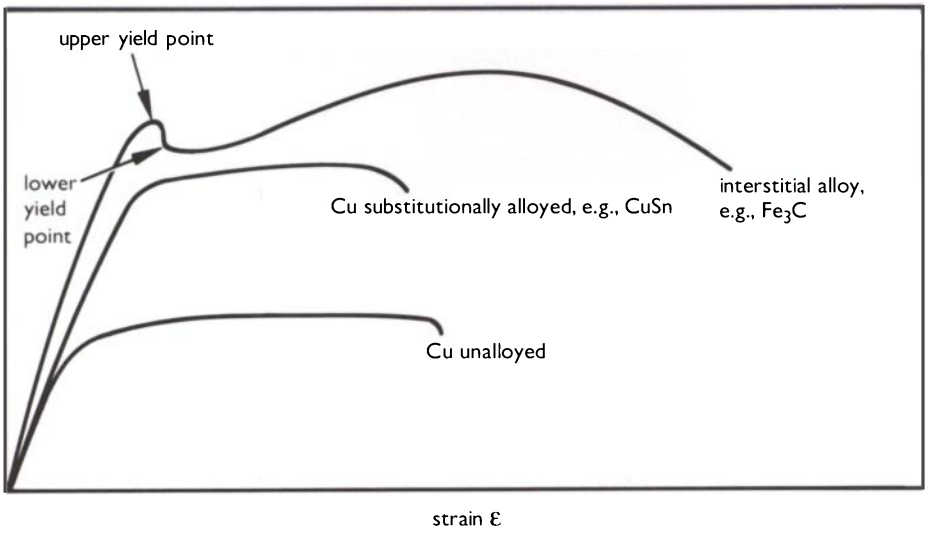

a metal is deformed then slip takes place until a tangle of dislocations builds up which prevents any further working (i.e., dislocation entanglement). As metal is worked, slip planes become thicker and immobile. If the metal is worked further, it must be annealed (heated up to bring about recrystallization). Before annealing, the metal can be said to be work-hardened. Work-hardening is accomplished by, for example, hammering at room temperature. This increases the metal hardness value, but decreases ductility.

Notes

1. The atomic packing factor is a measure of the space actually used by the atoms in the lattice. CPH and FCC lattices are both 0.74 while the BCC metals have a lower factor of 0.68. A complete infill of the lattice would be 1.00.
2. Ductility is often used in the sense of tensile movement (i.e., stretching) and malleability is used for ability to be worked (i.e., hammering).

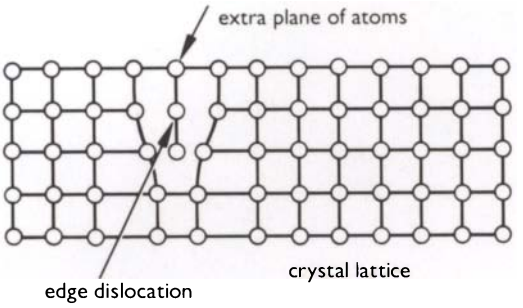

Figure 6. This figure shows an extra plane of atoms inserted in the original lattice. The plane of the edge dislocation and its direction of movement are perpendicular to the slip plane.

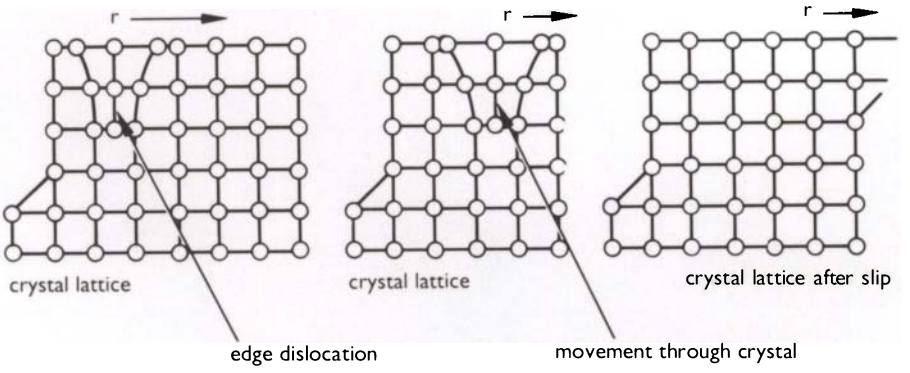

Figure 7. Progressive movement of an edge dislocation showing slip.

There are two basic means of manipulating metals: they can be cast or worked. All the various methods by which casting and working are carried out cannot be examined here in detail, but the different types of structures are described.

Casting

There are essentially three types of microstructure that can arise during the casting and cooling of a melt in a mold, regardless of the exact nature of the technology involved. Most ancient metals are impure or are deliberate alloys of two or more metals, such as copper and tin (bronze) or copper and zinc (brass). The fact that they are impure is an important one, for the kind of crystal growth that can occur is to a large extent dependent on the purity of the metal. This is one reason why the great majority of ancient castings show a dendritic structure. Dendrites look like tiny fernlike growths scattered at random throughout the metal. They grow larger until they meet each other. Sometimes outlines of grains form between them, and the rate at which the metal is cooled influences their size. Usually a microscope must be employed to make dendrites visible, but on objects that have cooled slowly, the dendrites have also formed slowly and may be visible to the naked eye or under a binocular bench microscope at low magnification (x10 or x20). The faster the rate of cooling, the smaller the dendrites. It is possible to measure the spacing between dendrite arms if they are well formed and to compare the spacings obtained from those from known alloys cast in different molds or under different conditions. Arms of dendrites are usually referred to as primary, secondary, or tertiary (Fig. 8).

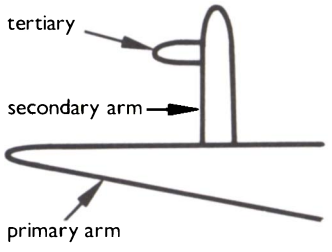

Figure 8. Dendrite arms.

It may be of interest to record dendritic arm spacing for comparative purposes, even if conditions are not precisely known or there is a lack of background information in the metallurgical literature. Dendrites may be rather fuzzy or rounded in outline or quite sharp and well-defined, depending on the nature of the alloy and the cooling conditions of the melt. Dendritic growth is actually one form of segregation that can occur during casting. It is a segregation phenomenon that often arises in impure metals or alloys because one of the constituents usually has a lower melting point than the other. For example, consider the cooling of an alloy of copper and tin. Copper melts at 1083 °C and tin at 232 °C. When the alloy cools and begins to solidify by dendritic segregation, the first part of the dendrite arms to form are richer in copper since this constituent solidifies first, while the outer parts of the arms are richer in tin. The result is that there is a compositional gradient from the inner region of a dendritic arm to the outer surface. Such dendrites are usually referred to as cored. Coring is a common feature in castings of bronze, arsenical copper, debased silver, etc. It is usually necessary to etch a polished section of the metal to investigate whether coring is present or not. Depending on the amount and nature of the alloying constituent present, the remaining fluid in the interdendritic channels or spaces will then solidify to form a different phase of the particular alloy system. A phase is any homogeneous state of a substance that has a definite composition. In practice this definition must be interpreted a little loosely because, very often, ancient metallic systems are not fully in equilibrium conditions, which means that the proportion and even the composition of the individual phases that are present in an alloy may not match the precise values that can be determined from a phase diagram. The subject of phases and phase diagrams will be taken up later in this section. Dendrites, then, dominate the world of ancient castings (see Figs. 9, 10), but there are occasions when other types of segregation occur in addition to dendritic segregation, or when cooling conditions give rise to completely different structures.

The other principal types of segregation are normal segregation and inverse segregation. Normal segregation occurs when the lower melting point constituent is concentrated towards the inner part of the mold, while inverse segregation— often associated with alloys of copper containing arsenic, antimony, or tin—can push the alloying element to the exterior of the surface of the mold. Inverse segregation may be responsible

Figure 9, right. Polished and unetched section through a "Darien"-style pectoral from ancient Colombia. Magnification (x160) shows selective corrosion of the dendrite arms. Note the very rounded impression of the dendritic shapes. The alloy is an 18% gold, 4% silver, 68% copper alloy cast by the lost-wax process.

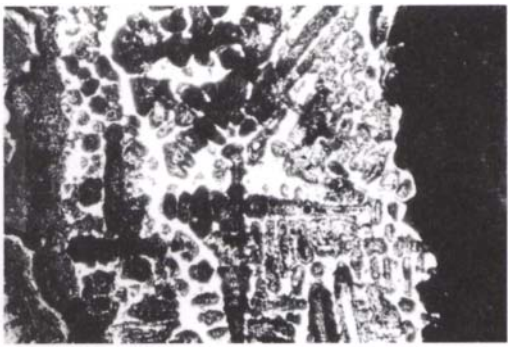

Figure 10, far right. Polished section of a small cast frog from the Tairona area of Colombia showing different dendritic structure. Here the magnification is x80 and the section has been etched with potassium cyanide/ammonium persulfate etchant.

for some of the silvery coatings occasionally reported in the literature, such as the antimony coatings on some cast Egyptian copper objects (Fink and Kopp 1933). Copper, lead, or gold castings can occasionally be relatively free of impurities and on slow cooling no dendrites may be visible. Under these circumstances, the metal may cool and produce an equi-axial, hexagonal grain structure. An equi-axed hexagonal crystal structure, in which all the grains are roughly the same size, randomly oriented, and roughly hexagonal in section, corresponds to an ideal model of a metallic grain or crystal. It is the arrangement of separate growing crystals that meet as they grow that gives the hexagonal nature to the ideal structure, since this results in the least energy requirement. It is an equilibrium structure for this reason, which the dendritic structure is not (see Fig. 11). One result of this is that it may be possible to obtain an equi-axed hexagonal grain structure by extensive annealing of the original dendritic structure. On the other hand, a dendritic structure cannot be obtained by annealing an equi-axed grain structure. Cast metals that do not show a dendritic structure can be quite difficult to etch and it may be difficult to develop any structure apart from the visible inclusions and any porosity in the metal. Cast metals often display characteristic spherical holes or porosity, which can be due to dissolved gases in the melt or to interdendritic holes and channels that have not been kept filled with metal during solidification. As the metal cools, the dissolved gases exsolve, creating reactions with the metal itself to form oxides (for example, the production of cuprous oxide [Cu_2O], the copper eutectic in ancient castings) or causing gas porosity in the metal. The third type of structure, which is particularly associated with chill castings, is columnar growth. Chill castings are formed when metal cools quickly on being poured into a mold. In this type of structure, long narrow crystals form by selective growth along an orientation toward the center of the mold. They may meet each other and thus completely fill the mold. It is rare to find this type of structure in ancient metals, although some ingots may show columnar growth.

Working

Working refers to a method or combination of methods for changing the shape of a metal or an alloy by techniques such as hammering, turning, raising, drawing, etc. A list of useful terms is given in Appendix E. Further details can be found in many of the texts mentioned in the bibliography, especially those by Untracht (1975) and Maryon (1971).

The initial grain structure of a homogeneous alloy can be considered as equi-axed hexagonal grains. When these grains are deformed by hammering they become flattened (their shape is altered by slip, dislocation movement, and the generation of dislocations as a result of working) until they are too brittle to work any further. At this point, the grains are said to be fully work-hardened. If further shaping or hammering of the metal is required then the metal must be annealed in order to restore ductility and malleability. Further deformation of the metal by hammering may then lead to work-hardening again and, if further shaping is required, then another annealing operation can be carried out. Many objects have to be

shaped by cycles of working and annealing in order to achieve sufficient deformation of the starting material, which may be a cast blank or ingot of metal that must be cut or shaped into individual artifacts. Typically, annealing temperatures would be in the range of 500–800 °C for copper-based alloys, iron, and steel. If the metal is an alloy, then, strictly, the type of annealing operation should be specified: process anneal, stress-relief anneal, solid solution anneal, etc. Time is an important factor as well: too lengthy an anneal may lead to grain growth and a weakening of the structure of the artifact; too short an anneal, and heterogeneity and residual stresses may not be eliminated sufficiently. There are other practical problems associated with annealing depending on the metal concerned; for example, when debased silver alloys (usually silver-copper alloys) are annealed by heating in air, they are liable to undergo internal oxidation. A black skin of cupric oxide forms (CuO), overlying a subscale of cuprous oxide (Cu_2O), while oxygen can diffuse into the alloy, attacking the readily oxidized copper-rich phase and producing internal cuprite embedded in a silver-rich matrix (for further details see Charles and Leake 1972; Smith 1971; Schweizer and Meyers 1978).

Cold-working and annealing can be combined into one operation by hot-working. The object to be worked is heated to near red heat and then immediately hammered out. The two processes, namely cold-working followed by annealing and hot-working, will give essentially the same microstructure of worked and recrystallized grains, so it is always not possible to know if cold-working and annealing has been used in a particular case, although there may be other indications that have a bearing on the interpretation of the resulting structure (see Figs. 11a–f, 12). Some metals, such as iron, usually must be worked into shape while they are red hot. The forging of wrought iron, which contains slag globules as impurities, produces a worked structure in which the slag gradually becomes elongated or strung out into slag stringers along the length of the object. It is important to note that most inclusions in ancient metals do not recrystallize as a result of hot working or working and annealing: they either are broken up into smaller particles or they are flattened out as the working process proceeds.

Face-centered cubic metals, except for aluminium, recrystallize by a twinning process.

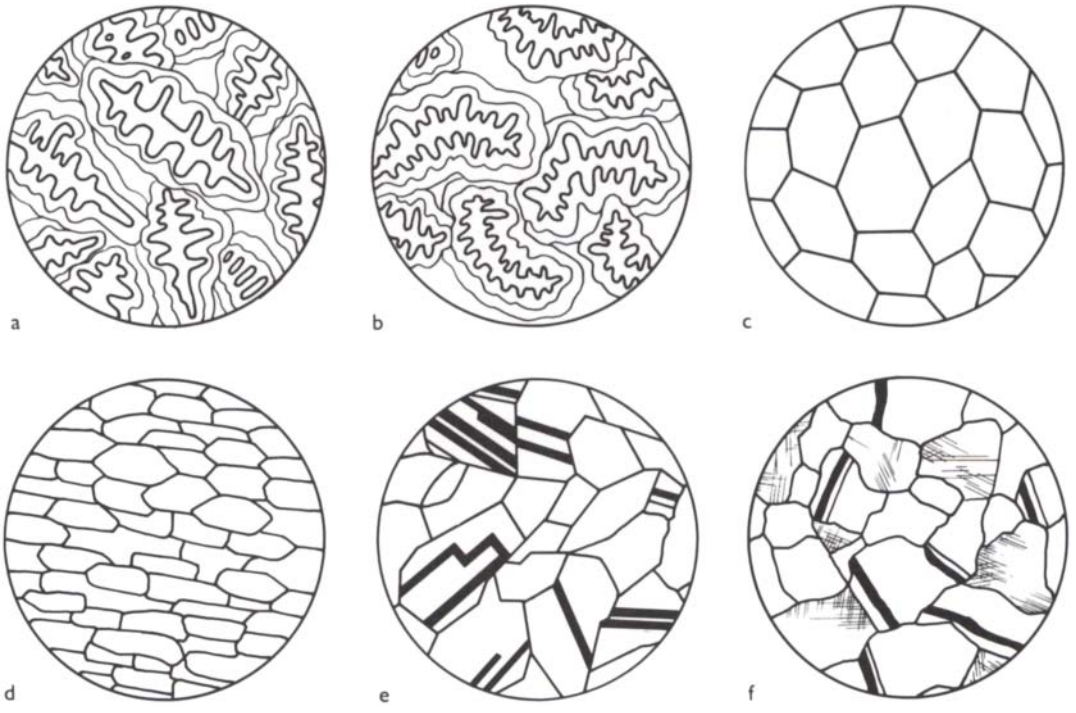

Figure 11a–f. Some microstructural features in solid solution FCC metals.
a. Cored grains with remnant dendritic structure.
b. Cold-worked cored grains.
c. Fully annealed homogeneous hexagonal equi-axed grains.
d. Cold-worked annealed metal with flattened grains.
e. Annealed after cold-working showing twinned grains.
f. Cold-worked after annealing showing distorted twin lines and strain lines in the grains.

Figure 12. Relationship between single-phase structures in FCC metals used in antiquity.

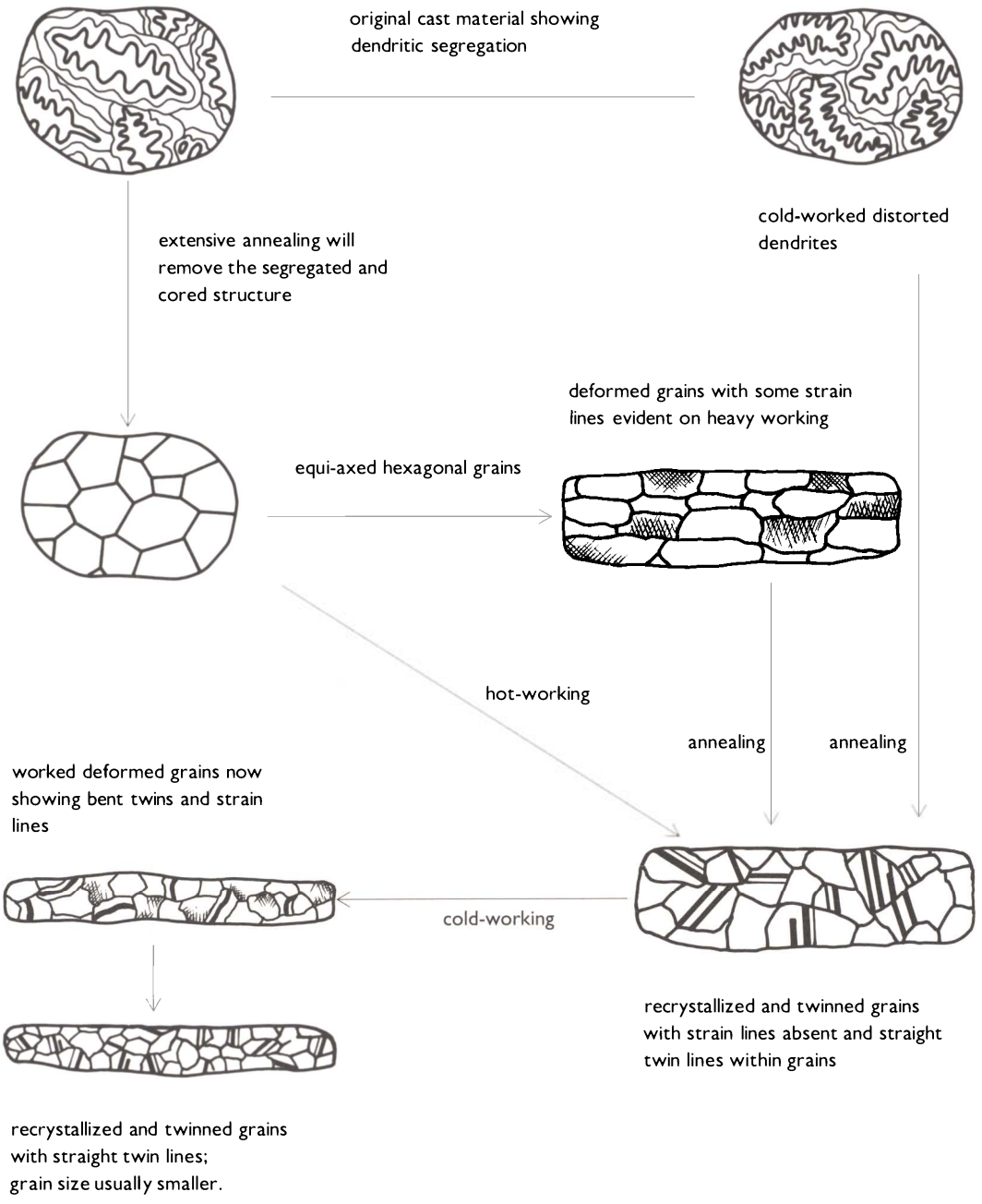

New crystals that grow following the annealing of cold-worked face-centered cubic metals such as gold, copper, silver, and their alloys, produce the effect of a mirror reflection plane within the crystals, with the result that parallel straight lines can be seen in etched sections traversing part or all of the individual grains of the metal (Fig. 12). After annealing, the twin lines in the crystals are perfectly straight: they may not run completely through every grain, but they are straight. If the grains are subsequently deformed, then the twin lines will also be deformed. In polished and etched specimens, they appear as slightly curved lines. In heavily worked metals, slip of crystal planes can occur in individual crystals resulting in a series of parallel movements that can be seen in

etched sections as a series of fine lines in some of the grains. These lines are called slip bands or strain lines. Another feature that may show that metal has been heavily worked is the presence of a fibrous morphology in the microstructure. This may occur when grains have been flattened out by hammering, producing an elongated structure commonly described as a "textured effect." When this metal is annealed to produce a recrystallized grain structure, the recrystallized material may still show a preferred orientation or a fibrous nature. This is an extreme example of the fact that recrystallized grains are not found to be completely randomly oriented. Depending on the amount of cold-working that the metal has received it will be able to recrystallize at successively lower temperatures, which are markedly different for particular metals. For example, heavily worked pure copper is capable of recrystallizing at 120 °C, iron at 560 °C, zinc at 10 °C, tin at -12 °C, and lead at -12 °C.

This is why metals like pure lead can be bent back and forth at room temperature without work-hardening: they are effectively being hot-worked at room temperature. Alloying elements and impurities will, of course, affect recrystallization temperature, as will grain size and the degree of cold-working.

The percentage of deformation, or degree of cold-work, is usually expressed in terms of reduction of height of the specimen, *h*.

$$\%\ cold\text{-}work = \frac{h_{initial} - h_{worked}}{h_{initial}} \times 100$$

It is often difficult to remove the segregation that occurs during the casting operation, and many ancient objects that were worked to shape from a cast ingot still show some coring or remnant dendritic structure, even though the object was subsequently worked to shape. Variations in composition are not confined by the new, worked grain structure and appear superimposed upon the grains when the specimen is etched (Figs. 13, 14).

The kind of twinning occurring in CPH metals is shown by the structure of the Indian zinc coin in Figure 15. While slip and twinning are the main methods by which zinc crystals accommodate plastic deformation, there are situations in which neither of these events can occur directly. This can happen when zinc crystals are compressed parallel to the basal plane or where crystals are restrained from movement, such as in

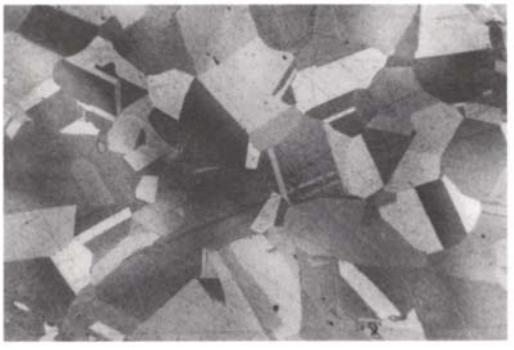

Figure 13. Photomicrograph of a section through a copper alloy axe from Iran showing twinned grains after etching with ferric chloride solution (approx. x300). Note that the porosity in the metal has not been eliminated by working.

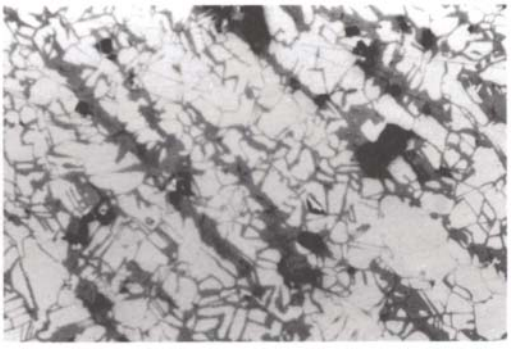

Figure 14. Twinned grains of gold-copper alloy sheet from pre-Hispanic Colombia, district of Nariño. Corrosion, which appears grey here, outlines twin grains of the crystals without etching. Striations through the section are due to selective corrosion as a result of segregation in the worked alloy. The segregation is due to unequal distribution of copper and gold in the hammered sheet. Annealing twins are straight showing that annealing was the final stage in manufacture. x120.

Figure 15, right. Twin planes in Indian zinc coin.

Figure 16, far right. Twin planes in zinc.

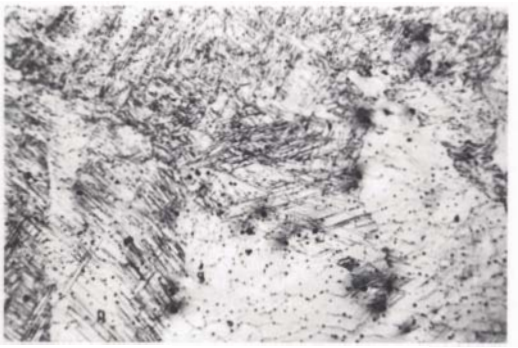

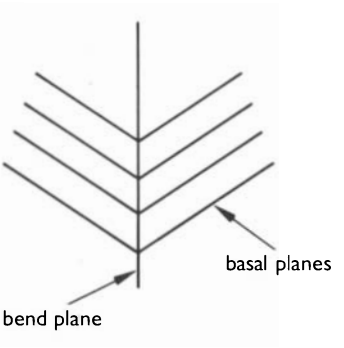

the usual polycrystalline solid. Under these conditions, stress can be relieved by the movement of the basal plane axis. The axes of the bend are contained in a bend plane which bisects the included angle of bend and which has no defined crystallographic indices. The bending mechanism involves slip, since individual basal planes must move relative to each other for bending to occur.

Although in some cases the volume of metal involved in a series of bends is sufficient to produce macroscopic kinks, bending often occurs around a very large number of closely spaced parallel axes giving the effect of a curve. When such deformed structures are annealed close to the melting point, a coalescence of the fine bend segments into coarser units occurs (Figs. 16, 17).

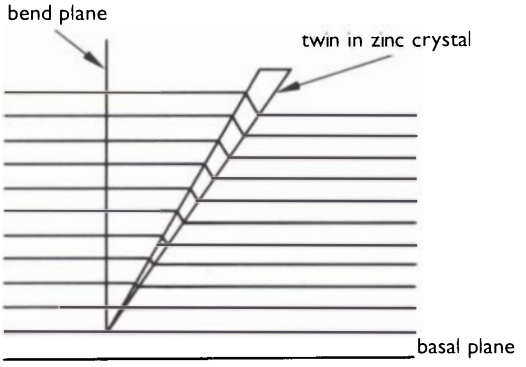

Figure 17. Twin planes in zinc.

Apart from compositional variations produced by segregation or by inclusions, the varieties of microstructure produced by the presence of two or more phases in metal have not been discussed. Some reasons why more than one phase can be present are discussed in the following sections:

1. Eutectic structures
2. Eutectoid structures
3. Peritectic structures
4. Widmanstätten transformations
5. Discontinuous precipitation
6. Intermetallic compound formation
7. Immiscible structures

When two (or more) metals are mixed together to form an alloy there are a number of different possibilities regarding their mutual solubility. Usually a phase diagram (or equilibrium diagram as it is also known) is employed. It is essentially a map that can be used to predict what phases should be present in the alloy at equilibrium. It is important to stress that diagrams usually only refer to very slowly cooled melts which rarely occur in archaeological materials. This does not mean that it is useless to consult phase diagrams: It means that the information must be interpreted with caution and, preferably, after experience with ancient alloys gained by microscopical examination.

When two metals are mixed together there are three main possibilities. The first is a solid alloy showing complete solid solubility of two metals. An example is the range of alloys formed between silver and gold. Gold is soluble in silver and silver is soluble in gold. The phase diagram that results from this kind of alloy shows just one solid phase present at all temperatures up to the solidus. The solidus line separates the region of solid metal from the pasty stage of solidification at temperatures above this line. As the temperature rises, the alloys pass through a pasty, semisolid region in which some liquid is present in equilibrium with some solid. This continues to the liquidus line and above this line the alloy is present as a liquid melt. The liquidus line separates the pasty stage from the liquid melt above (Fig. 18).

In cooling from the molten state, the alloy undergoes the following transitions:

$$L \longrightarrow L + \alpha \longrightarrow \alpha$$

where L = liquid and α = solid.

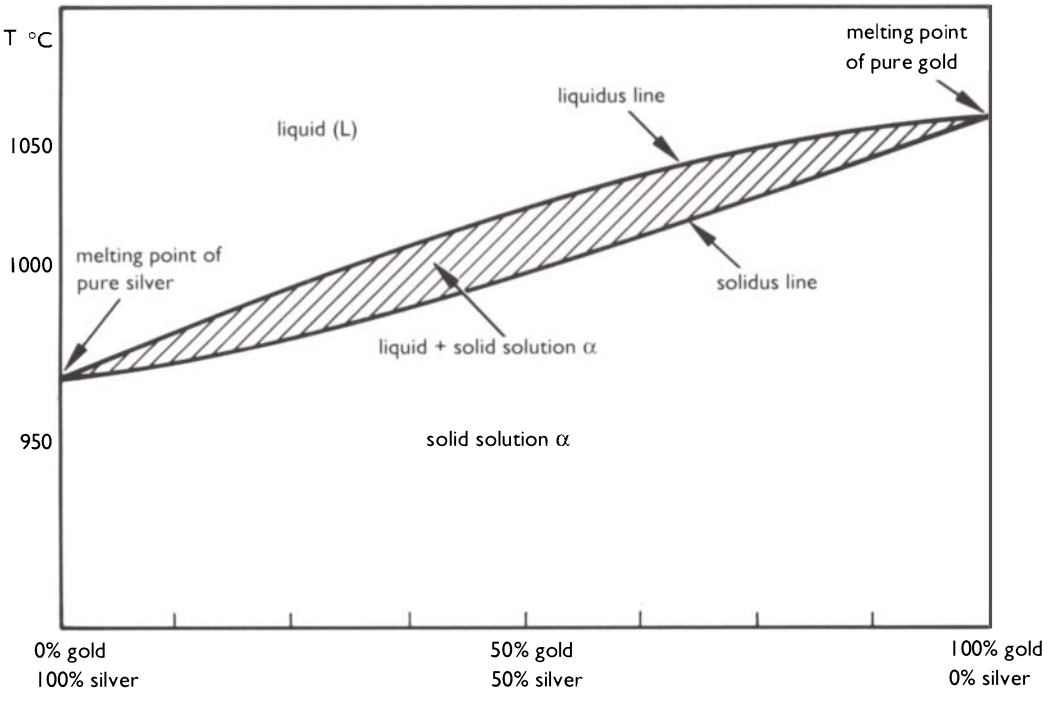

Figure 18. Phase diagram for the gold-silver system. Note that both metals are completely soluble in each other.

If no coring or other forms of segregation are present, then the microstructure will be a collection of equi-axed hexagonal grains of uniform composition—there will be only one phase present.

The second possibility is that a solid alloy can show only partial solubility of the metals in each other. One example is silver and copper. There are three principal types of phase diagrams that can arise from this situation. The most common is the eutectic type, second is the eutectoid, and third is the peritectoid. The third possibility is that the two metals are completely immiscible in each other.

Eutectic Structures

Silver-copper alloys are examples of the eutectic type and have the following characteristics: the solubility of copper in silver and of silver in copper falls as the temperature falls (this is a general characteristic for most alloys), and there is one temperature at which the liquid melt can pass directly to solid: The eutectic point. At this particular composition and temperature—which varies, of course, depending on the nature of the alloying constituents—the liquid melt passes to solid, which is two-phased and consists of fine plates of alpha phase and beta phase interspersed in each other (see Figs. 21–23, 25a, b).

There is a large area where alpha phase coexists with liquid and a similar region where beta phase coexists with liquid (Fig. 19). If an alloy of composition B is cooled down from the melt, then the following transitions will occur:

$$L\ (t_1\ ) \longrightarrow L\ (t_2) + \alpha$$

$$L\ (t_2) \longrightarrow (\alpha + \beta)$$

where t = temperature.

The final solid structure therefore consists of $\alpha + (\alpha + \beta)$. The original alpha will be present as either grains of alpha solid solution or as dendrites of the primary alpha, which will probably be cored. The infilling around the alpha grains will then consist of the alpha + beta eutectic as a fine interspersed mixture and under the microscope in etched section will look something like Figure 20a.

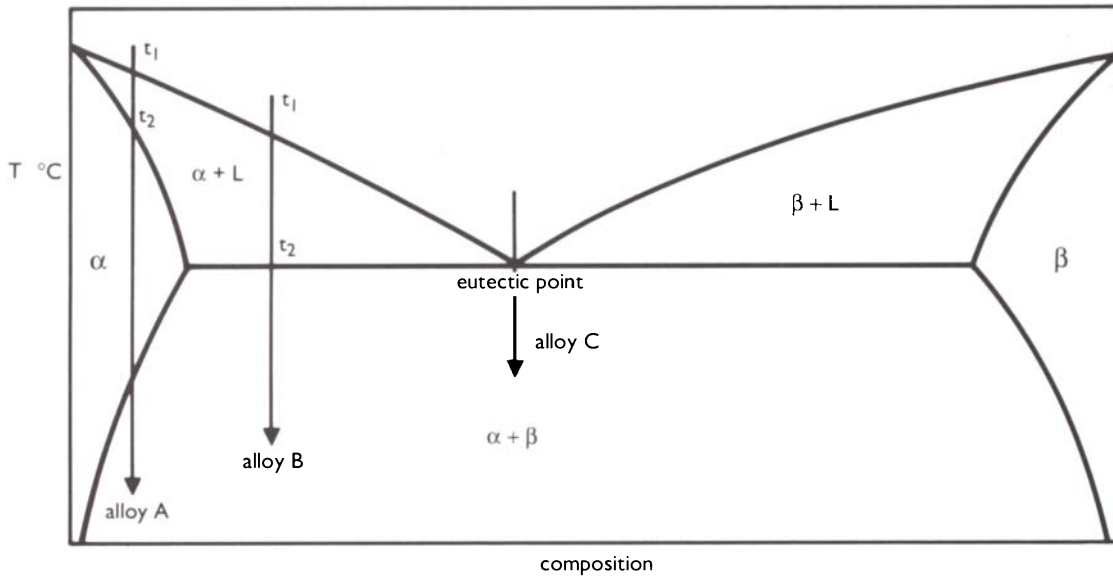

Figure 19. Eutectic phase diagram of silver-copper alloys.

Figure 20a, b. Eutectic-type microstructures.

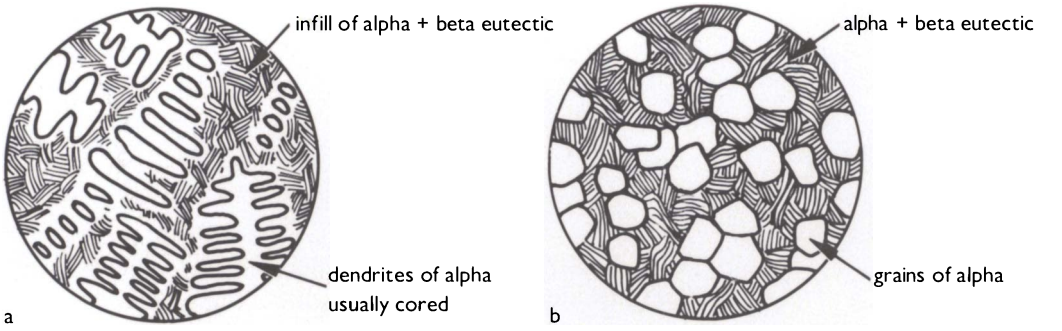

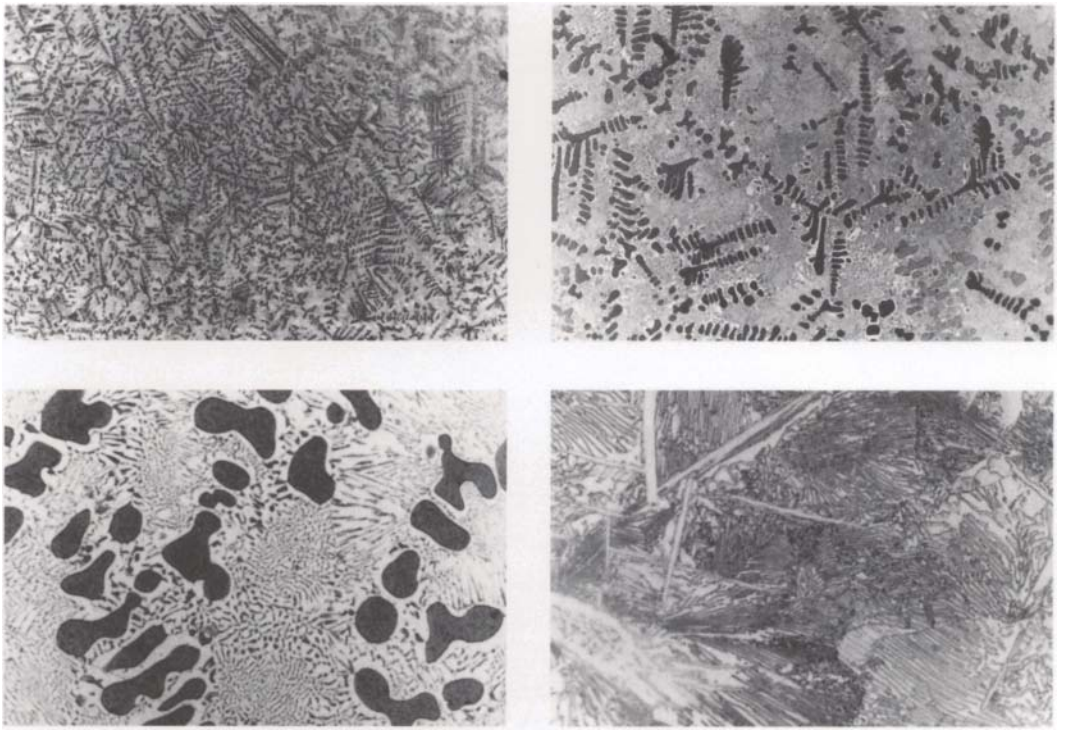

Figure 21, middle left. The feathery nature of dendritic α in a 60% Ag 40% Cu alloy that has been cast. Etched in potassium dichromate, x35. While the α dendrites can be seen clearly at this magnification, the eutectic infill of $\alpha + \beta$ cannot be seen.

Figure 22, middle right. The same alloy as Figure 21, 60% Ag 40% Cu etched in potassium dichromate, x100. The $\alpha + \beta$ eutectic phase is just beginning to be resolved into a fine series of lines in the section.

Figure 23, bottom left. 60% Ag 40% Cu alloy illustrating the nature of the eutectic infill in which the copper-rich α phase etches dark and the silver-rich β phase etches light. Electron-probe analysis of one of the dendritic arms that appear here as dark globules, gives an analysis of 92% Cu 8% Ag, corresponding very well in composition to the first solid formed from the melt in the phase diagram for Cu-Ag etched in alcoholic $FeCl_3$ and potassium dichromate, x160.

Figure 24, bottom right. Wootz steel ingot from India showing fragments of cementite needles with an infill of eutectoid pearlite ($\alpha + Fe_3C$, x300), etched in nital. Wootz steel ingots from India were high-carbon steels (often over 0.8% carbon), cast in crucibles, and used for the manufacture of sword blades and other quality products. The eutectoid may be similar to the eutectic.

The cooling rate determines whether the original alpha phase is present as dendrites or as hexagonal grains. Usually in archaeological materials the primary alpha will be dendritic and cored; later working and annealing may remove dendritic segregation and grains of alpha may become more apparent. It is beyond the scope of this text to provide a quantitative interpretation of the phase diagram, but what can be said is that as the eutectic point is approached, there will be correspondingly less initial phases of alpha or beta.

As the area of alpha is approached there will be less eutectic present and more alpha. As the alloys approach the beta side of the diagram the same variation is found: the alloys are progressively richer in beta and have less eutectic. In two-phase alloys where dendritic segregation has occurred, the proportion of the two phases will not be quite what it should be at full equilibrium.

The alloy at composition A (Fig. 19) will have a slightly different composition in terms of the distribution of the two phases. As it cools down the following sequence should occur:

$$L\ (t_1) \longrightarrow L\ (t_2) + \alpha$$

$$L\ (t_2) \longrightarrow \beta$$

The resulting structure will then be alpha grains with a thin film of beta surrounding them, or alpha dendrites with a fringe of beta (Fig. 25).

At the eutectic composition, the liquid melt passes directly to solid and ideally will consist of a fine, intermixed matrix of alpha and beta phase (Fig. 26).

A feature of the microstructure of eutectic-type alloys is that there may be a depletion of part of the eutectic phase near the grains or dendrites. For example, suppose the original dendrites are alpha phase, with an infill of alpha + beta eutectic. Some eutectic alpha constituent can migrate and join the dendritic alpha, which will leave a fringe surrounding the dendrites appearing to contain a more homogeneous zone before eutectic infilling is reached (Fig. 27).

One of the interesting changes that can occur when a two-phased alloy is worked is that either one or both phases can become elongated or strung out, much like slag stringers in wrought iron, along the direction of the working of the alloy. Slag stringers are the broken-up remnants of slag inclusions in wrought iron that become elongated upon hammering the iron to shape. In theory, one would expect the process of working and annealing to remove any original dendritic segregation and to produce worked and recrystallized grains with a eutectic infill, depending on the composition of the original raw ingot. However, it is often very difficult to remove the initial dendritic structure and instead the microstruc-

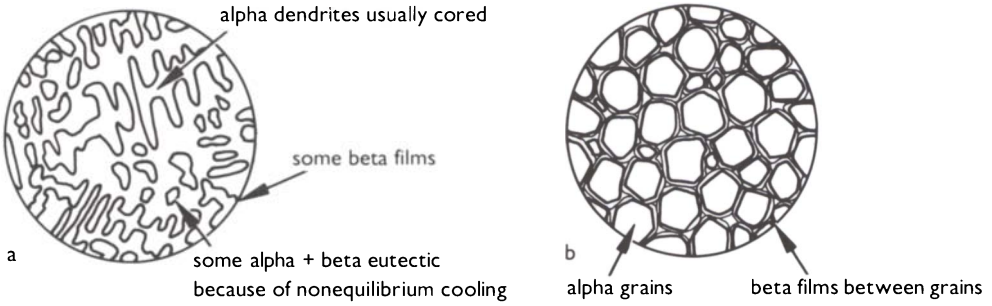

Figure 25a,b. α and β microstructures. A typical eutectic alloy microstructure.

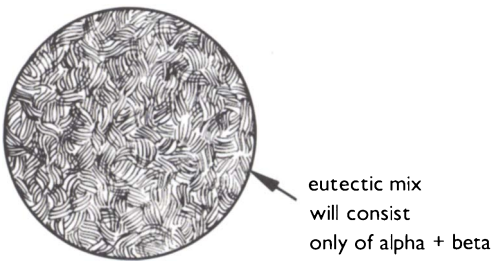

Figure 26. Eutectic α and β.

Figure 27, right. Eutectic and dendrites in a typical eutectic alloy.

Figure 28, far right. Fibrous structure in a typical heavily worked two-phase alloy.

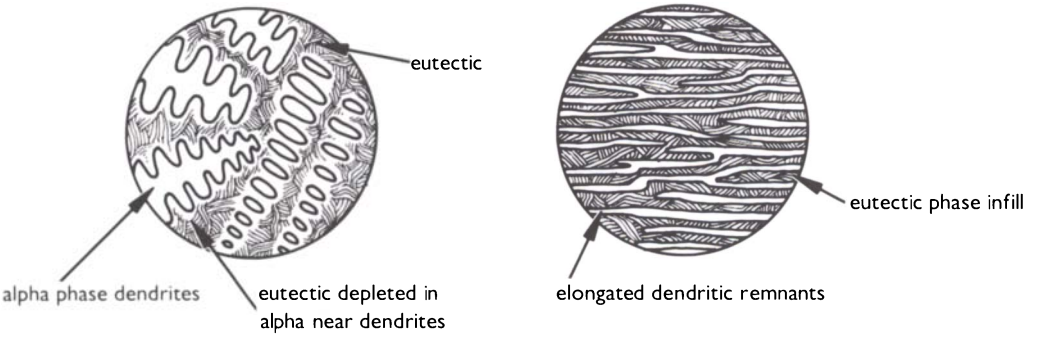

Figure 29. α and δ eutectoid in a tin bronze alloy.

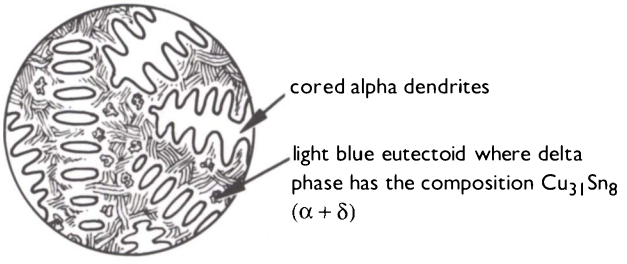

ture tends to consist of elongated ribbons of one phase with the eutectic in-between. The length-to-breadth ratio of these elongated stringers then gives some idea of the extent to which the alloy has been hammered out—very thin stringers suggesting more severe deformation during manufacture. Sometimes alloys also have a fibrous quality for the same reason (Fig. 28).

Common examples of simple eutectic systems in ancient metals are those of debased silver artifacts, which are usually silver-copper alloys and soft solders, which are lead-tin alloys.

Eutectoid Structures

The eutectoid phase is similar to the eutectic structure, the principal difference being that the eutectoid reaction occurs when an already existing solid solution transforms into two distinct phases. The types of phase diagrams that give rise to eutectoid-type transformations are necessarily more complex because there are series of changes in the solid as it cools to room temperature. There are two important eutectoid transformations in archaeological metals: those in tin bronzes and in carbon steels (for one example, see Fig. 24). The form the eutectoid takes in bronzes and steels is not the same. In bronzes, the eutectoid constituent is made up of the two phases, alpha (the copper-rich solid solution of tin in copper) and delta (an intermetallic compound of fixed composition, $Cu_{31}Sn_8$). This eutectoid phase begins to appear in the microstructure between about 5% to 15% tin (and above), depending on the cooling conditions of the alloy. It is a light blue, hard and brittle material that often has a jagged appearance. The structure is often shaped by grain boundary edges and the blue delta phase often contains small islands of alpha phase dispersed through it (Fig. 29). If there is a lot of this eutectoid phase present, the bronze is difficult to work. Proper annealing of bronzes with up to about 14% tin will result in a homogeneous solid solution of alpha grains that can then be worked to shape much more readily because the hard and brittle eutectoid has been eliminated.

Eutectoid in the bronze system originates from a complex series of changes that are not delineated in detail here, but are summarized as follows:

1. The alloy passes through the alpha + liquid region as it cools.

2. It reaches a transition at about 798 °C and a peritectic transformation occurs.
3. A beta intermediate solid solution results.
4. On cooling to about 586 °C, the beta phase transforms to gamma.
5. At 520 °C the gamma solid solution transforms to the final solid mixture of alpha + delta eutectoid.

Because the eutectoid in the copper-tin system is rather difficult to follow, most textbooks on the subject introduce the idea of eutectoid transformation by looking at the phases formed when carbon is added to iron to produce steels, and, as the carbon content increases, cast irons.

Most ancient steels were made from iron containing up to about 1% carbon, although not only is the carbon content of many ancient artifacts very variable in different parts of the same object, but many of them only contain about 0.1–0.5% carbon. These low-carbon steels were, however, very important products and could be used to produce excellent edged tools.

The eutectoid is formed when the austenite solid solution (gamma phase) decomposes at about 727 °C to form the two new solid phases, ferrite and cementite. The combination of these two constituents as a fine collection of small plates is called pearlite. The name ferrite is given to the pure iron alpha phase grains, while cementite (Fe_3C) is another very hard and brittle constituent, a compound of fixed proportions between iron and carbon.

Consider the cooling of an alloy from above 900 °C, in the austenitic region of the phase diagram with an average content of carbon, represented by the line for alloy A in Figure 30. As cooling proceeds, austenite (gamma-phase) grains will separate out, and as the temperature falls, ferrite begins to separate from the austenite at the grain boundaries. Also as the temperature falls, the gamma phase becomes richer in carbon, and the ferrite loses carbon until it reaches a low of 0.03% carbon, while the austenite reaches the eutectoid composition at 0.8% carbon. As the temperature falls below 727 °C, the austenite decomposes by a eutectoid reaction into ferrite + cementite. The changes can be represented as symbols:

$$\textit{Alloy A:}\quad \gamma \longrightarrow \gamma + \alpha \ \textit{(at about 820° C)}$$

$$\gamma + \alpha \longrightarrow (\alpha + Fe_3C) + \alpha \ \textit{(below 727° C)}$$

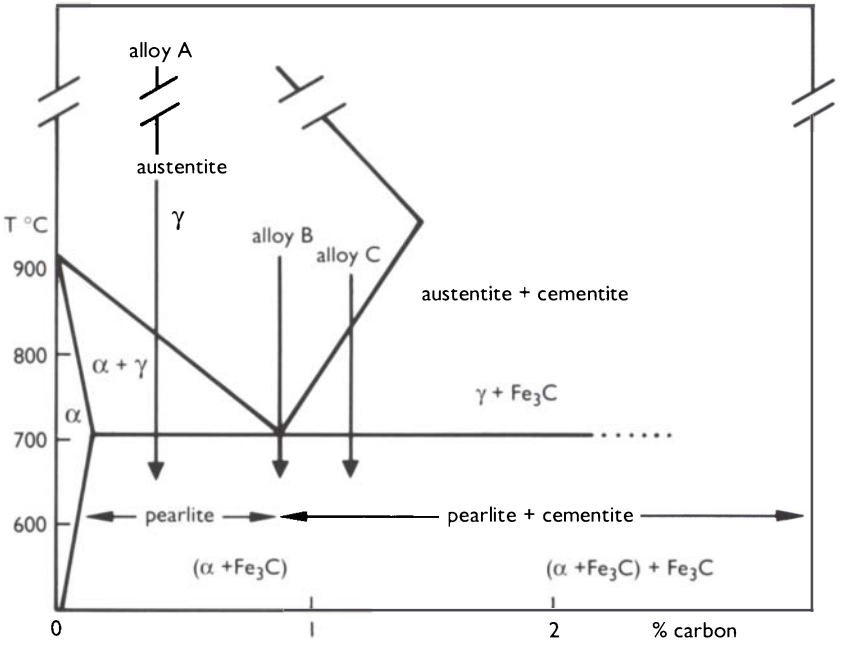

Figure 30. Significant region of the iron-carbon phase diagram.

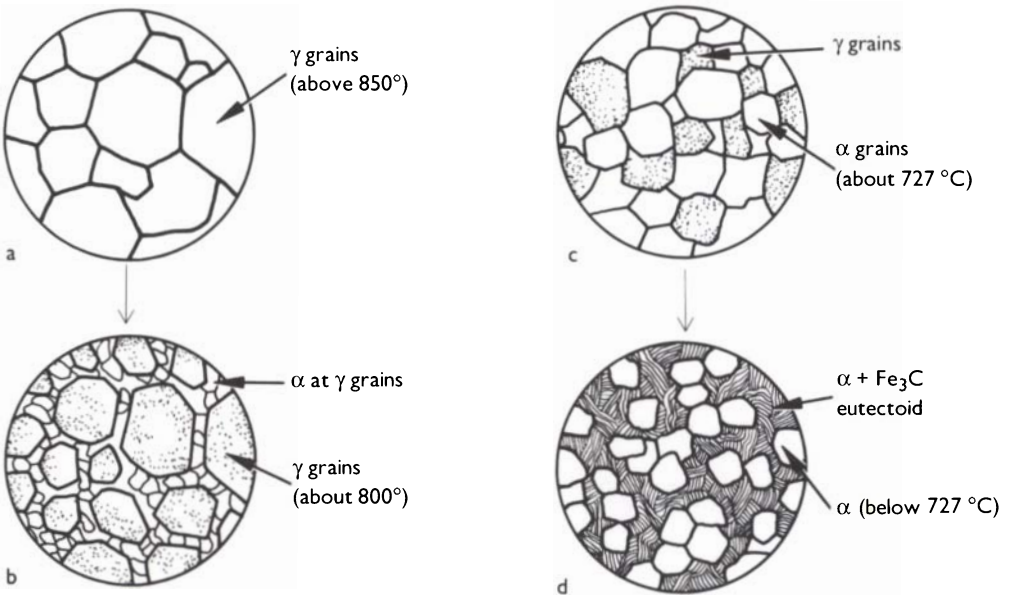

Figure 31a-d. Breakdown of γ grains in the iron-carbon system.

or as a series of drawings at different temperatures on the way to room temperature (Fig. 31a–d).

The cooling of alloy B, shown on the portion of the iron-carbon phase diagram (Fig. 30), follows a line leading through the eutectoid point with a composition of 0.8% carbon. For this particular alloy the microstructure, if cooled slowly, would consist of an intimate mixture of pearlite (alpha + Fe_3C). In the case of the iron-carbon eutectoid, the initial appearance is very similar to that of the eutectic mixture drawn previously (Fig. 26). If the rate of cooling of alloys containing pearlite as a constituent increases, then the spacing between eutectoid constituents becomes progressively finer. If the cooling rate is very fast, then the true nature of the phases that might form on a phase diagram cannot be shown because nonequilibrium cooling conditions would be involved. What happens in steels in fast cooling is very important, and new phases, such as martensite, can form, which has an extremely hard and brittle needlelike structure (see Chapters 6 and 7).

The cooling of alloy C (Fig. 30), whose position is shown on the phase diagram, produces a different but analogous series of transformations from the austenitic region:

$$\textit{Alloy C:}\quad \gamma \longrightarrow \gamma + Fe_3C$$
$$\gamma + Fe_3C \longrightarrow (\alpha + Fe_3C) + Fe_3C$$

The final structure will usually consist of cementite films or a continuous cementite network between the pearlite regions (Fig. 32).

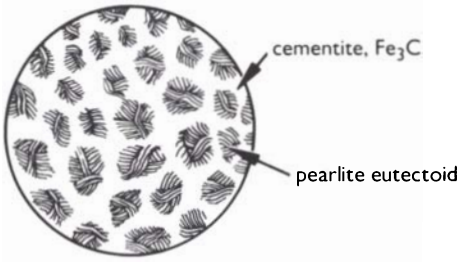

Figure 32. Cementite and pearlite.

Peritectic Structures

Peritectic structures arise from a type of transformation that may seem rather peculiar at first sight. It is unusual in the sense that a liquid reacts with an existing solid phase to form a new solid phase. An example can be taken from part of the copper-tin phase diagram (Fig. 33) to illustrate the typical shape of the phase system in peritectic alloys.

Alloy A cools down from the melt with about 18% tin content. Ignoring for the moment the complications produced by coring, as alloy A cools down, initially an alpha-phase solid solution of tin in copper separates out, while the liquid

Figure 33. Copper-tin phase diagram.

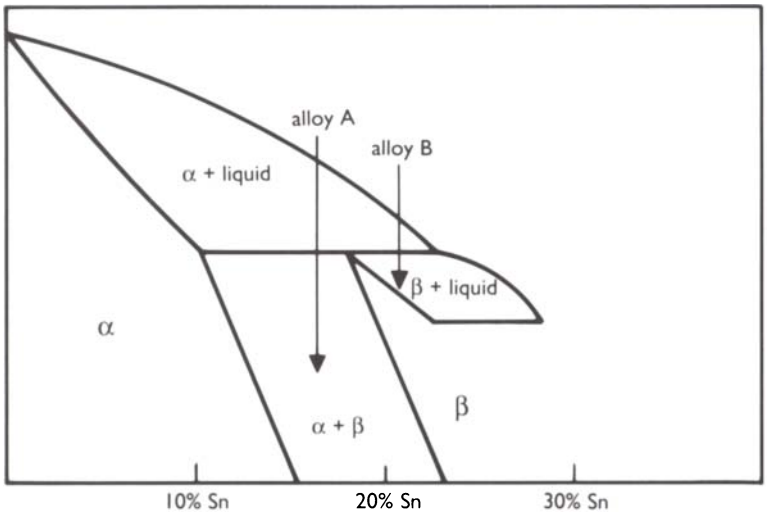

that is left gets progressively richer in tin. A reaction now occurs at about 800 °C between this liquid and the alpha phase, which produces a new phase, beta. Since alloy A occurs in the alpha + beta region of the diagram, all of the tin-rich liquid will be used up before the alpha phase is completely dissolved, and the alloy will then consist of alpha + beta crystals:

Alloy A: *liquid* ⟶ α + *liquid (tin-rich)*
liquid (tin-rich) + α ⟶ β
final structure: α + β *grains*

Often the peritectic reaction gives rise to precipitation of the new beta phase both within the alpha crystals and also at the grain boundaries so that the alpha has rather rounded contours (Fig. 34).

An alloy of composition B on the phase diagram (Fig. 33) starts to solidify by production of alpha phase grains, but these grains then react with the remaining liquid at about 800 °C and are completely converted to a new grain structure of beta grains:

Alloy B: *liquid* ⟶ α + *liquid (tin-rich)*
α + *liquid (tin-rich)* ⟶ β
final structure: β *grains*

One of the difficulties of the peritectic reaction is that it is rarely possible to get complete conversion of alpha grains into beta because alpha grains become covered with a coating of beta as they transform, and the film of beta then prevents the diffusion of tin-rich liquid to the alpha grains. The result is that there is very often a core of alpha grains left, even if the phase diagram suggests that all the material should have been converted to the second phase. A complicated example is given by the final structure resulting from an alloy containing 70% tin and 30% copper. Some of these alloys were used, usually with about 40% tin, as the alloy *speculum,* a white alloy used since Roman times for the production of mirrors. In

Figure 34, right. α and β peritectic.

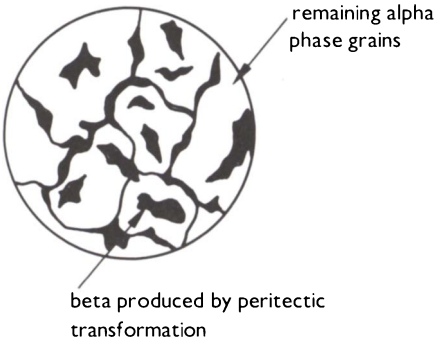

Figure 35, far right. ε phase grains.

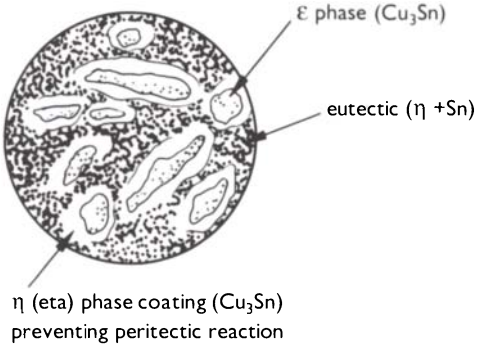

theory, this alloy should simply be a mixture of the eutectic (eta and tin); however, these alloys often show a nonequilibrium structure with epsilon (ε) phase grains (Cu_3Sn) coated with eta (η) phase grains (Cu_3Sn_3), in a eutectic mixture of (η + Sn; Fig. 35).

Many of the mirrors used in Roman times were either made using high-tin leaded bronze, with tin contents of 20–24% and lead variable (typically 5–12%), or they were made with a more common low-tin bronze alloy, which was then tinned on the surface to produce the desired color.

There are other unusual features in the copper-tin system (see Figs. 198, 199), such as that shown by the cooling of an alloy with about 41% tin. During cooling of this alloy, gamma (γ) phase crystals start to separate out at a temperature of about 715 °C. At slightly below 700 °C, freezing is complete and all the liquid is transformed to gamma solid phase. At about 650 °C, the eta (η) phase starts to form from the gamma (γ) until a temperature of 640 °C is reached. At about 640 °C the residual gamma (γ) decomposes to form simultaneously the liquid + eta (η) phase. A solid alloy melts as a result of cooling during these phase changes—a rather unique occurrence.

An alloy system of interest in which a series of peritectic transformations can occur is the copper-zinc system (brass; see Fig. 207). Most copper-zinc alloys of antiquity were made by a cementation process that had, as an upper limit, a zinc content of about 28%. Zinc ore was mixed with copper ore and the two were smelted together directly so that the zinc was absorbed into the copper during reduction, thus avoiding loss of zinc, which boils at 907 °C. Most ancient zinc alloys, therefore, possessed an alpha phase or cored dendritic structure. However, metallic zinc was also produced; for example, an alloy containing 87% zinc was reputedly found in prehistoric ruins in Transylvania, while in ancient India and China, metallic zinc was produced.

The brasses are generally divided into three categories depending on the phase type: alpha brasses with up to about 35% zinc; alpha + beta brasses with between 35% and 46.6% zinc; and beta brasses with between 46.6% and 50.6% zinc.

As zinc content increases the brittle γ phase begins to appear and thus alloys with more than

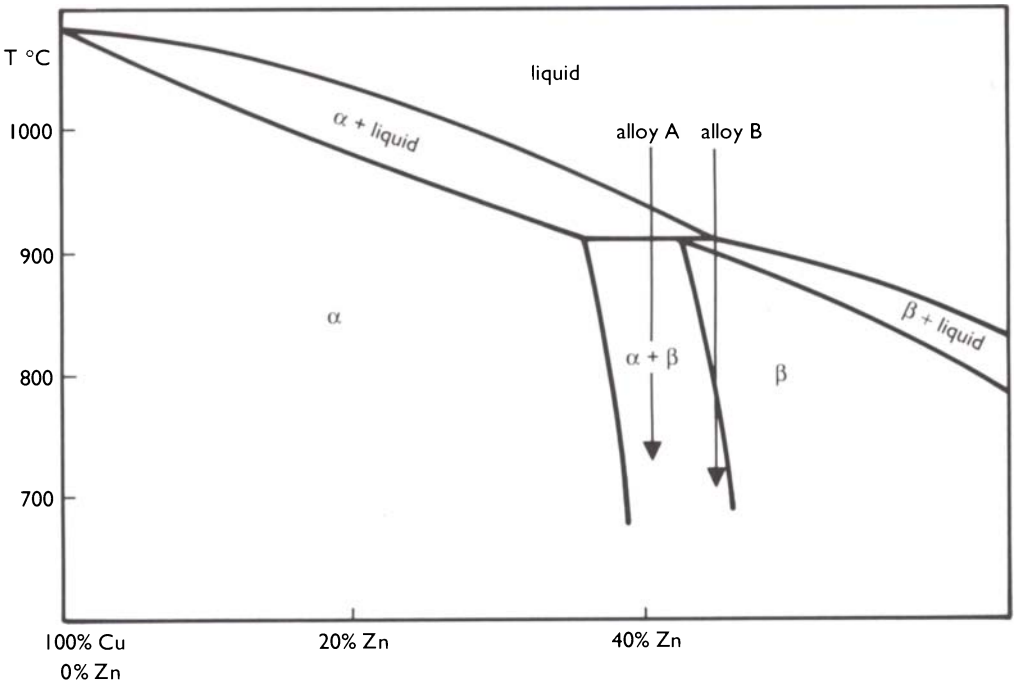

Figure 36. Copper-zinc phase diagram.

50% zinc are generally avoided. Beta (β) phase brasses are very much harder than the alpha and can withstand very little cold-working. The beta phase begins to soften at about 470 °C (as the lattice changes from an ordered to a disordered state), and at about 800 °C it becomes much easier to work. The alpha brasses, which include most of the ancient specimens, are much better when they are cold-worked and annealed rather than hot-worked because, if hot-worked, impurities tend to segregate at the grain boundaries and make the brass very weak.

These types of structures are essentially similar to the possibilities given for the section of the copper-tin diagram examined briefly earlier (Fig. 33). An alloy of composition A will, having passed below the liquidus line, begin to precipitate out alpha grains, which are then partially attacked and converted to beta during solidification so that the resulting structure consists of alpha + beta grains (Fig. 36).

Widmanstätten Transformations

The copper-zinc alloys may apply to a brief discussion of the Widmanstätten transformation. The Widmanstätten structure results from the precipitation of a new solid phase within the grains of the existing solid phase. It is thus quite different from the martensitic transformation, which is essentially a single-phased structure usually occurring as a nonequilibrium component of quenched alloys. Martensite is a collection of fine intersecting needles that can form in alloys cooled very quickly. Usually the alloy is quenched by plunging it into water or oil from a red heat. In contrast, the Widmanstätten precipitation is the result of one solid phase at a high temperature decomposing into two solid phases at a lower temperature. This precipitation usually occurs at the grain boundaries of the initial crystals and as plates or needles within the grains themselves, which have a particular orientation depending on the crystallographic structure of the original crystals.

In the case of alloy B (Fig. 36), a mixture of about 58% copper and 42% zinc, we can follow the precipitation of the alpha solid solution from the beta high temperature region.

In Figure 37a the beta grains are shown as they would appear at about 800 °C, or if the alloy was suddenly quenched in water, which would prevent it from decomposing into the alpha + beta region. The appearance of the grains is just a homogeneous solid solution of beta grains. Figure 37b shows the nature of the Widmanstätten precipitation upon cooling to room temperature. If the structure is annealed or heated to about 600 °C, then it can become quite coarse and the alpha phase may grow into large crystals with the background becoming a fine mixture of alpha + beta.

Widmanstätten structures also occur in ancient steels as a result of the working process or deliberate heat treatments used during manufacture. Very often Widmanstätten precipitation is only partially carried through the grains so that a jagged effect is produced. It is useful to return to the iron-carbon diagram (Fig. 30) at this stage in order to define a few common terms. Steels

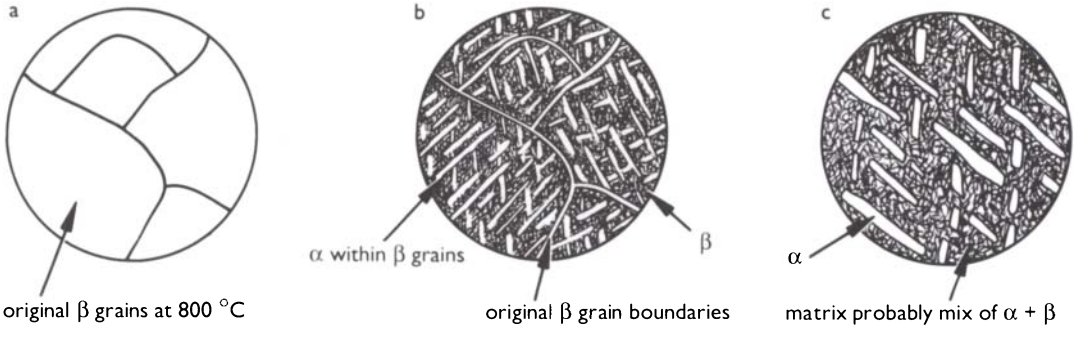

Figure 37. β grains in copper-zinc.

containing less carbon than the amount needed to make the eutectoid structure complete are called *hypoeutectoid steels*, whereas those containing carbon in excess of the eutectoid composition (and up to 1.7% carbon) are usually called *hypereutectoid steels*. The eutectoid composition itself occurs at 0.8% carbon. In hypoeutectoid steels there will generally be more ferrite than is required, and this is called the *proeutectoid* (or free) *ferrite*. In hypereutectoid steels there will generally be too much cementite to form a complete eutectoid, and this is called *proeutectoid cementite*.

Proeutectoid ferrite occurs in several different shapes. In the lower carbon steels of antiquity it is characteristically found as extensive areas among scattered islands of pearlite. This, according to Samuels (1980), should be called *massed ferrite*. In steels nearing eutectoid composition, the ferrite is usually found as thick films located at what were originally the *austenitic grains*. This is called *grain-boundary ferrite*. Ferrite may also be found in the form of broad needles, which can be sections of plates of ferrite occurring as a Widmanstätten pattern within the pearlite. A descriptive scheme for some of the various forms of ferrite has been developed by Dubé (in Samuels 1980; see Appendix A for names of ferrite shapes in low carbon steels and a glossary of terms).

Discontinuous Precipitation

Another type of phase separation of importance is discontinuous precipitation. A good example is afforded by copper-silver alloys used in antiquity. Very often the silver was debased to some extent with copper, partly to make the alloy harder and also to reduce the amount of silver. Debased silver objects then often consist of silver-rich grains in which the copper has not yet begun to separate out as it should according to the phase diagram. The solution of copper in the silver grains is therefore in a metastable state and can be precipitated slowly with time at the grain boundaries. Precipitation of this nature is called discontinuous when it occurs at the grain boundaries. The essential part of the phase diagram is shown below (Fig. 38).

A typical, slightly debased silver alloy is shown by alloy A on the silver-copper phase diagram. Note that it cuts across the $\alpha + \beta$ phase region where it cools down to room temperature. It can exist as a homogeneous solid solution alpha phase between temperatures t_1 and t_2. When the alloy gets to t_2, the decomposition of part of the solid solution into beta may not occur and instead a metastable solid solution will result. The copper-rich phase may precipitate out very slowly at room temperature, and Schweizer and Meyers (1978) suggest that the discontinuous precipitation of copper can be used to establish the authenticity of ancient silver. They extrapolate from experimental data to give a growth rate of about 10^{-3} microns per year for the rate of precipitation. This kind of growth can lead to age-embrittlement of ancient metals. Thompson and Chatterjee (1954) also found that lead formed at the grain boundaries of impure silver and led to embrittlement.

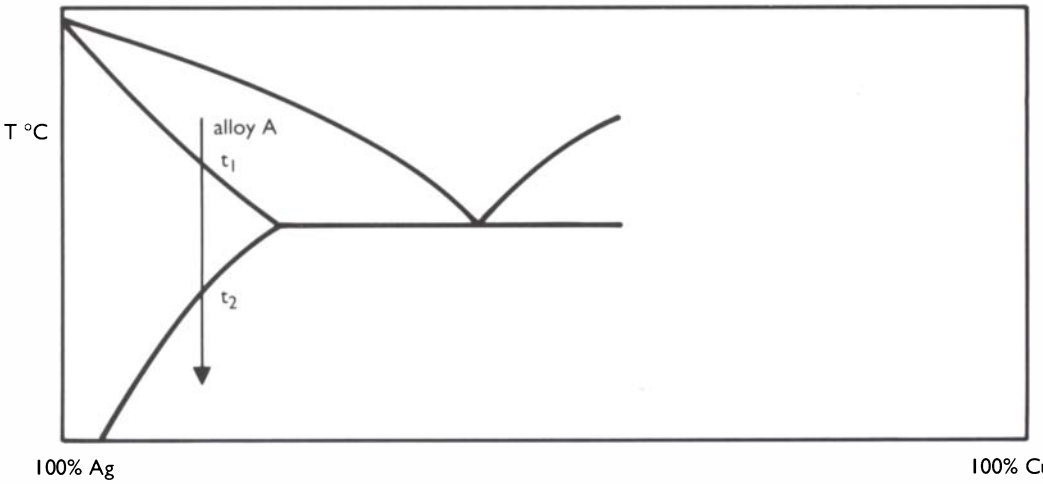

Figure 38. Discontinuous precipitation in Ag-Cu.

Intermetallic Compound Formation

When some metals are mixed together they can form phases that are essentially like ordinary chemical substances in that they are effectively compounds of fixed composition. An example is the gold-copper alloys. These alloys were used in antiquity, especially in the more base, copper-rich compositions in South America. This alloy was known as *tumbaga* and was used widely both for castings and for hammered sheetwork, often being finished by a depletion gilding process (Lechtman 1973, Scott 1983; see Fig. 39).

The diagram shows that copper and gold are completely soluble in each other with a eutectic-type low melting point, which occurs at a composition of 80.1% gold at 911 °C. The rounded shapes at the bottom of the diagram show the regions where the ordered phases can form. There are essentially three different ordered compositions: Cu_3Au, CuAu, and $CuAu_3$. $CuAu_3$ can form between about 85% to 92% gold. It is a superlattice formed by a *peritectoid* (a solid state peritectic reaction) at about 240 °C (Rhines, Bond, and Rummel 1955). Cu_3Au can form between 50% and 50.8% gold. CuAu can form between 70% to 85% gold.

Ordered phases such as these have to be distinguished from those phases normally called intermetallic compounds. Intermetallic compounds are usually represented on the phase diagram by a straight line that passes down vertically as the temperature falls. There may be two such lines close together that mark out a rectangular block on the phase diagram, showing the areas over which the intermetallic compound may form. The ordered phases are rather different because they may be formed over wider compositional limits, they do not show vertical phase boundaries in the form of straight lines, and they may pass easily between ordered regions and disordered regions.

However, these ordered phases are usually harder than the disordered alloy of the same composition, and they may make the process of

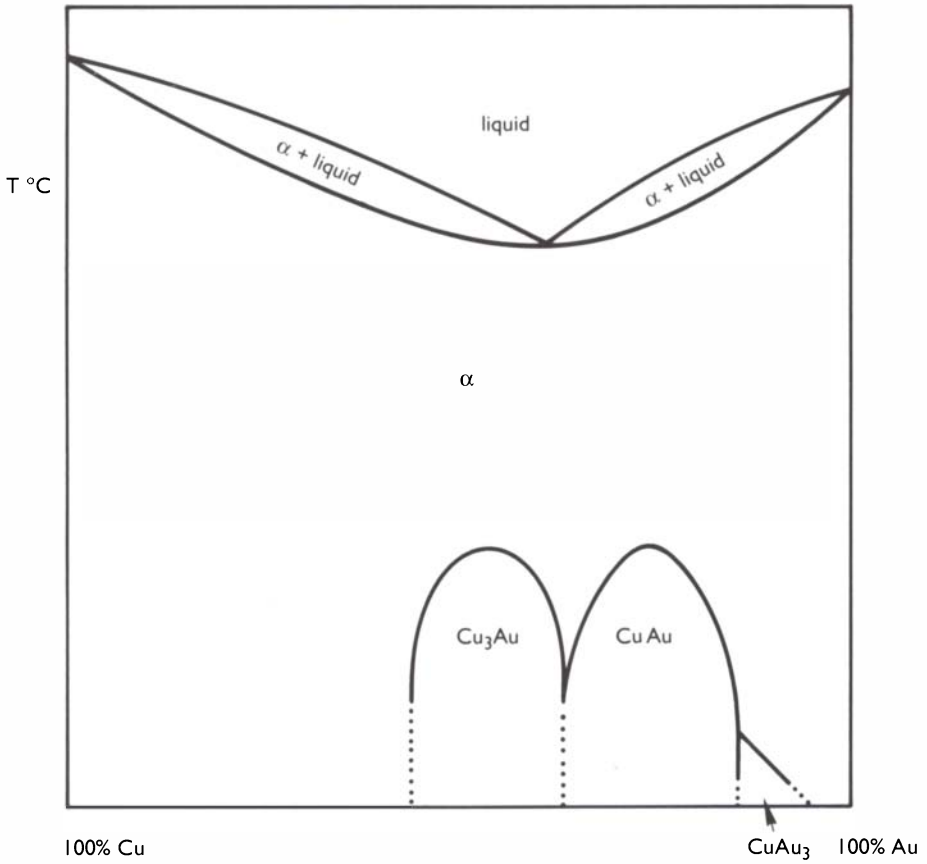

Figure 39. Cu-Au phase diagram.

working and annealing to shape more difficult. For example, the quenched alloys in the gold-copper system between about 85% gold and 50% gold are softer than the alloys that are allowed to cool slowly in air. This is the opposite of the situation that exists in alloys such as iron and carbon, where the material is dramatically hardened by quenching because of the formation of new phase, martensite. The reason why gold-copper alloys are softer is that the quenching process suppresses the formation of the ordered phases which need some time to form, and it is these ordered phases that give rise to higher hardness values and to the difficulty sometimes experienced in the working of these gold-copper alloys. South American Indians, in lowland Colombia for example, used water quenching after annealing in order to make their alloys easier to work to shape and to avoid embrittlement.

There are many examples of intermetallic compounds, such as cementite (Fe_3C), which contains 6.67% carbon and the delta phase in bronzes, which is an intermetallic compound of the formula $Cu_{31}Sn_8$.

Immiscible Structures

In some cases metals may be completely insoluble in each other. Examples of this type of microstructure are shown by the alloys of copper and lead, zinc and lead, and iron and copper. As the temperature falls from the melt of these mutually insoluble metals, one of them will be precipitated, usually as globules of one phase in grains of the higher melting point metal. An example is leaded copper, shown in Figure 40.

The diagram shows that the microstructure consists of two distinct phases and that the copper grains that form will contain globules of lead. Practically all the copper will solidify before the lead-copper eutectic forms. This lead-copper eutectic is, for all practical purposes, pure lead, as it consists of 99.9% lead and 0.1% copper. This means that the lead is segregated while the solidification process is taking place. Ordinarily, the separation of lead globules would be expected to result in massive segregation and an unusable material would result. There is a monotectic reaction at 955 °C, which occurs when the liquid from which the copper is separating out reaches a composition of 36% lead. At this point, a new liquid forms that contains about 87% lead. This new liquid is heavier than the first liquid, and so it tends to sink under gravity. However, in practice the gross segregation is limited by the formation of a dendritic structure upon casting in the copper-rich alloys and, with a high cooling rate, the lead is finely dispersed among the dendrites. With very high lead content alloys, the two liquids that separate out form an emulsion when they are cooled from about 1000 °C (Lord 1949). This emulsion results in a division into very fine droplets so that gross separation cannot occur.

With leaded copper, brass, or bronze alloys the lead usually occurs as small, finely dispersed

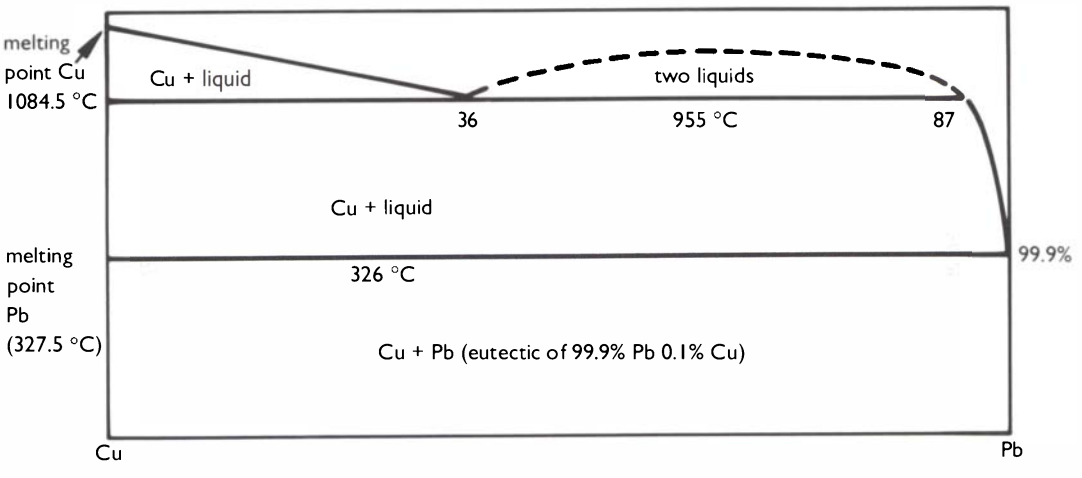

Figure 40. Cu-Pb phase diagram.

spherical globules scattered at the grain boundaries and within the grains themselves. Lead has the effect of making the alloys of copper easier to cast; it can, for example, improve the fluidity of the alloy in the melt. Lead also makes copper alloys easier to work since the lead acts as an area of weakness between the grains. This is of no practical use if the alloy is used for the manufacture of daggers or sword blades since they will be weakened by the inclusion of lead, but it is advantageous for the production of cast objects.

It is not strictly true that iron is insoluble in copper; the phase diagram is more complex than that, although the end result of admixtures of copper with small amounts of iron is the presence of small dendrites or globules of iron mixed with the copper grains. The phase diagram is given in Appendix G in this book. The cooling of a 6% iron in copper alloy is examined by Cooke and Aschenbrenner (1975). As the 94% copper and 6% iron alloy cools, it reaches the liquidus at about 1215 °C and solid gamma iron begins to separate out. This gamma iron will contain about 8.3% copper in solid solution. As the temperature falls, more of the gamma iron-rich phase separates until at 1095 °C the precipitating iron contains about 8.5% copper. At the copper-rich side of the diagram, the composition of the still liquid copper follows the liquidus until at 1095 °C the copper will contain something like 3% iron in solution. At 1084.5 °C, a peritectic reaction will occur between the liquid and the precipitated gamma phase to give a solid solution of 96% copper and 4% iron. This means that given a very slow cooling rate the alloy should consist of a solid solution (eta [η] phase) of 96% copper and 4% iron with residual gamma (γ) iron particles. As the temperature falls, the copper is gradually precipitated out of the alpha (α) iron and at the same time the eta (η) phase loses iron. In ancient specimens, so far no evidence has come to light to suggest that the peritectic reaction had occurred. Because of the presence of alpha-phase iron (ferrite), the copper alloys containing iron are usually ferromagnetic and can sometimes be picked up with a magnet.

Care must be taken when grinding and polishing leaded alloys to ensure that lead globules do not drop out (without notice being taken of their existence) in the process. If they do fall out, they leave small spherical holes and it may then become very difficult to distinguish between porosity due to casting defects and lead inclusions as an alloying constituent, since both appear as holes in the polished section.

Some of the features to be found in alloys of copper and tin, commonly referred to as bronze, or more correctly as tin bronze, have been discussed in previous chapters. The phase diagram for the copper-tin system is rather complex and cannot be discussed fully here, and the one given in this book ignores the low-temperature phase field of the alpha (α) + epsilon (ε) phase region (Fig. 33 and Figs. 198, 199 in Appendix G). This is because the ε phase never appears in bronzes of up to about 28% tin that have been manufactured by conventional means. Thousands of hours of annealing are necessary in order to make the ε phase appear and, of course, such conditions never occur, even in modern bronzes. Despite this, common forms of equilibrium diagrams contain no clue that equilibrium is practically never attained. Even more surprisingly, some modern metallurgical textbooks appear to be unknowledgeable on the subject and maintain that an alloy with 2% tin will decompose on cooling from the usual alpha + delta region to give alpha and eta without difficulty!

Tin bronzes may conveniently be divided into two regions: low-tin bronzes and high-tin bronzes. Low-tin bronzes are those in which the tin content is less than 17%. This is the maximum theoretical limit of the solubility of tin in the copper-rich solid solution. In practice, the usual limit of solid solution is nearer to 14%, although it is rare to find a bronze with this tin content in a homogeneous single phase.

When a tin bronze is cast, the alloy is extensively segregated, usually with cored dendritic growth, and an infill of the alpha + delta eutectoid surrounds the dendritic arms. The center of the dendrite arms are copper-rich, since copper has the higher melting point, and the successive growth of the arms results in the deposition of more tin. At low-tin contents, for example, between 2 and 5%, it may be possible for all the tin to be absorbed into the dendritic growth. This varies considerably depending on the cooling rate of the bronze and the kind of casting involved. If the cooling rate is very slow, there is a greater chance of reaching equilibrium, and the amount of interdendritic delta phase will be much reduced or disappear entirely. However, at tin contents of about 10% it is very unusual in castings from antiquity to get absorption of all the delta phase and the dendrites will usually be surrounded by a matrix of the alpha + delta eutectoid.

As the tin content increases the proportion of interdendritic eutectoid also increases. If a homogeneous copper-tin alloy is worked by hammering and annealing, then the typical features seen in face-centered cubic metals will be developed; namely, annealing twins, strain lines, progressively finer grains as a result of working, and flattened grains if left in the worked condition, as discussed earlier. The same features will develop if the alloy is two-phased, although the eutectoid is rather brittle and may be broken up to some extent. The usual microstructure shows the presence of small islands of alpha + delta eutectoid between the recrystallized grains of the alpha solid solution. If coring in the original cast ingot was pronounced, then this may be carried over in the worked alloy as a faint or "ghost" dendritic pattern superimposed upon the recrystallized grains. When a bronze section is etched with ferric chloride, this difference in alloy composition due to coring may only be apparent as vague differences in shading of the alloy, and a dendritic outline of the shading may be very difficult to see. Some experience in the examination of bronzes must be developed so that a worker can differentiate between uneven etching and uneven coloring of the specimen surface due to coring.

Apart from complications introduced by other alloying elements such as zinc, the structural features seen in most low-tin bronzes are the following:

1. Homogeneous bronzes, in which all the tin has dissolved with the copper and which do not display coring or residual cast features.
2. Cored bronzes, in which there is an unequal distribution of copper and tin, but no eutectoid phase present.
3. Bronzes in which both the alpha phase and

the eutectoid phase are present.

4. Bronzes in which the alpha phase is extensively cored and where the eutectoid phase is present.

Most ancient alloys have less than 17% tin. At this level of tin content, bronzes can be cold-worked and annealed; however, if the tin content is between 17% and 19% it has been found that the alloy is unworkable: it can neither be hot-worked nor cold-worked. A film of delta forms and this brittle phase then coats the grain boundaries with the result that the alloy breaks up into pieces. However, above 19% tin the bronze can be hot-worked. Bells and mirrors in antiquity were often made of ternary tin bronzes consisting of about 20–25% tin, 2–10% lead, the remainder being copper. Alloys of this type were almost invariably cast. Binary tin bronzes containing more than 17% tin often have about 23% tin, which corresponds closely to the equilibrium value of the beta phase of the bronze system, which has been mentioned in connection with peritectic transformations. Above 586 °C, a bronze in the beta region can be readily worked, whereas if allowed to cool slowly to room temperature, the bronze would decompose into alpha and delta and be impossible to work. One advantage of beta bronzes is that the beta phase can be retained by quenching. A complete account of this process is quite complex, but one of the most important points is that the beta phase is retained by quenching as a structure of martensitic needles. This quenched beta bronze is very hard, but a lot less brittle than the same bronze slowly cooled to the alpha eutectoid room temperature form. Apart from a few cast figurines, the majority of artifacts of beta bronze composition were made by the following series of operations. The alloy was made up as accurately as the technology of the time allowed, a blank was then cast in the approximate form of the desired object, and the object was shaped by hot-working at a temperature of about 650 °C. At the end of the working process, the alloy was uniformly reheated to about the same temperature and was then rapidly quenched (to preserve the high-temperature phase and to produce a martensitic structure). Hammer marks and oxide scale could then be removed by grinding with abrasives of various grades, often on a simple lathe, and then the object was polished. Surface decoration, if present, was cut into the surface with drills or an abrasive wheel before final polishing.

Although certain vessels made from this alloy possessed interesting musical properties, the principle reason for its use in regions where tin was plentiful, was its color. The color of typical beta bronze resembles gold. Beta bronzes were first found in India and Thailand from the early centuries B.C. and they spread slowly to the Near East. The Islamic alloy, white bronze, *safidruy*, is an example of a high-tin alloy. It was also found in Java and Korea, but when brass became more widely known, high-tin bronze use became much more limited.

The alloy known as *speculum*, which may contain up to about 35% tin, is said by some to have been used by the Romans for the manufacture of mirrors. However, Roman mirrors were often made by tinning; the alloy itself was often a low-tin bronze. At high levels of tin, such as those encountered in tinned surfaces, the following intermetallic phases of the copper-tin system must be considered carefully: (1) the delta (δ) phase which has already been discussed, $Cu_{31}Sn_8$, containing about 32.6% tin; (2) the epsilon (ε) phase, Cu_3Sn, containing about 38.2% tin; (3) the eta (η) phase, containing 61.0% tin, Cu_6Sn_5. Here, in tinned surfaces, the epsilon phase does appear and is important in understanding the microstructure. When tin is applied to bronze, layers of both the eta and the epsilon phase can develop by interdiffusion between the bronze and the molten tin, which then can develop layered structures in the following sequence: surface tin, eta phase, epsilon phase, substrate bronze.

Under the optical microscope, tin is light and silvery in appearance, the eta compound is slightly more grey-blue in color, the epsilon phase is the darkest grey-blue, and the delta is light blue. The range of features that may form on tinned surfaces is complicated: Cu_6Sn_5 is common and is

often misdescribed as tin (see Meeks 1986).

Many tin bronzes are leaded. With low-tin bronzes, typically castings, the lead does not alloy with the copper or tin and occurs as small globules throughout the structure. Some gravity segregation may take the lead down to the base or bottom of the casting, but generally in cast structures the distribution is fine and random.

With a higher percentage of tin, the structure may become difficult to understand if lead is present as well. This is especially true if the bronzes are quenched. There are several Roman mirrors made in bronzes approximating to: 24.7% tin, 3.2% lead, and 73.7% copper. When quenched from intermediate temperatures, a very fine particle matrix develops that is difficult to resolve under the optical microscope. This is due to the very fine dispersion of the lead and the development of a Widmanstätten structure in the bronzes. If quenching of bronzes of beta composition is not sufficient to retain beta, then decomposition into a Widmanstätten structure of fine alpha and delta may occur. Some Roman mirrors have this kind of structure. The situation is even more complicated, in fact, because in leaded-tin bronzes the melting points of the alloys are much lower than in the binary system. The ternary phase diagram shows that the presence of two liquids for many compositions above 734 °C may prevent quenching from temperatures high enough to retain beta (see Appendix G, Fig. 212).

Figure 41 shows a section through a cast toggle pin from Iran, etched in $FeCl_3$ at x450. The network of the $\alpha + \delta$ eutectoid can clearly be seen in the interdendritic regions. The toggle pin has a composition of 92.3% copper, 3.7% tin, 0.6% zinc, 0.4% iron, and 1.3% arsenic. Note that the α phase (the copper-rich component) appears light in color except near the eutectoid where some coring occurs. The coring looks as though some of the tin is being depleted in the region of the $\alpha + \delta$ eutectoid as some tin from the α solid solution region migrates to join up with $\alpha + \delta$. The darker regions around the $\alpha + \delta$ phases are copper-rich compared to the rest of the bronze.

The bronze structure of the incense burner in Figure 42 is atypical, consisting of small polygonal grains with patches of the eutectoid between them and interspersed with small globules of lead. This leaded bronze must have been cast followed by an annealing process during manufacture (see Figs. 109, 110 in Appendix F). There are very few traces of twinned grains present and these are not as prominent as the coring that still remains from

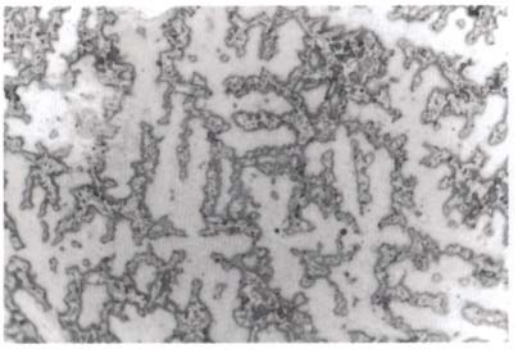

Figure 41, right. Cast toggle pin from Iran. Bronze with 3.7% tin and 1.3% arsenic. Etch: $FeCl_3$; x120.

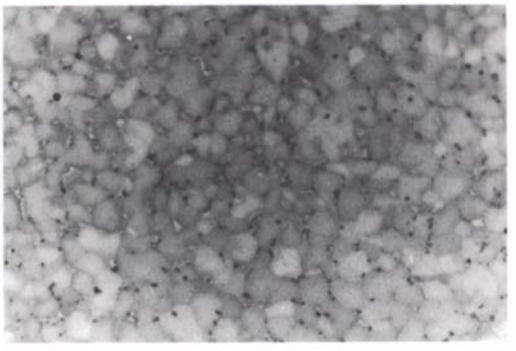

Figure 42, far right. Chinese cast-bronze incense burner of the 19th century. Bronze with 8% tin and 4% lead. Etch: $FeCl_3$; x80.

Figure 43, top right. A small mirror of beta-quenched bronze from Sumatra from Kota Cina, a 10th century A.D. trading complex. x150.

Figure 44, top far right. A high-tin bronze mirror from Java showing the classic development of the beta-quenched bronze structure in the microstructure. x130.

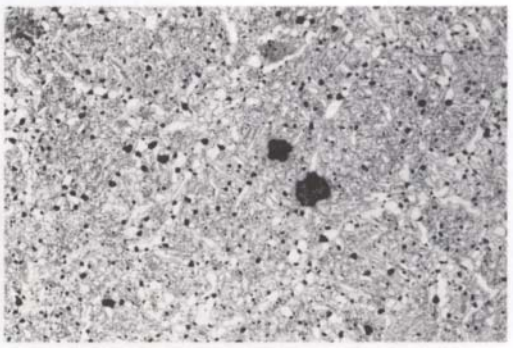

Figure 45, below right. Cast high-tin leaded bronze of composition 22% tin; 6% lead and 72% copper showing structure after etching in alcoholic $FeCl_3$. x80.

Figure 46, below far right. Laboratory quenched alloy of composition 24% tin, 76% copper that has been quenched in cold water at 650 °C showing a fine network of β needles. The β phase in this sample occupies the structure completely with only a few globules of copper oxide present as an impurity. x180.

the cast metal.

The bronze mirror in Figure 43 has slightly less than the required amount of tin to make a complete beta phase throughout, and small islands of α phase can be seen that often follow the previous grain boundaries of the high temperature β grains before quenching the alloy. The type of β needles developed here is sometimes mistaken for strain lines in a copper alloy, but the context and type of lines to be seen is unmistakable. It is etched with $FeCl_3$ at x150; about 22.5% tin, 77.5% copper.

The α islands that are also present in many of the high-tin beta bronzes, such as the mirror in Figure 43, are sometimes twinned as a result of hot-working the bronzes before quenching. The mirror possesses a highly lustrous dark green patina. Despite being a metastable phase, beta bronzes remain quite stable after thousands of years of burial.

Figures 45 and 46 are examples of laboratory-made bronze ingots, originally produced to study the structural aspect of ancient alloys. For example, Figure 45 was cast in a high-tin leaded bronze to replicate some of the structures that were found in a series of Roman mirrors. Figure 46 illustrates the microstructure for a laboratory prepared alloy made from an ingot of 24% tin, 76% copper quenched in cold water at 650 °C. The structure of this alloy consists of a fine interlocking network of β needles.

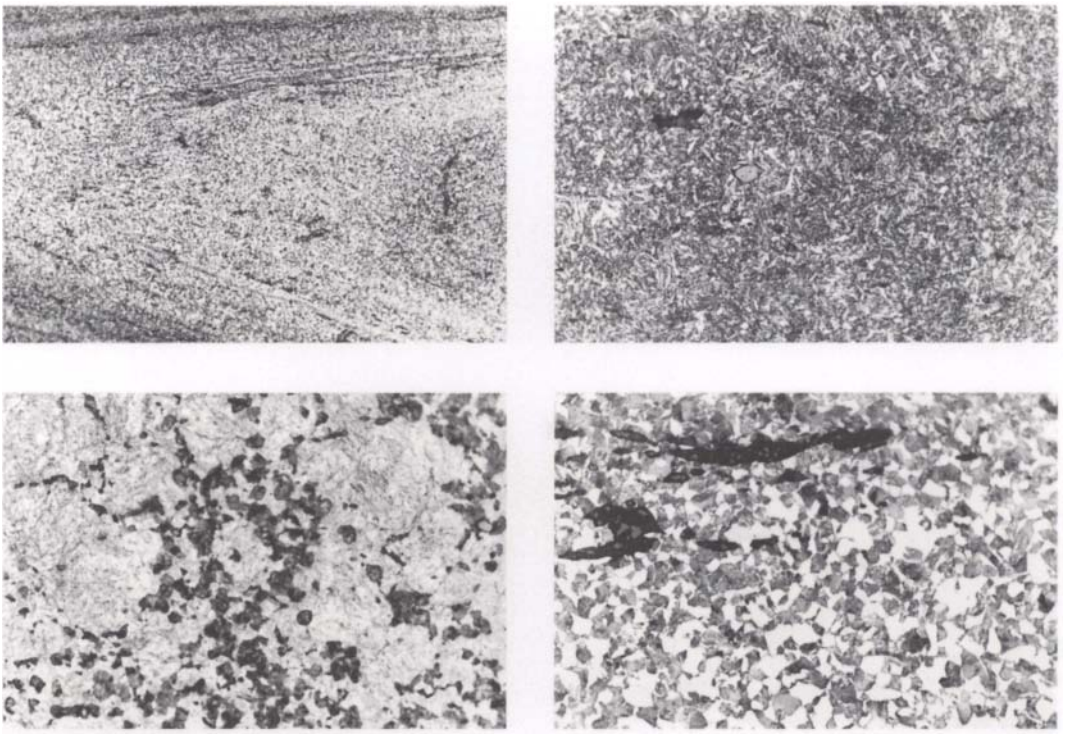

Figure 47, top right. Japanese sword blade fragment of the 18th century, close to the center of the blade, showing folds in the ferrite grain structure as a result of the forging operations used to make the blade. Etch: nital; x150.

Figure 48, top far right. Japanese sword blade fragment, close to the cutting edge, showing lath martensite which has been tempered. Note the great difference in structure between the center and cutting tip of the sword. Etch: picral; x300.

Figure 49, below right. Part of the section of a Japanese sword blade showing transition zone near to cutting edge where troosite (very fine irresolvable pearlite) nodules can be seen together with Widmanstätten pearlite. Etch: picral; x220.

Figure 50, below far right. Japanese sword blade section, further back from the cutting edge and closer to the center than Figure 48. Here the white phase is pure ferrite grains with an infill of the eutectoid pearlite (fine grey zones). Note the two-phased slag stringers in the section. Etch: picral; x220.

The type of structure seen in Figure 51, below, in low-carbon steel, could arise from heat treatment in the $\alpha + \gamma$ region of the phase diagram. At room temperature, the structure will be ferrite + pearlite, and after heating this will become:

$$\alpha + (\alpha + Fe_3C) \longrightarrow \alpha + \gamma$$

and after cooling the gamma phase will revert to:

$$\gamma \longrightarrow (\alpha + Fe_3C)$$

During cooling some of the ferrite will take a Widmanstätten structure.

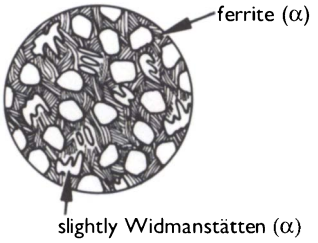

Figure 51. Partially Widmanstätten steel.

If the cooling rate is very fast then martensite can form. Even if the cooling rate is too slow for this transformation to occur the proportions of pearlite and ferrite in the solid will not be present in equilibrium amounts. The presence of more pearlite than ferrite will lead to an overestimation of the carbon content.

The structure in Figure 52 shows grain boundary cementite (Fe_3C) with a subgrain structure of cementite + pearlite. How can this type of structure arise? When cooling down an alloy from the gamma (γ) region, the alloy contains more than 0.8% carbon. Upon decomposition of the gamma phase, Fe_3C will be formed at the original austenitic grain boundaries after cooling from temperatures above 900 °C. If this alloy, typically with about 1.2% carbon content, is cooled down and then subsequently reheated to about 800 °C (in the gamma + [alpha + Fe_3C] region), then more Fe_3C will be formed on a finer scale, while the original austenitic grain boundaries will be preserved, so that on subsequent cooling, the gamma phase will decompose to

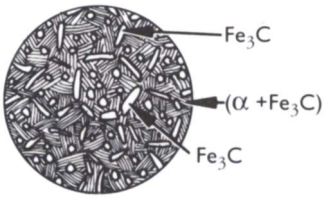

Figure 52. Grain boundary structure with subgrain features.

alpha + Fe_3C.

The section in Figure 53 shows small grain size in the cutting edge and a larger grain size in the body of a knife. There is some tempered martensite on the edge.

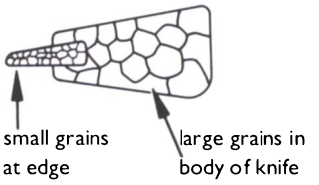

Figure 53. Grain size of knife edge.

This type of structure cannot originate from heating the tip of the blade followed by quenching. If the tip was made by heat treatment from the same metal then the grain structure would be larger. This indicates that the cutting edge must have been put in at some point during manufacture; it could not have been made in one piece.

When etching quenched structures, some areas of the martensite may etch rather darker than others. This can be due to tempering of the martensite or, if fuzzy nodular shapes appear, it could be due to the presence of troosite. Troosite patches appear because the cooling rate is not quite fast enough to produce a martensitic structure. There is often confusion between the terms troosite and sorbite. It is better to reserve the term sorbite for structures resulting from quenching followed by heat treatment (for example, martensite going to sorbite upon heating). Troosite should be used for structures resulting from the rapid cooling of a carbon steel, but not fast

enough for the production of martensite.

In the banded structure of the quenched sword blade in Figure 54, the question arises as to why, if the whole structure has been quenched, are there some areas of martensite and some that are apparently only a mixture of ferrite + pearlite. There are two possible reasons for the structural differences. First, the difference may be due to carbon content. The amount of carbon present will affect the production of martensite when the heated alloy is quenched. It is possible that the carbon content in the fine ferrite + pearlite regions is not sufficient to produce martensite. Second, the shift may be due to other alloy elements in the regions concerned, which would be apparent with further analysis.

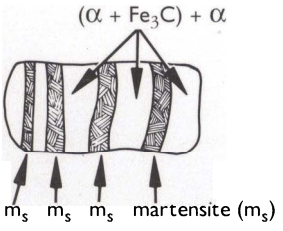

Figure 54. Banded structure of a quenched sword blade consisting of very fine pearlite and alternate bands of martensite.

Similarly, if in a homogeneous specimen the cooling rate is not sufficiently high to produce a totally martensitic structure, then it is possible to get a series of transitions between martensite, troosite, ferrite, and fine pearlite, with incipiently Widmanstätten ferrite between the pearlite regions.

In Figure 55, if the alloy is of composition A, then the structure will consist of alpha at the grain boundaries with pearlite infill, but if the alloy is of composition B, then the structure will be cementite at the grain boundaries with an infill of pearlite. Small changes in the direction of B make little difference to the visible amount of cementite at the grain boundaries, but a small movement in the direction of A makes a large difference in the amount of alpha at the grain boundaries.

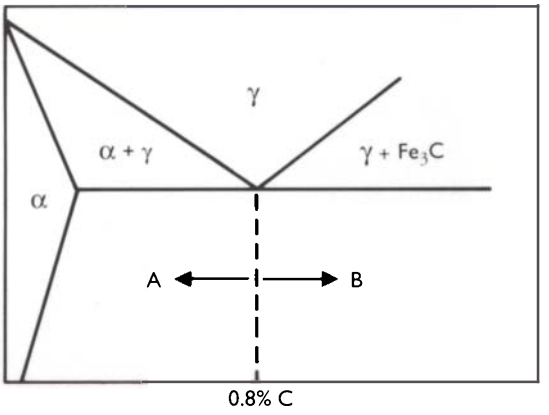

Figure 55. Part of the Fe-Fe_3C phase diagram.

Martensite is a very hard needlelike constituent of steels that forms when steels are quenched in water or other liquids at room temperature. A steel artifact is usually heated up to the austenite region of the phase diagram, about 800–950 °C, then quickly plunged into cold water, thus forming the extremely hard martensite constituent. Some of the hardness and brittleness could then be removed to various degrees by tempering, usually at temperatures between 200 and 500 °C.

Untempered martensite is difficult to etch in picral, but it can be etched in nital or sodium bisulfite. There are two essential types of martensite: lath and plate. Most steels below a carbon content of 0.6% give lath martensite. The individual laths cannot be resolved by optical microscopy even at x1000, and what can be seen is an aggregation of small lath bundles. The number of possible orientations for the growth of lath martensite within the parent austenite grain are less numerous than those in plate martensite, which becomes the dominant constituent as carbon content increases. Lath martensite has a more regular appearance in section than the plate form.

Mixtures of lath and plate martensite occur in steels up to about 1% carbon, while the plate form predominates over 1% carbon. Sometimes darker etching networks in bisulfite or nital are composed of plate martensite.

The hardness of martensite is determined by its carbon content which can vary from about 300 H_V at 0.1% carbon up to about 900 H_V at 0.6% carbon. Many ancient artifacts, however, were made under poorly controlled conditions, and the martensite may have tempered itself as the heated steel cooled down to room temperature; this is known as self-tempering. Tempered martensite reacts much more quickly to etchants than the untempered variety, and picral etchants can be used readily, as can bisulfite, although according to Samuels (1980) there is only a slight change in the response to nital.

During the quenching process it is also possible to retain some of the high-temperature austenite phase. Austenite can often be made apparent with Villela's etchant.

Although the tempering process simply involves heating the quenched artifact to temperatures that may lie between 100 and 600 °C, the processes involved are quite subtle and complex; for example, a particular form of carbide, epsilon (ε)-carbide, forms when steels containing more than 0.2% carbon are tempered between 100 and 250 °C, while if the tempering is carried out between 250 and 700 °C, cementite is formed instead of ε-carbide, in the form of small plates of spheroidal particles. It is difficult to see any fine detail of these changes using optical microscopy. Precipitation of ε-carbides can only be detected indirectly since they etch more darkly than untempered martensite. Similarly the formation of cementite at higher tempering temperatures (e.g., 500 °C) gives darker etching regions, and sometimes a mottled appearance can be seen at high magnification at x1000–x2000.

When tempering is carried out at 400 °C or higher, carbon is removed from the martensite and grains of ferrite can start to form. These can be platelike, but the morphology can barely be seen under the optical microscope.

The hardness of tempered martensite decreases as the tempering temperature rises, and the influence that carbon content has on the hardness of tempered structures decreases considerably.

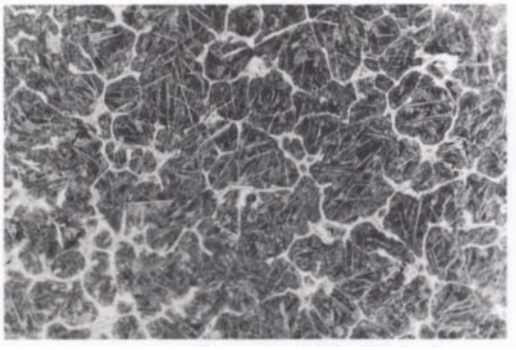

Figure 56. A good-quality steel prill from the lid of a Wootz crucible found in the Deccan area of India. The prill had become embedded in the crucible lining probably during agitation to test that a molten product had been produced. The carbon content of the prill is over 0.8%. The area shown in the photomicrograph, etched with nital at x65 shows some ferrite at prior austentic grain boundaries with cementite needles and fine pearlite as the dark phase which is not resolved at this magnification.

Figure 57. Martensite needles in the cutting edge of a medieval knife blade from Ardingley, Sussex, England. Etched in picral at x380 magnification. The needles are only just resolvable at this magnification. The overall effect is, however, typical for martensite in low-carbon steels; compare this with martensite seen in the cut-steel bead shown in Figure 59. This is lath martensite.

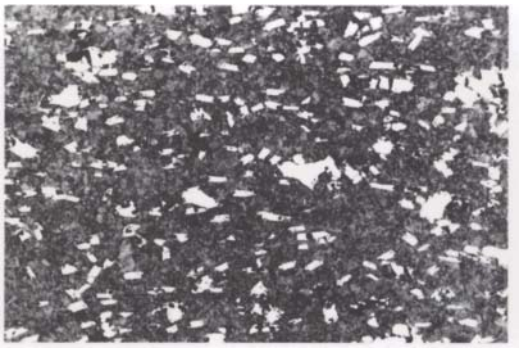

Figure 58. Photomicrograph of part of a small kris from India, showing the high carbon content of the blade. Broken fragments of cementite needles occur as white angular fragments throughout the section, oriented along the direction of working of the blade. The dark background is finely divided pearlite with practically no slag content. Etch: nital; x150

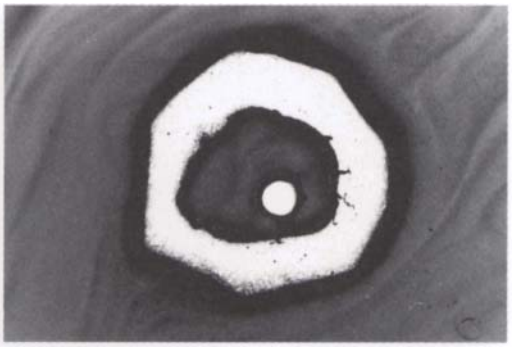

Figure 59. A cross section through an 18th century French cut-steel bead showing part of the support wire (center) and the octagonal faceted bead in section. Lightly etched; x20.

Figure 60. French cut-steel bead of the 18th century showing well developed plate martensite at a magnification of x420, etched in picral. The carbon content of the cut-steel bead is about 1.2% carbon, a very high carbon steel compared with most other European products of the time.

It is remarkable that ancient Chinese metalsmiths in the Han Wei period (206 B.C.–A.D. 534) and in the Western Han dynasty (206 B.C.–A.D. 24) were already producing spheroidal graphite cast iron. Just as remarkable are whiteheart malleable cast irons from the Province of Hubei, dating to the Warring States period of 475–221 B.C. (Hongye and Jueming 1983). Early apparatus for providing efficient blasts of air enabled the attainment of very high temperatures. The commercial production of cast iron in the West did not commence until the 13th century A.D., considerably later. But what is cast iron and what are the different microstructures associated with this material?

Cast irons have high percentages of carbon—greater than 2% but generally less than 5%—and are castable solely because they can be kept in a liquid state at temperatures as low as about 1148 °C (with a carbon content of 4–5%). Cast irons are difficult to describe fully without some analyses for additional alloying elements that are often present, besides carbon, and that can change considerably both the physical properties and the microstructure.

Present-day cast iron produced in a blast furnace is essentially pig iron and may contain silicon, sulfur, phosphorus, manganese, nickel, and chromium, in addition to carbon, and each of these elements produces changes in microstructure. The most important alloying additions or impurities as far as ancient and historical period cast irons are concerned are silicon, sulfur, and phosphorus. The special properties of cast irons may be summarized as follows:

- They may be cast into shape in molds.
- They have good fluidity and, when carbon is precipitated, they expand on cooling and thus take a good mold impression.
- Their melting point is low, on the order of 1200 °C.
- They have good wear properties since graphite is a good lubricant.
- They have a high damping capacity.
- They have a reasonable strength in compression, although they are weak in tension.
- They can be mixed with wrought iron and heated to produce a steel by lowering the carbon content.
- Grey cast irons may corrode badly and they present difficult problems for the conservator.

There are three principal groups of cast iron: grey cast iron, white cast iron, and mottled cast iron (mixed areas of white and grey).

In the grey cast irons there is free graphite in the structure—some of the carbon being rejected from solution and solidifying as flakes of graphite. In white cast irons all the carbon occurs as cementite. In the mottled, mixed group, both graphite flakes and cementite can be found in different regions of the same sample, sometimes deliberately made by chilling part of the mold and increasing the cooling rate, which favors cementite formation.

There are two important factors influencing the formation of graphite and cementite: solidification rate and composition. Since the iron-carbon phase diagram (Fig. 30), incorporating ferrite and graphite as stable products, is the nearest to equilibrium, slow cooling favors graphite production, while rapid cooling favors the metastable ferrite and cementite system.

The most important elements in cast irons are carbon and silicon, a high content of either favoring graphite formation. Other alloying or impurity elements that stabilize graphite are nickel, aluminium, copper, and titanium.

Manganese stabilizes cementite, although the situation is more complicated if sulfur is present as well. Sulfur stabilizes cementite as well, but sulfur also has a strong affinity for manganese and forms manganese sulfide particles if both elements are present. This compound, as a result, has little influence on carbon.

Primary additions, for example, of sulfur to an iron with a high manganese content, tend to stabilize graphite formation. Phosphorus acts chemically to promote carbide formation, but the presence of phosphorus produces a ternary phosphide eutectic (steadite) between ferrite (usually with some phosphorus content), cementite, and iron phosphide ($\alpha + Fe_3P + Fe_3C$). This

ternary eutectic melts at 960 °C and thus is the last constituent to solidify. This results in the $\gamma + Fe_3C$ solidifying slowly and allows any silicon present to promote graphite formation. With low amounts of phosphorus (about 0.1%), graphite can actually be enhanced rather than destabilized. Nickel, like silicon, dissolves easily in ferrite and also acts to stabilize graphite.

Because of the complexities introduced by alloying elements beside carbon, a carbon equivalent value (CE) is often quoted instead:

$$CE = total\ C\% + \frac{(Si + P)}{3}$$

This CE value may then be used to determine whether an iron is hypoeutectic or hypereutectic. In general, the lower the CE value, the greater the tendency for an iron to solidify as a white cast iron or as a mottled iron.

Irons that are hypereutectic (carbon equivalent more than 4.2–4.3%) will precipitate kish graphite[1] on solidification with normal cooling rates. Hypereutectic cast irons solidify by direct formation of graphite from the melt in the form of kish, which has a low density and can rise to the surface. When entrapped by metal it generally appears as long wavy or lumpy flakes. This phase is precipitated over a range of temperatures that will be examined with the aid of a phase diagram (Fig. 61) later in this section, starting at the liquidus surface and continuing until the remaining melt is at the eutectic point when crystallization of graphite and austenite occurs. This eutectic graphite in hypereutectic cast irons is usually finer than primary kish graphite.

As an example of the application of the CE formula, consider a white cast iron from Nang Yang City, Henan Province, China, dating from the Eastern Han dynasty (A.D. 24–220). The object is a cauldron with the following elemental analysis: C 4.19%, Si 0.14%, Mn 0.09%, S 0.06%, P 0.486% (Hongye and Jueming 1983).

$$CE = 4.19 + \frac{0.14 + 0.486}{3} = 4.39$$

This CE value places the Han cauldron in the hypereutectic region, although since the ledeburite eutectic occurs at 4.3% carbon (at a temperature of 1140 °C), the alloy is quite close to the eutectic region. Ledeburite is a eutectic comprising iron carbide and austenite.

Microstructural Constituents

The constituents, apart from graphite and transformed ledeburite, are similar to steels and in a typical grey cast iron would include graphite flakes, as well as varying amounts of ferrite and pearlite. The ferrite may be harder than in ordinary steels because of the silicon content. The usual white cast iron constituents are pearlite and cementite. The grey cast irons may have the following constituents:

1. Flake graphite, formed during solidification, can determine the properties of the iron by its shape, size, quantity, and distribution. Graphite flakes are usually found in the following forms: randomly distributed, dendritic, or rosette.
2. Pearlite, which may vary in composition between 0.5 and 0.8% because of alloy content.
3. Steadite, the ternary phosphide eutectic previously discussed.
4. Free ferrite, which appears in appreciable amounts only in low-strength cast irons. The ferrite is usually rounded in appearance compared with steadite or cementite because it precipitates from the austenite solid solution rather than from a liquid. It is often found in association with graphite flakes. Free cementite is unusual in grey cast irons.

Preparation of grey cast irons by metallographic polishing can give rise to problems because the graphite flakes may be smeared or removed preferentially upon polishing. Very corroded grey cast irons can also be very difficult to retain in a plastic mount because they may consist of little more than a loose mass of iron oxides in a graphite matrix. These have a tendency to lose part of the friable surface upon polishing with the consequent difficulty of obtaining a good polish.

Less corroded specimens polished with diamond abrasives usually do not present major difficulties.

A good test to determine if graphite is polished correctly is to examine the sample in reflected polarized light. Graphite is anisotropic[2] and exhibits reflection pleochroism.[3] When examined under ordinary bright field illumination with unpolarized light, graphite flakes appear to have a uniform brownish-grey color. If the same sample is then examined under plane polarized light, some graphite flakes appear light, some dark, and some have an intermediate color. If the sample is rotated 90°, the flakes formerly dark become light. The relationship between the plane of polarization of the incident light and the position of maximum or minimum brightness is such that when the plane of polarization is at right angles to the graphite flakes they appear dark, and when parallel they appear light (Nelson 1985). If the same sample is examined under polarized light between crossed polars, upon rotation through 360°, each graphite flake will lighten four times; this is expected from the hexagonal anistropy of graphite.

Picral is probably the best etchant for predominantly pearlitic grey, malleable, and ductile irons. Picral does not damage graphite which nital can, but for ferritic grey cast irons nital is preferable.

If the iron is sufficiently below the eutectic value, has a very low silicon content, and contains appreciable carbide stabilizers, or if the cooling rate is fast, then instead of graphite flakes solidification occurs by formation of austenite dendrites. Meanwhile the interdendritic regions solidify as ledeburite, a eutectic mixture of iron carbide and austenite. In appearance, ledeburite etched in nital would consist of light etching cementite in a background of unresolved and transformed austenite, which usually appears as dark etching pearlite.

As cast iron cools, the austenite transforms to ferrite and cementite. The structure of a white cast iron at room temperature therefore usually consists of primary dendrites of pearlite with interdendritic transformed ledeburite.

Heat Treatment of Cast Iron

Castings produced in white cast iron can be made malleable to some extent by a number of techniques. Two such methods are known as whiteheart and blackheart. These names refer to the respective fractures of the different irons after annealing, the whiteheart variety being white and crystalline due to the presence of pearlite and the blackheart being grey or black due to graphite. In whiteheart structures, annealing oxidizes some of the carbon producing a ferrite structure that gradually changes to a steel-like mass of ferrite and pearlite with interspersed nodules of graphite. In blackheart structures, the heat treatment does not result in much carbon oxidation and, depending on other alloying constituents such as silicon and sulfur, the cementite may break down to graphite aggregate nodules in a matrix of ferrite and pearlite.

Temper Carbon Nodules

When cast iron is in the white condition, annealing at temperatures in the range of 800–950 °C may produce graphite nucleation. At this temperature, white cast iron usually consists of a eutectic matrix of cementite, austenite and, if many impurities are present, inclusions. Nucleation of graphite then occurs at the austenite/cementite interfaces and at inclusions. Cementite gradually dissolves in the austenite and the carbon diffuses to the graphite nuclei to produce nodules. This kind of process of heat treatment appears to be responsible for the spheroidal graphite cast irons made in ancient China. Ancient Chinese smiths could cast a white cast iron and then, by high temperature heat treatment, produce spheroidal graphite. The graphite is slightly polygonal in shape, but in all other respects is the same as the spheroidal graphite cast iron produced today by alloying a variety of elements such as cerium or magnesium with cast iron. These alloying elements do not occur in ancient Chinese examples. Analysis by SEM indicates that spheroidal graphite nuclei are latent in white cast irons having carbon, low silicon, and the required ratio of manganese to sulfur.

In the microstructure of a typical cast iron, which cools down quickly, the nonequilibrium phase Fe_3C tends to predominate: the equilibrium constituent is free graphite. Line AB has been drawn on the iron-iron carbide diagram that represents the cooling of a typical cast iron (Fig. 61). At temperature t_1, the liquid material starts to solidify and austenite grains, or rather dendrites, start to form, surrounded by liquid. As the temperature falls, this liquid cools and reaches the stage at which a simple eutectic decomposition occurs. This eutectic is called ledeburite and consists of austenite + Fe_3C.

At t_1 $L_1 \longrightarrow \gamma + L_2$ *(dendrites of* γ *in liquid)*

At t_2 $\gamma + L_2 \longrightarrow \gamma + (\gamma + Fe_3C)$

As the temperature falls between t_2 and t_3 on the graph, so the carbon content of the austenite decreases and more Fe_3C is precipitated from both of the constituents present at t_2.

At t_2-t_3 $\gamma + (\gamma + Fe_3C) \longrightarrow$

$\gamma\ (+Fe_3C) + [(\gamma + Fe_3C) + Fe_3C]$

Finally, as cooling proceeds past t_3 itself, all of the austenite tends to decompose to pearlite. This means that the final change can be represented as:

At t_3 $\gamma\ (+ Fe_3C) + [(\gamma + Fe_3C) + Fe_3C] \longrightarrow$

$(\gamma + Fe_3C) + Fe_3C + (\alpha + Fe_3C) + Fe_3C + Fe_3C$

This series of reactions leads to the formation of typical white cast iron. There is a different series of phase changes that may occur if slow cooling is carried out or if there are alloying additions, such as silicon, made to stabilize the formation of graphite. The series of changes that take place at t_1, t_2, and t_3 are the same, except where Fe_3C occurs in the phase relationships, it is replaced

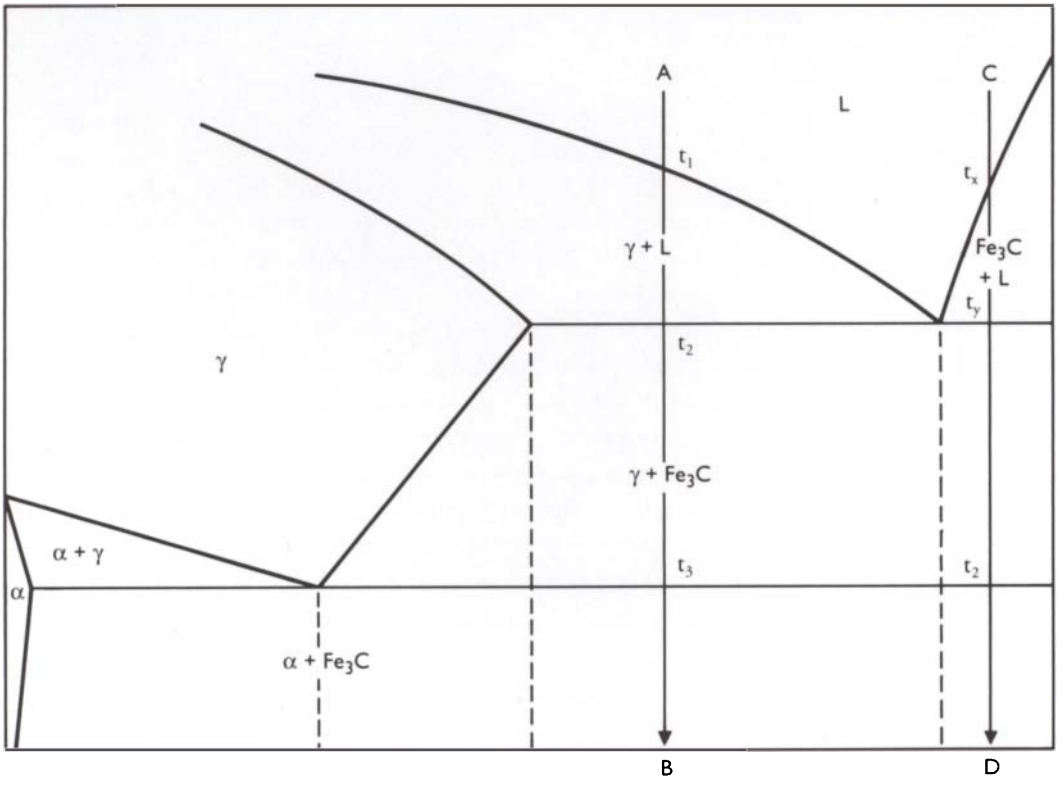

Figure 61. Part of Fe-Fe_3C phase diagram for cast iron.

with graphite (G):

$$\text{At } t_1 \quad L_1 \longrightarrow \gamma + L_2$$

$$\text{At } t_2 \quad \gamma + L_2 \longrightarrow \gamma + (\gamma + G)$$

$$t_2\text{-}t_3 \quad \gamma + (\gamma + G) \longrightarrow \gamma + G + [(\gamma + G) + G]$$

$$\text{At } t_3 \quad \gamma + G + [(\gamma + G) + G] \longrightarrow \gamma + G + G + \gamma + G + G + G$$

In practice, the last stage never fully takes place. More typically the first phase change is from austenite to austenite + graphite, but the austenite is much more likely to precipitate Fe_3C. The phases at t_3 then become:

$$\text{At } t_3 \quad \gamma + G + [(\gamma + G) + G] \longrightarrow (\alpha + Fe_3C) + G + (\alpha + Fe_3C) + G + G$$

This should lead to dendrites of pearlite in a matrix of ferrite and graphite which is most likely in grey cast iron.

Above a carbon content of 4% the primary reaction would be decomposition of the liquid to form Fe_3C and ledeburite (austenite + Fe_3C). The phase changes upon fast cooling of an alloy shown in Figure 61 would then be represented by:

$$\text{At } t_x \quad L_1 \longrightarrow Fe_3C + L_2$$

$$\text{At } t_y \quad Fe_3C + L_2 \longrightarrow Fe_3C + (\gamma + Fe_3C)$$

$$\text{At } t_y\text{-}t_z \quad Fe_3C + (\gamma + Fe_3C) \longrightarrow Fe_3C\,(+\gamma) + [(\gamma + Fe_3C) + Fe_3C]$$

White cast irons with a total carbon content of over 4% tend to be extremely hard with no elongation at all and are not normally used in the fast cooled state. With slow cooling, very large graphite flakes can form, and it is possible to get quite a large difference in the size of these flakes depending on where they form in relation to the phase diagram. Graphite formed with a carbon content of 3% can be quite small, whereas with a carbon content of 5% the flakes can be enormous (Fig. 62).

Although cast iron metallurgy was well developed in China, isolated examples of cast iron do occur in other Old World contexts, for example, the 1st century A.D. find from the classic excavations of Bushe-Fox at Hengistbury Head and also from the Roman period cast iron from Wilders-

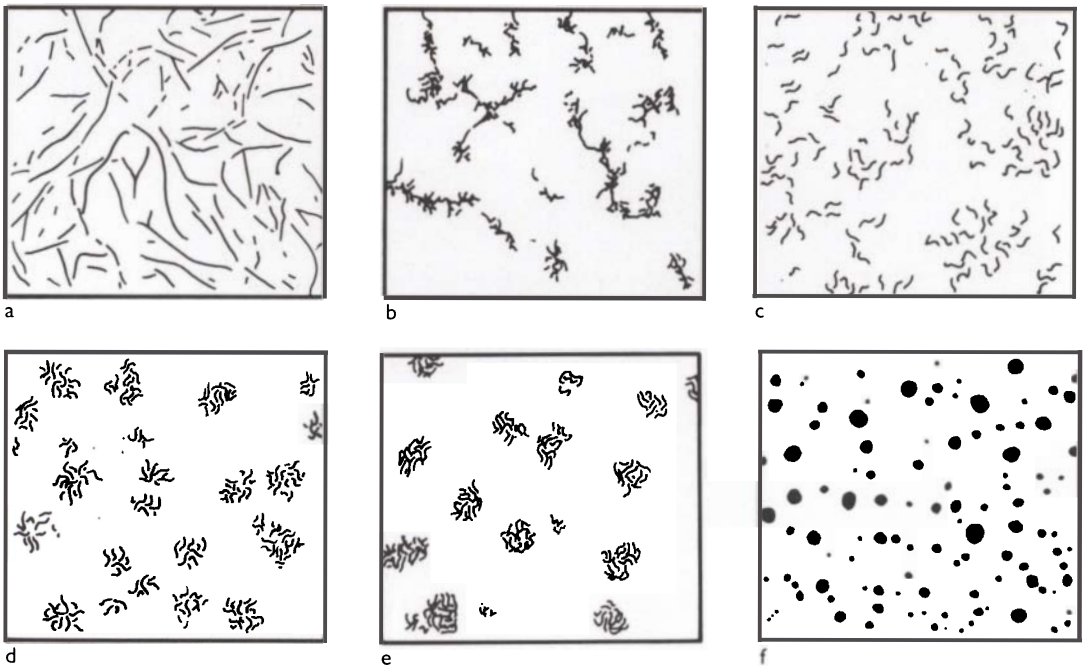

Figure 62. Flake graphite in cast iron. From ISO Standard R 945-1969(E). x100.
a. Flake graphite
b. Crab-type graphite
c. Quasi flake graphite
d. Aggregate or temper carbon
e. Irregular or open-type nodules
f. Nodular or spheroidal graphite

Figure 63. Cast iron scales from the 18th century. Typical example from England, showing the graphite flakes surrounded by white borders (ferrite). The grey infill is pearlite, which has variable spacing, while the white spotty phase is the ternary eutectic, steadite. Etched in nital; x90.

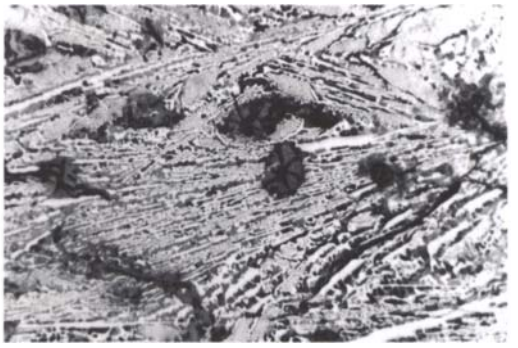

Figure 64. Heavily corroded fragment of a cast iron cannonball from the Tower of London, 18th century. Note severe corrosion of the ferrite regions around the course graphite flakes and corrosion of pearlite regions throughout the structure. The two phases that have survived best are the steadite eutectic (the fine spotty material) and the cementite laths (the long white crystals). Unetched; x40.

pool, Lancashire. Both of these pieces were of grey cast iron. The Hengistbury example had an analysis of: C 3.4%, Mn tr, Si 0.38%, P 0.18%, S 0.035%, while the specimen from Wilderspool gave: C 3.23%, Mn 0.403%, Si 1.05%, P 0.76%, S 0.49%.

Many of the Chinese examples have lower silicon content than these, ranging from 0.08% to 0.28% in the examples published by Hongye and Jueming in 1983. The Chinese examples span a considerable range of different material as can be seen from the following:

- An axe from the Warring States period (475–221 B.C.) excavated from the site of Tonglushan, Huangshie City, Hubei Province, was found to be an example of a whiteheart malleable cast iron with imperfect decarburization and a total carbon content that varies from 0.7 to 2.5%. The analysis for this axe gave: C 0.7–2.5%, Si 0.13%, Mn 0.05%, S 0.016%, P 0.108%.
- An example of a mottled cast iron is provided by a hammer from the same site with the following analysis: C 4.05%; Si 0.19%; Mn 0.05%; S 0.019%; P 0.152%.
- A white cast iron was found at Cheng Zhou City, Henan Province. This block dates to the Eastern Han dynasty (A.D. 24–220) and gave the following analysis: C 3.97%, Si 0.28%, Mn 0.30%, S 0.078%, P 0.264%.
- An example of cast iron with spheroidal graphite was found in the iron workshop at Trieshenggou dating to the Western Han dynasty (206 B.C.–A.D. 24). This site is located in Gong County, Henan Province, and gave the following analysis: C 1.98, Si 0.16, Mn 0.04, S 0.048, P 0.297.

Notes

1. Kish graphite is the graphite that separates from molten cast iron as soon as it cools to the solid. It may sometimes float on top of the molten alloy.
2. Anisotropic substances do not have the same physical properties in all directions of the material.
3. Reflection pleochroism results from different interactions in anisotropic solids when viewed under polarized light. Generally, pleochroic substances will show some color variation on rotation when viewed under polarized light.

9 Corroded Microstructures

Many ancient objects are, of course, covered with corrosion products that may have originated at the time of manufacture (if the object had been deliberately patinated, for example), or they may have arisen from corrosion during burial or in the atmosphere. Many books on the subject of corrosion do not discuss the types of structures that occur in ancient metals. Often they are subjected to several different corrosion processes, resulting in a nearly composite material consisting of metallic remnants and mineral alteration products. Normally corrosion produces a buildup of insoluble products, both within and overlying the original metal volume. Corrosion products may be very informative; indeed, they may be all that is left of the original object. Therefore, corrosion products should not be cleaned from the surface of antiquities before metallographic examination. Loose material, soil, and soil and mineral concretions usually should be removed because continual loss of them during polishing could create a very badly scratched surface unsuitable for microscopic examination. It is generally possible to polish corroded samples in much the same way as more robust specimens, although if the material is very friable, vacuum impregnation with a low-viscosity epoxy resin should be considered before mounting, or the whole sample could be mounted in resin under vacuum.

It is most important to examine all features of corrosion products before etching the specimen, since many corrosion products are severely attacked by the chemicals used to etch metal surfaces: they could be dissolved completely. Under normal bright-field reflected light microscopy most corrosion crusts have a grey color. Examination under reflected polarized light yields a great deal of valuable information. The polarizer in reflected light microscopes is usually housed in the chamber of the light source and can be rotated, while the analyzer is placed in a special holder in front of the eyepiece turret. By adjusting one or both of the polarizing elements, the "true" colors of corrosion products can often be revealed. Not only does this aid considerably in the interpretation of many microstructures but also many crystalline and other morphological details are revealed clearly.

It should be remembered that the interface of interest may not just be between the metal and the primary (or currently existing) corrosion products. Important information may also be preserved in some other interfacial event between layers of corrosion products of different composition or structure.

Corrosion products may pseudomorphically replace the metallic structure that previously existed. That is to say, the structural orientation (for example, dendritic structure) of the metal is preserved in the corrosion products that have replaced it. One of the ways in which this can happen is by epitaxial growth. This means, in general terms, the regular orientation of a particular growth on a crystalline substrate. Most ancient chemical corrosion processes (which are best modeled by electrochemical reactions), if they produce structural information preserved in the corrosion products, do so by chemoepitaxy. This is a subdivision of the epitaxy structure. Chemoepitaxy can be defined as a process leading to the growth of crystalline, regularly oriented reaction layers on a material resulting from a chemical reaction between this initial substance and any other substance. Examples of layers formed from such a process are cuprite (Cu_2O) growing on the surface or into the metal grains themselves, and Ag_2O, the initial thin film that can form on silver objects.

Valuable information can sometimes be retrieved from corroded metallic fragments; parts of the structure may remain uncorroded, or there may be pseudomorphic replacement of the phases by corrosion products. Appendix B illustrates some of the types of corrosion found in ancient specimens. Evidence of the authenticity of an artifact can be obtained from metallographic examination of small chips of corroded metal. In copper alloys, the presence of intergranular corrosion, intragranular corrosion, corroded slip lines, twin lines, or cuprite next to the metal would be very significant. It is extremely difficult to produce coherent cuprite layers by artificial corrosion

over short periods of time, and it is also practically impossible to fake the penetration of cuprite along selective planes in the crystal, such as twin bands or slip lines. If the corrosion process has not completely disrupted the original volume of the metal but has preserved some interface between internal and external corrosion, then this discontinuity may be recognized as preserving information relating to the original surface of the artifact.

When corroded samples are mounted for polishing, the difficulty of preparing scratch-free surfaces is evident. Abrasive particles frequently can become embedded in the corrosion products. During polishing some of these particles may be released, producing scratches on the metal. Prolonged polishing with intermittent etching to remove smeared material, or ultrasonic cleaning in baths of acetone or alcohol, may produce a better finish. One danger is that small specimens will become rounded at the edges and part of the corrosion crust or the edges of the metallic constituents may then be out of focus microscopically compared with the remaining polished surface. The polishing hardness of corrosion products and the metal from which they have formed is usually quite different. Surface relief effects are therefore common when examining corroded samples. It has been found that a much sharper preservation of detail in corrosion products is achieved by using diamond polishing compounds rather than alumina compounds (Figs. 65–68).

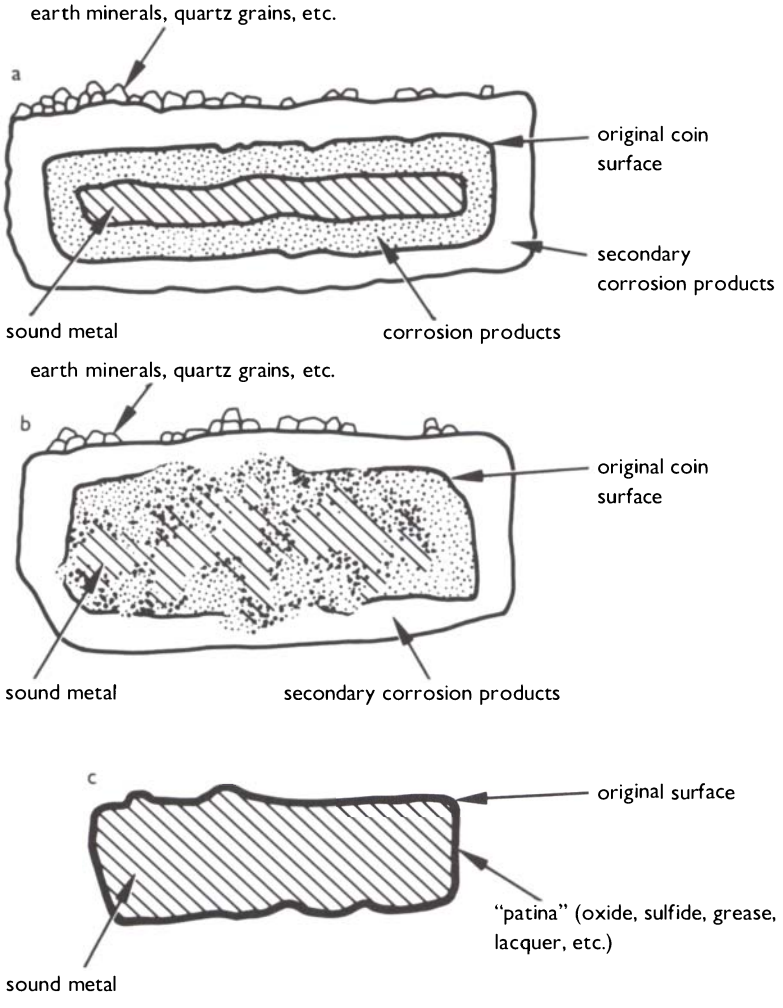

Figure 65. Typical variations in the preservation of surface detail as a result of corrosion. a. Preservation of shape in corrosion. b. Disruption of surface by corrosion. c. Sound metal with patina.

9 Corroded Microstructures

Many ancient objects are, of course, covered with corrosion products that may have originated at the time of manufacture (if the object had been deliberately patinated, for example), or they may have arisen from corrosion during burial or in the atmosphere. Many books on the subject of corrosion do not discuss the types of structures that occur in ancient metals. Often they are subjected to several different corrosion processes, resulting in a nearly composite material consisting of metallic remnants and mineral alteration products. Normally corrosion produces a buildup of insoluble products, both within and overlying the original metal volume. Corrosion products may be very informative; indeed, they may be all that is left of the original object. Therefore, corrosion products should not be cleaned from the surface of antiquities before metallographic examination. Loose material, soil, and soil and mineral concretions usually should be removed because continual loss of them during polishing could create a very badly scratched surface unsuitable for microscopic examination. It is generally possible to polish corroded samples in much the same way as more robust specimens, although if the material is very friable, vacuum impregnation with a low-viscosity epoxy resin should be considered before mounting, or the whole sample could be mounted in resin under vacuum.

It is most important to examine all features of corrosion products before etching the specimen, since many corrosion products are severely attacked by the chemicals used to etch metal surfaces: they could be dissolved completely. Under normal bright-field reflected light microscopy most corrosion crusts have a grey color. Examination under reflected polarized light yields a great deal of valuable information. The polarizer in reflected light microscopes is usually housed in the chamber of the light source and can be rotated, while the analyzer is placed in a special holder in front of the eyepiece turret. By adjusting one or both of the polarizing elements, the "true" colors of corrosion products can often be revealed. Not only does this aid considerably in the interpretation of many microstructures but also many crystalline and other morphological details are revealed clearly.

It should be remembered that the interface of interest may not just be between the metal and the primary (or currently existing) corrosion products. Important information may also be preserved in some other interfacial event between layers of corrosion products of different composition or structure.

Corrosion products may pseudomorphically replace the metallic structure that previously existed. That is to say, the structural orientation (for example, dendritic structure) of the metal is preserved in the corrosion products that have replaced it. One of the ways in which this can happen is by epitaxial growth. This means, in general terms, the regular orientation of a particular growth on a crystalline substrate. Most ancient chemical corrosion processes (which are best modeled by electrochemical reactions), if they produce structural information preserved in the corrosion products, do so by chemoepitaxy. This is a subdivision of the epitaxy structure. Chemoepitaxy can be defined as a process leading to the growth of crystalline, regularly oriented reaction layers on a material resulting from a chemical reaction between this initial substance and any other substance. Examples of layers formed from such a process are cuprite (Cu_2O) growing on the surface or into the metal grains themselves, and Ag_2O, the initial thin film that can form on silver objects.

Valuable information can sometimes be retrieved from corroded metallic fragments; parts of the structure may remain uncorroded, or there may be pseudomorphic replacement of the phases by corrosion products. Appendix B illustrates some of the types of corrosion found in ancient specimens. Evidence of the authenticity of an artifact can be obtained from metallographic examination of small chips of corroded metal. In copper alloys, the presence of intergranular corrosion, intragranular corrosion, corroded slip lines, twin lines, or cuprite next to the metal would be very significant. It is extremely difficult to produce coherent cuprite layers by artificial corrosion

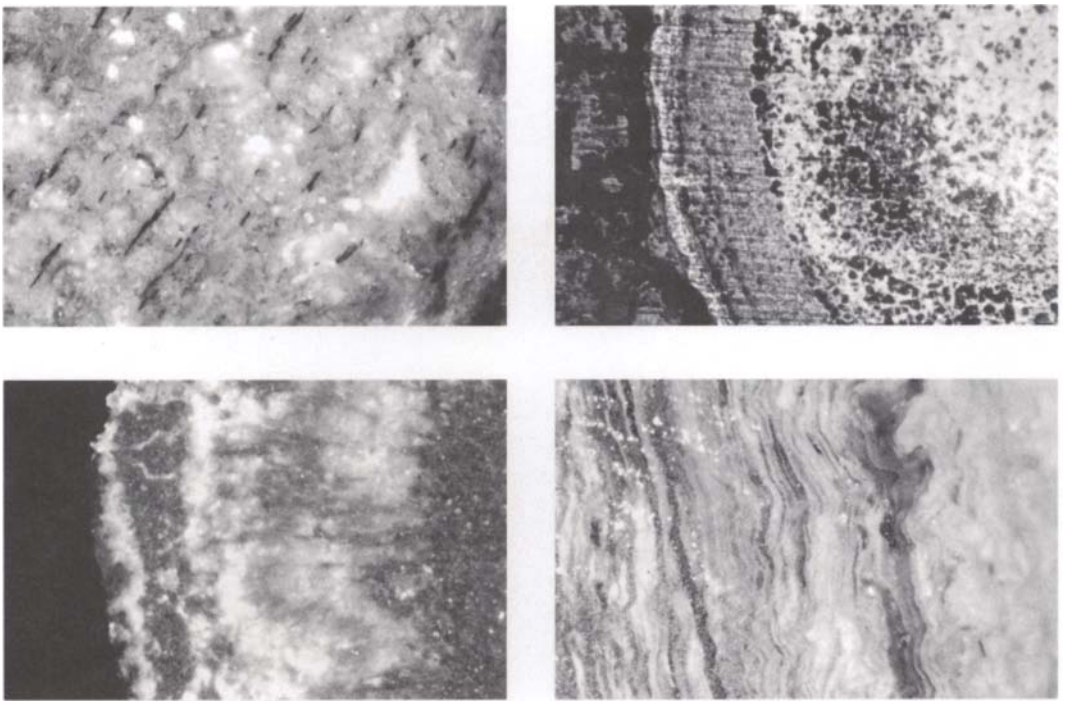

Figure 66a, top right. Completely corroded bronze pin from Palestine. The dark elongated phase are original copper sulfide inclusions from the worked and annealed pin, preserving their original location in the corrosion products. From their preservation it is possible to deduce that the object was not cast, but worked, even though no metal remains. x125.

Figure 66b, top far right. Part of a corroded bronze rod from Iran. The original surface of the rod is preserved in corrosion products only, but the circular cross section is clear. x50.

Figure 66c, middle right. Completely mineralized silver disk; radiating crystals of silver chloride and patches of silver sulfide (dark) preserve the shape of the object with some distortion. x65.

Figure 66d, middle far right. Multiple corrosion layers similar to Liesegang rings in a bronze fragment from Iran. The periodic precipitation of cuprite and malachite result in this finely banded corrosion structure in which surface outline is not preserved in corrosion. x100.

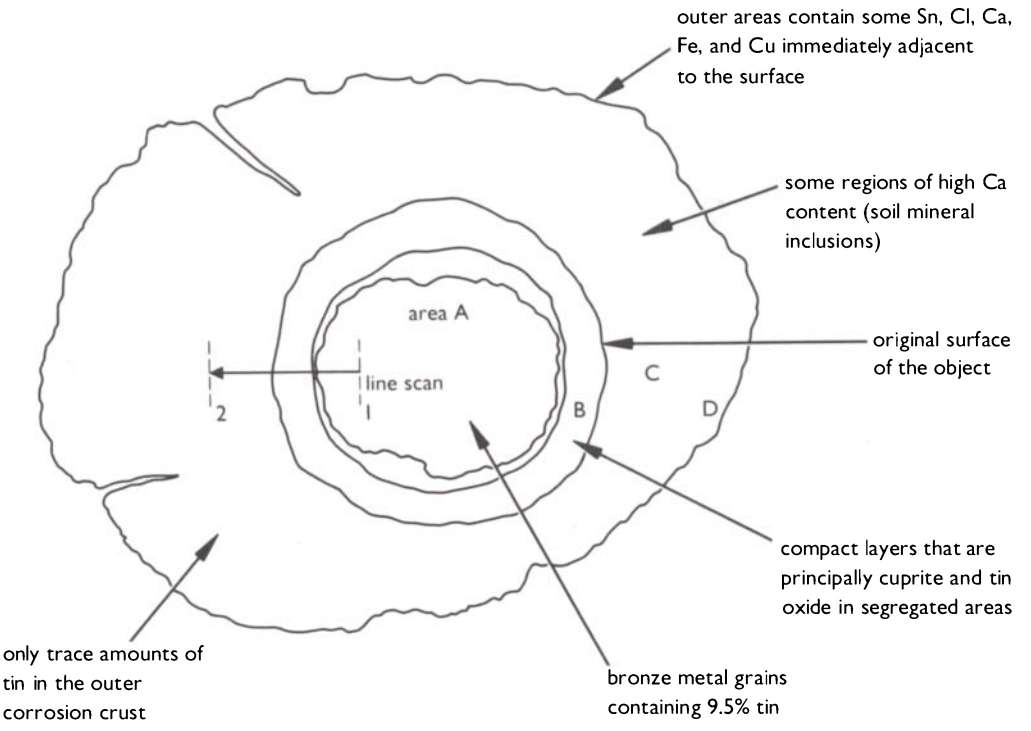

Figure 67. Drawing of the cross section of a bronze rod fragment. The location of the electron microprobe line scan is illustrated. A, B, C, and D indicate areas of analysis. The line scan was started approximately at position 1 and was terminated at position 2.

Figure 68a–d. Examples of corrosion of gold-copper alloys.

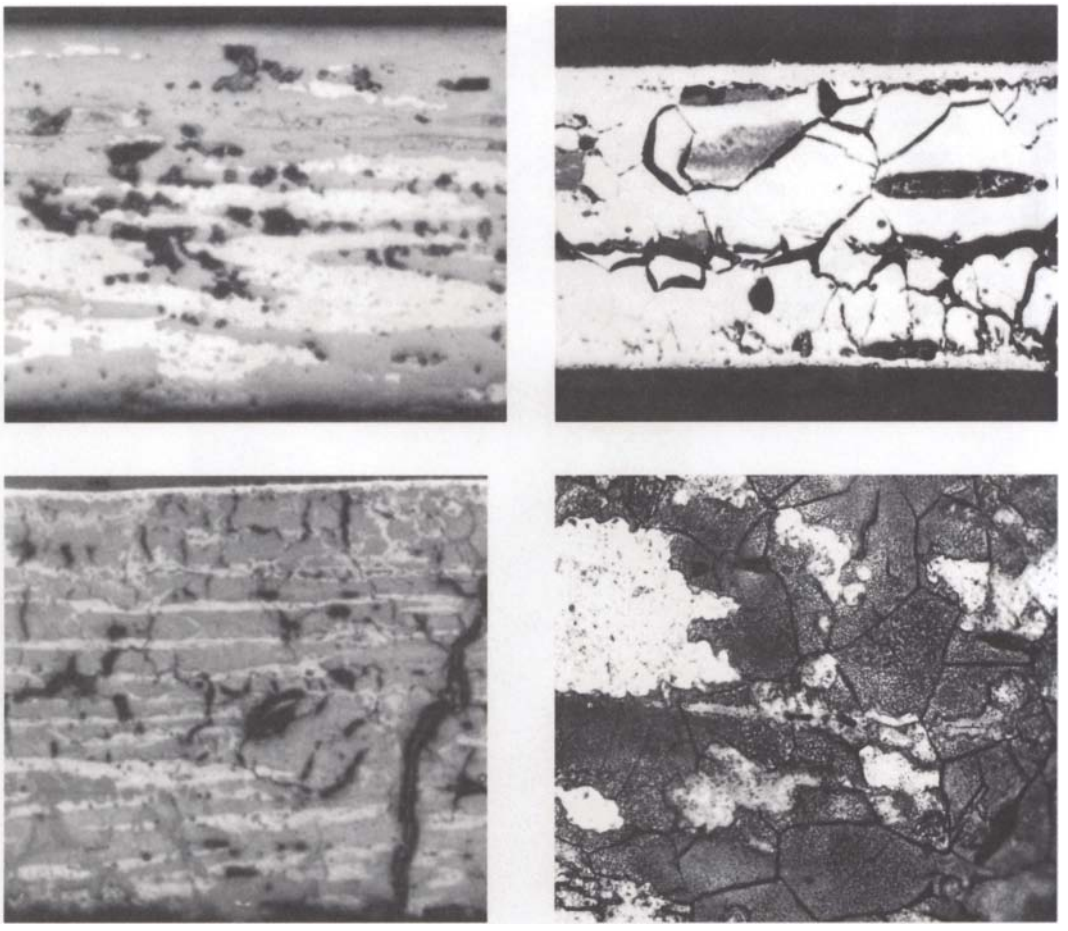

Top left, a. Sheet gold-copper alloy from the Sierra Nevada de Santa Marta, Colombia. A fragment of a large Tairona sheet with depletion-gilded surfaces. The composition is 15.2% gold, 65.4% copper, and 0.6% silver. The structure consists largely of dark grey corrosion products, mostly cuprite with gold and porosity (seen as black holes) as a result of corrosion. The sound metal is white. Unetched; x160.

Top right, b. Fragment of a Tairona ear ornament: 39.6% gold, 34.8% copper, and 2.5% silver. In the unetched condition at a magnification of x160, extensive cracking can be seen. Cracking results from volume changes upon corrosion. Some cracks run just under the surface of the alloy. Depletion-gilding has created a gold-enriched layer more resistant to embrittlement than the underlying layer.

Bottom left, c. Cross section of a corroded gold-copper alloy sheet from the Tairona area of Colombia. The composition of the sheet is 59.6% gold, 19.4% copper, and 7.1% silver, the low total reflecting internal corrosion and extensive conversion to cuprite. The polished section shows the corroded alloy with a number of fine lamellae of sound metal remnants that appear bright. The sheet has been depletion-gilded and the consistent gold-rich surface can be seen clearly on the top of the section. Unetched; x160.

Bottom right, d. Enlarged view of Figure 68c, x300. Etched in alcoholic ferric chloride, revealing a fine network of cracks running through the alloy. Some cracks in the principally cuprite matrix are related to the original microstructure, since a twin can be seen in one grain area and some of the cracks appear to be following grain boundaries. Sometimes the cracking appears to be unrelated to the grain structure, but here there is some pseudomorphic retention.

Figure 69, top. Luristan ceremonial axe showing interdendritic porosity (dark) with well-developed dendrites. Etch: $FeCl_3$; x30.

Figure 70, middle (see Fig. 69). Redeposited copper resulting from in-depth corrosion. Etch: $FeCl_3$; x150.

Figure 71, bottom. Section of a corroded fragment from an Ecuadorian gilded copper ceremonial axe, from Pindilig, Canton Azogues, Ecuador. A gold surface can just be seen as a thin bright line at the top of the section. This axe was gilded by the electrochemical replacement plating technique described by Lechtman (1982). The photomicrograph illustrates the extraordinary precipitation of copper as a result of the corrosion of the axe. The redeposited copper outlines areas of remaining uncorroded alloy, which is nearly pure copper. x120.

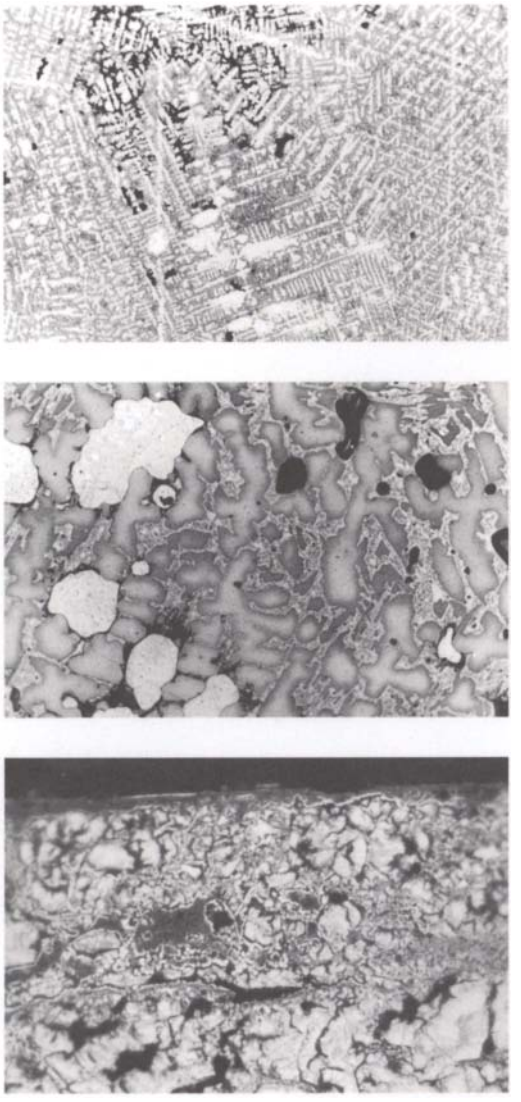

The samples illustrated in Figures 69–70 (see also Plate 10 and Figs. 112, 113), taken from the broken end of a hilt of a Luristan ceremonial blade show a well-developed dendritic structure consisting of an α dendritic system with the usual $\alpha + \delta$ eutectoid infill, showing that the hilt is in the as-cast condition. There is some porosity present in the section resulting from interdendritic holes, which could be due either to rapid solidification in the mold or to gas evolution in the casting. The hilt section has distinct copper globules, which originate from corrosion effects within the bronze structure and occur most probably in the former eutectoid spaces that are attacked selectively in this particular bronze in a burial environment. The dissolution of the eutectoid sometimes leads to precipitation of copper (as here), somewhat akin to the process of dezincification in brass. The copper globules often display twinned grain structures, barely visible here at x150.

Polarized illumination for the examination of ancient metallic samples has many applications. In bright-field unpolarized illumination, many nonmetallic inclusions, corrosion products, burial concretions, soil minerals, core materials, etc., appear as various shades of grey. By using polarized illumination and rotating the polarizer and analyzer until most or all normally incident light is excluded, fine color differentiation becomes possible between many of the mineral phases associated with ancient metals.

Some of the metals themselves also give rise to colored effects under polarized illumination if they are optically anisotropic, i.e., if they have two or three principal refractive indices. Some examples of anisotropic metals are antimony, tin, and zinc. In addition, some alloys may also produce anisotropic effects such as prior austenitic grain boundaries in martensitic steels, beta-grain structures in high-tin bronzes, different reflectivities in duplex alloys, and strain or slip markings within grains. Most of the common metals of antiquity, such as iron, copper, silver, gold, lead, and nickel are optically isotropic since they crystallized in the cubic system and are either body-centered cubic (in the case of alpha-iron) or face-centered cubic (as in copper, silver, gold, nickel, and lead). Nevertheless, even optically isotropic metals have grain boundaries, and optical effects with, for example, cast metals, do occur, although they rarely provide new information.

With completely clean and uncorroded samples there may be little advantage in the use of polarized light microscopy. However, this is rare among ancient metals which typically have both nonmetallic inclusions and corrosion products present, and often valuable information can be gained by examining them in polarized light. Voids that appear dark in unpolarized illumination suggest, for example, that they may be filled with quartz or calcite, although the chemical identity of the material examined is not easy to establish. In fact, there is no straightforward guide to the identity of any material of this kind. The best means of identification is by X-ray diffraction, electron-microprobe analysis, scanning-electron microscopy, or transmission-electron microscopy. The principal advantages gained by using polarized illumination are the visual manifestation of the morphology and the distribution of corrosion products by color and crystal size. There are some color effects that can be seen if the stage or specimen is rotated. Color change is due to pleochroism—as the vibrational direction of the polarized light is altered by rotation, so the resulting color of the observed anisotropic material will also change.

Grain boundaries in metals, twin lines, and slip planes may react differently even in isotropic materials such as copper or low-tin bronze. Dendritic structures that have preferred orientations of growth may also show chiaroscuro effects in polished section.

Care must be taken to avoid inference from the absence of an expected reaction to polarized illumination: the concomitant absence of the substance sought. For example, cuprite, which is usually a liver-red color in mineral form under macroscopic conditions, is expected to appear scarlet-red under the microscope using polished sections with polarized illumination. Often this is how it looks; however, some small cuprite inclusions give no bright coloration because the orientation of the crystal is not producing anisotropic effects in that particular position. Although it is not customary to use rotating stages with metallurgical microscopes unless the stage is an inverted one, it may be useful to change the stage if much polarized light work is to be carried out.

Massive corrosion, such as that preserving the surface detail on a copper alloy artifact, will usually produce a wide range of colors. The color observed with copper corrosion products is very similar to the color usually associated with the mineral concerned, as evidenced by cuprite. The same limitations that apply to visual identification apply to this type of microscopic examination. It would not be possible, for example, to know that a green mineral seen under polarized light was malachite. It is also not possible to say, with a mineral such as cuprite, that the material is solely composed of cuprite because a scarlet-red

color is visible under polarized light: there may be compositional variations or other minerals present in addition, such as stannic oxide, which alter the shade of the color. Thus the analyst cannot detect the presence of minerals by this means alone, although polarized light microscopy used in conjunction with electron-microprobe analysis can give very useful information (Scott 1986). Slags and other materials, such as matte, speiss, cements, and plasters, can also be examined effectively by reflected polarized light. Ancient plaster and cements are usually fine grained or contain fine-grained aggregates which makes examination difficult in thin section (usually 30 microns thick). More information can be gained about the crystalline and glassy phases in many slags under polarized light, although mineral identification is not usually possible.[1] An idea of the possible range of color can be shown by looking at slag composed of copper sulfides (matte) in globular form, surrounded by magnetite and fayalite crystals in a dark glassy matrix. In unpolarized light, the copper sulfides appear grey, the fayalite laths will be a different shade of grey, the magnetite is white, and the glassy matrix is dark grey. Under polarized illumination, the copper sulfides are light blue, the magnetite is black, the fayalite is grey, and the matrix can have various effects, but can appear translucent and glassy. Crystal size in cements and plasters can be revealed by polarized light examination, as can color variation, and layered mineral assemblages, as are commonly found in wall paintings, painted tesserae, or polychromed materials.[2]

Notes

1. For more information on the structure of slags and other metal by-products see Bachmann (1982) where many slag structures are illustrated, both in color and black-and-white.

2. For further information on polarized light microscopy (although little information has been published on ancient metals), refer to the works mentioned in the bibliography by McCrone et al. (1974) and Winchell (1964).

A useful quantitative aspect of metallography is the measurement of the grain size of the material or the dendritic arm spacing. Dendrite arm spacing is best obtained by measuring the number of arm intersections across a line traverse, the distance being measured by means of a stage micrometer or graticle, or on a photomicrograph of the area concerned. Large, coarse dendrites generally mean that the cooling rate of the alloy in the mold was fairly slow, usually implying that heated or well-insulated molds were employed. Finer dendrite arm spacings suggest faster cooling rates.

Grain size can be measured by a number of different methods. One of the simplest techniques is to use a grain size comparator eyepiece. This eyepiece has inscribed around its circumference ASTM (American Society for Testing and Materials) grain size scales. By direct visual comparison at an objective lens magnification of x10, giving a magnification of x100 overall (the magnification of microscopes is obtained by multiplying the objective lens by the eyepiece lens magnification), the ASTM number can be determined. Great accuracy in this type of measurement is seldom required: what is useful is the approximation to an ASTM number that can be readily compared by another investigator. The ASTM has prepared two typical series for ferrous and nonferrous materials which are reproduced in Figures 73 and 74. Strictly speaking, ferrous alloys are estimated on a logarithmic scale based on the formula:

$$y = 2^{n-1}$$

where n is the ASTM number, and y represents the number of grains per square inch. The most useful numbers in this series are from ASTM 1 to ASTM 8, with 8 being the smallest defined grain size. As well as ASTM numbers, it is possible to refer to a scale that gives average grain diameters, usually from 0.010 to 0.200 mm. With twinned nonferrous alloys, the structure of worked grains can sometimes be confusing because the grains appear fragmentary. The intercept method can also be used to determine the average grain size of the material. The equation relating the factors required is:

$$N(D) = \frac{\textit{length of intercept (mm)}}{\textit{magnification x no. of grain boundaries}}$$

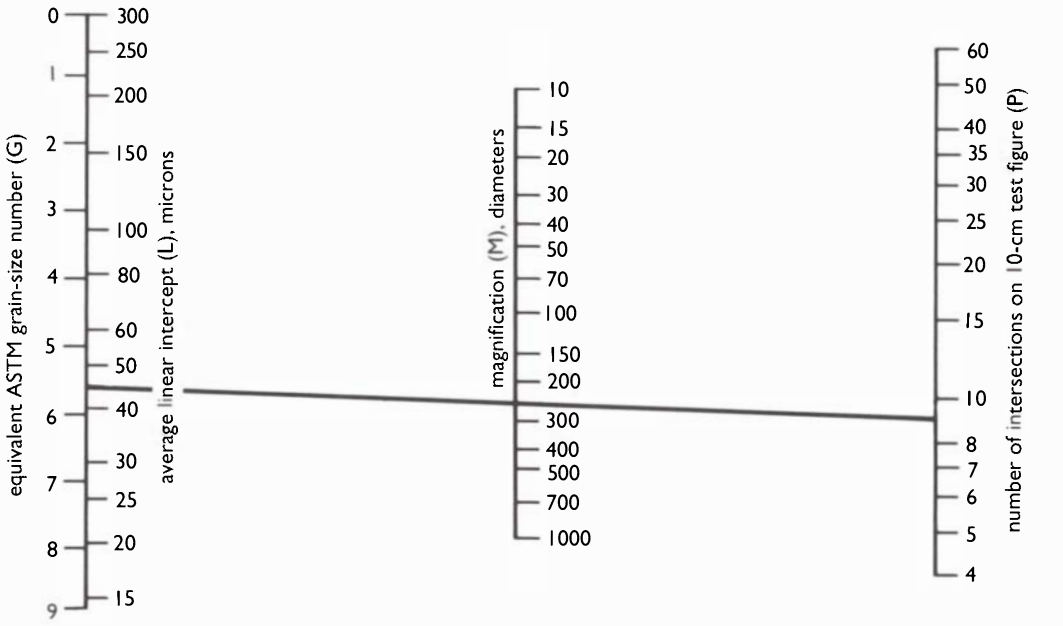

Figure 72. Nomograph for grain size. Estimation based on Hilliard's method.

Hilliard's circular intercept method can also be used. In this technique, a photomicrograph of known magnification is selected and a circle, drawn on a sheet of plastic of diameter 10 cm or 20 cm, is placed over the photomicrograph. The circle should intersect more than six grain boundaries for the method to give a reliable grain size estimation. The circle is used until at least 35 grain boundary intersections have been counted. One of the advantages of the circular intercept method is that it is easier to apply to deformed structures. A nomograph for the graphical solution of the Hilliard method is given in Figure 72.

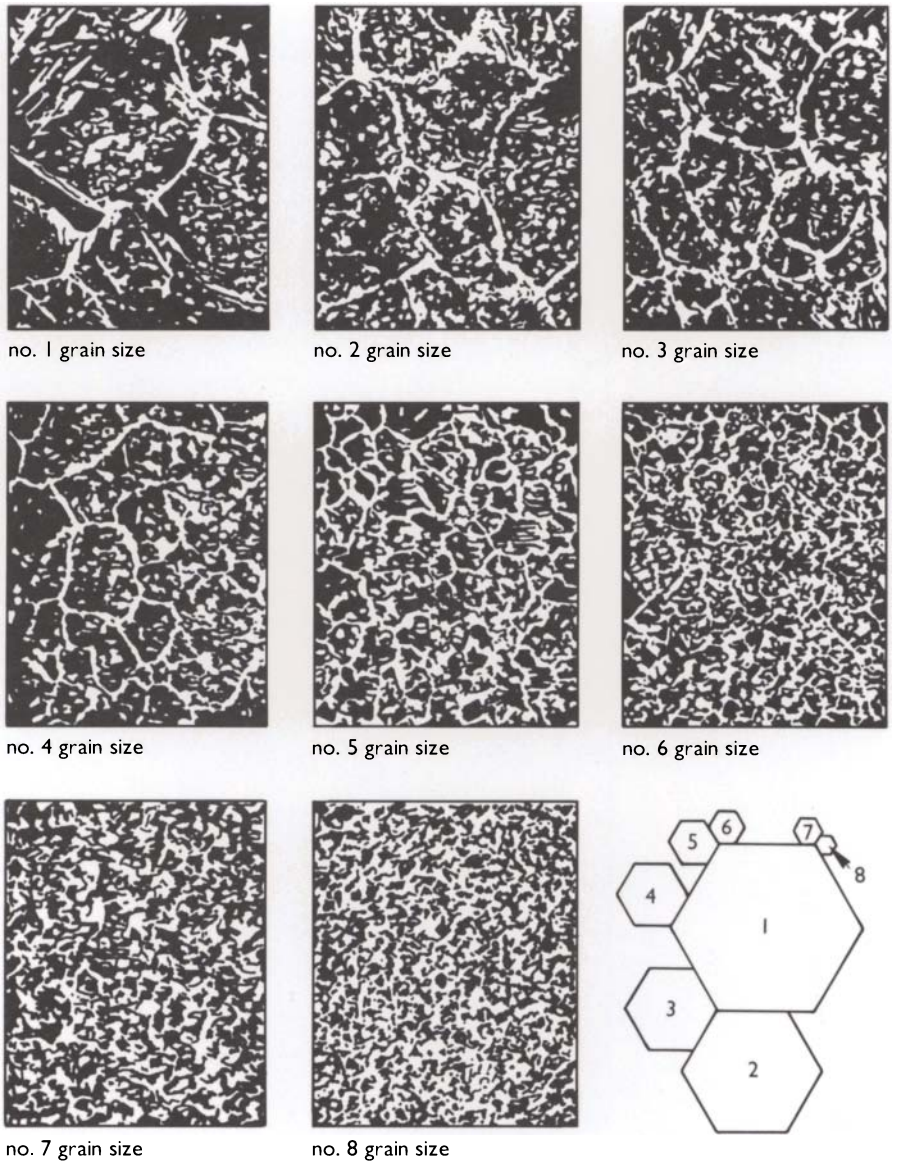

Figure 73. Typical standard for estimating the (austenitic) grain size of steel. Photomicrographs of samples carburized at 1700 °F (930 °C) for 8 hours and slowly cooled to develop the cementite network. From Samans (1963). Etch: nital; ×100.

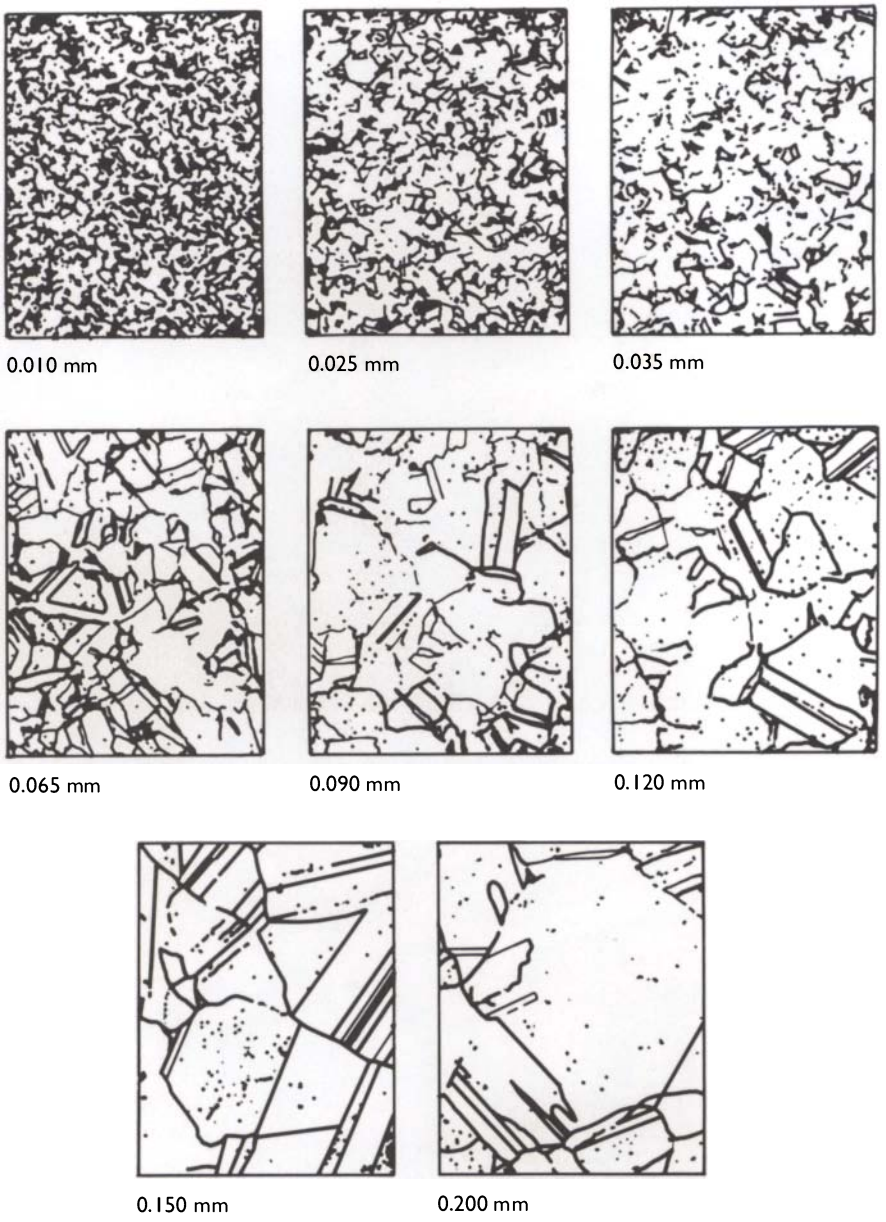

Figure 74. Typical standard for estimating grain size of annealed nonferrous materials such as brass, bronze and nickel silver. Actual diameter of average grain is noted. x75.

Figure 75, right. Mounting small specimens in silicon rubber cups. Embedding resin used here was Buehler epoxide resin which sets in about 6–8 hours.

Figure 76, below. Grinding the mounted sample on wet silicon carbide papers; usually papers of 240–600 grit are employed.

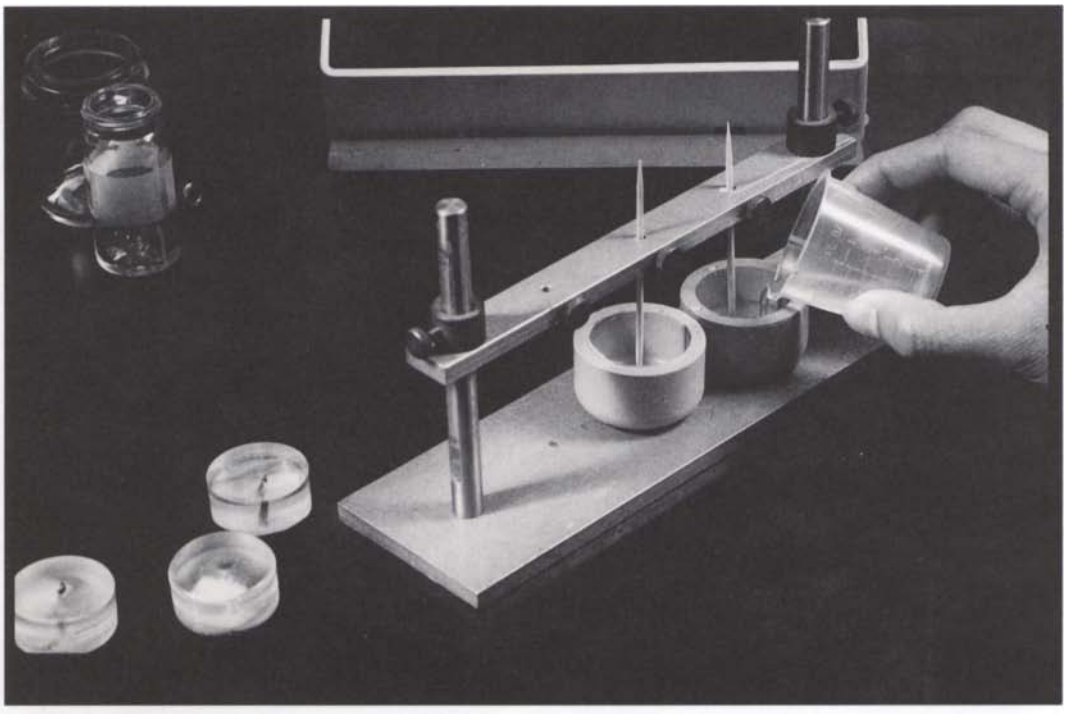

Figure 77, right. Polishing the mounted sample. Here Buehler Mastertex cloth is being used with 1-micron diamond spray abrasive and lapping oil lubricant.

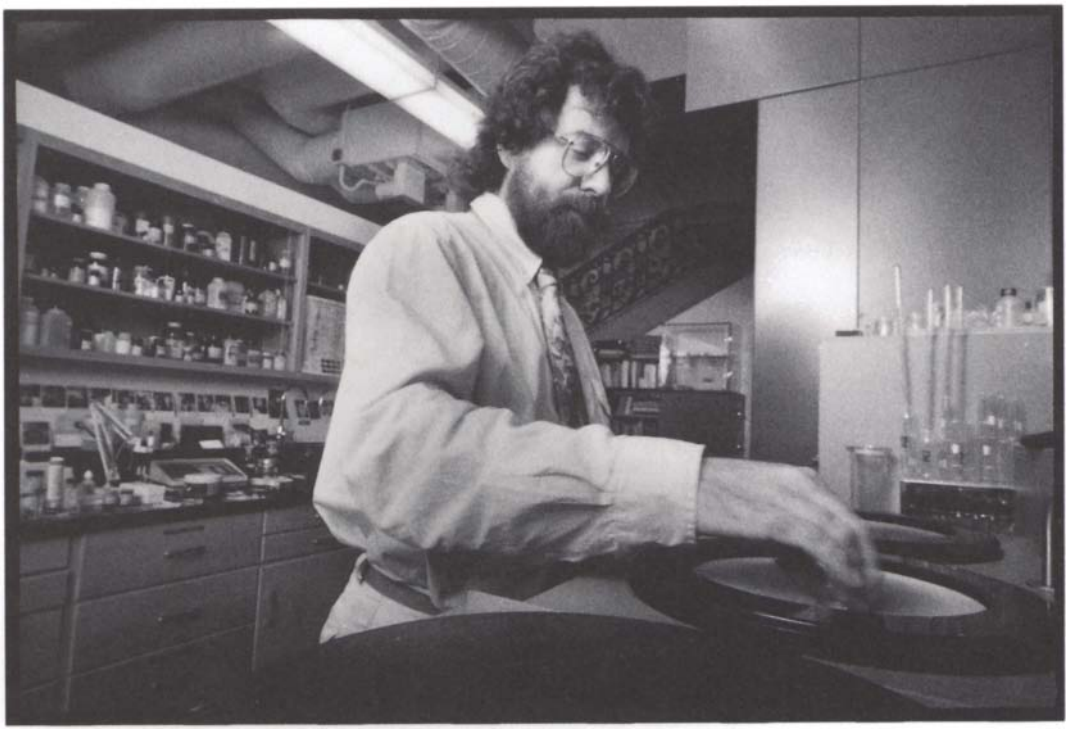

Figure 78, below. Sample storage and selection is best carried out in specially purchased metallography storage cabinets. Trays can be obtained in a variety of diameters for storage of different size mounts. Most of the samples here are 1 1/4" diameter polyester or epoxy mounted samples that have labels embedded in plastic on the back for easy identification.

Figure 79, right. Examination of pigments or corrosion products of metals can be best achieved by polarized light microscopy. This microscope can also be used for reflected illumination so that mounted samples can be examined.

Figure 80, below. Use of the inverted stage metallurgical microscope in which the specimen is placed on top of the microscope stage as illustrated here. The microscope illustrated is the Nikon Epiphot attached to a video camera, a 35-mm camera back, and a 4" x 5" color or black-and-white Polaroid film back. Dark field and reflected polarized light are both very useful features of this metallograph.

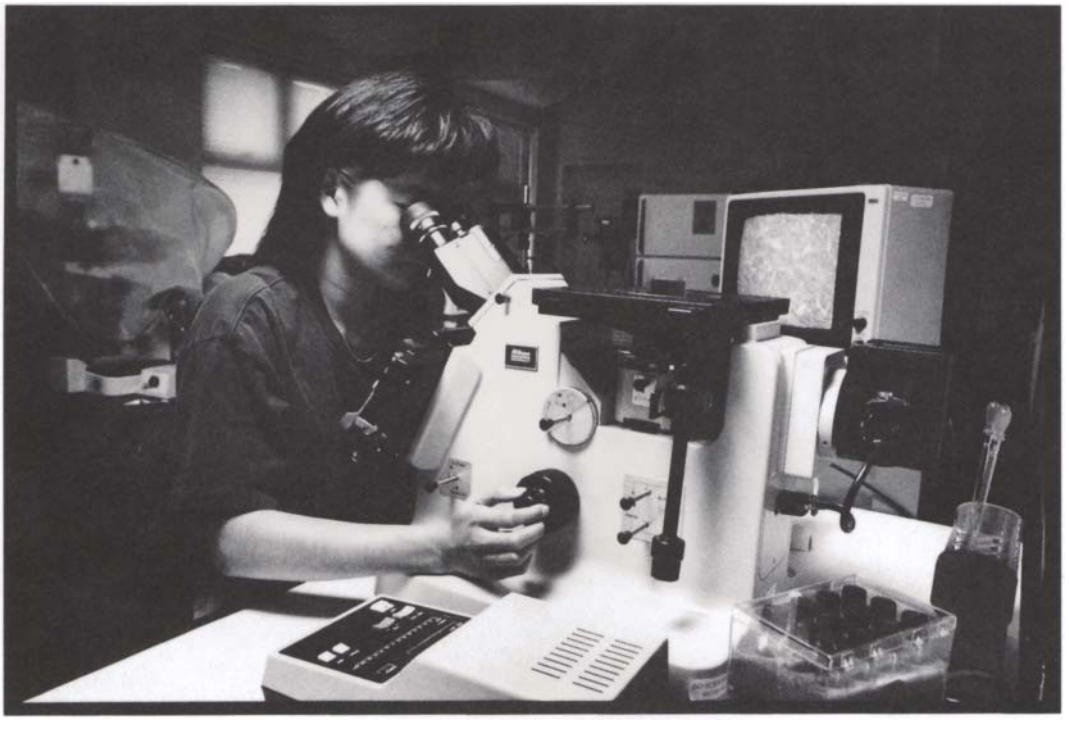

Metallography offers one of the most useful means for the examination of ancient metals. It is the study of polished sections of metallic materials using a special microscope that reflects light passing through the objective lens onto the specimen surface. The reflected light passes back through the objective to the eyepiece, which enables the surface structure of the section to be studied (see Fig. 80 for a typical example of a metallurgical microscope). Reflected light microscopy is used for metallographic examination because metals cannot transmit light in thin sections in the same way as ceramic or mineral materials. Apart from gold foil, which, if very thin, can transmit a greenish light through grain boundaries, metals are opaque substances.

It is usually necessary to take a sample, which can be quite small, from the object being studied. It is possible to polish a small area of a relatively flat surface on an object using a minidrill and fine polishing discs, but this method is quite difficult. With many antiquities, useful information can be obtained from samples as small as 1 mm^3, which can be removed from the object with a minimal amount of damage. Some methods of sampling applicable to ancient material are listed in Chapter 13. The sample itself need not be metallic: corrosion products, paint layers, core material from castings, niello, deteriorated enamels, patinations, and an array of other compositional materials are of considerable interest. Examination with a metallurgical microscope is often a useful first step in characterizing a particular component of an object. Some typical metallographic equipment is shown in Figures 75–80.

Metallography is, then, an important tool that may provide clues to the fabrication technology of the object or may assist in answering questions that arise during the treatment of an object by a conservator. It may be possible to provide information on the following range of topics:

1. The manufacturing processes used to produce the object. For example, whether cast into a mold or worked to shape by hammering and annealing.
2. The thermal history of the object. Quenching and tempering processes may produce definite changes in the microstructure that can be seen in section.
3. The nature of the metal or alloy employed to make the object. For example, many debased silver objects are made from silver-copper alloys and both constituents are clearly visible in the polished and etched section; they show up as a copper-rich phase and as a silver-rich phase. Sometimes it may be very difficult to obtain any idea of composition from looking at the microstructure and here additional evidence must be obtained using a suitable analytical method. One way of doing this if a sample has been taken and already mounted is to trim the plastic mount and place the sample in an X-ray fluorescence analyzer (XRF).
4. The nature of corrosion products. Much useful and varied information can be obtained from corroded fragments or pieces of corrosion crusts. For example, there may be residual metallic structures within the corrosion layers, pseudomorphic replacement of metal grains by corrosion products, the existence of gilded layers or other surface finishes within the corrosion layers, pseudomorphic replacement of organic fibers or negative pseudomorphic casts of fibers, unusual morphology of the corrosion products themselves, and changes brought about by methods of conservation. It should be noted that the scanning electron microscope is a very powerful tool for many of these investigations in addition to optical microscopy.

The principal difficulties with metallography applied to ancient material lie in the problems associated with sampling the object and the selection of the sample. If any damage is to be caused, the owner should always be consulted first so that necessary permission is obtained for the work. It should be made clear to the owner whether the sample can be returned when the examination is completed, and the kind of information that the sample is expected to provide. The owner should

receive a copy of any written report that is prepared as a result of the examination, together with any photomicrographs of the structure, clearly identified with the magnification of the print, the etching solution used, and the laboratory number assigned to the sample. It may be necessary to examine carefully a group of objects in the museum or laboratory before coming to a decision as to the number of samples to be taken or the objects from which it may be permissible to take a sample. If the damage is such that it can be repaired by filling the area concerned, the owner should be given the option of deciding whether or not to have the object gap-filled. It is preferable to fill small holes or missing corners with a synthetic resin colored to match the surface color of the object. A fairly viscous epoxy resin can be used for this purpose and can be colored with powder pigments.[1]

In many museum collections there are examples where large slices, pieces, or drillings have been taken from metallic antiquities causing gross damage to the objects concerned. Missing parts are sometimes filled with unsuitable materials such as Plasticine (normally a mixture based on putty, whiting, and linseed oil), which usually creates severe corrosion of exposed metal surfaces over a period of years in the museum collection. Sulfur-containing fillers such as Plasticine should never be used for mounting, display, or gap-filling of metallic objects. Great improvements in metallographic techniques over the last 20 years mean that it is no longer necessary to remove as much sample bulk from the object as many earlier investigations required. The extent of the damage is therefore greatly reduced; indeed, with much corroded metalwork or fragmentary objects, the loss may be insignificant and the resulting information may be very important indeed.

The only difficulty with taking small samples is the problem of the representative nature of the sample compared with the overall structure of the object. It does not follow, for example, that because the area sampled shows an undistorted dendritic structure (indicating that the piece was cast) that the whole of the object will reveal the same structure. Obviously there are cases in which this difficulty would be very unlikely to occur: worked, thin sheet-metal, pieces of wire, small items of jewelry, and so on, but with artifacts such as axes, knives, swords, large castings, etc., it may present a very difficult problem. If a complete interpretation of the metallographic structure of an artifact such as an axe is required, then it is almost essential to take two samples from the axe (Fig. 81).

Another example is that of a piece of wire or rod where both the longitudinal and transverse sections are of potential interest. Here the two sections can be obtained from a single sample by cutting the wire into two pieces and mounting them in a mold (Fig. 82).

The procedures for preparing metallographic samples are as follows:

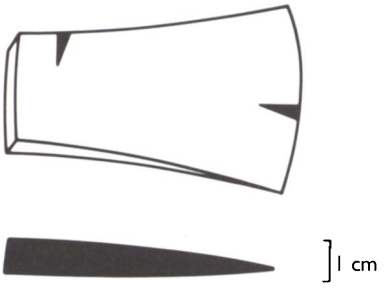

Figure 81, right. Drawing of an axe showing the ideal location of two samples removed for metallographic examination. Note that one of the cuts of the "V" section should be at right angles to the principal sides of the object to aid interpretation of any directional characteristics of the microstructure.

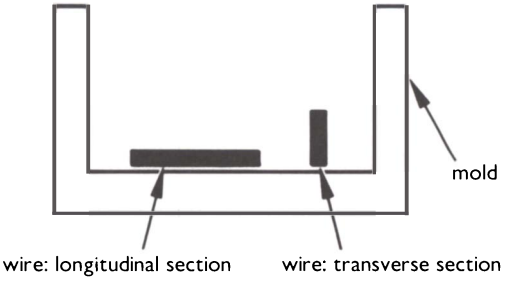

Figure 82, far right. Two samples of wire or rod mounted in different directions to obtain structural information relating to length and cross section. There are often different or diagnostic features visible in one section that may not be apparent in the other.

1. Selecting the sample
2. Mounting the sample in a synthetic resin cast into a small mold
3. Preliminary grinding of the embedded sample
4. Polishing, using rotary discs impregnated with alumina or diamond powders
5. Examining the polished section with a metallurgical microscope
6. Etching with a suitable etching solution
7. Preparing a written report
8. Doing photomicrography and drawings, if required, of the section to show microstructural details
9. Employing an orderly system of sample storage and documentation.

Note

1. For example, Araldite XD725 can be used with good quality artists' powder pigments mixed into the resin and hardener mixture. If a missing piece is being gap-filled and it is required that the restoration can be removed at a later time then the metal surface can be coated in the area to be filled with a reversible synthetic resin such as Paraloid B72 brushed on as a 10% solution in toluene applied in two coats. This should ensure that the fill can be removed, if it is not keyed-in, by soaking in acetone for a few minutes.

There are often severe restrictions on the quantity of metal that can be removed from an artifact for metallographic examination. On the other hand, even a very small sample, smaller than 1 mm^3 if necessary, can be mounted and polished for examination, although great care has to be exercised at all stages of preparation. It is much easier to work with larger samples, although by museum standards samples of 3 mm^3 are already unusually large, unless whole artifacts or substantial fragments are available for sectioning.

There are a number of criteria that samples should meet:

1. The object should be photographed or drawn before the sample is taken. This is especially important if the dimensions of the object are fundamentally altered by the material removed.
2. The microstructure of the samples should not be altered in the process of removal.
3. The sample should be representative of the object as a whole or of a selected feature or area of the object.
4. The orientation of the sample in relationship to the entire object should be carefully recorded and if it is not obvious where the sample was taken from, the position on the object concerned should be marked on a photograph or drawing of the object.

There are a number of possibilities for removing a sample depending, inevitably, on the nature of the object and on the metal or alloy of which it is composed.

1. A hacksaw with a fine-toothed blade can be used to cut large samples; however, high heat generated by friction during cutting can alter the original microstructure. The blade should be cooled periodically in water or ethanol. Removing a sample will usually entail considerable loss of solid as fine powder. This powder can be kept for analytical purposes although it may not be completely free from contamination. It can be used, for example, to provide X-ray fluorescence analysis for major constituents.
2. A fine jeweller's saw may be employed. These are easily broken if they get wedged in the cut, so a blade must be selected that is sufficiently robust for the job at hand. It is then possible to remove very small specimens quite accurately, often with minimal damage to the object concerned.
3. A hollow-core drill bit can be used to remove a core that can then be mounted for examination. While only robust or thick-sectioned objects would survive this technique, it is sometimes the only way a metallographic sample can be taken.
4. A wafering blade can be used to cut a thin slice or remove a small V-shaped section from the object. One suitable machine for this purpose is the Buehler "Isomet" diamond wafering machine with a cutting blade consisting of an oil-cooled copper disk impregnated with diamond powder along its circumference. The principal problem with this machine is the inherent difficulty of holding large or irregular artifacts, although a variety of clamps are provided for this purpose. If an object can be held securely and oriented in the proper direction, then the machine is extremely useful. Not only can the length and direction of the cut be precisely controlled, but the speed and weight applied to the cutting blade can be adjusted. The copper blade conducts generated heat to the oil bath so that the risk of any microstructural alteration is negligible.

   Friable material may break along lines of weakness, crystal planes, fractures, etc. and should not be cut using this machine, since transverse pressure on the blade in motion would result in cracking or chipping of the diamond-impregnated cutting edge, which would be costly (approximately $300 each in 1989).
5. With thin sheet or uneven edges it may be

possible to break off a small piece of metal by carefully gripping the area to be sampled with a pair of long-nosed pliers, medical forceps, or fine tweezers. Since many ancient sheet metals are corroded or otherwise embrittled, the lack of plastic deformability of the material may assist in allowing the removal of a sample, since slight and carefully applied pressure may enable the removal of very small pieces.

6. A scalpel may be used under a binocular microscope. This technique may enable the removal of small pieces of corrosion products or metal for subsequent examination. It is occasionally possible to detach a specimen under the microscope by patient chiselling with a scalpel. Some deformation of the specimen may result, but this zone can usually be eliminated in the grinding stage or, alternatively, one of the undeformed sides polished.
7. A broken jeweller's saw blade held in a vibrotool can be used. There are a number of applications for this technique, which allows the removal of small pieces from hollow sheet work, lost-wax castings, cavities, etc., since the vibratory action of the blade in combination with a gentle sawing action is not as limiting as using the blade rigidly held in its usual frame. A broken blade, about 3–5 cm in length, is satisfactory.

Once a sample is removed from an artifact, it must be mounted and prepared for examination under a metallurgical microscope. Before the sample is placed in a mold, it should be degreased thoroughly in acetone or ethanol and dried. This is especially important if the sample has been cut in a Buehler wafering machine. Very small samples, pieces of thin wire, or thin sheet may require physical support at the mounting stage, otherwise when they are embedded in resin and the block is ground and polished, there will be no control over the metal surface exposed to view. There are a number of ways in which this can be achieved:

1. A small brass jig, specially made for the purpose of holding specimens, can be used (Fig. 83a). The purpose of the jig is to allow the specimen to be attached to a toothpick with a very small amount of acrylic or nitrocellulose adhesive. The attached specimen and stick can then be rigidly held in the jig and angled or positioned as required in the mold.
2. Similarly, the specimen can be mounted on a toothpick and then supported with more toothpicks or matches laid across the mold as shown in Figure 83b. It is, of course, possible to support more than one sample in the same mold using this technique, but the samples are much more likely to move in the mold when resin is poured in, and simultaneous polishing of two or more very small samples is much more liable to result in the loss of the embedded specimens once the block has been ground and polished.
3. Some texts suggest adhering the sample to the bottom of the mold with adhesive or supporting the sample with a paper clip. These methods can be used but have disadvantages. For example, the adhesive may result in slight unevenness in the resin layer surrounding the edge of the sample with loss of good edge retention, or the paper clip may interfere with the polishing of very soft metals if it is in contact with the resin surface.
4. A disk of ash-toughened wax or a small quantity of molten beeswax can be poured over the bottom of the mold. When set in position, the specimen can be partially embedded before the resin is poured into the mold. When set and removed from the mold, the specimens will stand in slight relief and will have to be carefully ground before polishing. This technique is inadvisable for very brittle materials.
5. If the sample will be subjected to electrolytic or electrochemical polishing, it can be supported by a piece of wire in the mold using the jig method detailed in No. 2. The wire can be attached to the specimen using "aqua dag" or some similar conducting paint applied in two or more coats to effect good electrical contact. The wire is cut to allow about 3–5 cm excess above the top of the mold (Fig. 83b).
6. Larger specimens, especially if they have been cut, can usually be mounted directly by placing them in the required position in the mold. If the embedding resin is then poured carefully, the specimen should not move in its position at the bottom of the mold.

Embedding the Sample

There are a number of proprietary synthetic resins on the market that are designed as embedding materials for metallographic specimens. Epoxy, polyester, and acrylic resins are the most common. For routine use, "Scandiplast 9101" polyester embedding resin can be used with peroxide catalyst "Scandiplast 9102." One drop per ml of catalyst is stirred into the resin, which begins to gel after about five minutes, and thus must be used promptly. Fifteen ml of resin is sufficient to fill Metaserv or Buehler 1-inch diameter or 1-1/8-inch diameter molds, which are made of polyethylene or silicon rubber. Curing is best carried out at room temperature; samples can be removed from the mold after two–four hours, but do not attain their maximum hardness until about eight hours. Manufacturers state that the slightly sticky surface on

the set resin is due to oxidation reactions, which can be minimized by covering the mold while the resin sets. This, however, is rarely a serious problem and the resin gives satisfactory edge retention and low porosity upon curing.

With many archaeological materials, the major problem is to achieve good edge retention. There are a number of ways in which this problem can be tackled. One method is to use an epoxy mounting system that has low viscosity compared with polyesters and to add a filler of specially graded black alumina granules. These are hollow alumina spheres whose hardness can be matched to that of the material to be mounted.

Figure 83. Holding small samples.
Top, a. Use of one type of mounting jig to hold small samples in a set position.
Middle, b. Use of toothpick support over mold to attach to samples.
Bottom, c. Use of wax embedding method; only suitable for small samples.

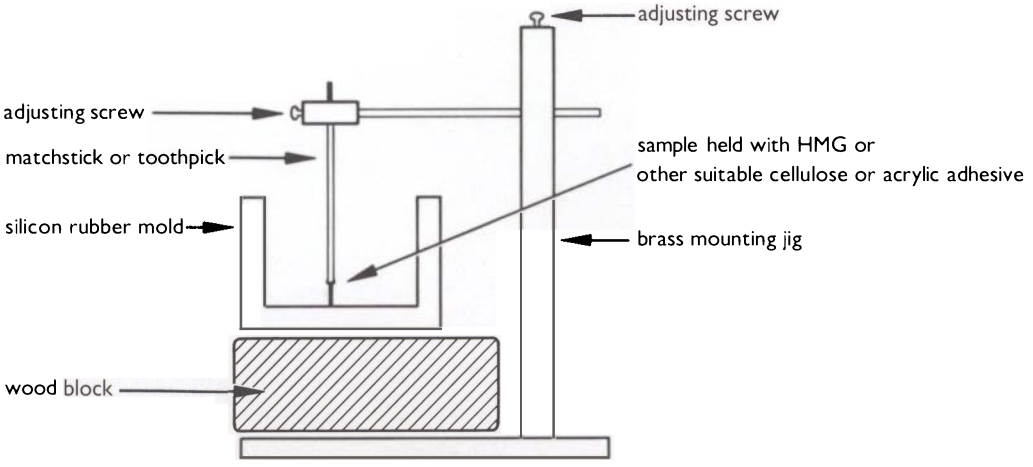

Use of one type of mounting jig to hold small samples in a set position.

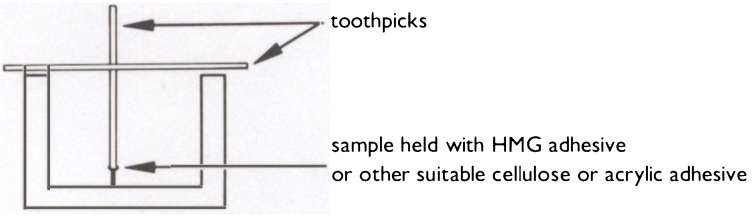

Use of toothpick support over mold.
to attach to samples

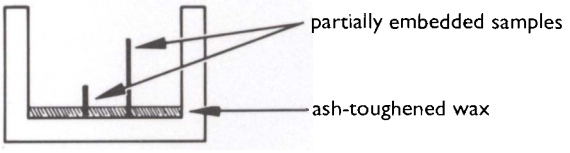

Use of wax embedding method.
Only suitable for small samples.

They also provide good edge retention, although they are time-consuming to use.

If the metallographic sample is embedded at an angle in the mold, some of the surface area of the sample will appear to be greater upon grinding and polishing. This technique can be used to provide a magnified view of surface layers or other features that might prove difficult to see in section. The sample, when embedded at an angle, is known as a taper section.

Other ways of solving the problem include electrolytic deposition of protective metallic coatings, such as nickel, or the use of electroless deposition solutions. Care, however, should be exercised when using these methods since a corroded sample is permeable to the penetration of applied layers and they will create a visually confusing result. A label should be incorporated into the top of the resin giving at least the laboratory number so that samples can be properly identified.

Another method of embedding very small samples, which is often used for paint cross sections, involves the use of a rectangular mold half-filled with resin (Fig. 84). The sample is carefully laid on the resin surface next to one edge of the mold and the mold is then completely filled with resin, embedding the sample without need of a support stick.

Grinding

Once mounted and set, the resin block must be ground flat. The standard procedure at this stage is to use wet silicon carbide papers with progressively finer grit sizes (120, 240, 400, 600). The sample must be held so that it does not rock or move out of one grinding plane, otherwise it will be very difficult to obtain an optically flat surface. Starting with the coarser grit paper, the sample is moved backwards and forwards over the paper until a uniform ground finish is obtained. It is then carefully washed under running water, examined, rotated 90°, and ground on the next grade of paper. This process is then repeated with the finer two grinding papers, rotating the specimen 90° on each paper. It is very important to eliminate completely the scratches from the previous grinding because they will not be removed by polishing.

With very important specimens, a fresh strip

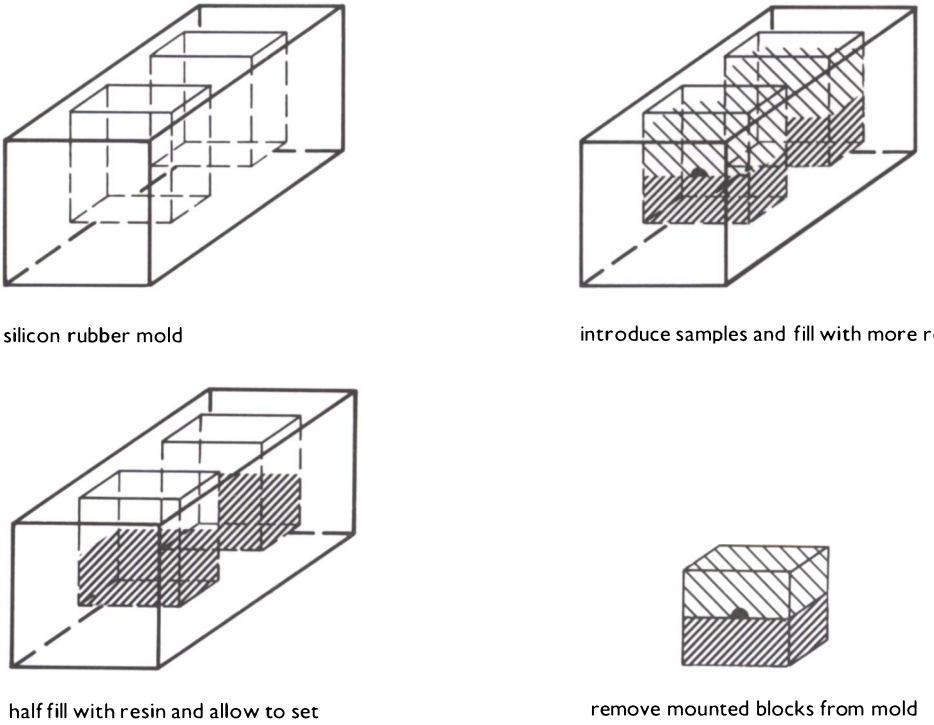

Figure 84. Embedding small samples.

of grinding paper should be used, and successively longer grinding times are necessary as the paper becomes finer. This ensures thorough removal of deformed material at the specimen surface before polishing. The quality of 600 grit paper seems to vary, and if any large particles are present they will produce surface scratches difficult to remove later. The care taken with metallographic preparation of soft metals, such as gold alloys, zinc alloys, or some copper alloys, has to be much more rigorous than is necessary with iron, steels, or cast iron specimens in archaeological contexts.

Polishing

For most ancient metals, the best results are to be obtained by polishing on diamond-impregnated rotary polishing wheels lubricated with mineral oil. Diamond powders are usually supplied as tubes of paste or in aerosol cans in an oil-based suspension. The usual range of diamond powder sizes are: six microns, one micron, and one-quarter micron. Some of the polishing can be carried out automatically using a variety of machines or polishing attachments. Hand-finishing, however, is usually preferable for best results with one micron or one-quarter micron diamond paste. Polishing with diamond powders produces less rounding of surface details than is apparent when using α-alumina, γ-alumina, or magnesium oxide pastes. Alumina often can be used for less detailed work and is frequently satisfactory for the preparation of iron and steel alloys. Magnesium oxide has to be used fresh as it undergoes atmospheric carbonation and the resulting magnesium carbonate that is formed may have a coarse crystal form.

Polishing is carried out by holding the specimen against the rotating polishing cloth. It is difficult to quantify how much pressure must be used: too little pressure retards the rate of polishing and may result in some pitting of the surface, too much pressure may distort the surface. The correct polishing pressure varies with different metals and can only be learned through experience.

After initial polishing on six micron diamond paste, the sample should be washed in water, rinsed in ethanol or acetone, and dried. It can then be polished on one micron diamond for at least five minutes. For many routine purposes this is sufficient, and the sample should then be carefully washed to remove all traces of polishing compound and oil before it is ready for examination under the metallurgical microscope. For very high-quality work, finish by final polishing on one-quarter micron diamond.

Electrolytic or electromechanical polishing can be employed from the grinding stage and may give a more perfect finish than that obtainable from hand-polishing. Disadvantages occur with many archaeological samples because of the extensive corrosion that they may have undergone; the presence of these corrosion products means that local anode/cathode reactions may occur with excessive sample dissolution as a result. If one phase of a two-phase alloy is slightly corroded it may be preferentially attacked at an accelerated rate. Mechanical methods are generally preferable unless there is a particular reason for the use of other techniques. For example, granulated gold spheres, difficult to etch, were polished and etched at the same time using an electromechanical polishing technique on an adaptation of the Struers "Autopol" machine.

A freshly polished section should be examined metallographically as soon as possible: some surfaces tarnish rapidly and will have to be repolished. Ancient metal samples should always be examined in the polished state to begin with since there may be many features already visible under the microscope.

Visual evidence should be described, preferably with accompanying photographic records of the microstructure at suitable magnifications. Inclusions or corrosion products that are present when the section is examined in the polished condition should be noted because these will either be dissolved or partially obliterated by etching. If necessary, a photograph should be taken in the unetched condition to show the range and type of inclusions present. They should also be examined in reflected polarized light, which may assist in identifying the range and composition of non-metallic material that may be evident.

It is important to obtain an overall view of the specimen at a low magnification (about x30–x50) before proceeding to look at particular features at higher magnifications. Some specimens will appear almost featureless before etching if the metal or alloy is uncorroded and relatively free from slag particles, oxide inclusions, or other impurities. In these cases, it is permissible to proceed to an etched surface quite early on in the examination. The details of the etching solution used should be recorded; it is not customary, however, to quote the time of immersion in the etchant because the conditions of use and strength of solutions vary from laboratory to laboratory, making exact comparisons difficult. The magnification should, of course, be recorded with any notes made about the structure, once detail can be observed.

The range of features that may be made visible by etching is variable, depending on the type of specimen examined. Details not apparent using one etchant alone may become visible after another reagent has been tried, so the assumption that all microstructural detail is evident by using one etchant should be resisted.

The following features should be noted:

1. The range and type of grains present. Their size can be compared with, for example, an eyepiece marked with grain sizes or with ASTM standard grain size numbers.
2. The presence of different phases.
3. Gross heterogeneity or differences between various areas of the sample.
4. Grain sizes, or surface deformation features, or heat-treated zones at cutting edges and worked surfaces.
5. The distribution of inclusions, weld lines, slag particles, or porosity.
6. The presence of any surface coating or gilding. Sometimes careful examination at high magnification is necessary to establish the presence of surface coatings, leaf gilding, amalgam gilding, etc.
7. The distribution of any corrosion products present and the existence within corrosion layers of pseudomorphic remnants of grain structure or other microstructural features, the presence of any remnant metallic grains, and layering or unusual features.
8. Indications of grain boundary thickening or precipitation of another phase at the grain boundaries.
9. The presence of twin lines within the grains and whether the twin lines are straight or curved.
10. The presence of strain lines within the grains.
11. Whether dendrites in cast alloys show indications of coring and the approximate spacing (in microns) of the dendritic arms, if these are clearly visible.
12. Do not forget that a polished section is a two-dimensional representation of a three-dimensional object. If the structure is complex, as in pattern-welded steel blades, for example, supplementary information, such as x-radiography to reveal the internal pattern, will be available.
13. The presence of intercrystalline or transcrystalline cracking in the specimen.
14. Indications of grain-boundary thickening.
15. The presence of second-phase precipitation at the grain boundaries (discontinuous precipitation) or precipitation within the grains (as in the case of Widmanstätten precipitation).
16. Evidence of martensitic transformation or heat treatment used in the fabrication process.

There may be, of course, other important structural details but this brief list covers most of the features that may be visible using the metallo-

graphic microscope.

Care should be taken not to confuse notes made on specimens under different conditions of polish or etching because it may be very difficult later to reproduce exactly the examined surface. Also, if careful note of the specimen number is not kept, it may become very difficult to establish which specimen had been examined. The same care should be applied to the photographic recording.

A satisfactory metallographic specimen for macroscopic or microscopic investigation must present a representative plane area of the material. To distinguish the structure clearly, this area must be free from defects caused by surface deformation, flowed material (smears), plucking of the surface (pull-out), and surface scratches. In certain specimens, edges must be well-preserved in order to investigate gilding, tinning, etc. Even for routine examination, poor specimen preparation can result in problems because the observation or conclusions may not be valid interpretations of the visual evidence.

Polished metal surfaces do not reveal details of structure. In order to examine grain boundaries, other phases, and effects of alloying additions the polished metal surface must be attacked with selected chemical reagents that will reveal differences in grain orientation and microstructure. There are three ways in which etching a polished metal surface can be carried out:

1. With chemical reagents either as a solution or as a gas.
2. With electrolytic etching, by applying small AC or DC currents to the specimen immersed in an electrolyte.
3. With electromechanical etching, which is a combination of anodic dissolution in an electrolyte and mechanical polishing of the specimen.

This section deals with etching solutions that are appropriate for archaeological metals. The polished metal surface must be free of all traces of oil from polishing, and of polishing compounds, grease, and particles of dirt. The usual procedure is to pour a small quantity of etching solution into a small petri or crystallizing dish so that the specimen can be immersed for a few seconds or minutes, as necessary. Some solutions need to be freshly mixed before each use since they either undergo very rapid chemical reaction (such as solutions of potassium cyanide mixed with ammonium persulfate) or they slowly deteriorate (such as solutions mixed with hydrogen peroxide). Once the surface of the sample has been exposed to the etching solution, it should not be touched; it can be dried, after rinsing in ethanol or acetone, by placing it in front of a specimen drier for a few seconds. Sometimes, at this stage, very obvious staining of the specimen occurs around the edges where it meets the resin mount. This is a consequence of the etchant seeping down any fine crack that may be present and then being drawn to the surface upon drying. Some specimens require considerable care if this problem is to be avoided. For example, it may be possible to dry the sample more slowly in air, or to dry it using a stream of cold air. After the sample has been etched, it is important to examine it immediately, as stored and etched specimens can rapidly become tarnished, and this obscures the surface detail the etchant is trying to reveal. The sample, if very delicate, should be leveled in such a way that the impact of the leveler does not fall onto the etched surface of the metal. Damage to the surface structure can result if the leveler is depressed into soft alloys, such as gold and silver.

Sound metallographic principle dictates that all specimens should be examined in an unetched condition before proceeding to the etched examination. This is partly because etching will often dissolve out any inclusions that may be present (this would mean repolishing the entire specimen), and partly because etching may not be necessary with some archaeological materials. If the specimen is two-phased or has surface enrichment or other visible features, all this should be noted in the unetched condition before proceeding to etching.

Etchants for iron, steel, and cast iron

Nital

100 ml ethanol, C_2H_5OH
2 ml nitric acid, HNO_3

Picral

100 ml ethanol, C_2H_5OH
2 g picric acid, $C_6H_2(OH)(NO_2)_3$

This is the most common etchant for wrought iron and iron carbon steels. Often useful for iron and heat-treated steels, pearlite, and martensite. Fe_3C is stained a light yellow. Nital and picral can be mixed together in 1:1 proportion.

Oberhoffer's reagent

500 ml distilled water, H_2O
500 ml ethanol, C_2H_5OH
42 ml hydrochloric acid, HCl
30 g ferric chloride, $FeCl_3$
0.5 g stannous chloride, $SnCl_2$ (add HCl last)

After etching, the section should be rinsed in a 4:1 mixture of ethanol and hydrochloric acid. Useful for steels and for segregation studies in irons (e.g., arsenic segregation).

Heyn's reagent

20 ml distilled water, H_2O
20 g copper (II) ammonium chloride, $CuCl(NH_4)$

Copper precipitates must be wiped from the surface with distilled water or washed off with distilled water from a wash bottle. Useful for phosphorus segregation in steel.

Klemm's reagent

50 ml saturated aqueous solution of sodium thiosulfate, $Na_2S_2O_3$
1 g potassium metabisulfate, $K_2S_2O_5$

Phosphorus segregation in cast steels and cast irons.

Baumann's print solution

100 ml distilled water, H_2O
5 ml sulfuric acid, H_2SO_4

Silver bromide paper is saturated with the solution and firmly pressed against the specimen surface. After one to five minutes, rinse and fix with a solution of 6 g $Na_2S_2O_3$ in 100 ml H_2O. Wash and dry. Useful for verification, arrangement, and distribution of iron and manganese sulfide inclusions.

Beraha's reagent

100 ml distilled water, H_2O
24 g sodium thiosulfate, $Na_2S_2O_3$
3 g citric acid, $CH_2COHCH_2(COOH)_3 \cdot H_2O$
2 g cadmium chloride, $CdCl_2 \cdot 2H_2O$

Use for 20–40 seconds. Chemicals must be dissolved in the sequence given. Each constituent must dissolve before adding the next. Store in the dark under 20 °C. Filter before use. Solution remains active for only four hours. Used as a tint etchant for iron and carbon steels. Ferrite is stained brown or violet. Carbides, phosphides, and nitrides may be only lightly stained.

With Beraha's reagent, ferrite is colored but cementite is not, so that both proeutectoid cementite and cementite in pearlite are in strong contrast to the ferrite, which can make even thin films of cementite easily visible.

Alkaline sodium picrate

2 g picric acid, $C_6H_2(OH)(NO_2)_3$
25 g sodium hydroxide, NaOH
100 ml distilled water, H_2O

This solution is useful for distinguishing between iron carbide and ferrite in steels. It can be used as a boiling solution for ten minutes or longer if required. The iron carbide, Fe_3C, is darkened by the reagent, while ferrite is unaffected. Etching in this solution may provide a good indication of pearlite lamellae spacing.

Beaujard's reagent

20 g sodium bisulfite, $NaHSO_3$
100 ml distilled water, H_2O

To ensure that the specimen is evenly wetted, it is often a good idea to etch in nital for two to four seconds beforehand. Beaujard's reagent can then be used for 10–25 seconds; the surface should be very carefully washed and dried, otherwise the deposited surface film will be disturbed. The reagent produces good contrast between ferrite grains and between lightly tempered martensite and ferrite, as well as delineating cementite networks. The reagent works by depositing a complex oxide-sulfide-sulfate film on the metal surface, in various shades of brown.

Dimethylglyoxime nickel test

Some ancient steels contain nickel as an important impurity. A simple test is to take a nickel print by pressing a blotting paper soaked in dimethylglyoxime against the polished section when the nickel-rich areas are revealed by brown-staining on the blotting paper.

Vilella's reagent

1 g picric acid, $C_6H_2(OH)(NO_2)_3$
100 ml ethanol, C_2H_5OH
5 ml hydrochloric acid, HCl

A reagent that can be used 5–40 seconds and reveals clearly the needles of plate martensite. It is useful for exposing the austenitic grain size of quenched and tempered steels if this feature is at all discernible.

Whiteley's method

5 g silver nitrate, $AgNO_3$
100 ml distilled water, H_2O

A technique for revealing sulfide inclusions in steel and other alloys. Soak the polishing cloth in the freshly prepared solution. The cloth is then washed to remove all excess solution. The polished surface of the sample is then rubbed carefully over the prepared surface of the cloth. Any sulfide inclusions that are present should be stained a dark brown.

Etchants for gold alloys

See ammonium persulfate/potassium cyanide (p. 72) used for silver alloys. A very useful solution for a wide range of gold alloys.

Aqua regia

40 ml nitric acid, HNO_3
60 ml hydrochloric acid, HCl

Used for a few seconds or up to one minute. Use fresh. Aqua regia is a strong oxidizing solution and highly CORROSIVE. In most alloys it provides grain contrast.

Hydrogen peroxide / iron (III) chloride

100 ml distilled water, H_2O
100 ml hydrogen peroxide, H_2O_2
32 g ferric chloride, $FeCl_3$

Sometimes useful for variable carat gold jewelry alloys and Au-Cu-Ag alloys.

Etchant for tin

Ammonium polysulfide

A saturated aqueous solution of ammonium polysulfide. Use for 20–30 minutes. Wipe off with cotton wool after etching. Can be used for all types of tin alloys. Nital or picral can also be used (see etchants for iron, steel and cast iron).

Etchants for zinc

Zinc alloys are difficult to prepare mechanically. Fake microstructures are common because deformation is difficult to prevent.

Palmerton's reagent

100 ml distilled water, H_2O
20 g chromic oxide, CrO_3
1.5 g sodium sulfate, Na_2SO_4 (anhydrous) or
3.5 g sodium sulfate, $Na_2SO_4 \cdot 10H_2O$

Can be used for seconds or minutes.

50% concentrated HCl in distilled water

50 ml conc. hydrochloric acid, HCl
50 ml distilled water, H_2O

This solution is sometimes useful for swab application as well as immersion.

Etchants for lead alloys

Glycerol etchant

84 ml glycerol, $HOCH_2CHOHCH_2OH$
8 ml glacial acetic acid, CH_3COOH
8 ml nitric acid, HNO_3

Use fresh only. Gives grain boundary contrast. Nital can also be used (see etchants for iron, steel and cast iron).

Glacial acetic acid

15 ml glacial acetic acid, CH_3COOH
20 ml nitric acid, HNO_3

Useful for lead solders and Pb-Sn alloys. If difficulty is experienced in the preparation of lead alloys, a good technique is to try finishing the polishing with fine alumina powder (1 or 1/4

micron) suspended in distilled water with a 1% solution of aqueous ammonium acetate.

Etchants for copper alloys

Aqueous ferric chloride

120 ml distilled water, H_2O
30 ml hydrochloric acid, HCl
10 g ferric chloride, $FeCl_3$

Produces grain contrast. Very useful for all copper containing alloys such as the arsenical coppers, bronzes, brasses, etc. Etching time is given as a few minutes in some books but ancient metals etch faster. Reduce time to 3–5 seconds at first.

Alcoholic ferric chloride

120 ml ethanol, C_2H_5OH
30 ml hydrochloric acid, HCl
10 g ferric chloride, $FeCl_3$

Same as aqueous ferric chloride, except that there may be some advantages in using an alcoholic solution (less staining, for example).

Aqueous ammonium persulfate

100 ml distilled water, H_2O
10 g ammonium persulfate, $(NH_4)_2S_2O_8$

Only a few seconds are necessary for all these etchants unless specified to the contrary. Produces grain contrasts. Must be used fresh; will not keep.

Saturated solution of chromium (VI) oxide

Chromium (VI) oxide solutions should be handled with great care. Mixtures of CrO_3 and organics may be EXPLOSIVE. Grain boundary etchant.

Ammonia/ hydrogen peroxide

25 ml distilled water, H_2O
25 ml ammonium hydroxide, NH_4OH
5–25 ml hydrogen peroxide, H_2O_2

Make up and use fresh only. Adding larger amounts of H_2O_2 creates better grain contrast; adding less H_2O_2 creates better grain boundary etching.

5% potassium ferricyanide

5 g potassium ferricyanide, $K_2Fe(CN)_6$
100 ml distilled water, H_2O

This etchant can be used to darken some precipitates such as Cu_3P which may coexist with alpha + delta eutectoid. Cu_3P can be seen as a purple shade against the very pale blue of the delta phase. After etching in $FeCl_3$, the distinction is lost. Some difficulties may be overcome by using a relatively high amount of aqueous ammonia in the final polish (e.g., 5% NH_4OH).

Etchants for oxide layers on iron

Solution 1

10 ml distilled water, H_2O
5 ml 1% nitric acid, HNO_3 solution
5 ml 5% citric acid,
$CH_2COHCH_2(COOH)_3$ solution
5 ml 5% aqueous thioglycollic acid,
HOCH · COSH

Swab for 15–60 seconds. Etches Fe_2O_3; Fe_3O_4 is not attacked.

Solution 2

15 ml distilled water, H_2O and
5 ml formic acid, HCOOH solution (a)
15 ml H_2O and
5 ml fluoboric acid, F_2BO_3 solution (b)

Swab for five seconds with solution (a) followed by solution (b) for two seconds. Etches Fe_3O_4 only.

Etchants for silver alloys

Acidified potassium dichromate

10 ml sulfuric acid, H_2SO_4
100 ml potassium dichromate, saturated
$K_2Cr_2O_7$ in water
2 ml sodium chloride, saturated NCl solution

Dilute 1:9 with distilled water before use. Can also be used without the sulfuric acid addition. Useful for silver and copper-silver alloys.

Ammonium persulfate / potassium cyanide

100 ml distilled water, H_2O and
10 g ammonium persulfate, $(NH_4)_2S_2O_8$ (a)
100 ml H_2O and

10 g potassium cyanide, KCN (b) POISON

Solutions (a) and (b) must be mixed before used in the proportion 1:1. After use flush down the sink with plenty of water. *Never* mix with acids. The solution of potassium cyanide is POISONOUS. Also useful for gold alloys, silver alloys, copper alloys. Make up the persulfate solution just before use.

Ammonia / hydrogen peroxide

50 ml ammonium hydroxide, NH_4OH
50 ml hydrogen peroxide, H_2O_2

Must be used fresh.

Acidified thiourea

10% aqueous solution of thiourea, $SC(NH_2)_2$
5–10 drops of either nitric acid, HNO_3 or hydrochloric acid, HCl

Interference film etchants for color effects

It is sometimes useful to investigate the application of color metallography to ancient metallic object specimens. One of the potential advantages to interference film metallography is that coring and segregation may be revealed when conventional metallographic techniques fail. Color metallography may also be used to enhance the visual appreciation of microstructural features. Further details concerning the techniques which may be employed can be found in Yakowitz (1970), Petzow and Exner (1975), and Phillips (1971). Some of the useful recipes are set out below.

Interference etchants for copper alloys

Acidified selenic acid

2 ml 35% hydrochloric acid, HCl
0.5 ml selenic acid, H_2SeO_4
300 ml ethanol, C_2H_5OH

This solution can be used after first etching the polished sample for a few seconds in a 10% solution of ammonium persulfate. Dry after etching in persulfate before using the selenic acid etchant.

Acidified thiosulfate / acetate

12 g sodium thiosulfate, $Na_2S_2O_3 \cdot 5H_2O$
1.2 g lead acetate, $Pb(CH_3COO)_2 \cdot 3H_2O$
1.5 g citric acid, $C_6H_8O_7 \cdot H_2O$
50 ml distilled water, H_2O

Use after first pre-etching with ammonium persulfate. A very useful etchant for copper alloys but must be made up fresh as the solution will not keep. Dissolve the thiosulfate before adding the other ingredients. Best made by placing the prepared solution in a refrigerator for twenty-four hours when a clear lead thiosulfate solution should form with a sulfur precipitate.

Acidified sulfate / chromic oxide

50 g chromium trioxide, CrO_3
5 g sodium sulfate, Na_2SO_4
4.25 ml 35% hydrochloric acid, HCl
250 ml distilled water, H_2O

Interference etchants for iron, steel, and cast iron

6 g potassium metabisulfite, $K_2S_2O_5$
100 ml distilled water, H_2O

This etchant is useful for both carbon and alloy steels.

2 g sodium molybdate, $Na_2MoO_4 \cdot 2H_2O$
200 ml distilled water, H_2O

Acidify to pH 2.5 to 3 using dilute nitric acid. Useful for cast irons after first pre-etching with nital.

60 g sodium thiosulfate, $Na_2S_2O_3 \cdot 5H_2O$
7.5 g citric acid, $C_6H_8O_7 \cdot H_2O$
5 g cadmium chloride, $CdCl_2 \cdot 2H_2O$
250 ml distilled water, H_2O

Useful for cast iron and steels without pre-etching. Must be freshly made. This solution will not keep longer than a week.

Saturated thiosulfate solution

100 ml saturated sodium thiosulfate, $Na_2S_2O_3 \cdot 5H_2O$ in distilled water
2 g potassium metabisulfite, $K_2S_2O_5$

Can be made up fresh and used for cast iron and steel alloys.

Selenic acid solution

10 ml 35% hydrochloric acid, HCl
4 ml selenic acid, H_2SeO_4
200 ml ethanol, C_2H_5OH

Can be used for ferritic and martensitic steels.

Interference etchants for aluminum alloys

Molybdate / bifluoride

2 g sodium molybdate, $Na_2MoO_4 \cdot 2H_2O$
5 ml 35% hydrochloric acid, HCl
1 g ammonium bifluoride, NH_4FHF
100 ml distilled water, H_2O

Can be used for etching both aluminium and titanium alloys.

Notes on use of these reagents for color etching and tinting of copper alloys

Pre-etching, which is sometimes necessary, should be carried out with 10% ammonium persulfate solution, after which selenic acid etchant or thiosulfate/acetate etchant can be employed. In either case it can be difficult to follow the change of colors in very small samples. The pre-etched sample should be immersed in the interference etchant and the color change observed. The sequence of colors should be from yellow, orange, red, violet blue and finally bright silver. Etching should not be allowed to continue beyond the blue or violet stage.

Chromic acid/sulfate etchant should be used without pre-etching and is useful for improving grain contrast. The thiosulfate/acetate etchant, for example, when used on an α–β brass results in the α grains turning light green, while the β grains become orange-yellow. With a 5% cast tin bronze, the dendritic α regions are colored blue, yellow, or brown depending on orientation; the $\alpha + \delta$ eutectoid can also be colored brown in the thiosulfate/acetate etchant (after pre-etching in ammonium persulfate).

Mounting resins come in different types and some manufacturers offer several grades for different purposes. The most suitable are epoxy or polyester resins that have been specially adapted for metallography or mounting of small specimens.

Two suitable resins used by the author are given as examples, one an epoxy resin and the other a polyester.

Epoxide

Manufactured by Buehler Ltd., 41 Waukegan Road, P.O. Box 1, Lake Bluff, Illinois 60044, U.S.A.

Epoxide 20-8130-032, with hardener 20-8132-008, is a cold-mounting epoxy resin system which is excellent for almost clear mounts for metallographic samples. The resin adheres well to samples and shows a very low shrinkage rate during curing. It sets in about eight hours at room temperature. Although the setting time can be inconvenient, it is better to wait for room-temperature curing than to speed up the process by curing in an oven at a higher temperature; shrinkage would be more likely to occur. Buehler Ltd. also manufactures a complete range of good quality metallographic equipment and many other resin types.

Polyester

Scandiplast 9101 UK Distributor:
(Hardener 1% Scandiplast 9102)
Manufactured by Polaron Equipment Ltd., 60-62 Greenhill Crescent, Holywell Industrial Estate, Watford, Hertfordshire, U.K.

This polyester resin, which is green, can be used as an embedding resin for sample examination in reflected light or as an adhesive for some applications. Scandiplast 9101 is used with a peroxide catalyst, Scandiplast 9102. One drop of catalyst is added for each milliliter of resin. Stirring should be carried out carefully and not violently so that air bubbles are not incorporated into the resin. The polyester must be used within six to eight minutes; it can achieve a workable hardness after 45 minutes. The polymerization of the resin can be accelerated by heating to about 45 °C. In fact, the manufacturers recommend heating because extended hardening time at room temperature may result in some surface oxidation, which can lead to incomplete polymerization and a lowered chemical resistance of the cured resin, although this is rare. Similarly, to avoid a tacky surface on the set resin, it should remain in the mold until it cools down to room temperature. This prevents oxidation reactions at the surface of the hot resin. Because of excessive heat generation, the resin should not be cured in a drying oven or any similar closed container.

The sample should be thoroughly cleaned and degreased; this will aid in the adhesion of the polyester resin to the sample. Scandiplast 9101 will cure fully after eight hours and can be ground and polished to give a perfectly adequate mounting material. The manufacturer maintains that there will be a complete absence of air bubbles in the cured resin, but this is not always the case. In any event, care must be taken when pouring the resin into the mold so that air bubbles do not become trapped on the surface of the sample, since they will interfere with the production later of a scratch-free surface by retaining abrasive particles.

To ensure particularly good edge retention of the sample, a small amount of the resin can first be made up and poured into the bottom of the mold to form a layer about 1–2 mm deep. Once this layer has cured, the mold is then filled up in the usual way. (For further details concerning the molds and sample preparation see Chapter 9, p. 43.) The best molds are made of silicon rubber; Polaron Equipment supplies Scandiform embedding molds which are excellent for this purpose as the Scandiplast resin is easily removed from the silicon rubber surface.

Scandiplast 9101 is not suitable for vacuum impregnation, and if a vacuum-potting technique is necessary a low-viscosity epoxy resin is preferable.

Metals are rather different from minerals in that Mohs' scale of hardness cannot be used accurately to assess the hardness of a metal. Usually, methods must be used that deform the metal in a hardness-testing machine under a certain load, employing a specially shaped indenter to press into the surface of the metal.

An early method, avoiding the need for deformation at the surface, was to drop a steel ball onto the surface of the object and measure the distance that the ball rebounded after impact. Although this device, called the scleroscope, is now a historical curiosity, some early archaeological reports refer to this method of hardness testing, thus its mention here.

Brinell hardness testing (H_B) was the first method to find universal acceptance. With this technique, a steel ball of known diameter is forced into a metal surface under a certain applied load. The diameter of the impression left on the surface can be measured accurately and a scale of hardness calculated. Subsequent industrial developments have brought other scales and methods into operation, such as the Rockwell method (H_R), the Knoop method (H_K), and the Vickers method (H_V). The only suitable scales for archaeological metals are the Brinell and the Vickers scales. The Vickers method utilizes a four-sided, 136°, diamond pyramid indenter and the results of the scale are sometimes quoted as DPN numbers (from Diamond Pyramid Number). This is the same as the H_V, merely being a different abbreviation for the result. The Brinell and Vickers scales are roughly the same, although for accurate work they differ and a table of equivalents must be resorted to for some comparisons (see *The Metals Handbook,* 9th Edition for the most recent information).

Macroscopic scale hardness tests leave impressions in metal that can be seen with the naked eye—in most ancient metals, sound metal is not found at the immediate surface and hardness testing must usually be carried out on a micro rather than a macro level on a polished and mounted section using a special microhardness testing machine. Microhardness testers usually operate on the Vickers scale and are available as attachments for inverted stage metallurgical microscopes, such as the Vickers metallurgical microscope, or as attachments for stage microscopes that use reflected light.

One such instrument is the McCrone low-level microhardness tester which can be attached to the Vickers metallurgical microscope. Four readings of the hardness of a sample are taken, the sample must be mounted in embedding resin in a 1" or 1-1/4" mold and the surface must be polished, otherwise the impression of the indenter may not be visible.

The exact relationship between the macrohardness and the microhardness of a particular sample may be difficult to compare because of a number of complications that may arise. One example is grain size: if the microhardness indentation falls across only one or two grains it may not compare with a macrohardness reading which averages the result of deformation over many grains and grain boundaries.

APPENDIX A | COMMON MICROSTRUCTURAL SHAPES

Figure 85. Shapes of ferrite in low-carbon steels.

grain boundary allotriomorphs

Widmanstätten side plates

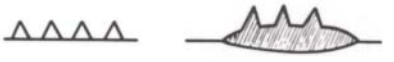

Widmanstätten sawteeth

idiomorphs

intergranular Widmanstätten plates

massed ferrite

Figure 86. Common descriptive terms.

equi-axed hexagonal grains

annealing twin

strain lines (slip lines)

mechanical twinning

intracrystalline (also known as transgranular) crack

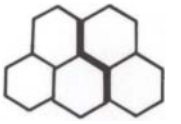

intercrystalline (crack)

polygonal

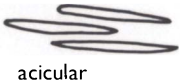

acicular

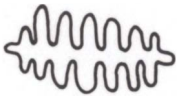

dendritic

banded

fibrous

nodular

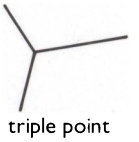

triple point

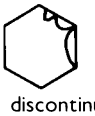

discontinuous precipitate

continuous precipitate

martensitic (needle-like)

Widmanstätten precipitation

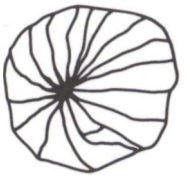

columnar grains

lenticular

fusiform

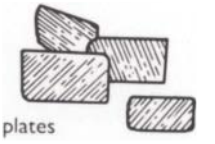

plates

botryoidal

rhomboidal

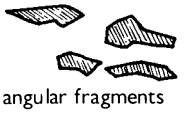

angular fragments

APPENDIX B MICROSTRUCTURE OF CORRODED METALS

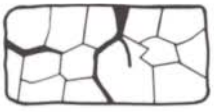

intergranular corrosion

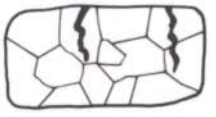

intragranular corrosion

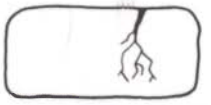

stress-cracking corrosion

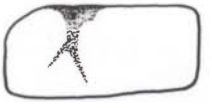

selective corrosion (parting)

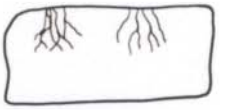

cavitation corrosion

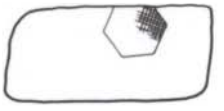

slip lines outlined by corrosion

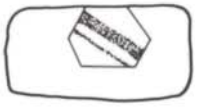

twin lines outlined by corrosion

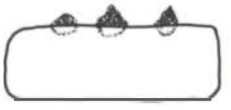

warty corrosion

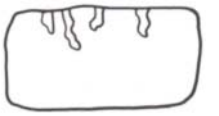

pitting corrosion

uniform corrosion through metal

selective corrosion

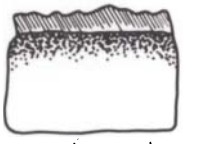

corrosion products over the original surface

remnant metallic grains in a mass of corrosion

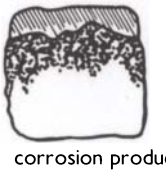

corrosion products and disruption of the surface

APPENDIX C Microhardness Values for Different Alloys and Metals

The values given in the tables below for the variation in microhardness of some of the copper-based alloys illustrate the advantages of using tin bronzes for obtaining hard materials. The increase in the Brinell hardness for arsenical copper in the range of 1–3% arsenic is of some interest, since the proportion of arsenic included in the alloy beyond the 3% level has relatively little effect on the ability of the alloy to be hardened any further by working.

This is in contrast to the tin bronzes where increasing amounts of tin produce successively harder alloys when they are cold-worked. An even greater effect is noticed when the tin bronzes are compared with low-zinc-content brass and cupro-nickel alloys, both of which are not greatly hardened by cold-working at the 50% reduction level. These figures have a practical importance. The color of the product upon casting may be strongly affected by inverse segregation of arsenic to the surface of the mold but as far as strength or hardness is concerned there is little or no advantage in having 7% arsenic in the alloy compared with 3% arsenic. It should be borne in mind from a practical point of view, that it is very difficult to compare the results of hardness tests on ancient alloys where different hardness scales have been used.

The scale used should always be specified and the same scale employed whenever possible for all comparisons with similar materials in different degrees of working or composition.

The following list gives some values or ranges for the microhardness of materials of interest in the Vickers Scale (H_V), which is one of the most generally useful scales.

Metal or Alloy	H_V
pure copper, cast	40–50
pure copper, worked and annealed	50–60
pure copper, cold worked	100–120
70:30 brass, annealed	50–65
70:30 brass, cold worked	120–160
gunmetal, cast	65–70
1.8% arsenic copper, cast	48
1.8% arsenic copper, worked	65–70
2.6% arsenic copper, cast	65–70
2.6% arsenic copper, worked	150–160
cast leaded bronze, 10%Sn 5%Pb	70
cast leaded bronze, 10%Sn 10% Pb	65
cast leaded bronze, 9%Sn 15%Pb	60
pure lead	3–6
pure tin	6–10
pure aluminium	14–22
pure silver, cast	15–30
silver, work hardened	80
20% copper 80% silver, annealed	45–50
40% copper 60% silver, annealed	45–50
60% copper 40% silver, annealed	65–70
80% copper 20% silver, annealed	65–70
12% tin bronze, fully worked	220
0.45% C steel, water quenched	546
0.45% C steel, annealed 400 °C	418
0.45% C steel, annealed pearlite	184
0.55% C steel, water quenched	876
0.9% C steel, water quenched	965
0.93% C steel, normalized	323
0.93% C steel, water quenched	836
ancient file, tempered martensite	535
ancient arrowhead, tempered martensite	390
knife blade, tempered martensite	720
ancient saw, ferrite	185
mortise chisel, ferrite	129
axe, pearlite and ferrite	269
sickle, pearlite and ferrite	171

Hardnesses of some important alloys on the Brinell Scale (H_B) in the 50% reduction cold-rolled (i.e., worked) condition and in annealed condition.

Alloy	H_B	
	50% Reduction	*Annealed*
Bronze		
1% Sn	110	50
2% Sn	115	52
3% Sn	130	54
4% Sn	140	59
5% Sn	160	62
6% Sn	178	72
7% Sn	190	80
8% Sn	195	82
Arsenical copper		
1% As	118	50
2% As	138	51
3% As	144	52
4% As	146	53
5% As	148	54
6% As	148	55
7% As	149	56
8% As	150	58
Cupro-nickel alloys		
1% Ni	102	52
2% Ni	104	52.5
3% Ni	108	53
4% Ni	110	54
5% Ni	112	55
6% Ni	114	56
7% Ni	119	57
8% Ni	121	58
Brass alloys with low zinc content		
1% Zn	102	51
2% Zn	104	51.5
3% Zn	106	52
4% Zn	107	52.8
5% Zn	110	53
6% Zn	112	54
7% Zn	114	55
8% Zn	118	56

APPENDIX D | ALLOYS USED IN ANTIQUITY

Copper

- copper-tin (bronze); also high-tin bronzes such as safídruy and speculum)
- copper-arsenic (arsenical copper or arsenic bronze)
- copper-antimony
- copper-zinc (brass)
- copper-silver (shibuchi)
- copper-gold (tumbaga, shakudo)
- copper-zinc-lead (bidri)
- copper-zinc-tin (latten, sometimes Pb)
- copper-cuprous oxide
- copper-tin-arsenic
- copper-nickel (cupronickel)

Gold

- gold-mercury (amalgams)
- gold-copper (tumbaga)
- gold-silver (electrum)
- gold-platinum (sintered alloys)
- gold-iron (Egyptian rose golds)
- gold-lead (sometimes used for gilding)

Silver

- silver-copper
- silver-gold
- silver-lead (sometimes from cupellation)
- silver-silver oxide
- silver on iron (example of gama hada)

Iron

- iron-nickel (meteoric/unusual ores)
- iron plus slag (wrought iron)
- *Iron-Carbon Alloys*
  - grey cast iron (free C)
  - white cast iron (no free C)
  - *Steels*
    - hypereutectic (>0.8)
    - hypoeutectic (<0.8)
- iron-nitrogen (nitriding)
- iron-hydrogen (embrittlement in steels)

Lead

- lead-tin (soft solders, ancient pewters)
- leaded bronzes, brasses, etc.
- lead-gold (for gilding)

Tin

- tin-lead (ancient pewters)
- tin-antimony (modern pewters)
- tin-copper (e.g., coatings, such as Cu_6Sn_5)

APPENDIX E | TERMS AND TECHNIQUES IN ANCIENT METALWORKING

Joining Techniques

Mechanical Joins

- crimping
- overlapping seam
- overlapping sheets
- riveting
- tab-and-slot

Metallurgical Joins

- brazing
- hard soldering
- fusing welding (2 parts locally heated)
- fusion weld
  - filler of same composition in solid state
  - filler of same composition in liquid state
- pressure welding (solid state)
- reaction soldering (as in granulation)
- soft soldering

Surface Treatment Techniques

Surface Coloration

- chemical solution treatments
- gold powder in binding medium
- pigments and dyestuffs

Surface Coatings

- amalgam gilding
- arsenic coatings
- fusion gilding
- gold-iron alloys
- gold or silver electrochemical deposition
- leaf gilding
- platinum coatings
- silver coatings over copper
- tin coatings

Surface Enrichment

- depletion gilding of Au-Cu alloys
- depletion silvering of Ag-Cu alloys
- gravity segregation
- inverse segregation
- natural corrosive processes
- selective surface etching
- selective surface removal

Casting and Working Techniques

Casting

- casting on
- lost-wax
  - solid
  - over a core
  - from a master matrix
  - other refinements (e.g., mold carving)
  - centrifugal casting
- open mold
- piece mold
  - two-piece
  - multi-piece
- slush casting

Working

- annealing
- chasing
- cold-working
- drawing
- engraving
- filing
- hot-working
- machining
  - turning
  - drilling
  - boring
  - milling
- piercing
- punching
- quenching
- raising
- repoussé
- spinning
- stamping
- tempering

This section contains a miscellany of microstructures with a limited amount of information concerning the composition of the objects studied. Most of the microstructures have been chosen because they are of good quality and illustrate a wide range of features seen in ancient metallic alloys, many of which have no modern equivalent. It would be ideal if the section included representations of the full range of microstructures to be found in ancient and historic metalwork, but this is very difficult to achieve. The selection that follows is therefore somewhat arbitrary, but includes a good range of copper alloys, iron, and steel, and some examples of silver and gold alloys.

The Metals Handbook, Volume 9, published by the American Society for Metals, includes many microstructures relevant to the study of ancient metals and the 9th edition has been expanded to cover precious metals, such as silver, so that the text is more useful to a broader audience. In order to make this appendix accessible, examples are indexed with regard to type of microstructure, alloy, object, and period or provenance. These appear in italic type in the index at the back of this volume.

Figure 87. Base silver-copper alloy coin of Skandagupta, Western India, c. A.D. 470. 11 mm.

Silver-copper alloy coin

This is a late and degraded form of the drachm, whose origins may be traced back over 600 years to the Indo-Greek kings. This coin bears the king's head on the obverse side and a fire altar on the reverse. It is small, thick, and struck in a much-debased silver-copper alloy that was almost certainly surface-enriched by pickling, resulting in copper depletion at the outer surfaces.

In the unetched condition, the two-phase nature of the coin can be seen, although it becomes much more evident upon etching in either potassium dichromate or ferric chloride. The dendrites, which are silver-rich, are not continuous, indicating a rather low silver content, about 18%, analogous to other struck silver-copper alloy coins. The silver-rich phase is elongated and flattened along the length of the coin. Also, the contours follow the depressions in the surface suggesting the coin was struck while hot. The corrosion is quite limited and does not extend much below the surface into the interior of the alloy.

Figure 88, top. Low magnification showing part of the struck surface. Note the curvature in the structure as a result of deformation. Etch: $FeCl_3$; x32.

Figure 89, bottom. The copper-rich grains can now be seen with the flattened remnants of the silver-rich phase passing along the length of the coin. Note the dendritic remnants are not continuous but occur as discrete elongated plates. From similar cast and worked sections, the silver content can be roughly estimated at about 15–20%. Etch: $FeCl_3$; x123.

Figure 90, above. Islamic inlaid inkwell from the eastern Iranian province of Khurasan.

Figure 91, top right. Coring is evident, as are some globules of lead. The larger dark holes are porosity in the alloy. The structure is difficult to interpret fully because of coring. Some strain lines are visible (near bottom right). Etch: $FeCl_3$; x63.

Figure 92, middle right. Overall view of the section at x21 etched in alcoholic $FeCl_3$ showing coring, lead globules, and complex structure.

Figure 93, bottom right. Some of the second phase areas may be gamma phase from the copper-tin-zinc system which appears as light-colored regions in the picture. The lead globules appear dark grey. Etch: $FeCl_3$; x41.

Islamic inlaid inkwell cast in a copper-tin-zinc-lead alloy

The inlay on this fine inlaid inkwell has been carried out in silver, copper, rock asphalt, and probably, ground quartz. It was made in the eastern Iranian province of Khurasan, probably in Herat during the period from the late 12th through early 13th century A.D. The inkwell measures 103 mm high (with lid) and has a diameter of approximately 80 mm. The composition of the metal used in the manufacture was found to be: copper 65%, tin 5%, zinc 20%, lead 10%, with smaller amounts of iron and silver.

A sample taken from the rim of the body of the inkwell was removed using a fine jeweller's saw. Although there are four major constituents, the alloy can be considered a ternary mix of copper, zinc, and tin because lead is immiscible in copper. There is a random scatter of lead globules visible in the polished section. The section etches well with alcoholic ferric chloride and reveals a cored structure to the grains showing that the inkwell has been cast to shape. The inner areas of each grain are richer in copper and the outer areas richer in zinc and tin. Also evident in this section are a number of holes that are due to some porosity present in the casting. The prominent coring shows that the inkwell was not extensively worked or annealed following fabrication. However, some strain lines can be seen near the surface suggesting some final working in the as-cast condition, probably due to chasing of the surface to receive the inlaid metal strips (see Plate 11).

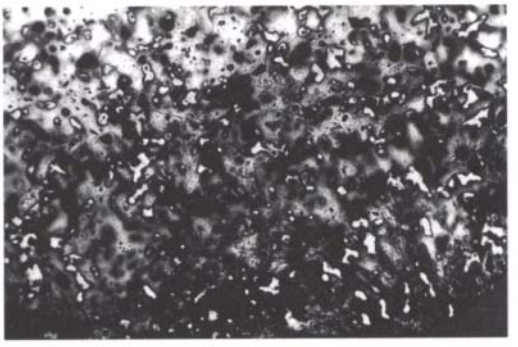

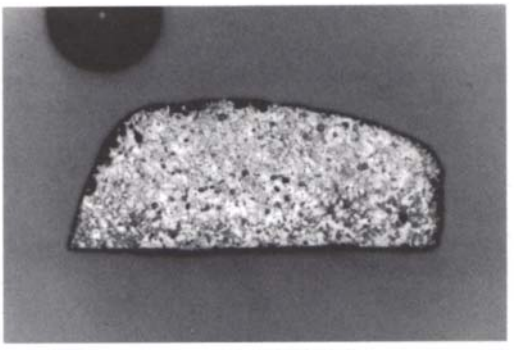

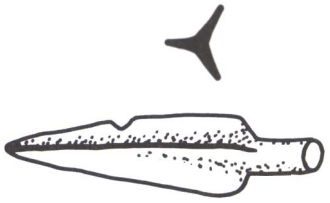

Figure 94. Drawing of cast bronze arrowhead from Palestine.

Cast bronze arrowhead

This arrowhead is from Palestine and was excavated by Sir Flinders Petrie between 1930 and 1938 from the site at Tell Ajjul. During his excavations Petrie found many artifacts associated with buildings and graves dating to the early XVIIIth Dynasty. This arrowhead, as well as the Palestinian bronze sword (below), were found during the excavations.

The composition of the arrowhead is a ternary copper-tin-arsenic alloy with some lead present (Ghandour 1981): Sn 9.86%, Pb 1.49%, As 3.87%, Zn 0.85%, the remainder copper. The arrowhead is 30 mm in length and triangular in shape with three fins and a hole for the socket on the tang.

The microstructure of the arrowhead can easily be observed after etching in ferric chloride for 3–5 seconds. The central region of the arrowhead as well as the three fins, which are seen here in section, all have the same undistorted, cast, dendritic pattern. This is clear evidence that the arrowhead was cast in a mold directly to shape and that the fins were not beaten out or work-hardened after manufacture. At low magnification, very long and finely developed dendrites can be seen together with some of the interdendritic eutectoid infill. The eutectoid itself is difficult to resolve, some structure becoming apparent at x600.

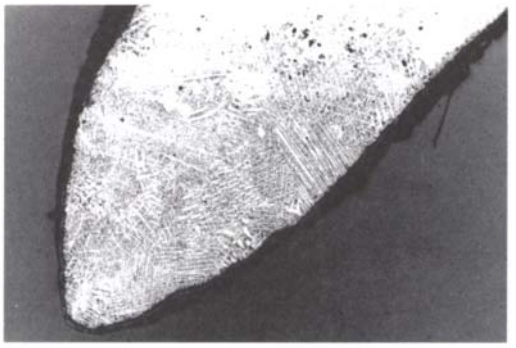

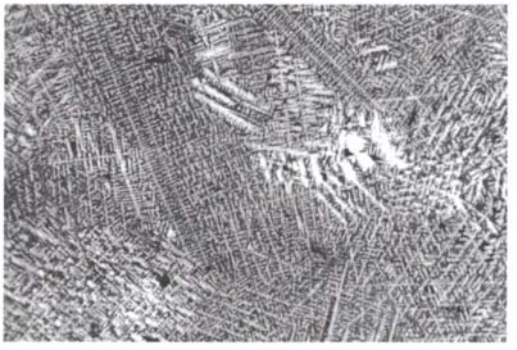

Figure 95, top. Fine, very long, and undistorted copper-rich dendrites with eutectoid infill of $\alpha + \delta$ phases between the arms. Note the occasional interdendritic pores. Etch: $FeCl_3$; x32.

Figure 96, bottom. The dendritic structure is clear and the occasional $\alpha + \delta$ eutectoid areas are more resolved at this magnification than at x32. Etch: $FeCl_3$; x65.

Figure 97. Drawing of Late Bronze Age sword. Etch: $FeCl_3$.

Palestinian bronze sword

This sword is dated to the Late Bronze Age. It has an intact tang rectangular in cross section and a blade about 285 mm long and 31 mm wide at the maximum width. There is a pronounced midrib (see "Cast bronze arrowhead," above, for a brief background reference).

The sword is composed of Sn 8.20%, Pb 0.27%, As 0.66%, Zn 1.72%, the remainder copper. In the unetched state, some grain boundaries are evident, as well as quite large but irregularly distributed pores. There are no visible sulfide or oxide inclusions present in this section. Etching

in alcoholic ferric chloride reveals the grain structure to be rather variable. Toward the cutting edge of the sword the grains appear quite large, possibly from over-annealing during some stage in its working. Toward the midrib, the grain size is smaller but still rather variable in size. Some of the grains are clearly twinned with straight twin

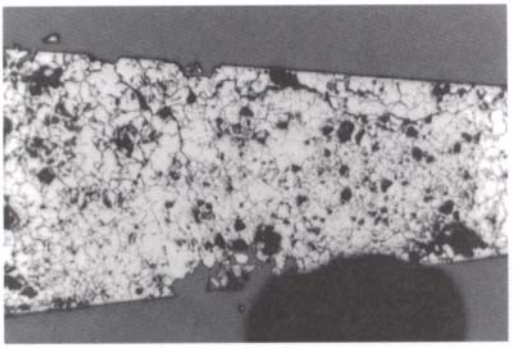

Figure 98, right. Overall view showing intercrystalline cracks, large grains, and some porosity in the section. Unetched; x30.

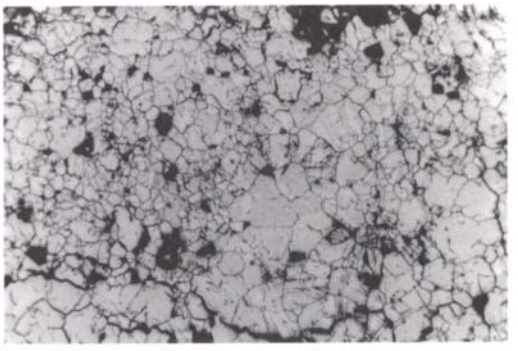

Figure 99, far right. Recrystallized grain structure with twinned crystals and corrosion along slip bands. Etch: $FeCl_3$; x62.

lines, showing that the sword was finished by a final annealing operation. The dark, thick lines that outline most of the grain boundaries are due to corrosion advancing through the alloy in an intergranular form of attack. The copper has also corroded along slip planes within the grains, outlining many slip bands in some parts of the structure. The extent of these slip bands suggests that the final annealing operation was not sufficient to remove the stresses within all the grains as a result of working the sword to shape (see Plate 17).

Roman wrought iron

This sample is a section from a large Roman billet (bar) of iron about 25 x 7 x 7 cm and weighing about 6 kg. It represents the primary forging of the bloom. During this stage of production most of the incorporated slag was squeezed out and the iron was consolidated in preparation for trade or manufacture into functional artifacts.

As with the bloom, this iron can have varying degrees of carburization. Forging can remove or introduce carbon depending on the area of the forge to which the iron is exposed. Near the tuyere (blast of air), conditions are more conducive to oxidization and carbon is lost from the structure. Variable carbon content can be advantageous when iron is forged, since ferrite regions (low-carbon areas) are malleable and easily worked, while pearlitic regions are tougher.

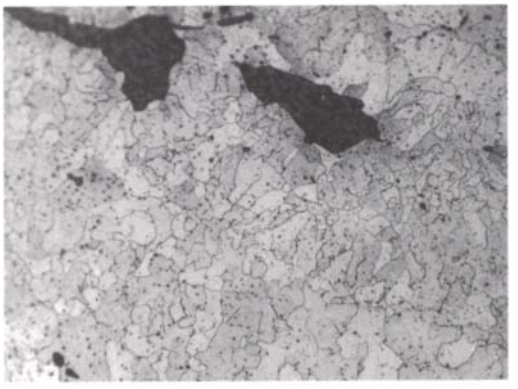

Figure 100. View showing variable grain size of the wrought iron with extensive slag particles and some larger slag fragments. Note that the slag is a two-phased material and typically consists of wüstite (FeO) as rounded dendritic shapes in a glassy matrix. Etch: nital; x83.

Figure 101. Depletion-gilded disc of *tumbaga* alloy showing matte gold and burnished gold surface design made by surface-etching the enriched gold after depletion-gilding. From the Municipio of Pupiales in the Department of Nariño, southern Colombia, and probably dates from the Piartal period, about 10–12th century A.D.

Gold-copper alloy sheet

This fragment is a circular disc approximately 110 mm in diameter. These gold-copper alloys are usually referred to as *tumbaga* alloys. They were usually finished by a depletion-gilding process. This particular fragment has deep-yellow colored surfaces with some patches of purple-brown staining. A circular hole has been pierced through the sheet which shows some fine surface scratches in the metal surrounding the hole. These scratches probably arose as a result of finishing the pierced hole when metal burrs were removed with an abrasive. Analysis of sound metal grains with an electron microprobe analyzer revealed a composition of about 80.6% copper, 17.1% gold, and 2.6% silver.

The polished section shows a typical worked sheet with small grains and a lot of intergranular corrosion. The grains can be etched, with difficulty, in an ammonium persulfate and potassium cyanide mixture that shows the nature of the gold-enriched surface as well. The grains are twinned with most of the twin lines being straight, but a few are not. There are some cuprite inclusions as well as cuprite lamellae running along the length of the section which also appears to be very even in thickness (see Scott 1983).

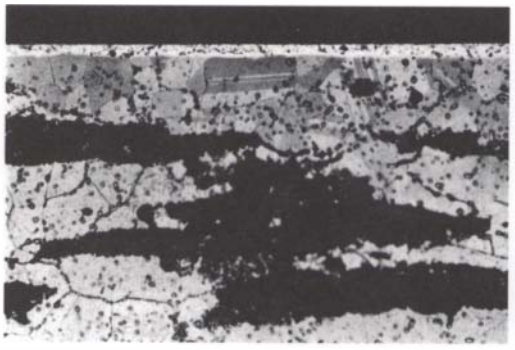

Figure 102. The depletion-gilded structure on the surface of the worked sheet is clearly evident. The etchant has left the gold-rich surface largely unattacked while etching the grains which are now visible as recrystallized with straight twin lines. The alloy is single-phased. Etch: $KCN/(NH_4)_2S_2O_8$; x200.

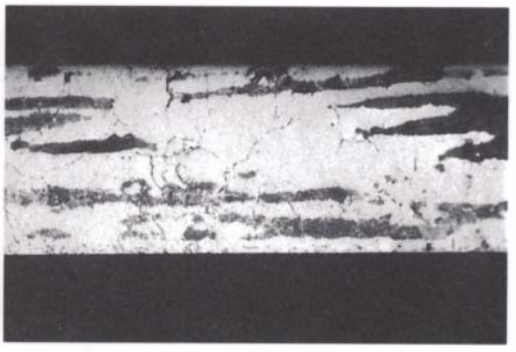

Figure 103. Note the very even thickness of the sheet and the small globules of cuprite that can be seen following some of the grain boundaries. The dark, elongated lamellar regions are caused by some corrosion to cuprite during burial. Unetched; x64.

Ecuadorian copper-alloy nose-ring

The object is one of several metal finds from the secondary chimney urn burial at La Compañia, Los Rios province, Ecuador. It is of intermediate size in the collection of nose ornaments from this burial of the late Milagro phase. The section through the nose ornament shows that the copper incorporates a considerable amount of cuprous oxide inclusions that run along the length of the object in a striated form, typical of worked copper. The nose-ring has on its outside surface a very thick (about 0.1 mm; 1000 microns) coating of a two-phased silver-copper alloy.

There is a very clear demarcation between the applied silver coating and the copper body of the nose-ring. The polished section was etched in alcoholic ferric chloride, resulting in a well-formed twinned crystal structure with perfectly straight twin lines in the copper grains. The grains near the center of the nose-ring are quite large with prominent twinning (ASTM grain size number 2-3), while on the outer surfaces of the nose-ring, which have received slightly greater

hammering and recrystallization during manufacture, the grain size drops to about ASTM 4-5.

The silver coating is a duplex structure consisting of copper-rich islands of alpha phase with an infilling of the copper-silver alpha + beta eutectic in which the eutectic phase forms a continuous network throughout the alloy. The junction between the applied silver coating and the copper base is quite abrupt, and the silver coating has not received anything like the degree of deformation and recrystallization to which the copper has been subjected. It is quite apparent from this fact, and from the very narrow diffusion zone between the silver alloy coating and the copper, that the silver alloy must have been applied at a very late stage in the manufacturing process, i.e., when the nose-ring was practically completed. The copper-rich alpha phase in the silver alloy coating betrays occasional slip lines and a few bent twins are also evident. This suggests some relatively light working and annealing followed by some cold-working of the coating after application to the shaped copper base.

The silver coating has itself been superficially enriched, or depletion silvered, as is apparent from a metallographic examination of the intact surface. This is not uniformly apparent on the section taken because some has broken away during burial as a result of corrosion or during preparation for metallography during the cutting stage. The observation that the silver alloy coating has itself received only slight working and has, essentially, a slightly modified cast structure, means that it must have been applied hot, i.e., in a molten condition, probably by dipping the cleaned nose ornament into a molten silver-copper alloy. The manufacturing process can therefore be almost entirely reconstructed from the metallographic evidence.

1. A raw, cast copper blank, which contained extensive cuprite inclusions as large globules, was worked and annealed in cycles to shape the nose-ring.
2. Oxide scale was removed from the surface to present a clean surface for coating.
3. An alloy of silver and copper was made up containing about 30–40% silver, which melts at approximately 200 °C below the melting point of pure copper. The alloy had to be held in a suitable container whether dipping or surface brush coating was employed.
4. The copper nose-ring was dipped or coated with the molten silver alloy.
5. The nose-ring received some final working to smooth out the silver coating and the surface was cleaned by an acid plant or mineral preparation to remove oxidized copper and to create a good silvery appearance.

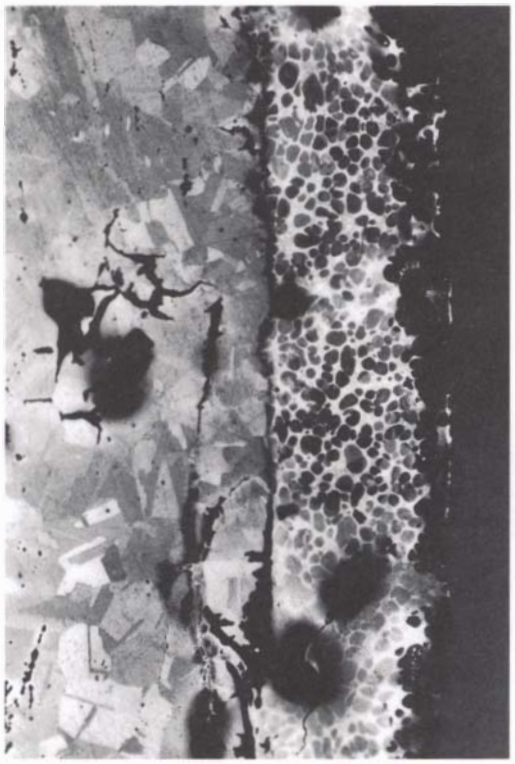

Figure 104, right. View showing the nature of the silver-copper alloy coating over worked and recrystallized grains. A few bent twins in the alpha region of the silver-copper alloy coating suggest some light working following the application of the coating to the shaped nose-ring. Etch: $FeCl_3$; x120.

Figure 105, far right. Lower magnification view in which the twinned grains of the base copper are clearly revealed. The thick silver-copper alloy surface coating is well-contrasted by the ferric chloride etchant. x78.

Figure 106, above. Small copper axe from Guayas, Ecuador. 70 mm.

Figure 107, top right. The structure is surprisingly clean. There is the expected porosity of a cast metal but no oxide or sulfide inclusions. The subtle shading passing across the grains is due to residual coring or the casting that persists despite the twinned grains which are clearly visible. Etch: $FeCl_3$; x32.

Figure 108, bottom right. Note that the twin lines are straight showing that an annealing process was probably the final stage in manufacture. The relatively large grains, the absence of strain lines, and undistorted porosity indicate that the amount of working was not extensive. Etch: $FeCl_3$; x65.

Cast arsenical copper axe

Simple axes of this kind were common, not only in many parts of the New World but also throughout the Old World, and the methods of production and manufacture are essentially the same. Many of these axes were made by casting into simple, open molds. The molds themselves could be made of stone, clay, or metal. It is sometimes possible to obtain evidence for the position of casting by metallographic examination. For example, slag and dross may be segregated to the top surface of an open-mold casting with the result that one side viewed in section looks quite clean while the other may contain more oxide inclusions and gross impurities in the form of debris or slag. This is not the case with this axe, although we know from other examples that axes were cast horizontally into one-piece molds.

Bushnell (1958) believes that the axe is from the Manteño period. Spectrographic analyses showed that the axe was made of arsenical copper with about 1% arsenic content. The other elements detected were present only in very small amounts (all less than 0.05%). These were antimony, bismuth, iron, lead, manganese, nickel, and tin.

It is difficult to cast copper into open molds without extensive oxidation occurring and yet the microstructure of this axe is remarkably clean: there are no cuprous oxide inclusions to be seen. The axe has been cast—that is evident from the pattern of distribution of porosity as well as from the coring resulting from dendritic segregation. Coring occurs as subtle patches of darker etching material that ignores the grain structure and is clearly evident upon etching. The fact that the axe has a recrystallized grain structure with twin lines, as well as coring, and virtually undisturbed porosity, indicates that it was finished by a working and annealing process, probably to improve the shape of the axe rather than to work it extensively. The grains have straight twin lines indicating that the final process was either hot-working or an annealing operation.

The achievement of casting the copper alloy into a mold and making an axe like this with no apparent oxide or sulfide inclusions present demonstrates considerable metallurgical skill.

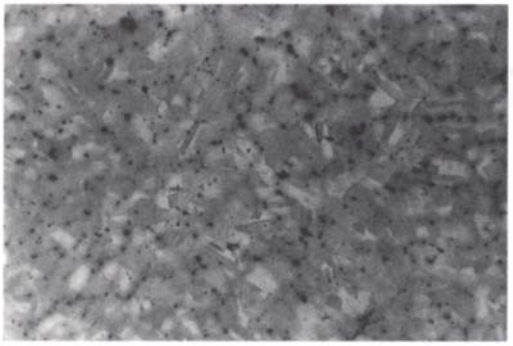

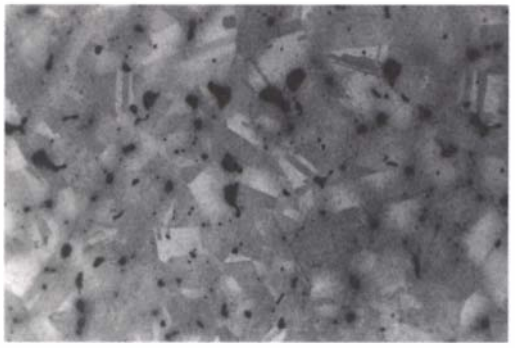

Figure 109. Chinese 19th century ancestral incense burner, usually placed on the ancestral table. Height 190 mm.

Chinese bronze incense burner

The fragment mounted for study shows a cross section through the lid of the incense burner. The sample shows an undistorted cast structure with a fair amount of delta tin-rich eutectoid.

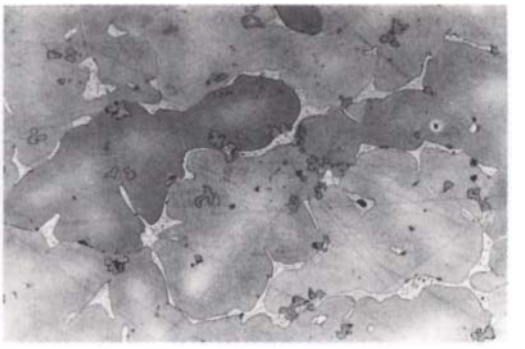

Figure 110. The outline of the equi-axed structure can be clearly seen. The $\alpha + \delta$ eutectoid phase occupies the grain boundaries for the most part, with small cuprite inclusions scattered through the section. This structure is unusual for a normal cast bronze and indicates annealing. Etched in alcoholic $FeCl_3$; x98.

Thai bronze cast bell

A bronze bell from Ban Don Ta Phet (see Rajpitak 1983) with a smooth surface and dark green patina, cast by the lost wax process. The composition is Cu 85.6%, Sn 3.5%, Pb 15.5%, As 0.1%, Ag 0.3%, Ni 0.1%, Co 0.01%. The microstructure shows the bell was cast in one piece. It has a coarse dendritic structure with extensive porosity which is evident in the section.

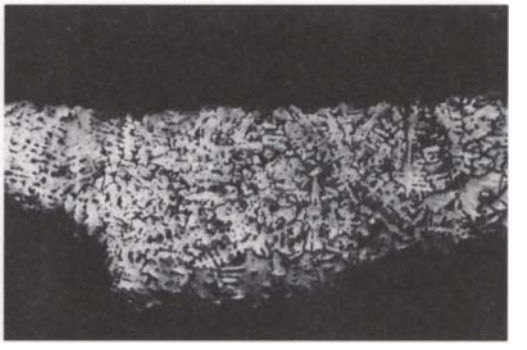

Figure 111. Note the large, coarse dendrites, the extensive corrosion, especially toward the bottom, and the segregation of the lead and tin to the interdendritic areas. Etch: $FeCl_3$; x35.

Luristan dagger handle

The materials used to make the handle and blade were well-chosen. The tin content of the handle is about 20%, while the hilt of the blade has a tin content of about 13.5%. The casting-on of the handle over the finished blade involved the use of a clay mold built up around the blade into which molten bronze was poured.

It is important that the alloy used in casting-on has a lower melting point than the metal to be incorporated in the cast-on product. This was facilitated in this case by the careful selection of materials. The blade has a worked microstructure, but the structure of the hilt incorporated into the handle is an annealed casting. The hilt is equi-axed compared with the heavily dendritic structure of the handle.

The redeposited copper that occurs in the crevice between the two components may have been caused by low oxygen availability in corrosive burial environments. That sort of situation would be ideal for this form of corrosion-redeposition phenomena. A slight potential gradient could also be set up between the two components themselves, that is, between the hilt and the blade. Redeposited copper also replaces delta, tin-rich regions in the hilt (see Plate 10 and Figs. 69–70).

Figure 112. Fragment of a Luristan blade from Iran: Cu 76.6%, Sn 20.8%, Pb 0.9%, Ni 0.5%. The handle was cast-on in a tin-rich bronze; analysis of the dagger hilt yielded: Cu 83.6%, Sn 13.5%, Fe 0.3%, Pb 0.8%, As 0.4%, Ni 0.6%. Length 89 mm.

Figure 113. The left side of the photomicrograph is the hilt of the blade, while the region on the right is the cast-on handle of the dagger. The irregular strip between the two regions is redeposited copper resulting from corrosion of the bronze. This is the result of the corrosion of the $\alpha + \delta$ eutectoid phase in the higher tin content alloy of the handle. x90.

Fragment of a Thai bronze container

This fragment is part of a circular container with a polished outer surface and a rough inner surface. Also, the alloy is corroded on the surface, rim, and part of the body. The diameter is approximately 3.4 cm and the thickness of the metal about 1.5 mm.

The object is one of a group of metal finds from Ban Don Ta Phet, a village in the Amphoe district of Phanom Thuan, Kanchanaburi Province, southwest Thailand. The date of the site is thought to be about 300–200 B.C. The composition of the alloy was determined by inductively-coupled plasma spectroscopy as Cu 70%, Sn 22.19%, Pb 0.3%, As 0.03%, Sb 0.01%, Fe 0.03%, Ag 1.2%.

Examination of the container reveals a well developed dendritic structure with an infilling of a matrix that appears superficially to be scratched. However, this structure is due to the development of a martensitic structure in the bronze as a result of quenching the bronze alloy following casting. The quenching procedure prevents the bronze alloy (which is high-tin) from decomposing into the usual alpha + delta eutectoid structure. This was carried out as a deliberate process in the manufacture of the container with the result that the

Figure 114, top right. Cast dendritic structure of cored alpha grains with an infill of beta-phase needles. There seem to be two types of needles present: fine martensitic needles and thicker lenticular needles. Etch: $FeCl_3$; x62.

Figure 115, bottom right. Enlarged view of the same area in which the beta martensitic structure is clearly visible. The needlelike martensitic phase is designated β_1 and the dendritic copper-rich phase is the alpha. Microhardness measurements were made and gave results of 188 H_V for the dendritic phase and 227 H_V for the beta phase. Etch: $FeCl_3$; x250.

delta-phase formation is suppressed and, instead, a beta-phase martensite grows due to the retention of the high temperature beta phase. The microstructure makes it possible to reconstruct the manufacturing process of the container. The object was first cast in a mold. After casting, it was briefly annealed and then quenched. The temperature at which the quenching was carried out is estimated to have been 586–798 °C.

The needlelike martensitic phase is designated as beta, and the dendritic copper-rich phase is the alpha. Microhardness measurements were made and gave results of 188 H_V for the dendritic phase and 227 H_V for the beta phase.

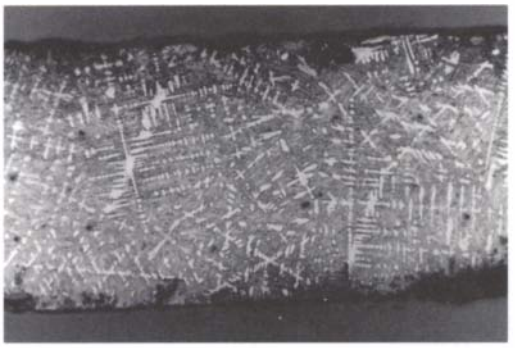

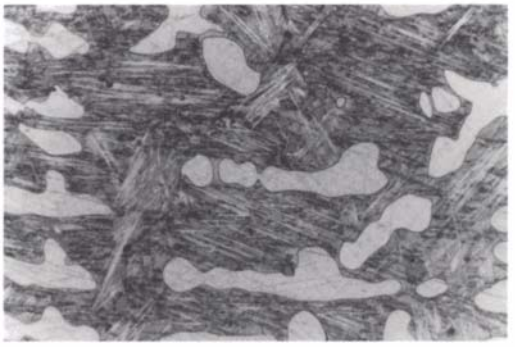

Figure 116. Part of an ear ornament from the Sinú zone in northwestern Colombia. 42 mm.

Colombian cast Sinú ear ornament

This type of fine filligree ear ornament was originally thought to be made by the soldering together of a number of wires. However, metallographic examination has proven that they were made by the lost-wax process.

The section cut transversely through the ear ornament shows the cast nature of the gold-copper alloy.

The loop for suspension is slightly uneven at the top, as is common in many other ear ornaments from this area, showing that the probable casting position was with the funnel and channels situated above the suspension loop, attached to it at the uppermost point.

The polished section shows an undistorted cast dendritic structure in which considerable corrosion has taken place. An estimation of the dendritic arm spacing gave a value of 33 microns averaged over nine arms (Scott 1986). Analysis yielded: Au 16.9%, Cu 71.2%, Ag 1.7%, Pb 0.07%, Fe nd, Ni nd, Sb nd, As nd (nd = not detected).

Figure 117. The orientation of the corroded copper-rich region of the cored dendrites reveals the original cast structure of the gold-copper alloy. Structures like this are difficult to etch satisfactorily with either KCN/$(NH_4)_2S_2O_8$ or HNO_3/HCl. $FeCl_3$ alone will only etch copper-rich gold alloys with up to about 30% gold by weight. Unetched; x36.

Cast iron cannonball from Sandal Castle

This polished fragment is a section from a cannonball used in the siege of Sandal Castle in 1645 between July and September of that year. One of the reasons for examining these cannonballs is to see if there are any differences between the 64-pound balls brought from Hull specially for the purpose, and the 32-pound cannonballs used earlier in the campaign. The structure of both types, in fact, proved to be the same. (Further details concerning the history and the cannonballs themselves can be found in Mayes and Butler 1977.)

Examination of the sample shows the cannonball to be made of a fairly typical grey cast iron. The structure consists of rather variable-sized but quite large graphite flakes set in a matrix that is principally pearlite. Some of the pearlite eutectoid is very finely spaced and is barely resolvable at x1 000 magnification. Much pearlite can clearly be seen, however, and there are a few areas that look ferritic. In some places, a white phase can be seen that has a patchy appearance with small globular holes. This is a ternary phosphide eutectic between ferrite (usually with a little phosphide content), cementite, and iron phosphide, Fe_3P. This ternary eutectic, called steadite, has a melting point of about 960 °C (Rollason 1973) and so it is the last constituent to form as the cast iron cools down. It is a very brittle phase, but is usually only present in small amounts scattered as isolated islands (see Plate 13).

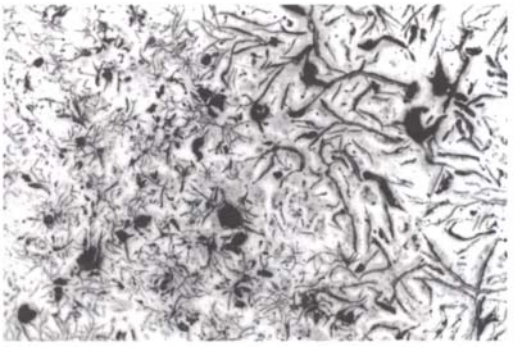

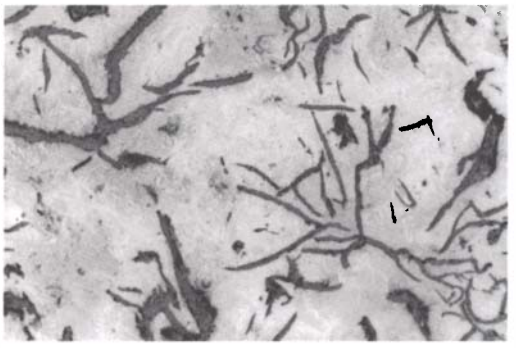

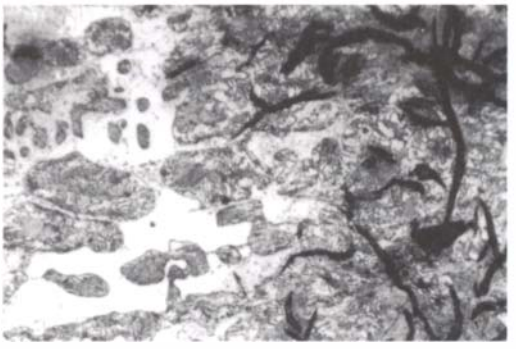

Figure 118, top right. Overall view showing the large graphite flakes with infilling of pearlite and the white, unetched ternary phosphide eutectic, which cannot be readily resolved at this magnification. Etch: nital; x70.

Figure 119, middle right. Fine pearlite with variations in the size of the graphite plates. Etch: nital; x150.

Figure 120, bottom right. The pearlite is clearly visible. Some pearlite regions have very fine spacing and appear grey. The white phase on the left is the phosphide eutectic, steadite, while carbon, in the form of graphite flakes, appears as dark lines. Etch: nital; x390.

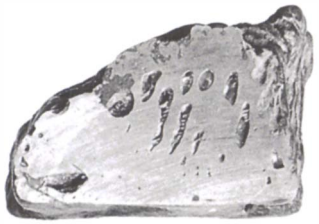

Figure 121, above. Copper ingot found in association with Bronze Age material in Hampshire, England. 27 mm.

Figure 122, right. Overall view showing the large grain boundaries and the scatter of cuprite globules at the grain boundaries and within the grains. Note also the presence of some porosity in the ingot and the absence of any twin lines or strain lines in the copper grains. Etch: $FeCl_3$; x105.

Bronze Age copper ingot

The small plano-convex ingot illustrated here was sectioned. It is typical of the convenient products used for trading cast copper. The cut face shows a columnar appearance, which suggests directional solidification. XRF analysis detected a small amount of nickel as an impurity in otherwise pure copper.

The microstructure shows a remarkable scatter of cuprous oxide inclusions. Grains are large (ASTM 1-2), with no annealing twin or slip lines present, indicating that the copper was cast. The purity of the copper explains the absence of coring and visible dendrites. The large and numerous globular oxide inclusions occur both within the grains and as slightly lenticular shaped discs that run along the grain boundaries. There is some porosity present. With this particular cast ingot, the copper produced would need refining or remelting and alloying before being used to produce small artifacts because of the unusually high cuprite content, otherwise the grain boundaries of the material would be very weak.

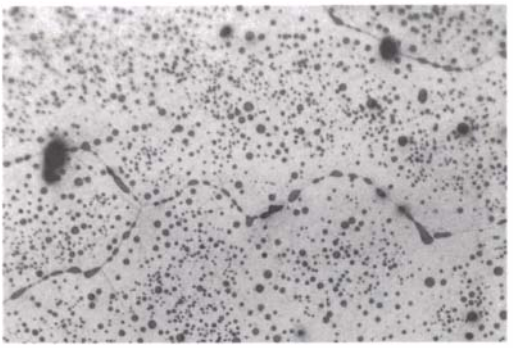

Figure 123. This Roman brass coin is from the period of Augustus, who reigned during the first century A.D. 48 mm.

Roman brass coin

Many Roman coins were made from brass rather than bronze. The microstructure of this coin, etched with ferric chloride, shows a typical recrystallized grain structure with extensive evidence of deformation produced in the process of striking the coin. Both twin lines and slip lines can be seen in the sections. Many fine sets of parallel slip (or strain) lines can be seen, both at x66 and x132 magnification. Some of the twin lines are more difficult to observe, and there is some variation in their appearance. Many of the twin lines seem quite straight, while others seem curved, indicating either hot-working or some cold-working after the final stage of recrystallization. Since the usual manufacturing technology involved striking heated coin blanks, there may be a dual character to these type of structures.

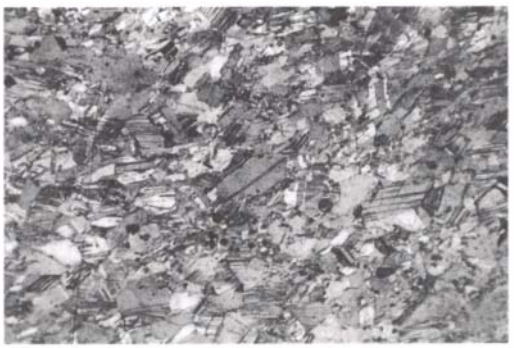

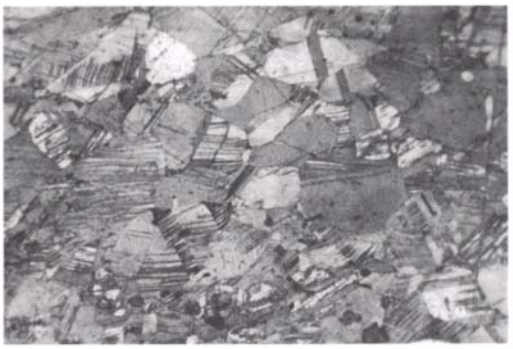

Figure 124, top. Roman brass. Etch: $FeCl_3$; x66.
Figure 125, bottom. Same as Figure 120. Etch: $FeCl_3$; x132.

Thai bronze container fragment

This is a fragment from the rim of a Thai bronze container from the site of Ban Don Ta Phet with an associated radiocarbon date of 1810 ± 210 B.P. The alloy is 77.22% copper, 22.7% tin, with traces of iron and lead.

Examination of the section reveals alpha-phase copper-rich islands, which are sometimes jagged and occur in areas with specific orientations as well as random scatter. The background matrix of these alpha-phase copper islands is difficult to establish. It could be either gamma phase or a homogeneous beta phase. Banded martensite is present and this modification is sometimes called beta'. The acicular martensite is often labeled as $beta_1$.

Judging by the microstructure and composition, one can say that the object was probably cast initially and then allowed to cool. It was then heated to between 520 and 586 °C, which corresponds to the alpha + gamma region of the phase diagram. After annealing, the container was quenched, preserving some of the high-temperature beta phases.

Microhardness readings from the two principal phases gave the following results: alpha phase, 257 H_V; gamma or beta grains, 257 H_V.

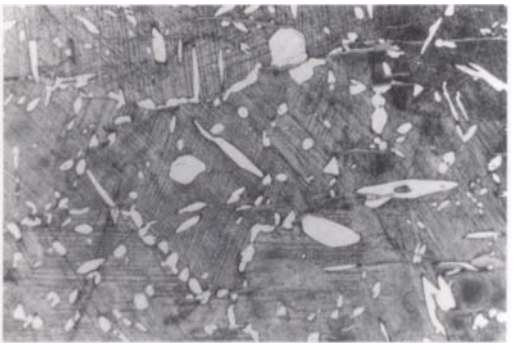

Figure 126, top. α-phase islands, some clearly outlining grain boundary regions. Etch: $FeCl_3$; x40.

Figure 127, bottom. The very fine β needles appear to be stain lines, but are not. Note that the orientation of the α precipitates is not random but occurs as grain boundary and as intragranular forms. This form of martensite is called banded martensite. Etch: $FeCl_3$; x280.

Figure 128. Gold necklace bead from Colombia. Calima cultural area.

Gold necklace bead

The bead consists of eight small gold spheres joined together. It comes from a necklace in the collection of the Museo del Oro, Bogotá, Colombia.

This bead weighs 0.245 g and is 2.41 x 2.39 x 2.38 mm. It is from the area of Calima-style metalwork in the zone of the western Cordillera of Colombia. The necklace bead was faceted on two opposing sides after joining.

In the polished state the beads appear to be made of a homogeneous gold-rich alloy. There is some porosity present, mostly as spherical holes, but there are no inclusions present.

Etching is best carried out with a potassium cyanide and ammonium persulfate mix, when the slightly cored dendritic structure can be clearly seen. There are also a few recrystallized grains in the vicinity of the joins between the spheres, showing that the bead was made from eight individual small gold spheres welded together without the use of copper salts to create a granulation mixture. The heating of the positioned spheres had to be carefully controlled to avoid melting the bead entirely.

Analysis by atomic absorption spectrophotometry showed the bead to be made of a gold alloy containing 84.3% gold, 13.3% silver, and 0.8% copper. It is a typical native gold composition for this area of Colombia.

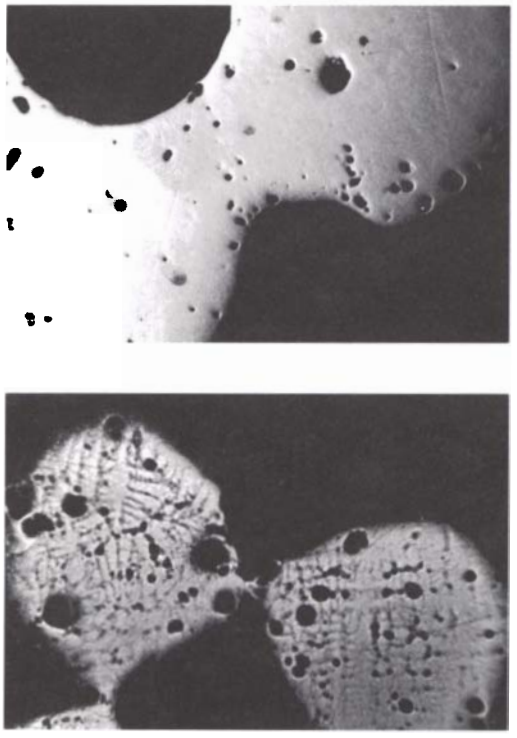

Figure 129, top. Unetched view of join region between spheres showing porosity. x55.

Figure 130, bottom. Etched in cyanide/persulfate showing dendritic structure. x55.

Figure 131. Fragment of a Calima ear spool made in a gold-rich alloy. From pre-Hispanic Colombia. 45 mm.

Gold alloy nail and gold ear spool

The ear spool is made up of sheets of beaten gold that were held to some internal support by means of fine gold nails that pass through the sheets. This internal support, which was probably wooden, has now disappeared, leaving the small nails projecting out on the inside of the sheet. This form of construction is characteristic of the Calima style of working.

A section was cut through the sheet so that a nail could be examined together with the surrounding sheet. The polished section examined showed that the object consisted of three layers of gold sheet. The nail did not appear to have a large head but instead tapered slowly to a point rather like a wedge.

The polished section showed no visible inclusions, little porosity, and no sign of any depletion gilding. The section was etched in a diluted aqua regia which revealed the grain structure.

Large equi-axed grains with prominent twinning can be seen. The twinned grains were slightly deformed by working after the final annealing as the twin lines are slightly curved.

The nail appears to be made of the same gold

alloy as the sheet itself. It has been worked rather more heavily, as the grain size is smaller and there are some flaw lines resulting from lamination of the structure during working.

Microhardness	Weight	Diagonal average	H_V
1	50g	15.5	56
2	50g	16.5	49
3	50g	15.0	60
4	50g	19.0	37
5	50g	16.5	49

Results 1, 2, and 3 were obtained from the nail, with the highest reading of 60 obtained from the nail tip. Results 4 and 5 were taken from the gold sheet and show that the hardness values are quite low. However, it seems unlikely that the nail would be able to penetrate the sheet effectively and the evidence suggests that the sheets were pierced after positioning them and before the nails were applied. Analysis: Au 83.7%, Cu 1.5%, Ag 12.8%, Fe nd, Pt nd, Sb nd, Ni nd, As nd, Pb nd, Si 50 ppm.

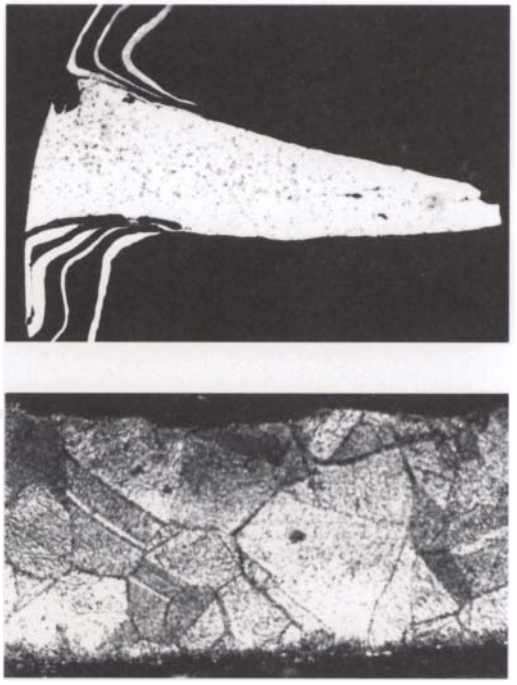

Figure 132, above. Section through a nail showing the folded gold sheet and the overall shape of the nail. x60.

Figure 133, bottom. Gold sheet etched in aqua regia with large twinned grains and bent twins showing some deformation after final annealing. x160.

Blade section

The section through the blade reveals that a steel strip was welded to a principally ferritic strip. Therefore, the variations in structure are due to the change in the rate of cooling and in carbon content between ferrite grains and tempered martensite. The angular holes evident in the microstructure correspond to the position of slag inclusions, many of which have fallen out during grinding and polishing.

A blade forged from a strip of steel and a strip of wrought iron was a fairly common method of manufacture.

Vickers DPN hardness measurements on different constituent areas of the blade gave the following results: ferritic area in the center, 89–93 H_V; tempered martensite towards the edge, 185–294 H_V.

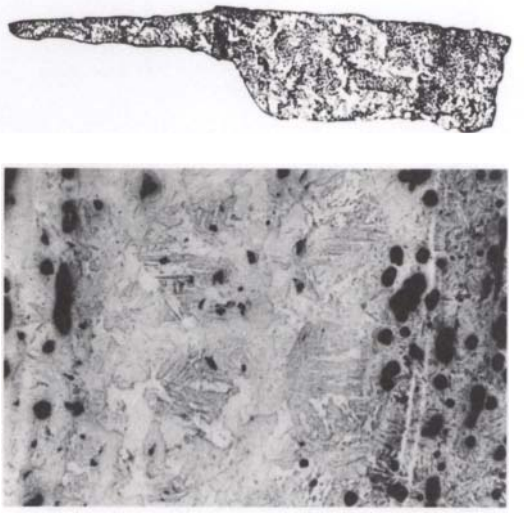

Figure 134, top right. Tang and blade from a late medieval site at Ardingley, Sussex.

Figure 135, bottom right. This is the transition zone between martensite at the right side, through a Widmanstätten structure to the beginning of some ferrite grains. Etch: nital; x140.

Iron knife

The polished and etched section shows that the entire blade was made from carbon steel quenched to produce martensite throughout. Martensite etched in nital is a dark straw color toward the edges. Slag content is moderately low with glassy fragments flattened out along the length of the section. The martensite near the two surfaces of the blade appears tempered with occasional suggestions of troosite. The fact that the martensite etches darker could be due to a change in the carbon content near the surface or to tempering after quenching. No weld lines are evident in this section. The carbon content near the middle region of the blade shows some banding, otherwise it appears to be very even.

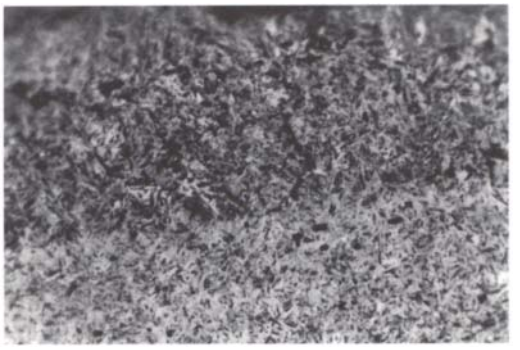

Figure 136, top. Blade section from a late medieval site at Ardingley, Sussex.

Figure 137, bottom. Shows transition between light etching and dark etching tempered martensite towards a cutting edge of the blade. Etch: picral; x280.

Roman copper alloy coin

The structure shows a well-formed, recrystallized grain matrix with straight twin lines and very little porosity present. The inclusions present are not attacked by ferric chloride during etching, suggesting that they may be sulfide inclusions rather than cuprite inclusions, which are extensively dissolved by ferric chloride solutions. The inclusions are flattened out along the length of the coin and are small—smaller than the grain size, which is about ASTM 6. There is no evidence of any second phase. X-ray fluorescence analysis carried out on the coin itself showed that only minor alloying constituents occur, with copper being the only major constituent; tin, zinc, and antimony were detected in small amounts. This evidence fits the metallographic evidence that the alloy is single-phased.

Figure 138. Coin of the Emperor Domitian which dates from A.D. 81. It is from the Mint of Rome, COS.VII DES.VIII (Roman Imperial Coinage 237). The inscription on the obverse is IMP. CAES. DIVI VESP. F. DOMITIAN AUG. P. M. with a head laureate. The reverse is TR. P. COS.VII DES.VIII P.P.S.C., Minerva advancing, brandishing a javelin and holding a round shield.

View of the etched, twinned, and recrystallized grains with part of the midsection crack through the coin showing as a black line. Note that the structure appears single-phased. Etch: $FeCl_3$; x39.

A deep crack penetrates the midsection of the coin. This crack does not appear to have been formed as a result of corrosion of the coin, but rather as a manufacturing fault. Midsection cracking is often associated with over-working at some stage during manufacture. This can produce cracks in the worked alloy which, although the grains are recrystallized upon annealing, are not removed by subsequent working and annealing.

Roman iron nail

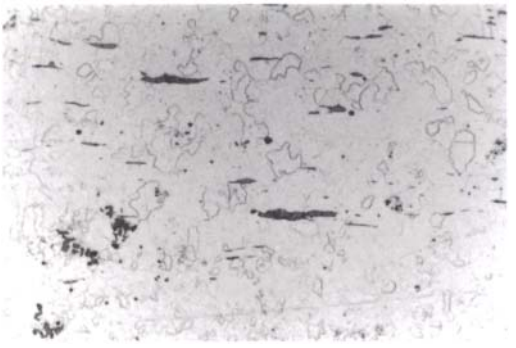

Figure 139. Roman iron nail from the site of Inchtuthil, Perthshire, Scotland. 140 mm.

Figure 140. Part of the nail shank showing small ferrite grains with elongated slag stringers passing along the length of the shank. The slag stringers in this nail are two-phased (glassy matrix and wüstite, FeO). This is a typical wrought iron structure. Etch: nital; x90.

At the Roman Agricolan fortress built at Inchtuthil in Perthshire, an enormous mound of iron nails was uncovered. The outer crust of the nails had corroded and protected the interior of the mound from extensive corrosion. The cache of nails, numbering hundreds of thousands, dated the abandonment of the settlement by the Roman army to A.D. 100 ± 80.

The section taken from the nail is a longitudinal cut through the head of the nail shank. The shank and head appear to have been made in one piece by forging from bloomery iron. A few slag stringers can be followed from the section through the head as they curve down along the length of the nail. These slag inclusions do not recrystallize when the iron bloom is heated by the blacksmith to forge the nail and, as a result, they become elongated into stringers upon heavy working. This can be seen in several areas in the polished section. Toward the center of the nail shank there is a large, elongated slag inclusion which at a magnification of x100 can be seen to be composed of two phases. There is a glassy dark-grey phase with a fine dispersion of globular dendritic wüstite precipitates (FeO). This kind of two-phase slag inclusion is a common feature of ancient bloomery iron, although high-quality products may show very little evidence of slag content. The veined, grey areas intruding into the nail surface are scale and corrosion products that can be seen under polarized light to be red-brown and are typical features of lightly corroded ironwork.

There is a slightly corroded area near the head of the nail where iron oxides outline some parts of the grain boundaries of the wrought iron. No further features are visible in the unetched condition.

The nail was etched in nital for 5–10 seconds and this revealed a primarily ferritic grain structure with no indication of carbon content. The raw material varies somewhat in carbon content, because another nail from the same site showed some pearlitic regions. The grain size in the shank of the nail is slightly larger (ASTM 5-6) compared to the heavier worked area of the nail head (ASTM 6-7).

Native copper

Figure 141. Native copper from the Great Lakes region in North America. 42 mm.

This sample is cut from a dendritic mass of native copper. In its polished condition, there are few inclusions present in the copper mass which appears to be broken up into a number of large segments. The cracks between the different segments are filled with cuprite and green-colored copper corrosion products. The outer surface of the cut sample also shows the ingress of corrosion with patchy conversion to cuprite.

In the etched condition (etch in alcoholic $FeCl_3$), large grains can be seen with some very long twin lines that are quite clearly curved. In some parts of the specimen, strain lines are evident, but there are other features to be seen as well. Long-zoned lines appear to mark the position of impurities or growth spirals within the cross section of the dendritic arms.

Figure 142, top right. Cross section through the dendrite arm etched in $FeCl_3$, x20, showing large grain size and unusual structural features within the grains.

Figure 143, top far right. A closer view of Figure 138 at x165 showing unusual features within the grains and well-defined grain boundaries.

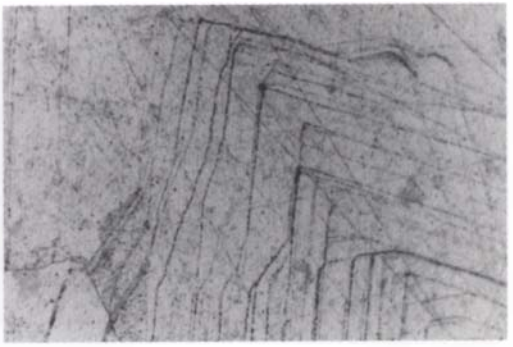

Figure 144, lower right. A high magnification view of Figure 138 at x500 showing a fine train of small precipitates occurring within banded regions of the dendrite arms that may be depositional features occurring as a result of growth phenomena in the native copper.

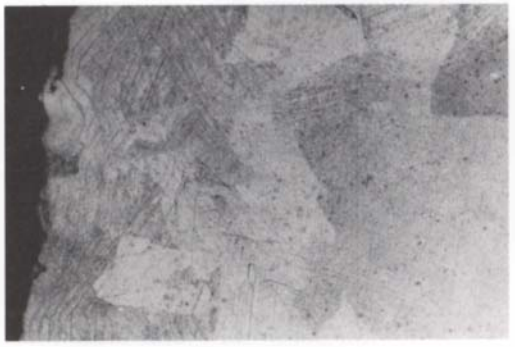

Figure 145, above. Toggle pin head from Iran. 20 mm.

Figure 146, top right. Etch: $FeCl_3$; x50.

Figure 147, bottom right. Etch: $FeCl_3$; x100.

Head of a toggle pin

This fragment is the head of a toggle pin, probably dating from the Late Bronze Age to the Early Iron Age period. The microstructure of the toggle pin head can be clearly seen after etching in ferric chloride for 3–5 seconds. The micrograph at x50 magnification (Fig. 146) shows that the structure is of cored dendrites with considerable interdendritic porosity, which appears in the photomicrograph as black zones between the dendrite arms. The structure is heavily cored, as can be seen from the photomicrograph at x100.

The eutectoid infill that also occupies the spaces between the dendrite arms has a different character from that which can be seen, for example, in Figures 95–96. Because of the range of composition and of the different rates of cooling, the extent of coring and the appearance of the eutectoid in tin bronzes can be quite variable.

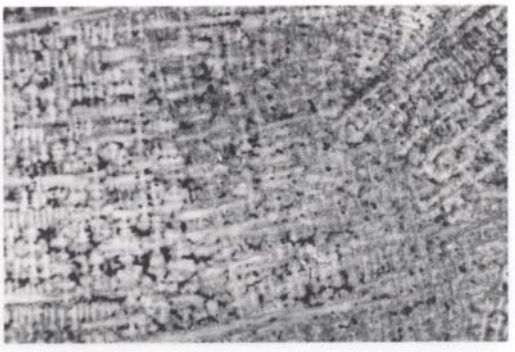

Javanese iron blade

This blade fragment from Java is thought to date from about 10–12th century A.D. It is potentially of interest since very few Javanese objects of this date have been examined. It is thought that nickel occurs in some of these products as an additional alloying constituent in addition to carbon.

A section taken through the complete length of the blade fragment reveals quite a complex structure. There are a number of different features that should be described. Overall the fragment has a piled structure made from a number of different components forged together. A drawing of some of the features is illustrated in Figure 149.

Parts of the structure show flattened ferrite grains, which is rather uncommon. This may have arisen from cold-working of the iron at some stage during manufacture. There is some pearlite present at the ferrite grain boundaries as well as a few small slag inclusions. This region also displays a banded structure. The bands are free from pearlite and have only occasional grain boundary precipitates crossing the bands perpendicular to the length. This type of banding is generally associated with other alloying constituents besides carbon, such as nickel, arsenic, or phosphorus. Toward the other side of the blade there are some grains that show subgrain structure. The grains themselves are quite large (ASTM 4) and they etch a light straw color in nital. The subgrains appear as occasionally equi-axed small areas outlined by fine dark lines that may be, in some cases, fine precipitates (not resolved at x1000). At high magnification some precipitates can be seen at the grain boundaries in this region. The carbon content is greater in one of the piled strips and the amount of pearlite is greater and the grain size smaller (ASTM 8). Towards the butt end of the blade the iron strip has clearly been folded over. There is a middle piece also, which occurs clearly in the midsection region of this sample, and joins with one of the hammered over pieces toward the cutting edge.

The area that contains a large scatter of angular slag inclusions passes along the length of the section. The slag is a glassy-phase material which here appears homogeneous, and it has been broken up into small angular remnants upon working.

There is no indication that this blade was quenched. The carbon content is well below the eutectoid composition, and in some areas would not have been sufficiently high to produce much change in properties upon quenching.

The etching has revealed in some grains the "α veining" substructure that arises when the nital attacks subgrain boundaries as well as grain boundaries (Samuels 1980). It is thought that this develops as a result of etch pitting at the walls of the dislocations at the subgrain boundaries. Both the development of subgrain structure and the ease with which the etch pits develop is dependent on the physical and thermal history of the sword. It can arise from hot-working or from quench-ageing effects due to the emergence of carbide growth and etch pitting in ferrites due to heating at low temperatures (e.g., 50–150 °C will suffice).

Figure 148. Fragment of Javanese iron blade. 110 mm.

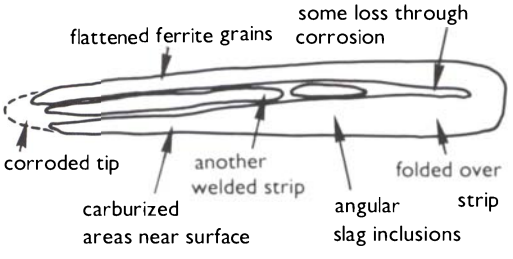

Figure 149. Illustration of cross section of iron blade.

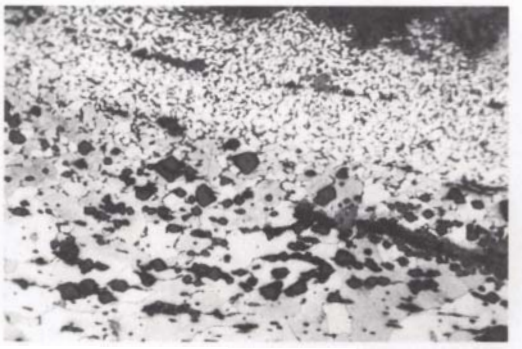

Figure 150, right. Part of the structure with carburized surface, angular slag region, and ferrite grains. Etch: nital; x70.

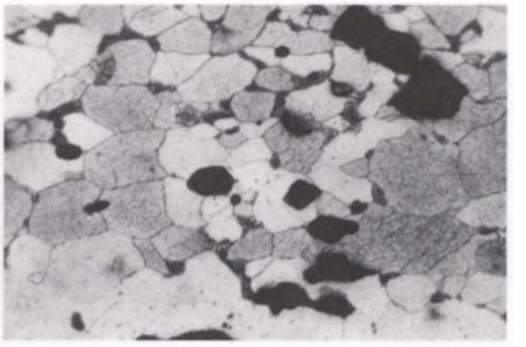

Figure 151, far right. Angular inclusions with some pearlite and subgrain structure that can be seen as veined lines passing through the ferrite grains. Very dark regions are angular slag fragments which are mostly glassy single-phased slag inclusions. Etch: nital; x280.

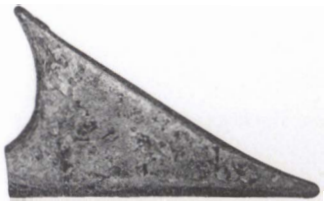

Figure 152. Bronze axe fragment from Iran. 90 mm.

Bronze axe fragment

This fragment is thought to be a part of a Luristan-style ceremonial bronze axe dating to about 8–10th century B.C., from Iran, composed of 87.1% copper and 7.2% tin, with no other elements detected by X-ray fluorescence analysis. The sample is taken from the cut end of the triangular fin which was probably integral with the blade. The triangular plate is carefully made and has smooth surfaces with a flange around the circumference on both sides of the plate. The sample removed for examination is a transverse section through part of the broken end of one of the projections of the plate.

Figure 153, above. Slight coring visible together with porosity and recrystallized grains with well-developed twinned crystals. Note that the twin lines are straight. This evidence suggests that the axe was roughly cast to shape and lightly finished by working and annealing, with annealing being the final fabrication process. Etch: $FeCl_3$; x62 (see Plate 19).

Figure 154. Well-developed hexagonal grain structure, usually outlined with a precipitation of α-phase (the copper-rich whiter material) showing variation in color as a result of different grain orientations in the brass: 60 Cu, 40 Zn, α + β brass. Etch: $FeCl_3$; x31.

Laboratory cast 60:40 brass

This 60% copper, 40% zinc alloy is etched with $FeCl_3$ in which case the β phase region appears darker or black. Note the well-formed Widmanstätten precipitation of α within the β grains producing α precipitates only on certain crystal planes. See page 20 for a brief discussion of the Widmanstätten precipitation.

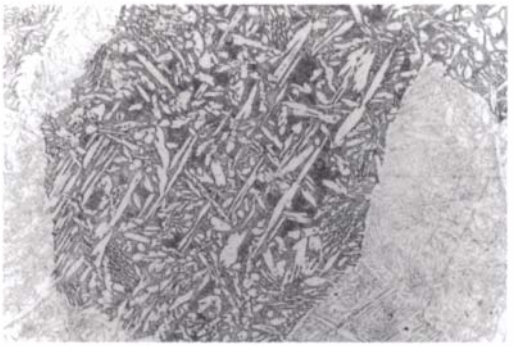

Figure 155. 60 Cu 40 Zn brass. Two-phased α + β brass showing detail of the Widmanstätten formation of α plates within the β crystals. Etch: $FeCl_3$; x100.

Note that the fundamental difference between the Widmanstätten and martensitic transformation is that the Widmanstätten involves the decomposition of *one* solid phase into *two* phases while the martensitic transformation involves the rapid cooling of one phase producing *one* metastable phase on cooling.

Figure 156, above. Drawing of gilded silver earring from Jordan. 22 mm.

Figure 157, top right. Part of the gold foil covering with overlapped join in the outer gold foil. The foil has been diffusion-bonded to the silver beneath. Note that the silver rod is heavily corroded with few remaining sound metal regions. Unetched; x21.

Figure 158, middle right. Hexagonal grain boundaries in the silver rod. The dark areas are corrosion, and the grain boundaries that can be seen are not straight lines. This is a consequence of the age of the silver. Over the past 3,500 years, copper has precipitated from the silver rod and the grain boundaries have moved as a result. Etch: acidified potassium dichromate; x200.

Figure 159, bottom right. "Wiggly" grain boundaries as a result of discontinuous precipitation of copper from the silver alloy. Etch: acidified potassium dichromate; x500.

Gilded silver earring

The complete earring, drawn in Figure 156 is one of a pair from the site of Tell Farah in Jordan and is dated to the Middle Bronze Age (first half of the second millennium B.C.). They were both made from gilded silver, the second example being in a fragmentary condition from which a sample could be taken across the broken end by careful sawing with a fine jeweller's saw. Both objects were decorated with granulated gold spheres attached to the gilded surface. The terminals of the earrings end in loops, which are secured with twisted gold wires. Before conservation, both objects were covered in dark grey corrosion of a waxy consistency. X-ray diffraction analysis showed that the main constituent of this corrosion was silver chloride. Conservation work was carried out both chemically and mechanically using 15% ammonium thiosulfate and hand tools. The corrosion products had erupted through the gilding in several places and had forced the gilding outwards. Characteristic features of leaf gilding were observed, in particular the overlapping and corrugating of the thick gold foil.

The metallographic sample, revealed a partially corroded silver substrate covered with a thick layer of gold. The gilding had become detached from several corroded areas, but in some areas a good interface between the gilding and the silver could be seen. This interface is several microns thick and suggests that a deliberate diffusion bond was created between the applied leaf gilding and the silver core. Analysis with the electron probe yielded 92.9% silver, 2.9% chlorine, 1.47% copper, and 0.7% gold.

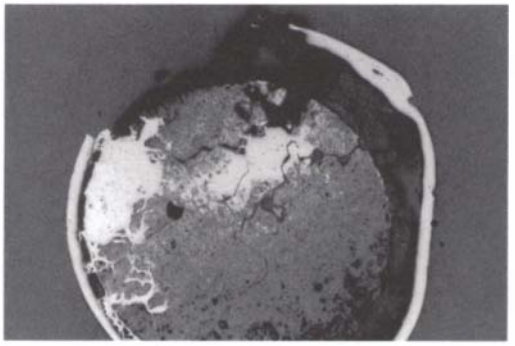

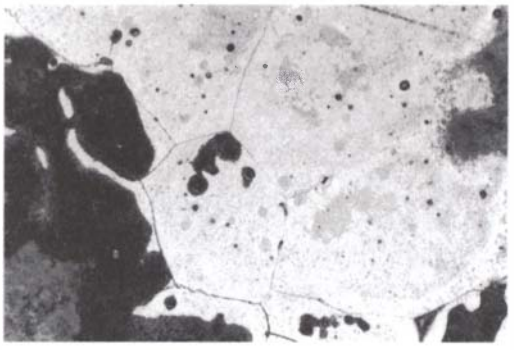

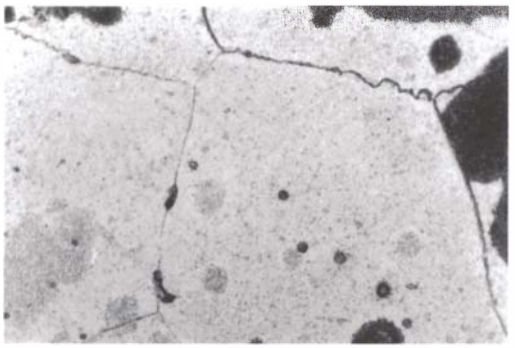

Figure 160, top right. Fragment of a brass medallion from the La Perouse, which sank off the coast of Australia in 1726. Unetched; x20.

Figure 161, bottom right. Etch: $FeCl_3$; x75.

Fragment of a brass medallion

This brass has major constituents of copper and zinc, with minor amounts of tin, lead, iron, and chromium. The first micrograph, unetched at x20 magnification shows the remarkable depth of corrosive penetration into the brass. Corrosion has outlined the dendritic forms of the cast brass medallion which has been lightly etched with ferric chloride. Although loss of both copper and zinc has occurred here, it should be noted that the dendritic arms have been preferentially corroded while the interdendritic areas are in some regions preferentially preserved. This is evident in the second photomicrograph at x75 magnification and suggests that the dendritic arms are rich in zinc compared with the interdendritic fill, since normally zinc is lost preferentially in sea-water burial such as this shipwreck site (see Plate 4).

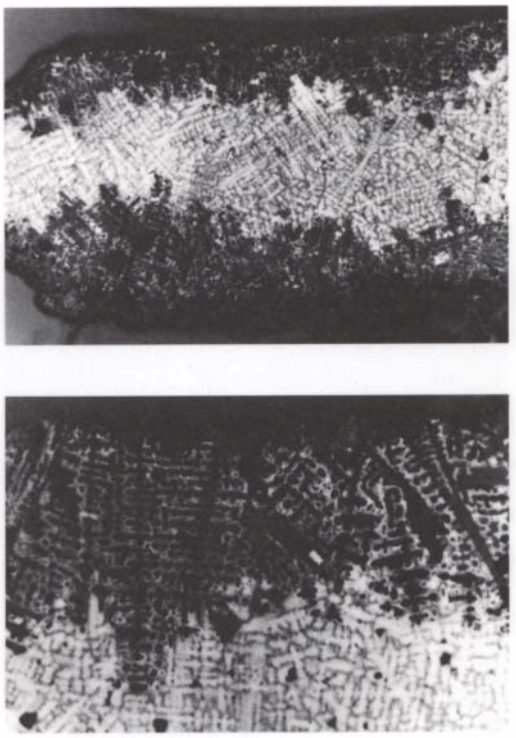

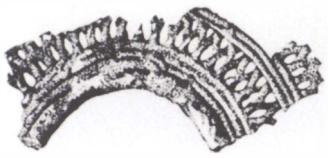

Figure 162. Sinú ear ornament fragment. Pre-Hispanic Colombia.

Fragment of a small Sinú ear ornament

These ear ornaments were cast as pairs by the lost-wax process and represent very skillful "false-filigree" wire work. The whole ornament is modeled in wax in one operation and then cast.

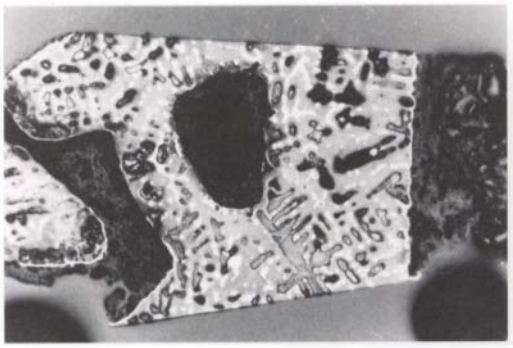

Figure 163. Unetched, low magnification view at x20 showing extensive corrosion to the gold-copper alloy wire section. The evidence shows that the ornament has been cast by lost-wax without any working. The dendritic structure of the alloy is clearly evident.

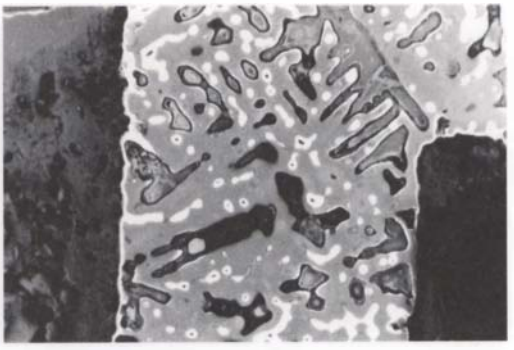

Figure 164. Enlarged view at x100 showing the light enrichment in gold at the surfaces as well as the selective retention of some areas of the dendrites as a result of coring of the gold-copper alloy on casting. The grey matrix is principally cuprite.

Roman mirror fragment

The early examples of Roman mirrors made in Europe, in a specialized production center in Germany, were often made in a leaded high-tin bronze which is partially quenched to fragment the $\alpha + \delta$ eutectoid phase. The mirrors date to the early centuries A.D. and this example is from Roman Canterbury and dates to the 4th century A.D. It is made in an alloy of 8% lead, 19% tin and 73% copper (see Plate 5).

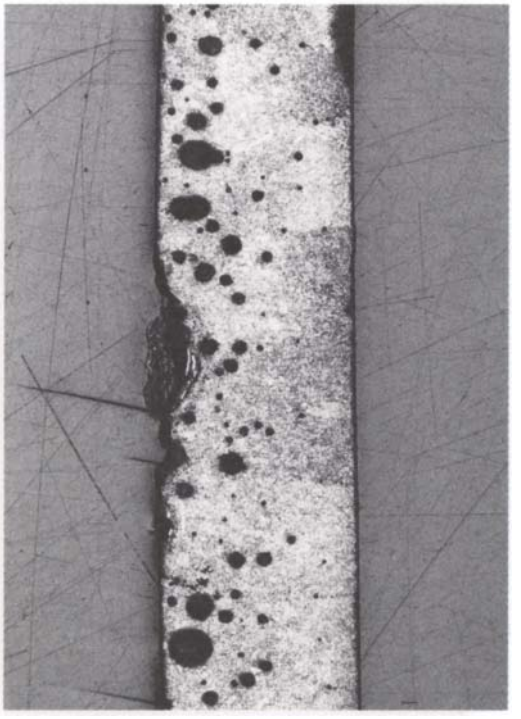

Figure 165. Section of a Roman mirror fragment at x35 magnification, etched in alcoholic ferric chloride showing the precipitation of large lead globules at the bottom of the cast mirror (on the left-hand side of the picture). The grain boundaries can just be seen as a result of the different etching of the surface with ferric chloride. It is a very fine structure for a cast bronze showing that despite the gross segregation of the lead globules, the cooling of the alloy was fast enough to prevent the usual dendritic structure from developing.

Roman bronze figurine

This small figurine, about 33 cm in height, is from the Julio-Claudian period of A.D. 40–68 and she is shown wearing a short Amazonian tunic. The torso and head were hollow cast in one piece with the left leg just above the knee. The right arm was attached by casting-on or solder. The legs and feet were then cast-on. The Roma was cast in a leaded bronze of 89.8% copper, 7.1% tin, 2.7% lead, with traces of zinc, iron, nickel, and silver.

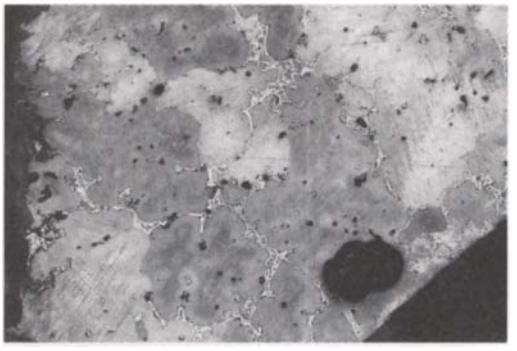

Figure 166, next page. Roman bronze figurine of Roma A.D. 40–68.

Figure 167, right. Roma bronze microstructure. The proper surface of the Roma casting is to the left hand side of this photomicrograph which shows the annealed cast structure of the bronze. The grain size is large with small inclusions of lead and copper oxides or sulfides. Etch: $FeCl_3$; x90.

There is an unusual feature on the back of this Roma: a series of hexagonal networklike structures appear in the metal. A core sample was taken in this area on the back to try to resolve the question concerning the nature of the grain structure in this area. The microstructure is shown here in Figure 167. The structure is etched in alcoholic ferric chloride with the cast surface of the Roma at the left of the photomicrograph. The structure of the bronze is essentially that of an annealed casting. The α grains appear hexagonal in shape in many areas of the section with the $\alpha + \delta$ eutectoid preferentially occurring at the grain boundaries and outlining some of the hexagonal α grains. Small oxide or sulfide inclusions can be seen scattered through the section along with some small lead inclusions and porosity. The absence of a typical dendritic structure suggests that there may be a microstructural explanation for the network of hexagons observable on the surface of the bronze, since the hexagonal annealed appearance of the section is unusual for a cast bronze. The microstructure shows that the grains are not mammiform but are equi-axed. The coalescence of these hexagonal grains during solidification could be responsible for the surface appearance of the bronze.

Figure 168. Renaissance silver basin from Genoa dated to about A.D. 1625. 755 mm.

Renaissance silver basin

This basin is an elaborate repoussé work with many cast additions and soldered components. It has been finished by chasing, engraving, and the addition of many components to the worked sheet of the basin itself. Before the late 16th century, forks were uncommon in Europe and eating was carried out using the fingers. This bowl was probably only for show, and many were probably melted down when they went out of fashion and turned into silver knives and forks.

The plate is made of an alloy of 94.9% silver, 3.2% copper; small amounts of lead, arsenic, zinc, tin, and antimony are also present (Scott 1991).

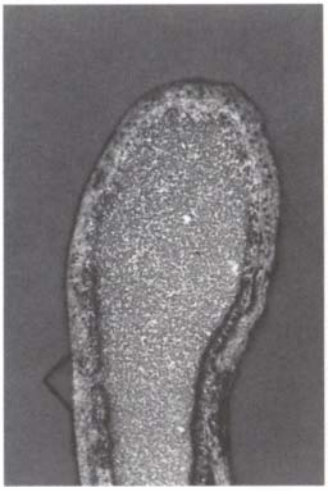

Figure 169. Part of a solder blob from a repair to the outer radial panel. The solder shows a cast morphology of the copper-rich and silver-rich phases, which are not equilibrium phases of the silver-copper binary system, but have individual phase compositions removed from their predicted values. This structure of alternate dendritic morphology is typical of many cast silver-copper solder alloys. The overall composition of the solder used here is about 50% silver, 50% copper. Etch: $FeCl_3$; x30.

The samples for study were removed with a diamond-tipped core drill, 1.5 mm internal diameter, after removing some of the components of the silver basin, so that no damage was visible from the front of the object when the parts are reassembled.

It was customary in the Renaissance to start important projects by preparing a detailed wax or gesso model, usually full-scale. The silversmith then carefully copied the model in silver, first working the parts that needed to be raised. This repoussé working was carried out to enable the metalsmith to model the location of the cast additions. The cast components were modeled in wax, most probably on the basin itself and then removed and prepared for casting. When cast and soldered in place, all the surfaces were finished by chasing and engraving exactly as if the entire basin had been made in one piece.

Figure 170, top right. Photomicrograph of part of the section through the basin, etched with acidified potassium dichromate under partially polarized light to reveal the continuation of the grain structure of the silver crystals across the boundary into a surface-altered zone. This micrograph illustrates the continuity of the overall microstructure within two apparently very different structural regions of the silver basin. x155.

Figure 171, middle right. Overall view of a core-drilled plug from the silver basin. The top surface of the basin is uppermost in this photograph and shows the extent and nature of the surface-altered zones of the silver basin. An unusual feature is the surface crack and corresponding surrounding zone of oxidized metal. The surface alteration zones here are due to the agglomeration of copper particles and their oxidation to cuprite, since silver is very susceptible to oxygen absorption during annealing. This oxygen can then combine with the copper to make cuprite. Etch: acidified potassium dichromate; x50.

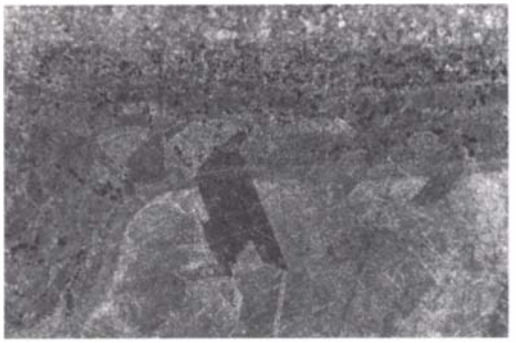

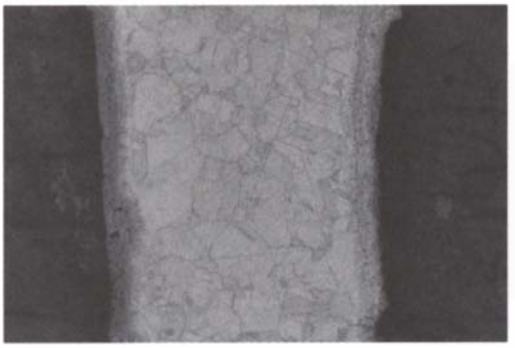

Figure 172, bottom above. View of part of the silver sheet, etched in acidified potassium dichromate. The grain structure of the silver can be seen. The grain boundaries are not straight and have a "jigsaw" appearance in places, but the precipitation of copper seen here occurs as continuous zones at the grain boundaries, suggesting that the basin had been heated subsequent to its manufacture, probably for repairs and for the casting of the small additions. x40.

Figure 173, top right. Overall, the structure is typical of a cast alloy; the bracelet has been cast integrally and joined near the center region. Large areas of extensive porosity are clearly evident together with smaller zones, sometimes filled with corrosion and, interestingly, a patch of casting core material in the hollow between the two regions of the bracelet. The casting core has been prepared as a fine mix and appears in reflected light as a grey mineral assemblage. The casting core appears to be principally mineral in composition with no organic debris apparent. One or two small areas that are of darker color may be remnants of the $\alpha + \delta$ eutectoid, now rather corroded. There is also a thick crust of corrosion surrounding the surfaces of the bracelet section.

The dendritic structure of the bracelet has probably been modified by heating during manufacture since it is not very pronounced, and the coring that remains is subtle. Unetched; x40.

Circular bracelet from Thailand

This is a transverse section cut across a circular bracelet from Thailand. It is from the site of Ban Chiang and is dated to about 500 B.C. In composition, the bracelet is a tin bronze with 89.2% copper, 5.4% tin, and 0.6% zinc. The inclusions present in the metal are copper sulfides and when analyzed one was found to contain 76.5% copper, 0.5% tin, and 19.1% sulfur, with silver, lead, and zinc undetected. The second inclusion studied contained 71.8% copper, 5.7% lead, and 18.3% sulfur with tin, zinc and silver undetected. Cuprite inclusions also occur and the tin content can vary up to about 10.7%.

Examination in the unetched condition reveals a number of different features. Toward some of the shaped edges of the bracelet fine cross-hatching outlined in corrosion can be seen, which indicates that there has been some working of the bracelet following casting, probably to finish the surface rather than to produce a great change in shape.

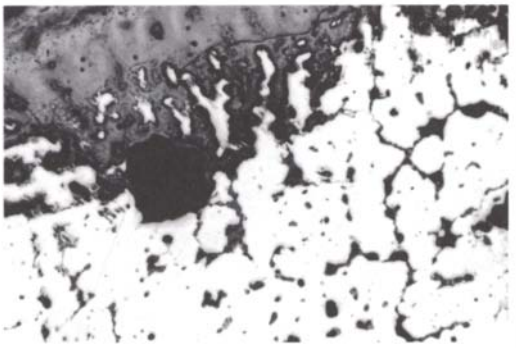

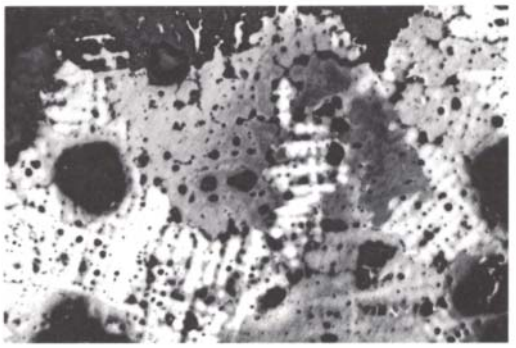

Figure 174, middle right. Structure after etching in alcoholic ferric chloride. Some coring can be seen in the structure together with evidence for slip planes (some evident as pseudomorphic remnants in the principally cuprite corrosion crust adjacent to the remaining metal). Some of the inclusions are not affected by etching in this way and may be copper sulfide inclusions; other rather dark grey regions appear to be corroded metallic regions, which again suggests remnants of the eutectoid phase. Another interesting feature of this sample is the many copper-colored areas present in the eutectoid regions or as small scattered blobs. This copper, unalloyed with tin, may be present as a result of insufficient melting in the original cast or as a pseudomorphic replacement of the original $\alpha + \delta$ eutectoid regions. It is more likely to be present as a result of corrosion-redeposition mechanisms that have resulted in the corrosion of the tin-rich phase preferentially. x70.

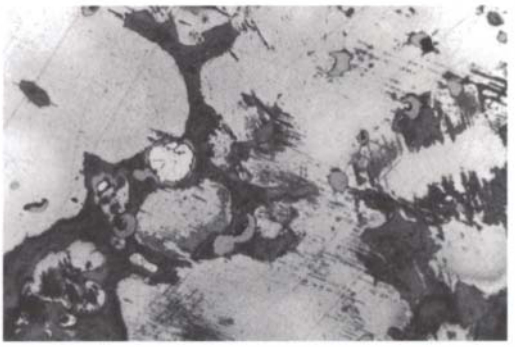

Figure 175, bottom right. High-magnification view showing a small globule (light in color) of redeposited copper in a corroded $\alpha + \delta$ region, together with copper sulfide inclusions (light grey) and bronze metal showing strain lines from working. Etch: $FeCl_3$; x170.

Roman bronze bowl

The sample was examined carefully in the unetched condition. Extensive intergranular corrosion has occurred outlining most of the grain boundaries with cuprite very clearly. Some straight lines of cuprite corrosion can be seen passing occasionally into a grain interior suggesting that the metal must have been stressed at some stage during manufacture to produce some slip, although no twin lines are apparent in the section before etching. Some of the inclusions present in the metal are of cuprite, often continuous now with the network of corrosion through the grain boundaries. There are other regions where the typical variegated surface appearance of lead inclusions occur and these are more concentrated in the thicker region of the section where they appear to have segregated. Note also that there is considerable porosity as well as some areas where lead globules may have fallen out as a result of grinding and polishing. That the alloy in question here is a leaded tin bronze, can almost certainly be deduced from the occasional presence of some regions of the $\alpha + \delta$ eutectoid. Where the eutectoid phase occurs, it is usually surrounded by islands of corrosion where the copper-rich grains have been attacked. In this example then, the primary corrosion process is the attack of the α grains surrounding the $\alpha + \delta$ eutectoid region: the α within the eutectoid is also attacked.

If the corrosion crust is carefully examined, some areas of remaining eutectoid can be clearly seen within the corrosion surrounded by copper oxides. This is an interesting example of the preferential retention of the copper-rich α phase. Careful examination of the corrosion layers under polarized light is also useful in the study of this material since the crust can be resolved into different layers.

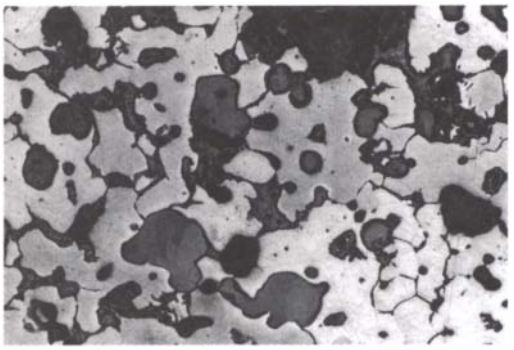

Figure 176. Section from the base of a Roman bronze bowl. The bowl has a composition of 87.0% copper, 11.5% tin, and 0.9% arsenic, with silver, lead, zinc, sulfur and iron undetected. x100.

The section has to be etched for about 10–12 seconds in alcoholic ferric chloride to bring out the grain contrast. The grains are not twinned which shows that this sample is essentially an annealed casting. Some of the grains show coring where the distribution of copper and tin in solid solution is still unequilibrated. Note that the thin strip that appears to be bent back to produce a uniform edge has multiple strain lines apparent in the crystals. A small island of metal grains in this region outlined by corrosion is also heavily strained. The $\alpha + \delta$ eutectoid is much easier to see in this section in the etched condition, and the grains have color contrast as a result of differing orientation in the polished section.

The overall structure is a cast one that has been annealed and then partly worked in some areas to produce the strain lines visible in some regions. The casting has resulted in some segregation of the lead component, while annealing has not been extensive enough to eliminate all of the eutectoid.

Early Medieval brass sheet

This fragment of a broken bronze sheet has three studs pushed through the plate. The sheet is English from the Early Medieval Period and has 83.6% copper, 15.7% zinc.

Before etching, the sample was examined in the polished state which reveals the features of corrosion to be seen in the section. Corrosion of the bronze stud head can be clearly seen outlining the worked and recrystallized grain structure in this part of the artifact. Corrosion has selectively removed part of the grains of the metal, advancing along twin boundaries or slip planes.

After etching in alcoholic ferric chloride for a few seconds followed by etching in potassium dichromate, the microstructure can be examined. It is immediately clear that the sheet brass has been cast to shape, as is apparent from the undistorted dendritic structure, which is cored. There are some depressed areas on the surface of the cast sheet that show the presence of strain lines from some surface working of the casting. The stud, on the other hand, has been extensively worked to shape and has a completely recrystallized grain structure in which most of the twinned crystals have straight twin lines indicating that a final annealing operation overall was the last stage in manufacture. However, just past the area of the cast metal sheet, there is a zone of the stud that shows a concentration of slip lines that could only have resulted from severe strain of the bronze stud in this particular region. This is perhaps due to hammering to attach the cast plate to a backing.

The stud appears slightly bent when examined by eye and this may have been caused by hammering into place, although the cast plate would probably have had the holes for the studs cast in situ. Hammering through such a thickness of metal could not have been accomplished with this stud, and there is no indication of deformation to the cast structure in the vicinity of the hole which would have occurred had the hole been drilled for the insertion of the stud.

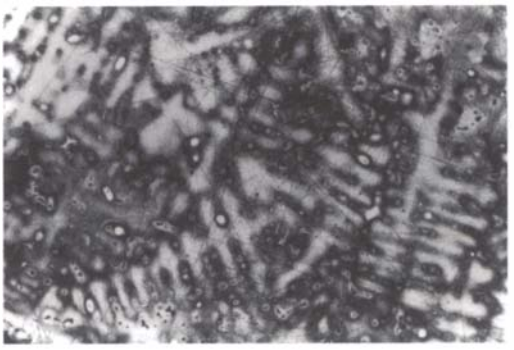

Figure 177, top right. Brass sheet, etched in alcoholic ferric chloride and then potassium dichromate. Heavily etched section reveals the cored dendritic structure of the brass. Small lead globules can be seen in interdendritic regions. x50.

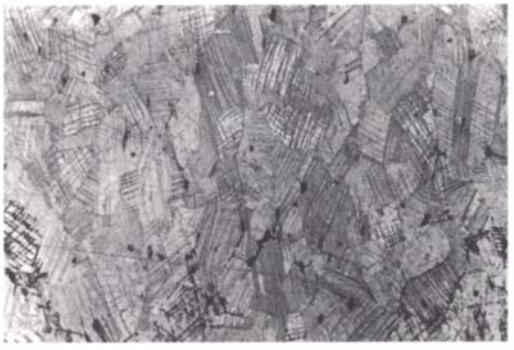

Figure 178, bottom right. Recrystallized and heavily worked grain structure of the stud probably hammered at this point to attach to the brass sheet. The grains are heavily strained and deformed, probably by additional hammering after working and annealing cycles to shape the stud. Corrosion has outlined some of the strain lines by dark corroded regions passing through the grains. Etch: potassium dichromate; x140.

Romano-Greek iron arrowhead

This small iron arrowhead is square in cross section and tapers to a point. It is Romano-Greek of about the 2nd century A.D. and is made of wrought iron.

In the polished state the wrought iron shows a scatter of slag inclusions, some of which are elongated across the width of this section while others are rounded and globular. All look like wüstite in a glassy matrix. The ingress of some iron oxides as corrosion products can also be seen on the surfaces of the section.

After etching in nital for about 10–15 seconds, the ferritic grain structure can be seen. The ferrite would technically be described as massed ferrite grains and, if properly etched, the subgrain structure can be seen within some of the ferrite. The grain size in many areas of the arrowhead approximates to about ASTM 8. Toward one surface of the arrowhead, the carbon content rises, almost certainly due to deliberate carburization here, since there is no carbon content to be seen elsewhere in the section. The ferrite begins to assume Widmanstätten characteristics and pearlite makes up the infill showing that a steel edge has been produced here. The depth of penetration of carbon is quite limited, as might be expected for a case-carburized steel.

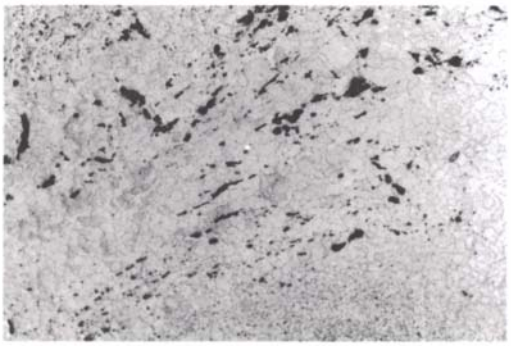

Figure 179. Part of the arrowhead's microstructure showing a typical wrought iron with slag stringers (dark in this photomicrograph) passing along the length of the arrow. The grain size of the ferrite is variable and it is typical for a piece of bloomery iron to find this kind of variation in apparently homogeneous material. Etch: nital; x75.

Byzantine leaf-shaped blade

The section from this small Byzantine leaf-shaped blade is taken across part of the edge of the blade. It is made in a low-tin bronze with about 92% copper, 7% tin.

There is very little metal remaining in this sample, which has mostly been converted to cuprite. The metal that does remain shows rather fine dissemination of corrosion at the surface, suggesting that the grain structure is quite fine.

After etching with alcoholic ferric chloride, the grain structure can be seen, in fact, to be very small suggesting that the alloy used to made the blade has been well-worked and annealed in a number of cycles to shape the blade. Many twinned crystals are visible as well as extensive strain lines throughout the grains. There are some blue-grey inclusions in the metal that may be small sulfide inclusions hammered out along the length of the section.

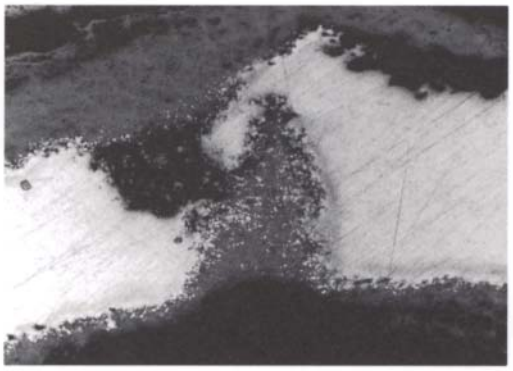

Figure 180, top right. Unusual corrosion pattern through the bronze blade resulting in the gradual isolation of small grain remnants in a matrix of cuprite. The ingress of corrosion is also severe and both surfaces of the blade are retained in a thick corrosion crust. Unetched; x70.

Figure 181, bottom right. Heavily etched view, in which some surface scratches are visible as well as the bronze grains and corrosion crust, showing twinned grains with some strain lines just evident. The shading in the metallic area is due to coring from the original cast ingot, still not entirely removed by working and annealing, and the grains continue across areas of slightly different composition. Etch: $FeCl_3$; x160.

Medieval iron knife

This iron knife blade is from Medieval Britain and is mostly wrought iron rather than steel. The sample taken is across the cutting edge.

In the polished state the heavily elongated slag stringers can be seen passing along the length of the section. Corrosion of the surfaces is also apparent: the structure of the corrosion here does not reveal any pseudomorphic preservation of the structure of the iron.

After etching in nital, the comparatively large size of the original austenitic grains can be seen toward both long surfaces of the section, where decomposition of the austenite has occurred upon cooling resulting in grain boundary ferrite with an infill of ferrite and pearlite. In some areas the beginnings of a Widmanstätten structure can be seen in the ferrite, but this is not very pronounced which means that the blade has been cooled fairly slowly from the austenitic region and has not been quenched, at least not in this part of the structure. The low-carbon steel edges gradually grade into a ferritic grain structure.

Another steel region with low carbon content appears about midway through this section which suggests that some welding of different carbon-content pieces may have been used to fabricate the blade.

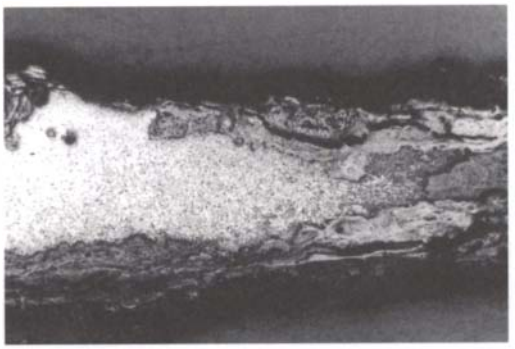

Figure 182, top right. Overall view of the corroded blade showing darker etching region toward cutting tip where the carbon content is greater. Outer areas are corrosion products, mostly iron oxides. Etch: nital; x30.

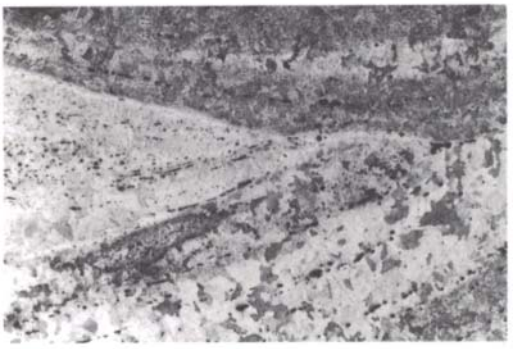

Figure 183, middle right. View of a weld where different pieces of iron have been joined together. The carbon content in the upper and lower zones is greater while the center triangular region is just wrought iron with some slag stringers. Etch: nital; x70.

Figure 184, bottom right. Low carbon steel area of the blade with partial Widmanstätten structure of ferrite and pearlite. Etch: nital; x120.

Set of panpipes

This is a fragment of *tumbaga* alloy from a set of panpipes from the Department of Nariño, Colombia, dating to about the 8–10th century A.D. Found in the municipio of Pupiales. The analyses of this sample gave 25.9% gold, 62.4% copper, 4.0% silver, and 0.01% platinum.

The structure has become quite corroded as a result of burial and the fact that it is a *tumbaga* alloy (a South American gold-copper alloy) that is quite debased. There are some dark striations passing along the length of the curved section which are areas of loss due to some segregation passing over from the cast ingot into the worked sheet of the panpipes. This segregation from casting has resulted in unequal distribution of the gold and copper of the alloy, with the consequence that the copper-rich segments of the worked sheet are preferentially corroded. Apart from this gross removal, there is also corrosion along twin bands, slip lines, grain boundaries,

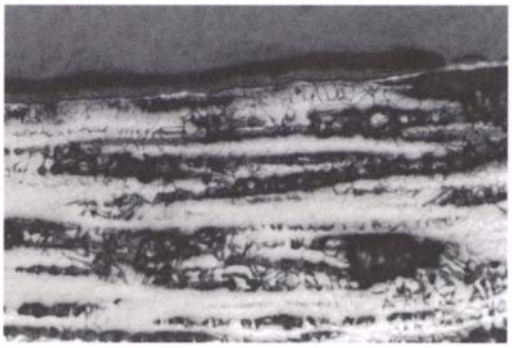

Figure 185. This section is etched in cyanide/persulfate. The depletion gilded surface appears at the top of the photomicrograph. The lamellar structure in the gold-copper alloy interior is created by differential corrosion of the worked and annealed sheet. Some twin crystals can be seen in the gold alloy, showing that annealing was the final stage in manufacture. x65.

and through some of the grains themselves, isolating small patches of residual metal. Note that in some areas there is very good pseudomorphic replacement of the original grain structure with cuprite, especially along some twin lines. Corrosion has already outlined most of the features of this gold-copper alloy, and there is little point in attempting to etch the sample. The grain structure can be seen to be worked and annealed with recrystallized grains and predominantly straight twin lines. Careful examination of the surface cuprite layers reveals a thin line embedded in the corrosion which is more golden in color than the alloy itself and which is, in fact, the remnants of the depletion gilded layer on this *tumbaga* alloy.

The depletion gilded layer here is deceptively thin and could easily be mistaken for some other form of gilding if the alloy itself did not contain gold, and the technology of the region was not understood.

Byzantine dagger blade

Figure 186. Photomicrograph of part of the blade edge, showing a low-carbon steel with Widmanstatten side plates and sawteeth in a ferrite and pearlite steel of about 0.4% carbon. Etch: Villela's reagent; x100.

This is a fragment of a Byzantine iron dagger blade, with the section taken across the cutting edge of the blade.

In the unetched condition, the sample section is quite corroded, with thick crusts of iron oxides evident. There is a fine scatter of glassy slag inclusions, slightly elongated, toward the center of the blade section and some finer slag stringers more heavily elongated along part of the length of the blade.

After etching in nital for about 10 seconds, very little relief could be seen and instead, Villela's reagent was used for about eight seconds. This revealed that the blade has been made from a steel of variable carbon content. One side is predominantly rich in carbon with Widmanstätten side plates and sawteeth visible. The carbon content in this region must be of the order of 0.4%. In most other regions the structure is that of blocky ferritic grains with some fairly uniform pearlite infill.

The edge of the blade, the detail of which is still preserved in corrosion, can be seen to have the same structure as the carbon-rich zone in which the Widmanstätten ferrite and pearlite appears to continue down into the edge, showing that the blade had not been quenched, but had been made from a low-carbon steel.

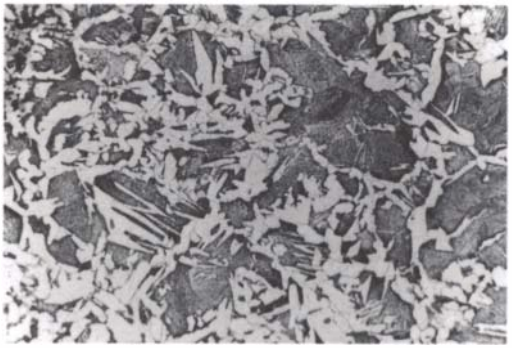

Roman coin of Victorenus

This is a debased silver coin of the Roman Emperor Victorenus, from A.D. 268–270. In composition the coin is about 96.1% copper, 2.5% silver.

The corrosion products were examined under reflected polarized light. Below the immediate surface, a very crystalline mass of green corrosion products are to be seen and there are some blue crystals also, and adjacent to that, some bright red cuprite layers together with corrosion products passing into corroded metal.

There are deep blue azurite crystals on the surface of this coin, while in the microstructure there are thin zones of grey corrosion which appear to be formed around some of the grain boundaries.

After etching in alcoholic ferric chloride for about 10 seconds, the grain structure can be seen. Parts of the structure of the coin betray an almost cast structure towards one end of the coin flan where it has not been effectively deformed on working: the punch has not touched this region. Here there are some recrystallized and twinned grains superimposed on the as-cast structure where some limited working of the coin has occurred.

This type of partially recrystallized structure is very suggestive of hot-working of the cast coin flan. There is some silver content to the alloy, but the amount of the silver-rich phase, which can be seen elongated along the length of the coin, is not very great.

Passing along the section one sees the heavily worked grain structure; again the form of the definition of these grains against the slightly cored background suggests hot-working to shape. Note the flow in the grain structure of the coin towards parts of the design which are less heavily worked by the die. Strain lines also occur in this region. Passing along to the other end of the section, there is a very uniform degree of grain size apparent, with twinned crystals in which the twin lines are straight.

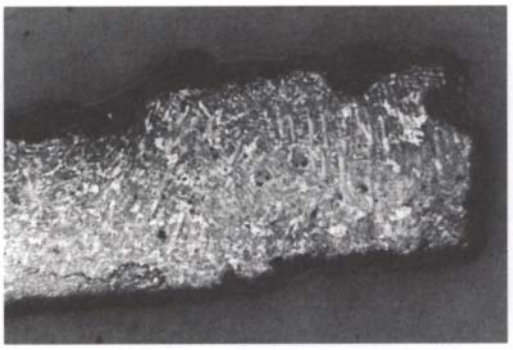

Figure 187, bottom left. Overall view of the coin, showing a cast structure with superimposed recrystallized grain structure indicating that the flan was cast to a suitable size and then struck. Etch: $FeCl_3$; x30.

Figure 188, bottom right. The grain structure of the coin is clearly shown in this photomicrograph. The crystals are lightly twinned showing that some working and annealing (in this case hot-working) has been carried out. The light particles present between the grains are silver-rich particles. Variation in shading is due to coring in the original cast structure. Etch: $FeCl_3$; x145.

Grey cast iron

This grey cast iron of the early 20th century contains about 4% carbon and a little phosphorus.

Before etching, the outlines of some of the thick graphite flakes can be seen at low power, while at higher power the coarse nature of the structure is apparent. After etching in nital for about 8 seconds, the high carbon content of this cast iron can be seen, since the whole of the infill surrounding the graphite flakes is made up of pearlite of different spacings. Some white, unetched regions in this cast iron are of the ternary eutectic, steadite. This is a common constituent of many cast irons because of the phosphorus content.

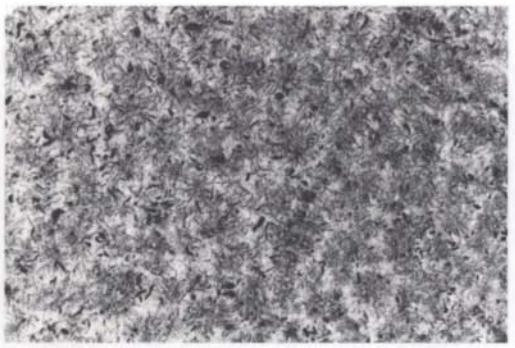

Figure 189, top right. Overall view of the cast iron microstructure, showing distribution of graphite flakes. Light areas are mostly ferrite. Etch: nital; x35.

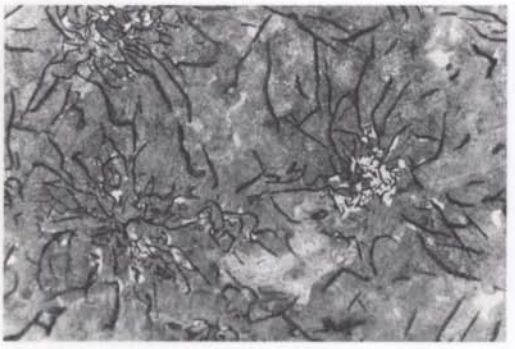

Figure 190, bottom right. View of the graphite flakes and pearlitic infill. The white areas associated with the graphite are ferrite. The pearlite is mostly dark grey here due to the fine spacing of the ferrite and cementite. Etch: nital; x130.

Grey cast iron

This is a grey cast iron, circa 1920, with about 3% carbon and 0.2% phosphorus.

In the polished state, the fine graphite flakes can be seen in this fairly typical grey cast iron, together with small inclusions that are probably sulfides. In some areas, clear rosettelike regions of growth of the graphite flakes can be seen, together with some zones in which thicker flakes have been deposited. After etching in nital for about 8–10 seconds, the structure can be seen to consist of small graphite flakes in a ferritic surround with fine pearlite accounting for the remainder of the structure. These are the typical constituents of many modern and historical cast irons.

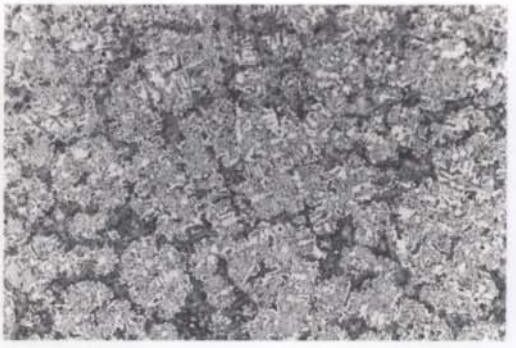

Figure 191, top right. The cast structure of this iron-carbon alloy can be seen in some dendritic areas revealed by etching in nital and picral. Grey areas are fine pearlite. x40.

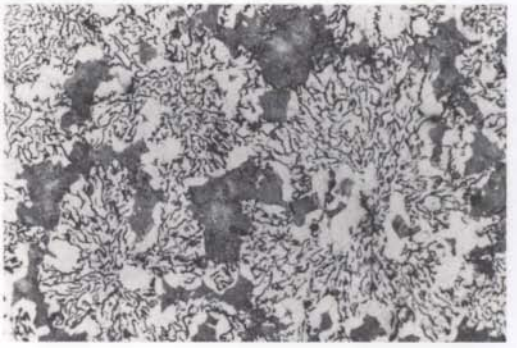

Figure 192, bottom right. Graphite flakes in a ferrite matrix with an infill of pearlite containing some steadite patches. Etch: nital and picral; x130.

White cast iron

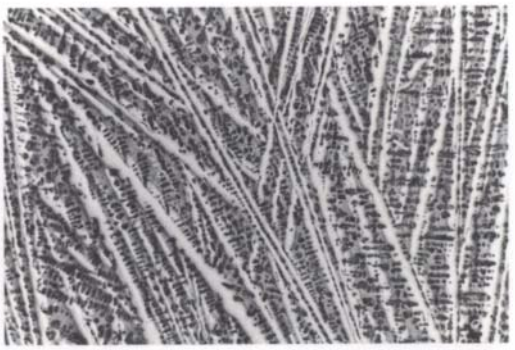

Figure 193, top right. Overall structure of white cast iron showing long cementite laths and small globular regions of pearlite. Etch: picral; x40.

This white cast iron dates to the early 20th century and has about 4% carbon and 2% phosphorus.

Before etching, some structural detail can be seen in the form of slightly whiter and harder needlelike growths in a more cream-colored matrix. Note that there are several intergranular cracks that affect this sample, as well as a region of porosity on one side of the ingot.

After etching in picral, the structure can be seen to consist of cementite laths with a fine infill of pearlite some of which can be resolved under the microscope. The remaining material between the cementite laths and the pearlite is the ternary eutectic, steadite. Here it tends to be present as fine particles of ferrite, sometimes showing a herring-bone effect set in a white matrix of iron carbide and iron phosphide.

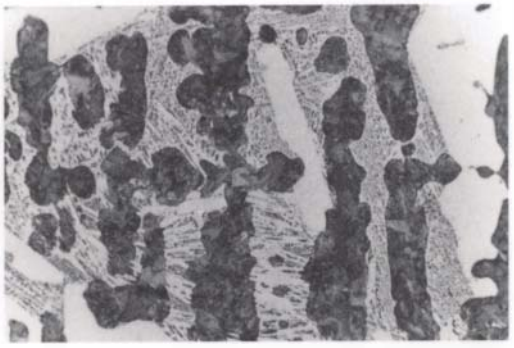

Figure 194, bottom right. Cast iron etched in Murakami's reagent and picral. The solid white areas are cementite, dark grey zones are pearlite with occasional non-metallic inclusions and the finely structured white areas with dark spots are ferrite in a white matrix of iron carbide and iron phosphide. x160.

Using alkaline sodium picrate etch or picral will darken the carbide, although it should be used hot, while Murakami's reagent can be used for examination of the iron phosphide in these cast irons.

Tin ingot from Cornwall

Figure 195, above. Tin ingot from Cornwall. 85 mm.

Many tin ingots have been recovered from marine excavations off the coast of Cornwall, England. This small tin ingot is heavily corroded and fragmentary with little metallic structure remaining. The components are now mostly the tin oxides cassiterite, romarchite, and hydroromarchite. The first of these is SnO_2 while the other minerals are SnO and hydrated SnO respectively.

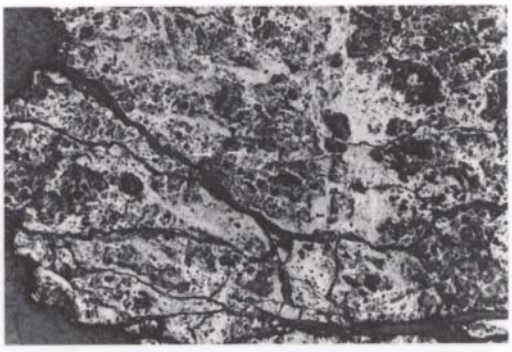

Figure 196, right. Heavily veined and corroded fragment from the tin ingot in which no metal remains, nor is there any clear pseudomorphic retention of the original cast structure of the ingot. The shape of the ingot is preserved entirely in corrosion products. Unetched; x35.

The following phase diagrams have been selected as being the most useful for investigations into ancient metals. Many of the figures drawn earlier in the text are schematic representations of the complete phase diagrams included here. In most cases the different regions of each diagram have been labeled with the appropriate Greek letter by which the phase region concerned is usually known. Some ternary diagrams are given although discussion of their application has not been dealt with in the text. They have a direct relationship to some of the binary phases and ternary mixtures that may occur in ancient metals and are given here because of their usefulness as reference material. For further details concerning phase diagrams the reader is referred to the books by Cottrell (1975), Lord (1949), West (1982), and Bailey (1960). Since the ε phase in ancient bronzes is not present below about 28% in tin, some different versions of the copper-tin diagram are included to represent the variable limits of a solid solution in practical terms, such as under normal casting conditions or if well annealed.

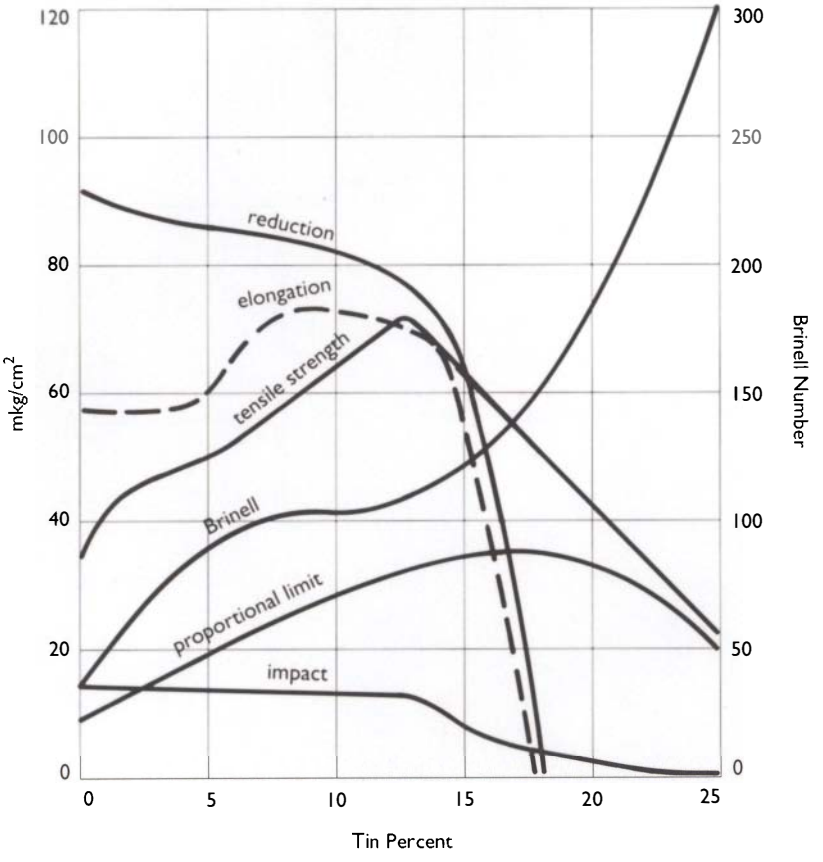

Figure 197. Tensile properties, impact value, and hardness of wrought copper-tin alloys.

Figure 198. Copper-tin system.

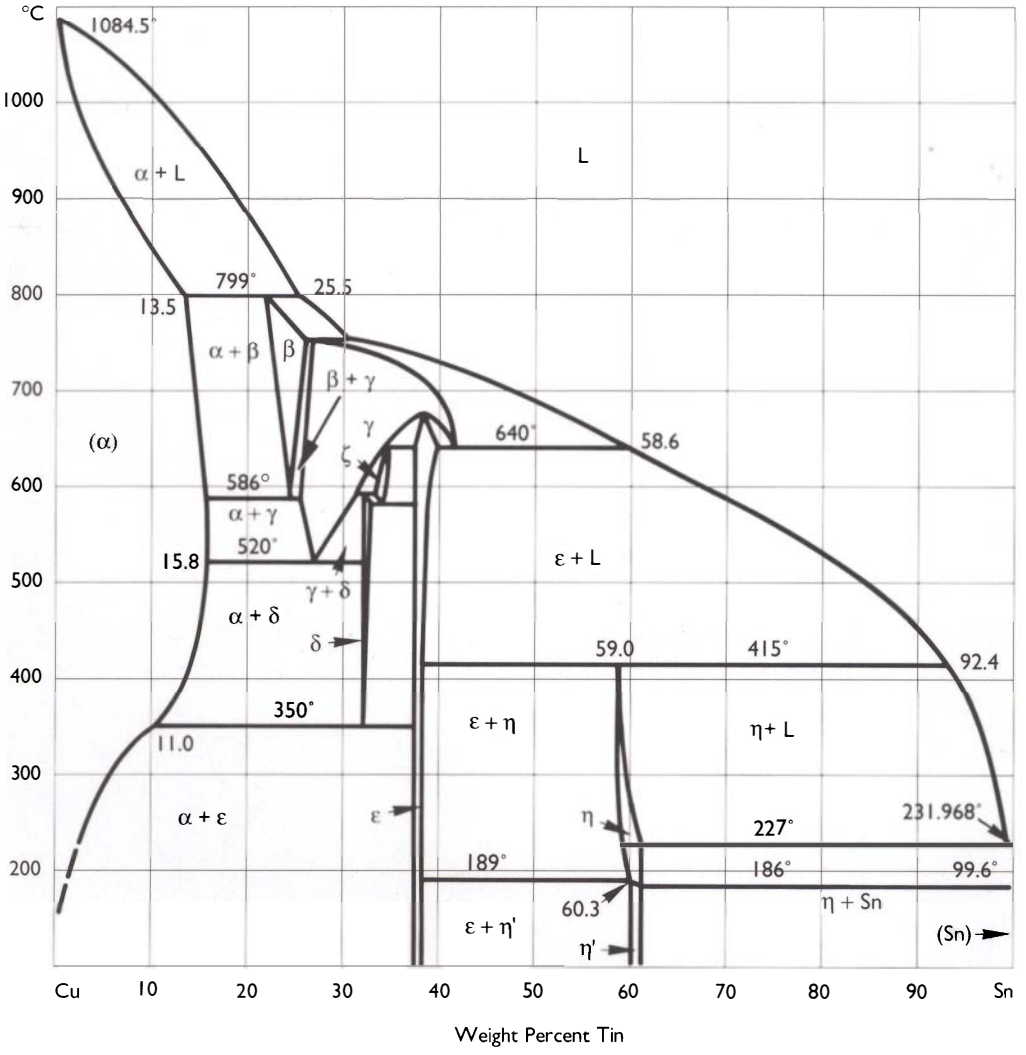

Figure 199. Part of the copper-tin diagram under different conditions.

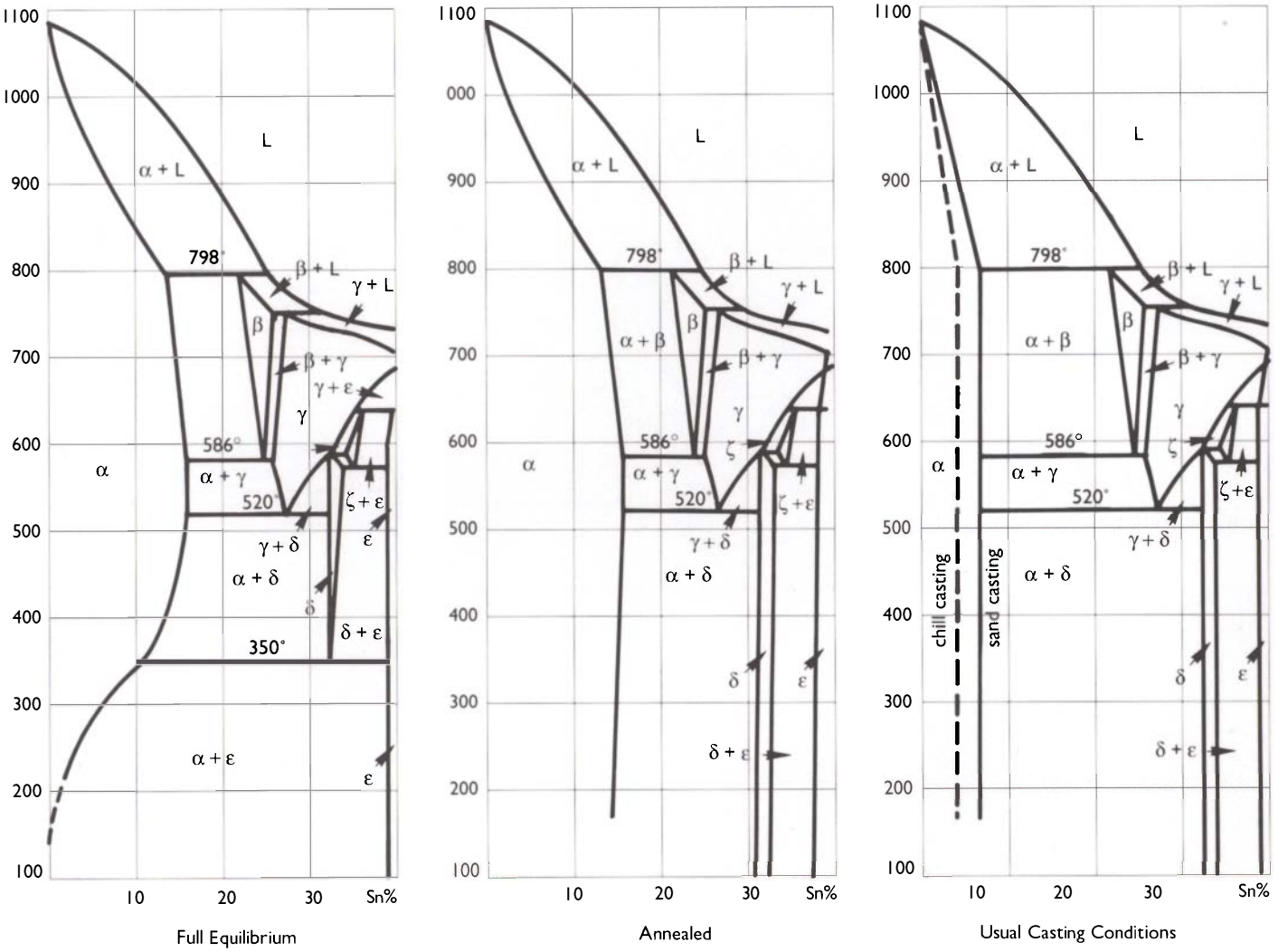

Full Equilibrium

Annealed

Usual Casting Conditions

Figure 200. Copper-arsenic system.

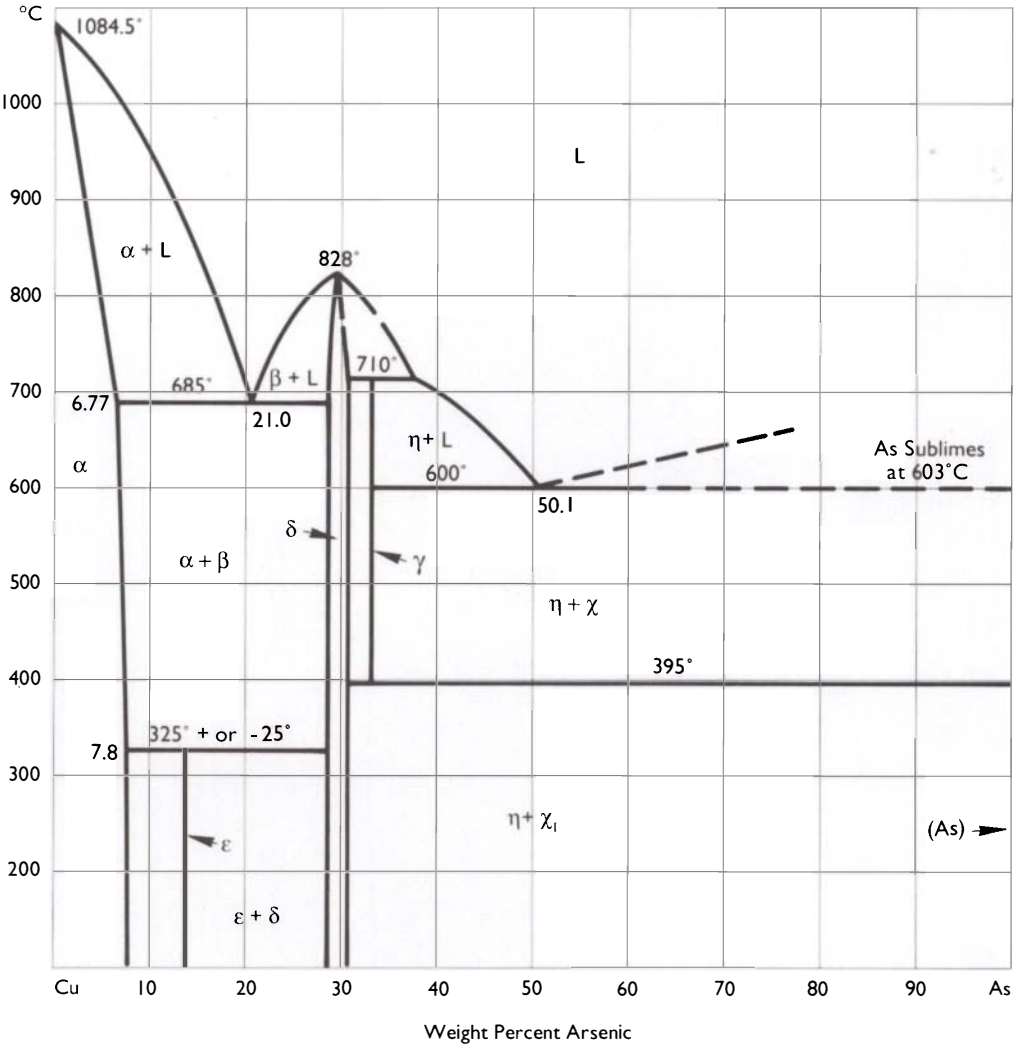

Figure 201. Copper-lead binary system.

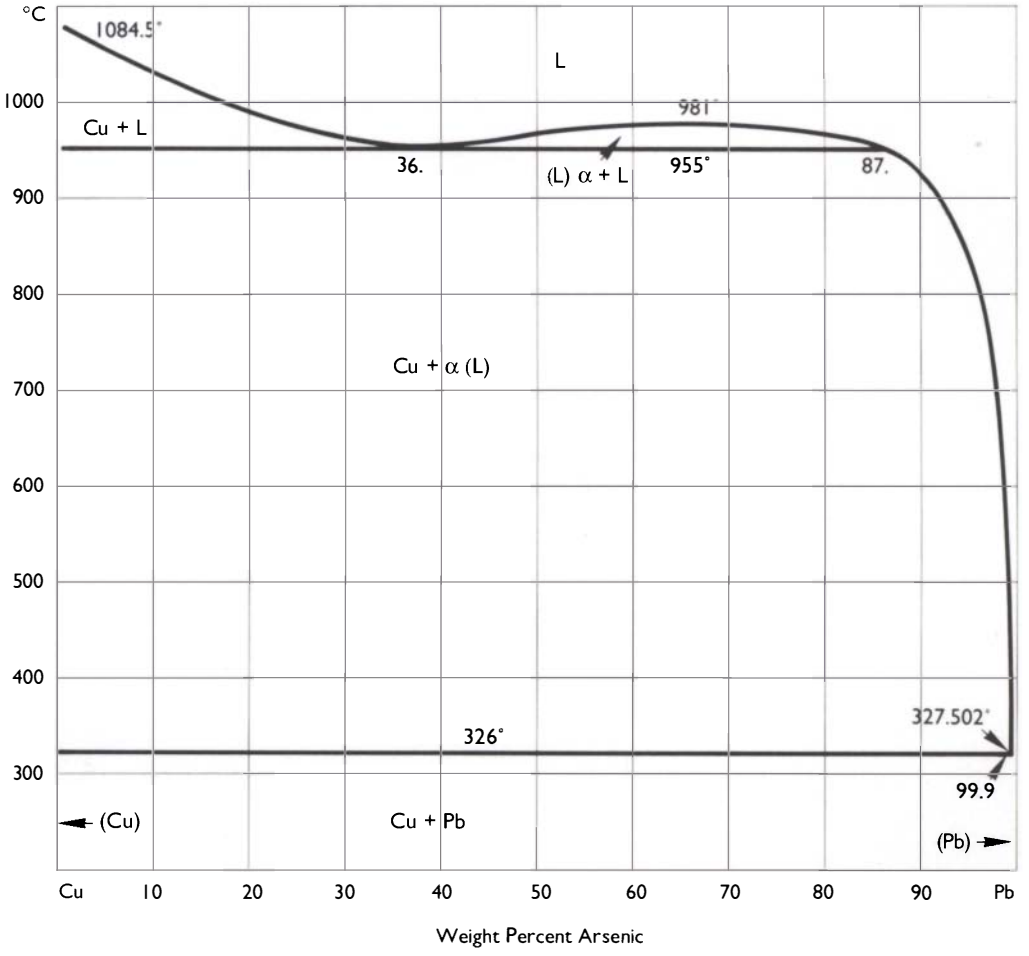

Figure 202. Copper-iron binary system.

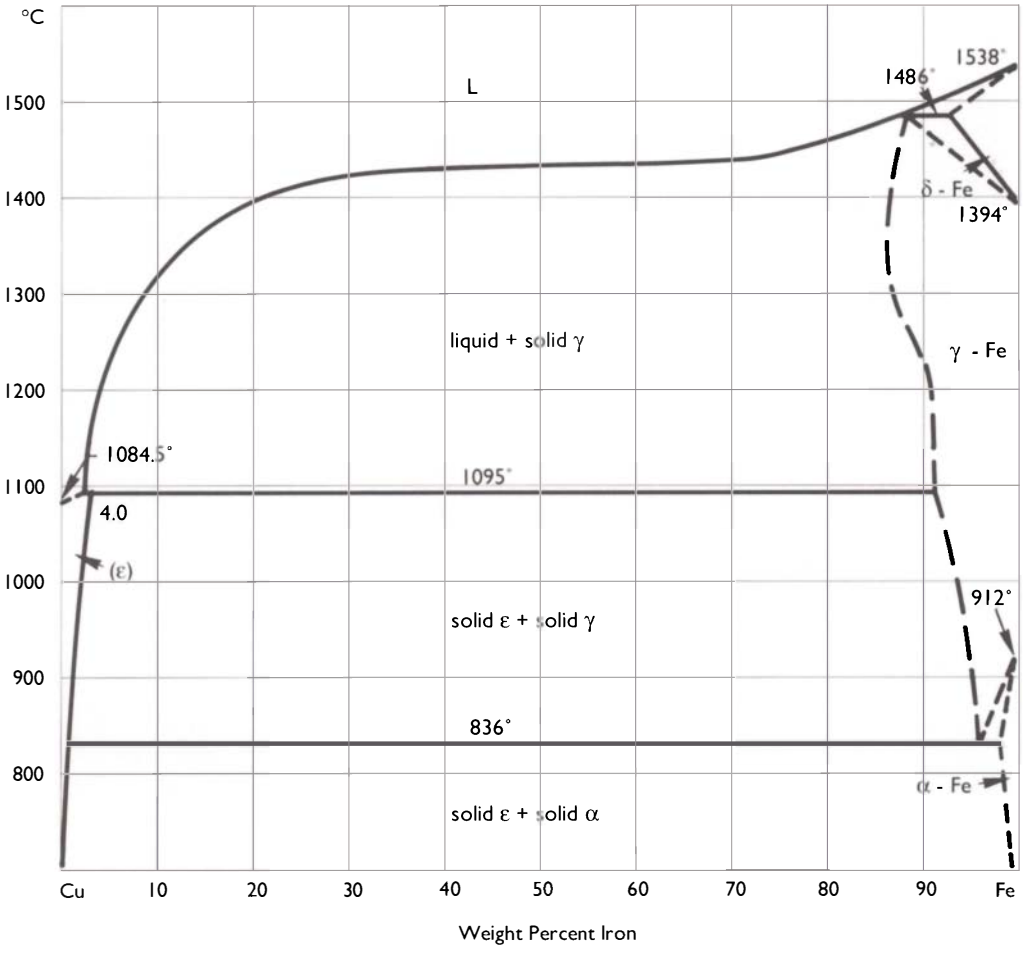

Figure 203. Copper-gold binary systems.

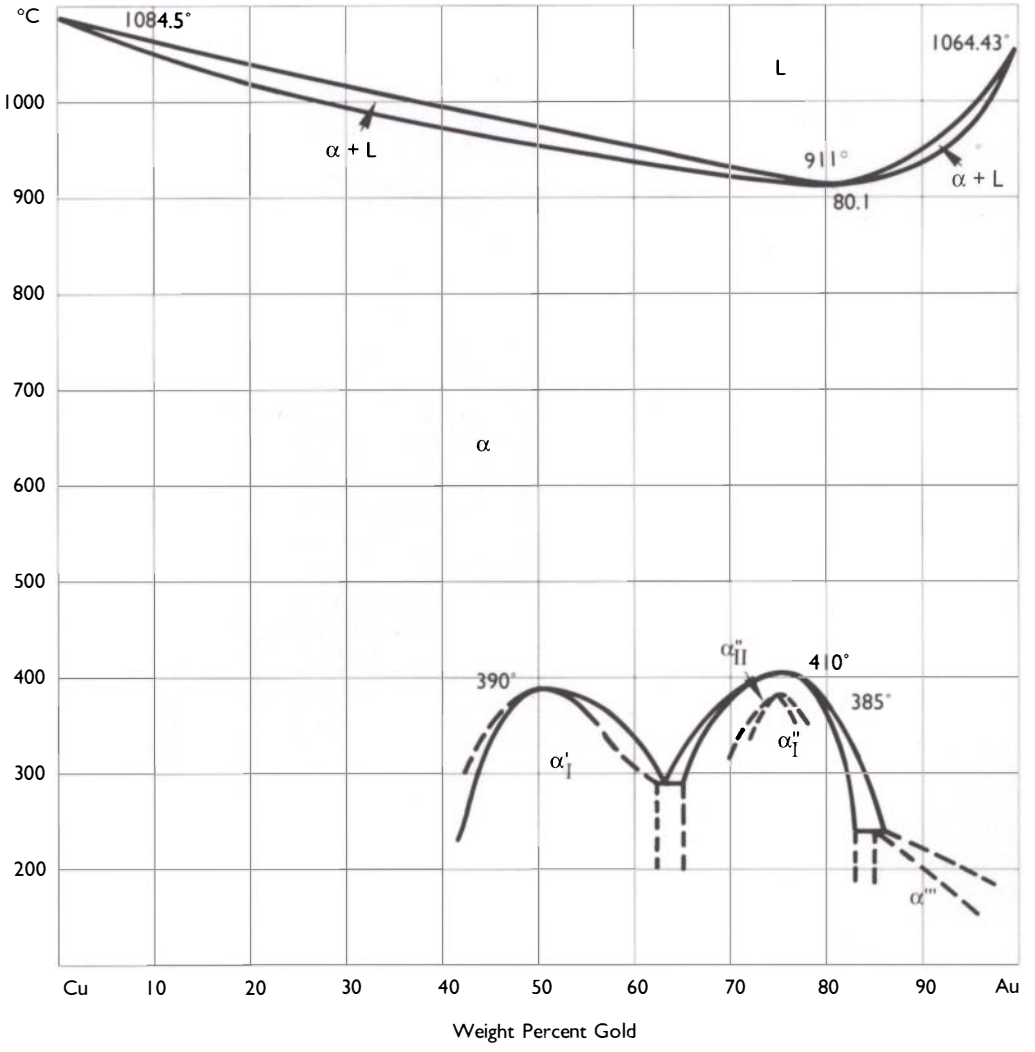

Figure 204. Copper-antimony binary systems.

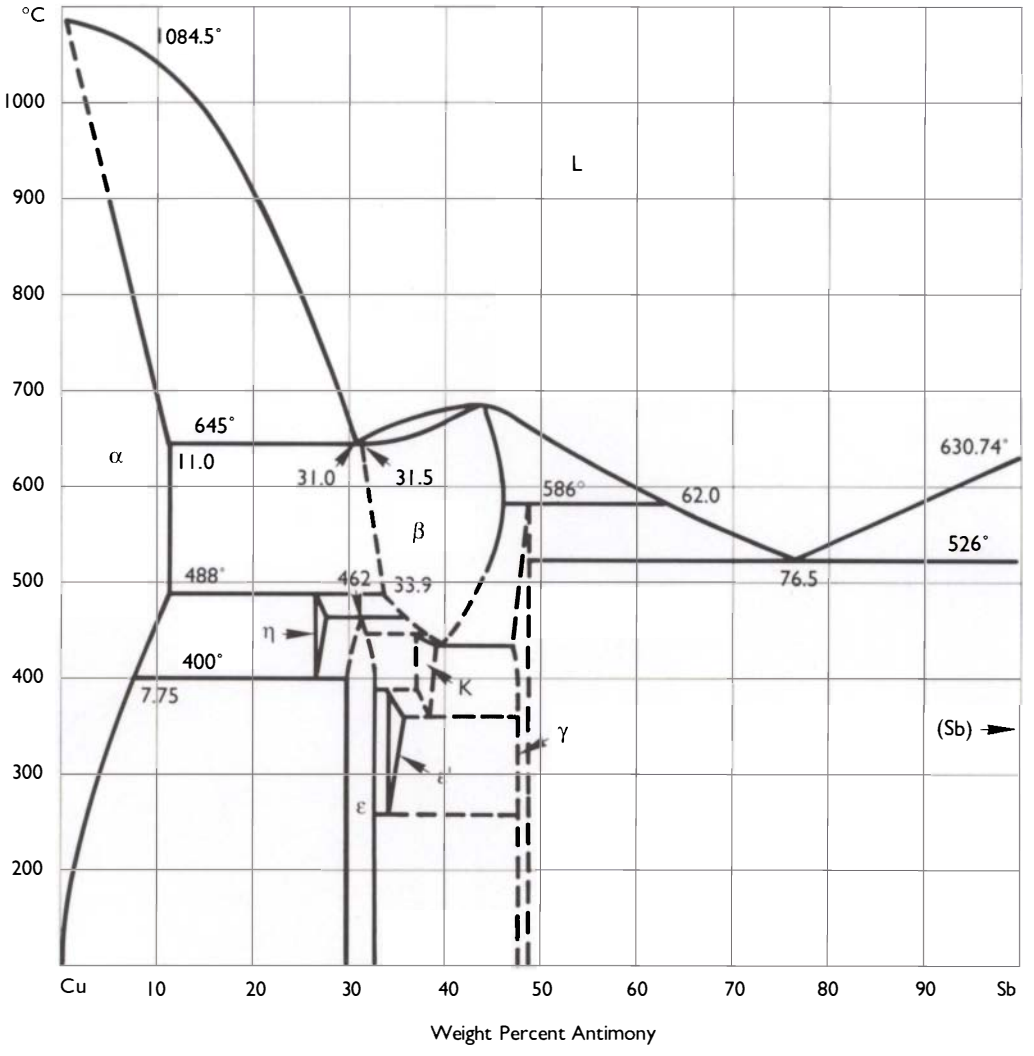

Figure 205. Copper-silver binary system.

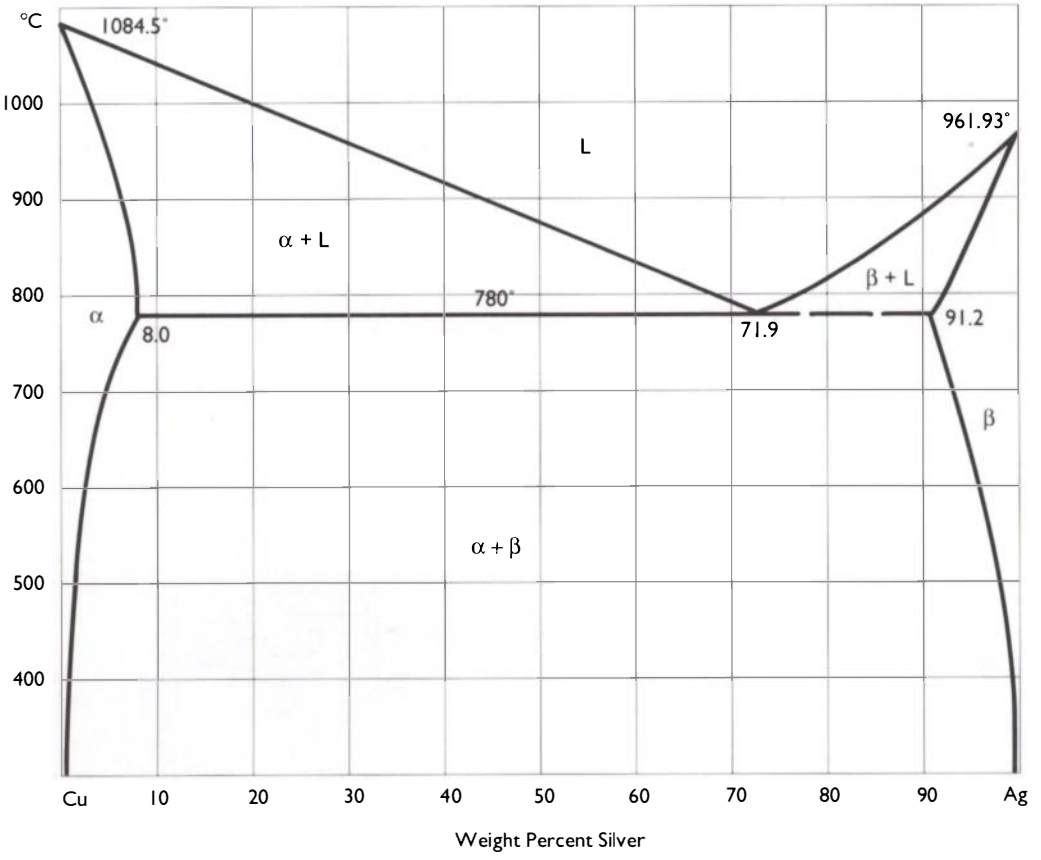

Figure 206. Copper-nickel binary system.

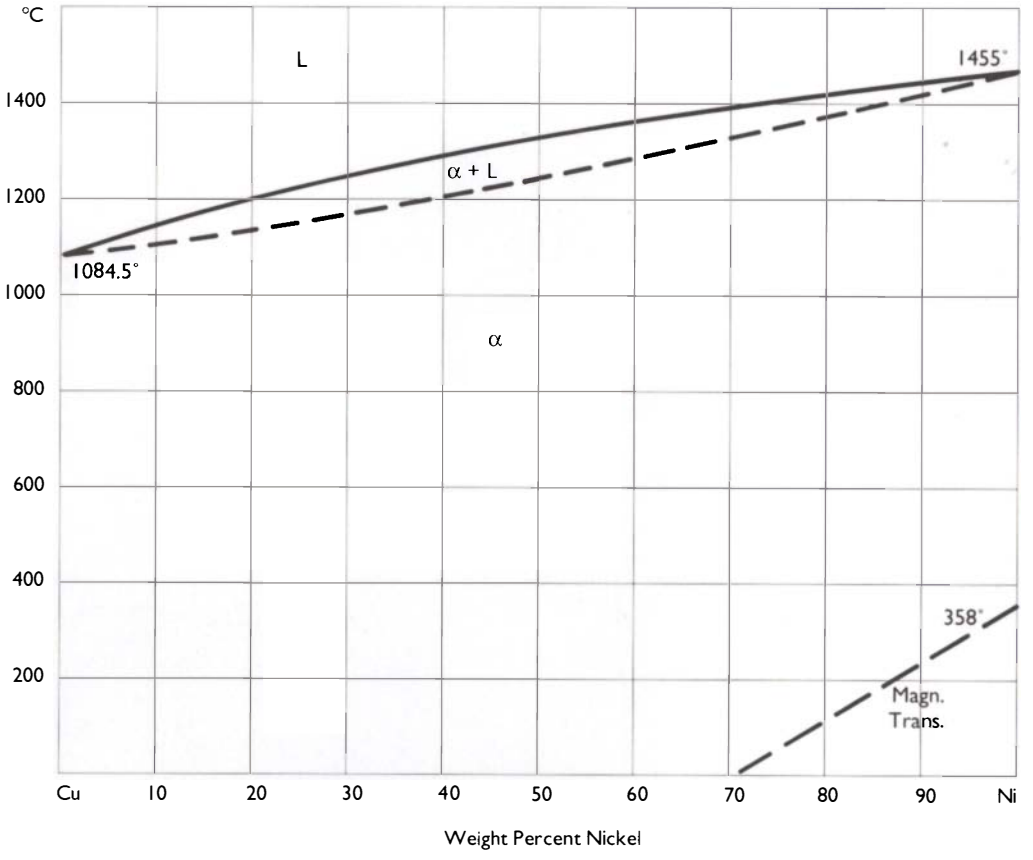

Figure 207. Copper-zinc binary system.

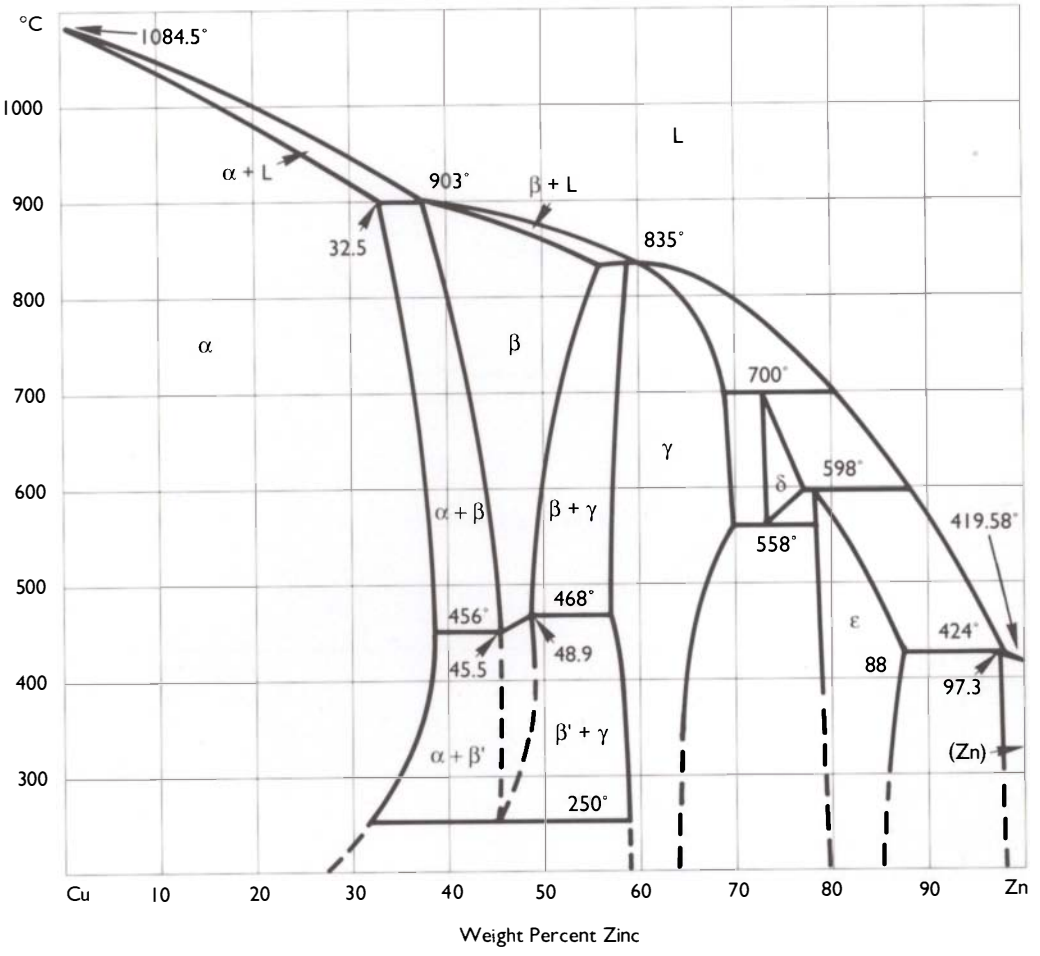

Figure 208. Iron-carbon system.

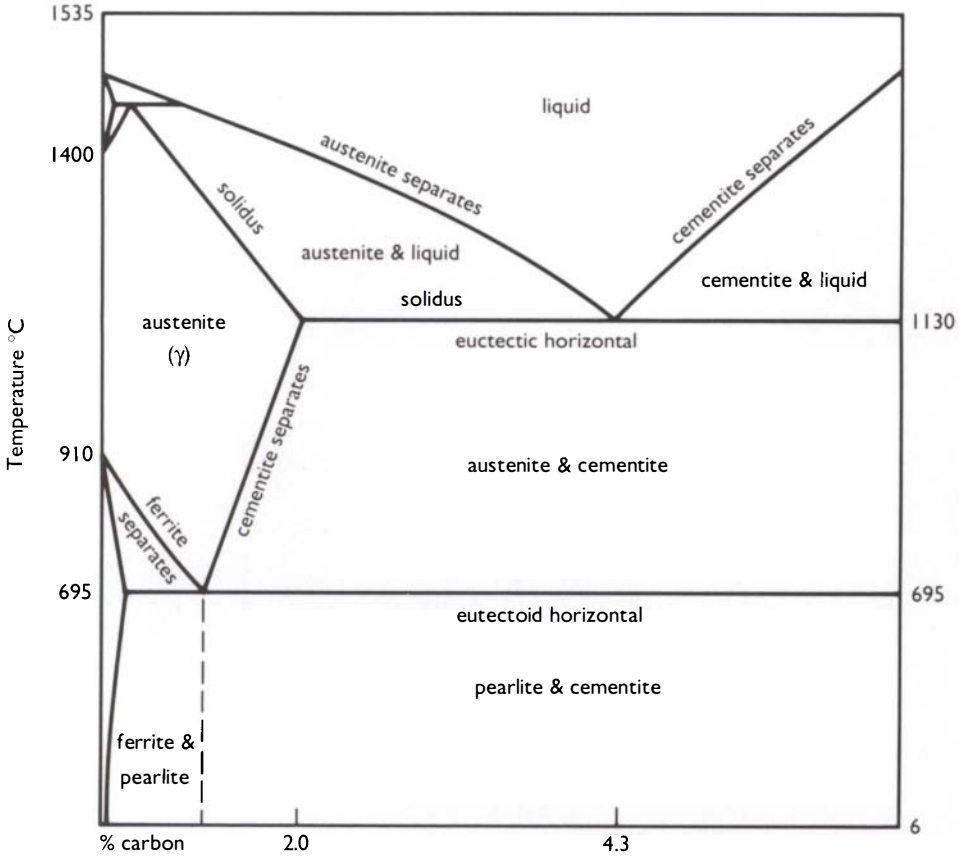

The Complete Iron-Carbon Diagram

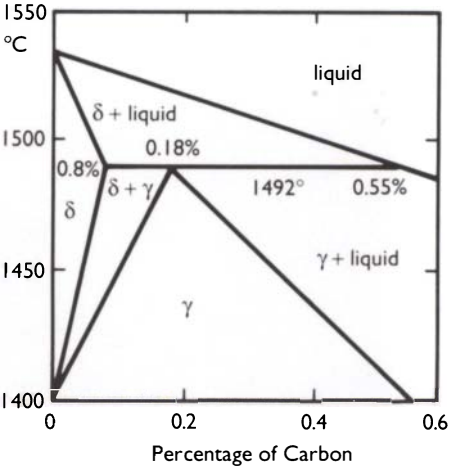

The δ-Region of the Iron-Carbon Diagram

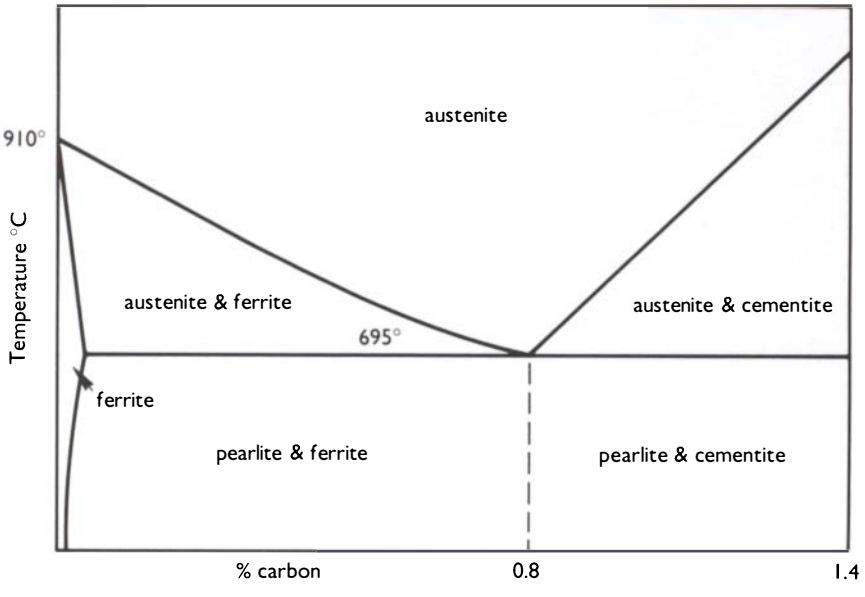

The Steel Portion of the Iron-Carbon Diagram

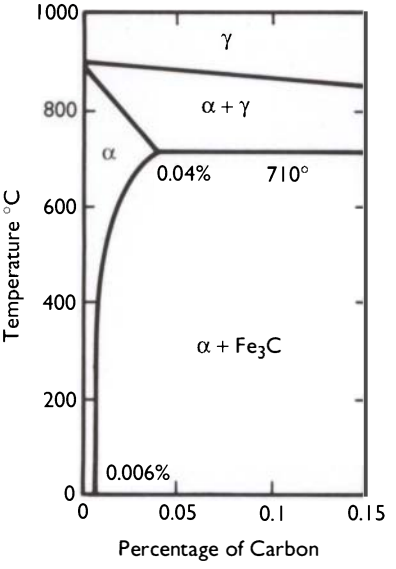

Constitutional Diagram Indicating Solubility of Carbon in α-Iron

Figure 209a. The lead-tin system (pewters).

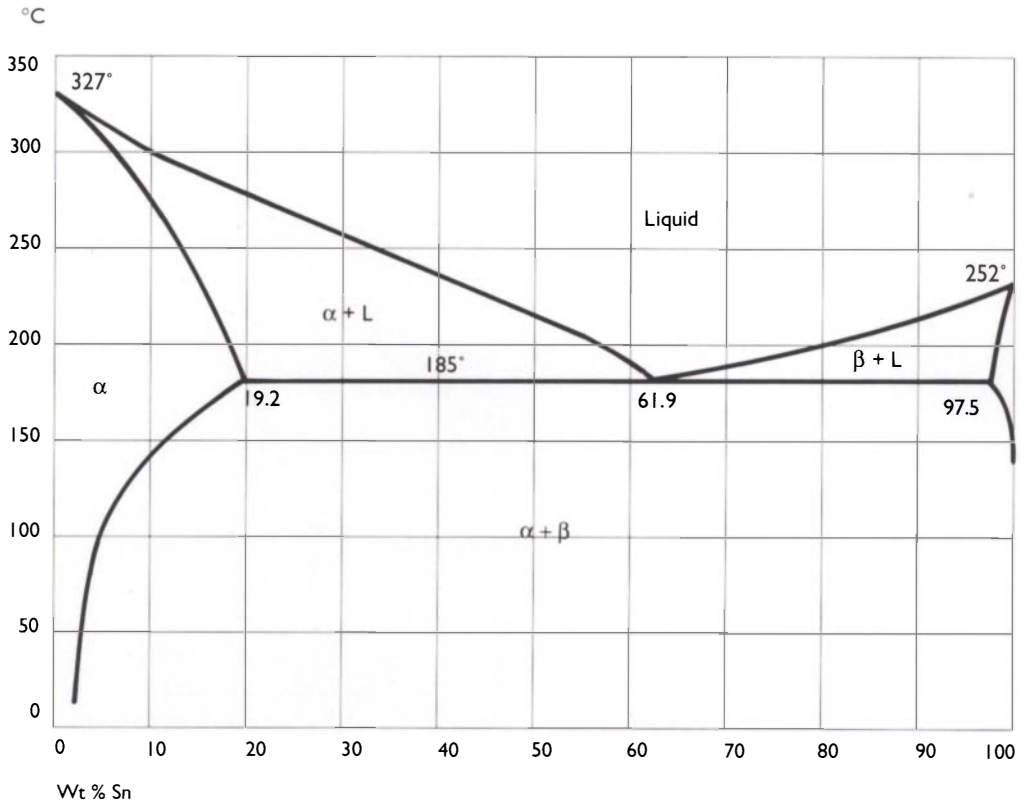

Figure 209b. The gold-silver system.

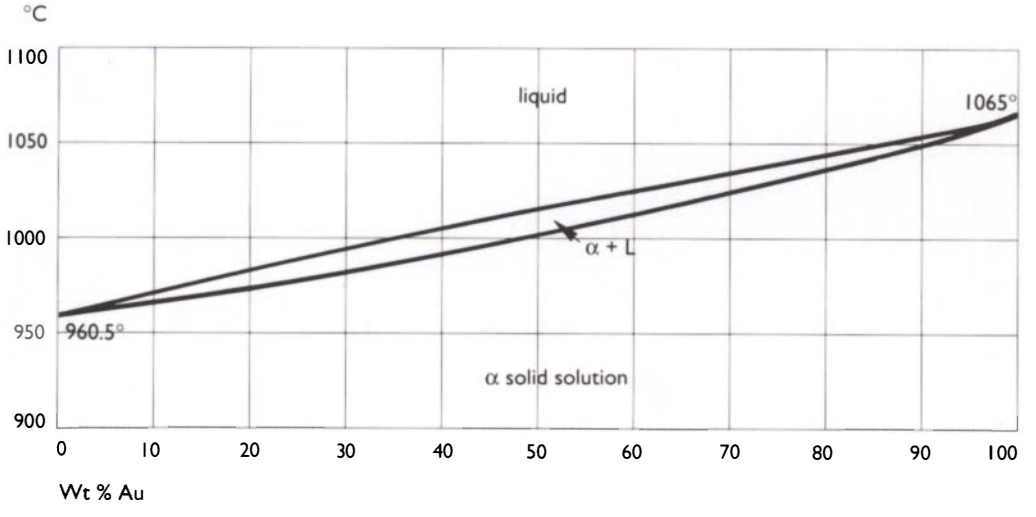

Figure 210. Copper-silver-gold ternary liquidus.

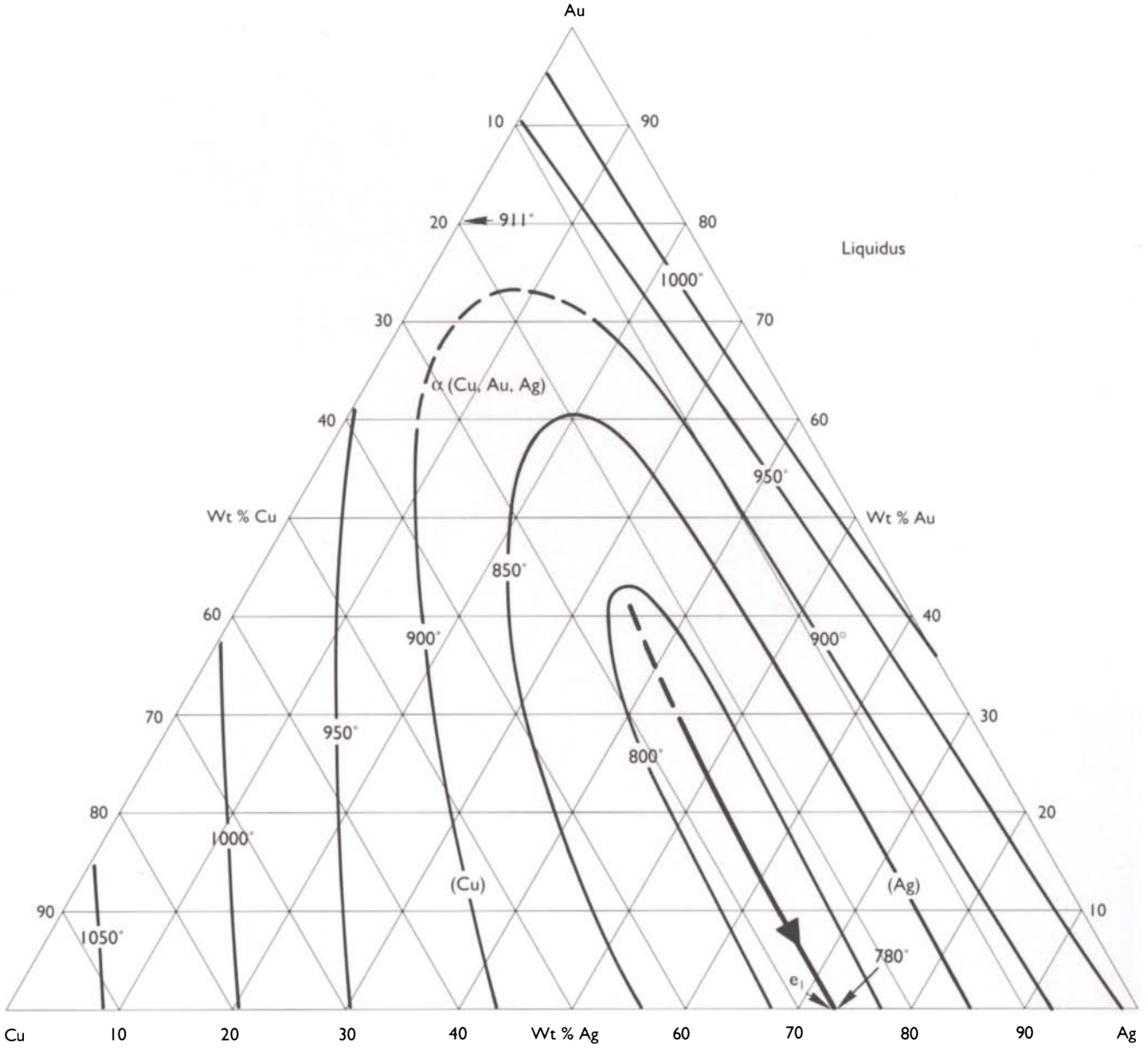

Figure 211. Copper-silver-gold ternary solidus.

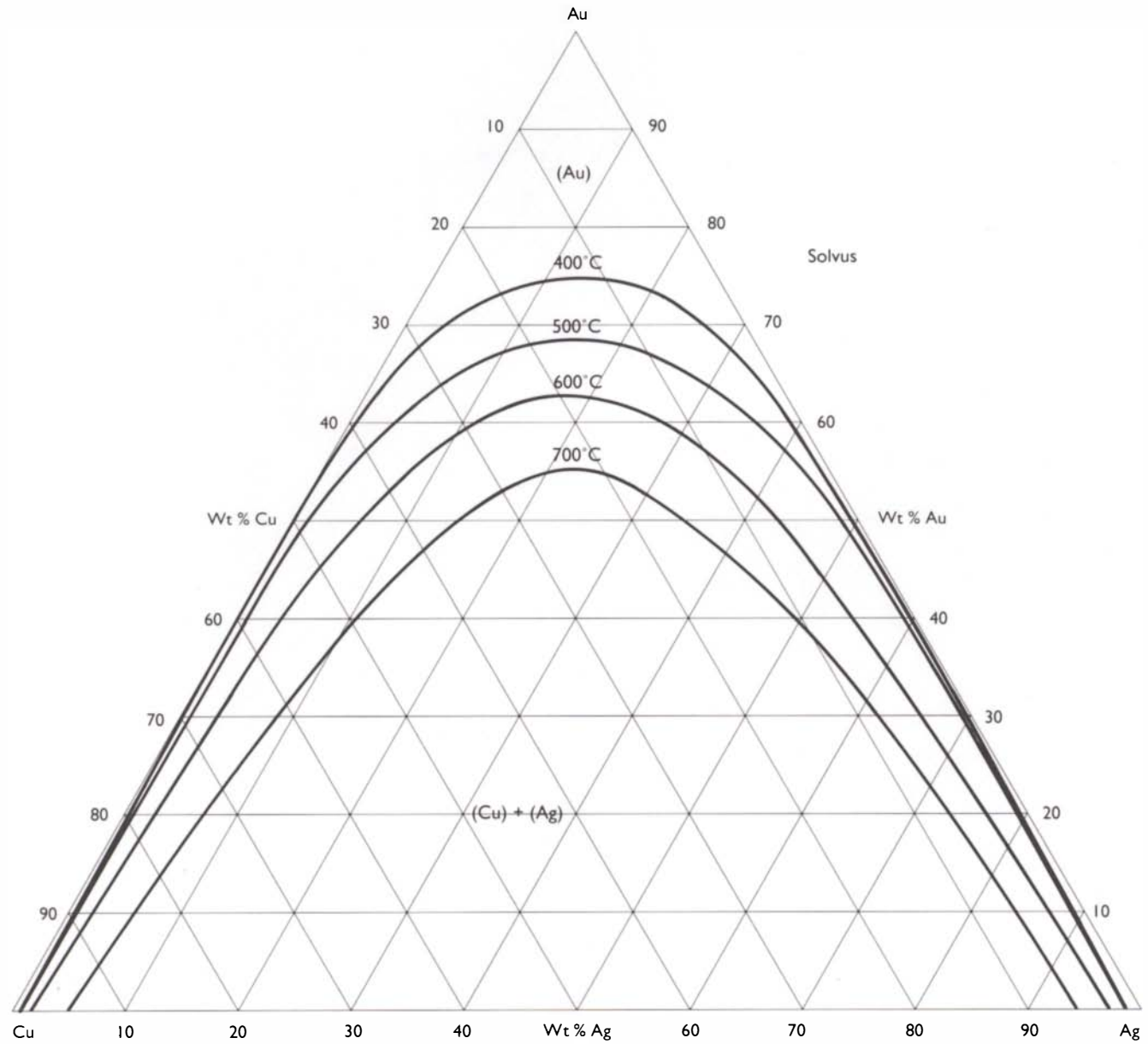

Figure 212. Copper-tin-lead ternary system.

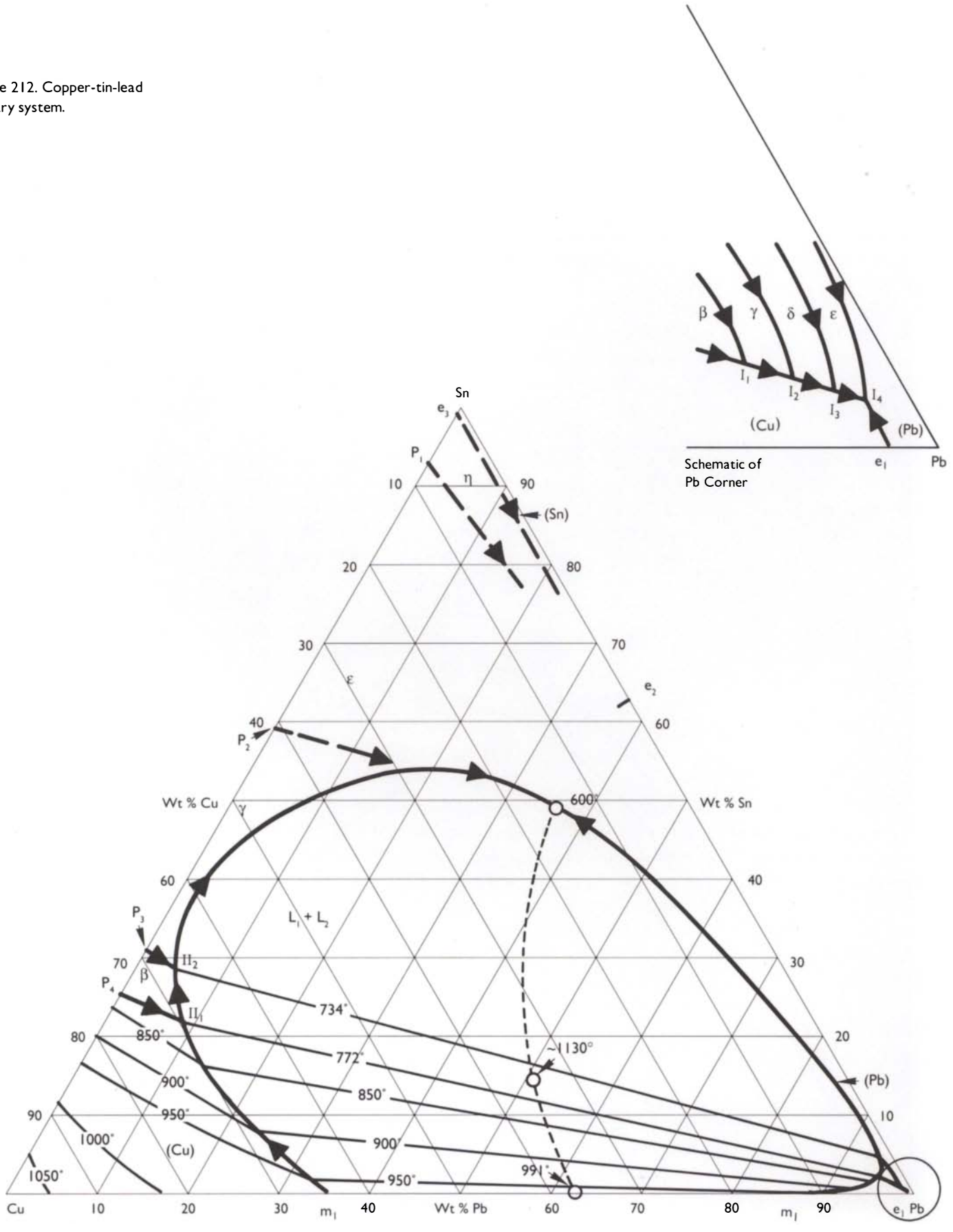

Glossary

Acicular
Possessing an elongated or needle-shaped structure.

Admiralty brass
An outdated term for an alpha brass in which some zinc is replaced by tin; usually only about 1–2% tin is added.

Age-hardening
The process of hardening spontaneously over time at ambient conditions. Some steels age-harden as do other alloys. The process was first studied in aluminium-copper where coherent regions of different structure form as the first stage of the process.

Alloy
A mixture of two or more metals. The term alloying suggests the mixture was deliberate.

Alpha brass
An alloy of copper and zinc with no more than 38% zinc. In antiquity, the cementation process for the manufacture of brass meant that only up to 28% zinc might be absorbed in the copper when the zinc ore was reduced in situ. Most ancient brasses do not contain over 28% zinc.

Aluminum
Atomic weight 26.98, atomic number 13, mp 660.37 °C, specific gravity 2.69. It is the most abundant of the metallic elements but is very difficult to extract and was not properly known until 1827.

Amalgam
An intermetallic compound or mixture of mercury with other metals. Mercury may form an amalgam with gold, silver, tin, zinc, lead, copper, and other metals. The microstructure of these amalgams may be complex.

Amalgam gilding
The process used for the gilding of many copper alloys in ancient and historic times. Gold becomes pasty when mixed with mercury and may be applied as a paste over a surface. This can be followed by heating to drive off most of the mercury, or the mercury can be applied to the clean surface of the object to be gilded, followed by the attachment of gold leaf or foil.

Antimony
Element with atomic number 51, atomic weight 121.75, mp 630 °C, specific gravity 6.62. A lustrous metal with a bluish silvery-white appearance. The metal does not tarnish readily on exposure to air and can be used as a decorative coating. Antimony is found in some copper alloys of antiquity and in the region of 3% has a considerable hardening effect.

Annealing
A process of heat-treatment carried out on a metal or alloy, usually to soften the material to allow further deformation. Strictly speaking, if an alloy is involved, annealing should be further described by such terms as stress-relief anneal, solid solution anneal, normalizing, etc.

Annealing twin
In FCC metals, a process of recrystallization (often of worked and annealed metals) in which a mirror plane in the crystal growth results in two parallel straight lines appearing across the grain when the metal is etched.

Anode
Component of a system that is usually corroded. In an electrochemical reaction, the electrode at which oxidation occurs.

Arsenic
Element with atomic number 33, atomic weight 74.9214, specific gravity (grey form) 5.73. The usual variety is grey arsenic which sublimates at 610 °C. Arsenic is a steel-grey color with a metallic luster and was the first alloying element of importance. Arsenical copper alloys precede the use of tin bronzes in most areas of both the Old and New Worlds. Arsenic contents usually vary from about 1 to 8%.

Bainite
A term more commonly applied in the past to the decomposition of martensite in steels by tempering at about 200–350 °C.

BCC
Body-centered cubic. A unit cell in which atoms are situated at each corner of a cube with one atom in the center of the cube. Each atom at the corners is shared by each neighbor. Because of the close packing, BCC metals such as barium, chromium, iron, molybdenum, tantalum, vanadium, and tungsten cannot be heavily worked but they have a good combination of ductility and strength.

Bidri
Name for an Indian copper-zinc-lead alloy, finished by surface treatment to color it black and often inlaid with silver.

Bloom
A roughly finished metallic product; specifically, the spongy mass of iron produced in a bloomery furnace in which the iron is reduced in situ and is not molten during reduction. The crude iron bloom must be extensively worked at red heat to consolidate the iron and remove excess slag and charcoal.

Brass
An alloy of copper and zinc, usually with copper as the major alloying element and zinc up to 40% by weight. Early brasses were binary alloys containing 90–70% copper and 10–30% zinc. The color of brass changes with increasing zinc content from a rich copper-red through pale yellow to white as the zinc increases.

Gilding metal containing 10–15% zinc is suitable for cold working. It is used for ornamental work and jewelry. Red brass contains 30% zinc and 70% copper and has good working properties. The common form of brass is 60% copper, 40% zinc and is known as yellow brass or Muntz metal (see also alpha brass).

Brazing

Joining of metals together with an alloy of copper and zinc. Modern brazing alloys may contain copper, zinc, and silver and are often called silver solders. In ancient times, silver-gold, copper-silver, and silver-gold-copper alloys were used for brazing (or soldering) operations on precious metals in particular.

Bronze

In antiquity and historical usage, an alloy of copper and tin. Usually with up to 14% tin, but many examples of ancient alloys are known with higher tin contents. 14% tin is the limit of solid solution of tin in well annealed α bronzes. In modern usage, the term bronze is associated with a number of copper alloys that may contain no tin at all and the composition of the alloy must be specified.

Brinell

The Brinell Hardness Scale in which the hardness is measured by the resistance to indentation of a small steel ball. This method is becoming less common, but does allow some comparison with results from the Vickers Scale, or other scales used more for industrial purposes, such as the Rockwell Scale.

Carat

A term used to express the degree of purity or fineness of gold. Pure gold is 24 carat or 1000 fine. The fineness of alloyed gold can be expressed in the number of parts of gold that are contained in 24 parts of the alloy. For example, 18 carat gold contains 18/24 parts of gold and is 75% gold or 750 fine.

Carburization

The process of increasing the carbon content of the surface layers of a metal (often wrought iron) by heating the metal below its melting point with carbonaceous matter such as wood charcoal.

Case-hardening

A process consisting of one or more heat-treatments for producing a hard surface layer on metals as in carburization. In the case of steel the carbon content of the surface can be increased by heating in a medium containing carbon followed by heat treatment.

Casting

The operation of pouring metal into sand, plaster, or other molds and allowing it to solidify. More generally, a metallic object that has been made by casting the metal into a shape. The simplest forms are open molds that are uncovered at the time of casting. This form was often used for simple early Bronze Age axes. Piece molds are made of two or more fitting pieces in stone, bronze, or refractory clay. Hollow-cast objects are usually piece molds with false cores. A figure was modeled in clay and a piece mold was built up around the model. The model was removed and could be shaved down in size to provide the core around which the mold pieces and mother molds would be assembled. Many variations are possible (see also lost-wax casting).

Casting-on

The process of making a cast part attached to an already existing object or component. In antiquity, a lost-wax addition, made by creating a small mold around part of an object and casting on metal directly to it. Often used for dagger handles or repair or construction of large bronze figures.

Cast iron

An iron-carbon alloy that usually contains 2–4% carbon. Generally divided into three groups: (1) Grey cast iron in which free carbon occurs as flakes of graphite. It has excellent casting properties and can be machined. (2) White cast iron in which all of the carbon is taken up as cementite, Fe_3C and as pearlite. These irons are usually hard and brittle. (3) Malleable cast irons are usually obtained by heat-treatment of white cast irons by converting the combined carbon into free carbon or temper carbon. In the whiteheart process, for example, a certain amount of carbon is removed from the surface by oxidation.

Cathode

In an electrochemical cell, the component on which reduction takes place. In many corrosion processes, the cathodic regions are protected during corrosion, while attack takes place at anodic regions.

Cementation

The term has several meanings. Cementation of gold alloys with salt in a cupel may remove silver leaving pure gold behind. Carbonaceous material may be used to cover the wrought iron, which is then heated. Carbon can diffuse into the structure creating a low-carbon steel surface by cementation.

Cementite

The hard, brittle component of iron-carbon alloys, containing about 6.6% carbon, corresponding to the phase Fe_3C and crystallizing in the orthorhombic system. It is soluble in molten iron, but the solubility decreases in austenite to about 0.9% at the eutectoid temperature. Pearlite, the eutectoid of ferrite and cementite, is the most common component

containing cementite in ancient and historic steels.

Centrifugal casting
Casting by the lost-wax process (usually) followed by rapid rotation of the casting mold to force the molten metal into the casting spaces. Often used in modern dental casting techniques and more associated with modern castings than with ancient practice.

Chaplets
Small pegs, wires, or other materials used to hold a hollow lost-wax casting in position in the mold by securing the investment or casting core to the mold so that it will not move when the wax is molten out.

Chasing
Displacement of metal by use of a chasing tool, often of brass or bronze or wrought iron. Unlike engraving, metal is distorted around the chased design and is not removed.

Cire perdue
Term meaning lost-wax casting.

Coherent precipitation
An atomic rearrangement of structure that is imperceptible by optical microscopy.

Cold-working
The plastic deformation of a metal at a temperature low enough to cause permanent strain hardening. The treatment usually consists of rolling, hammering, or drawing at room temperatures when the hardness and tensile strength are increased with the amount of cold-work, but the ductility and impact strength are reduced.

Columnar
Long columnlike grains that can form when a pure metal is cast into a mold.

Continuous precipitation
The formation of a precipitate or inclusion distribution uniformly through the grains themselves.

Copper
An element with atomic number 29, atomic weight 63.54, mp 1083 °C, specific gravity 8.96. Pure copper is reddish in color and malleable and ductile. It occurs in native copper in dendritic masses and has been known for thousands of years. Many copper minerals were used to extract copper metal in primitive furnaces, in the form of copper prills and later as cakes and ingots of copper. There are about 240 copper-bearing minerals and both copper oxides and sulfides were smelted to obtain the metal.

Coring
The segregation of an alloy on successive freezing to the solid. Zones are formed, especially in dendritic castings, in which a continuous series of small changes in composition occurs as the dendrite arm is formed. Especially common in ancient cast bronzes and cast silver-copper alloys. Coring is accentuated in alloys with a wide separation between liquidus and solidus curves.

CPH
Close-packed hexagonal. A hexagonal net in which the atoms are arranged in a repeating sequence ABABABA..... One unit lattice has a hexagonal prism with one atom at each corner, one in the center of the bottom and top faces, and three in the center of the prism. CPH metals tend to be brittle, e.g., cadmium, cobalt, titanium, and zinc.

Crimping
Mechanical join between two pieces of metal in which they are deformed to shape an overlap or attachment.

Cupel
A porous ceramic, often made from bone-ash or other refractory components. The cupel is used to melt small amounts of metal, usually silver for the extraction of lead, or the assay of gold. In the extraction of lead from silver, the oxidized lead is absorbed into the cupel leaving a button of silver. The cupel can then be broken and smelted to recover the lead.

Cupellation
Often applied to the removal of basic metals from silver or gold by use of a cupel and either oxidation of base metallic constituents or chemical combination with salt.

Cupro-nickel
Alloys containing copper and nickel, usually from 15% to 70% nickel, but in ancient alloys often with less nickel than this. Alloys with about 25% nickel are now used for coinage metals. Early examples of copper-nickel alloys are also known, the most famous being the Bactrian coinage.

Damascening
An ancient process of ornamenting a metal surface with a pattern. In the early Middle Ages swords with this pattern were said to be from Damascus, made by repeatedly welding, drawing out, and doubling up a bar composed of a mixture of iron and steel. The surface was later treated with acid to darken the steel areas. Ferrite remains bright. In the East the process of inlaying metal on metal is common, particularly in parts of Iraq and India, where it is known as Kuft work.

Dendritic
Shaped like the branches of a tree. Dendrites are common in cast alloys and may look like an intersecting snowflake pattern.

Depletion gilding
Gilding by removal of one or more baser components. Commonly used in ancient South America for the gilding of *tumbaga* or gold-silver-copper alloys by removing copper from the outer surfaces by pickling.

Depletion silvering
Silver-copper alloys usually develop a scale when worked and annealed. Removing oxide scale enriches the surface in silver, creating a depleted copper zone and making the alloy silver in color.

Diffusion
The migration of one alloy or metal into another. Interdiffusion also occurs with the secondary metal migrating into the first. Usually heat is required for this process to occur.

Diffusion bonding
Bonding or joining of two metals by heating them together. Each will diffuse into the other, at different rates, creating a strong and permanent metallurgical bond.

Discontinuous precipitation
Precipitates laid down at grain boundaries, often by a process of aging or of exsolution of metastable phases. An example is the precipitation of copper from silver-copper alloys.

Dislocation
Defects in the crystal structure of a metal that allow movement of planes or atoms within the lattice. Edge and screw dislocations are two common types.

Dislocation entanglement
The density of dislocations increases on working the metal until dislocation entanglement is reached. At this point the metal is brittle since no further movement can occur. Annealing will restore working properties.

Drawing
The act of pulling a wire, usually of silver or gold through a drawplate of hard material. Drawing is not thought to have occurred before the 6th century A.D.

Ductility
The ability of a metal to be drawn or deformed. Ductile metals are usually FCC types such as silver or gold.

Electrochemical corrosion
Corrosion of a metal in which anodic and cathodic reactions result in metallic dissolution. The most common form of corrosion of buried or marine metals.

Electrochemical replacement plating
Cleaned copper will exchange with gold solutions to form a thin gold surface. Used in ancient Peru as a gilding technique.

Electrum
Naturally occurring alloys of gold and silver, usually white or silvery in color and containing up to about 40% silver.

Engraving
Use of an engraver, usually of hardened steel to remove metal from a surface.

EPNS
Electroplated nickel silver. An alloy of copper, nickel, and zinc typically with 60% copper, 22% nickel, 18% zinc, electroplated with silver.

Equilibrium diagram
A synonym for a phase diagram.

Equilibrium structures
Microstructures that represent full equilibrium phases predicted from phase diagrams. In ancient metals the structure may be far from equilibrium.

Equi-axed
Of equal dimensions or properties in all directions. Equi-axed grains are hexagonal in form.

Eutectic
In binary alloys the composition with the lowest melting point. The eutectic is a fixed composition in binary alloys and is often a fine intermixture of two phases, typically α and β.

Eutectoid
Decomposition from a solid phase into two finely dispersed solid phases creates a structure called a eutectoid. The eutectoid point is fixed in binary alloys and in morphology may resemble the eutectic.

Fayalite
The most common component of ancient slags, often occurring as slag stringers in wrought iron. Fayalite is an iron silicate, $2FeO.SiO_2$ which melts at about 989 °C, crystallizes in the orthorhombic system, and usually takes the form of broken, elongated grey laths in silicate based slags.

Filing
Removal of metal with a file. Filing is uncommon in ancient metalwork since hard steel files were not available.

FCC
Face-centered cubic. In this lattice system there is an atom at each corner of a cube and an atom at each center of the cube faces. Face-centered cubic metals tend to be soft and easily worked, such as silver, aluminium, gold, copper, lead, and platinum.

Fusion gilding
A process used in ancient South America, especially Ecuador, for the gilding of copper alloys by dipping or fusion of molten gold alloys to the surface, resulting in thick gold alloy coatings. May also be used to

create silver alloy coatings over copper.

Gama-hada
Japanese decorative technique making use of immiscible metals, such as silver or silver-copper alloy droplets on iron.

German silver
Alloys of copper, nickel, and zinc usually comprising about 52–80% copper, 5–35% nickel, and 10–35% zinc. This alloy was formerly used for many decorative purposes as a cheap substitute for silver, since it does not readily tarnish and is of silvery hue.

Gilded
Covered with gold.

Gold
Element with atomic number 79, atomic weight 196.96, mp 1063 °C, specific gravity 18.88. Native gold usually contains some copper and silver. Typical gold concentrations are 85–95% with the remainder being mostly silver. Gold is bright yellow, but with increasing silver content the color is white, while copper provides red tints to the color. Platinum from 20 to 25% and nickel make the alloy with gold white.

Gold leaf
Leaf in ancient technology is rare. The term is reserved for gold less than 1 micron thick.

Gold foil
Any gold sheet greater than 1 micron thick.

Grain
In crystalline metals, the grain is an area or zone of crystal growth in a uniform and homogeneous form. Most metals consist of grains and the grain boundaries are the interface between a succession of grains in the solid mass of crystals.

Grain boundary segregation
The precipitation of a phase or inclusion at the grain boundaries of a polycrystalline solid.

Granulation
Usually refers to small gold grains attached to an object with solder, either made in situ by reduction of a copper salt with glue or by use of diffusion bonding of the gold grains. Common in Etruscan goldwork.

Graphite
An allotropic form of carbon, occurring in the trigonal system as grey, soft, lustrous plates. It is the form of carbon found in steels and cast irons and usually occurs in grey cast irons as thin flakes or nodules.

Grey cast iron
Cast iron with a grey fracture. The fracture color is indicative that the cast iron contains free carbon as graphite.

Gunmetal
May have different compositions, but usually an alloy of copper, tin and zinc.

Hard soldering
An alternative term for the use of a brazing alloy or a copper-silver alloy for joining, as opposed to the use of lead-tin alloys.

Hot-working
Deformation of the metal or alloy above the temperature necessary for plastic deformation of the metal.

H_V
Hardness on the Vickers or Diamond Pyramid Number (DPN) scale.

Hypereutectoid
Containing a greater amount (often of carbon steels) than that required to form a completely eutectoid structure. In steels this would require more than 0.8% carbon, the amount needed to create a completely pearlitic structure.

Hypoeutectoid
Containing a lesser amount (often of carbon steels) than that required to form the eutectoid structure of 0.8% carbon. Most ancient steels are hypoeutectoid, except for Wootz steels made in a crucible, or later historical products, such as cut steel beads from France.

Intaglio
The process of engraving or removing metal to create a design. The depression so formed may be filled with niello or enamel.

Interstitial
A small element that may occupy lattice spaces without causing too great a distortion of the original lattice structure. An example is carbon in iron. Carbon is a small element and can insert into the cubic iron lattice.

Iron
An element with atomic number 26, atomic weight 55.85, mp 1528 °C, specific gravity 7.87. A heavy whitish metal and one of the most abundant and widely distributed. Iron was known early as meteoric iron, which usually contains some nickel. Extraction by the bloomery process was common by the early centuries B.C., and this continued until the invention of the blast furnace. Later methods of extraction in the Western world were able to melt iron and, by the 13th century A.D., make cast iron. In China, iron (with carbon) could already be molten during the time of Christ and cast iron was produced much earlier than in the West.

Latten
Copper-zinc-tin alloy (sometimes with lead as well) used in the medieval period for cheap

decorative and functional metalwork.

Lead

Atomic number 82, atomic weight 207.19, mp 327.4 °C, specific gravity 11.35. Pure lead recrystallizes at room temperature when deformed. The metal can readily be extruded into pipes or rod but lacks the tenacity to be drawn into wire. Lead was commonly extracted from galena, lead sulfide, and was often a by-product of the extraction of silver from galena, since many of these lead ores are argentiferous. Lead is a useful addition to bronzes and brasses, especially for making castings and is used as an alloy with tin as a soft solder.

Leaf gilding

Covering with gold by the application of gold leaf (or foil). Sometimes held mechanically by roughening the surface or by a diffusion bond to the substrate metal.

Ledeburite

Name applied to the cementite-austentite eutectic at 4.3% carbon which freezes at 1130 °C. During cooling the austenite in the eutectic may transform into a mixture of cementite and austenite.

Liquidus

The line on a binary phase diagram that shows the temperature at which solidification begins upon cooling from the melt. In a ternary diagram the liquidus is a surface, not a line.

Lost-wax casting

Casting from a wax model. The object to be made is shaped in wax (either solid or hollow) and is covered in a clay mold. When the wax is molten out, the space can be filled with molten metal, usually bronze or brass.

Martensite

Often used only for the hard, needlelike component of quenched steels, but more generally, any needlelike, hard transformation product of a quenched alloy. The most common in ancient materials is martensite in low-carbon steels, or martensite in beta-quenched bronzes.

Martensitic transformation

A product formed by rapid cooling of an alloy. Some alloys may be specially formulated to allow martensitic events to occur on cooling.

Mechanical twinning

Twinned crystals produced by mechanical strain alone, as in zinc.

Mercury

Atomic number 80, atomic weight 200.59, mp -38.84 °C, specific gravity 13.55. Mercury has been found in Egyptian tombs of 1500 B.C. and was widely known in the centuries B.C. in China and India. A silvery white metal which is liquid at room temperature. The earliest extractions were carried out by roasting cinnabar, mercury (II) sulfide, in an oxidizing atmosphere and collecting the mercury by distillation.

Meteoric iron

Iron from outer space. Usually an alloy of iron and nickel. Small amounts of cobalt and manganese are typical. Some early iron exploitation made use of meteoric iron.

Nitriding

In steels, the hardening due to nitrogen content that may result in nitrides being formed in the alloy.

Open mold

A primitive form of casting into an open-shaped depression in stone, sometimes covered partially to prevent excessive oxidation.

Pearlite

The fine mixture of ferrite and cementite found in steels. The eutectoid, pearlite, will be complete when the carbon content reaches 0.8%. In most ancient steels, a mixture of ferrite and pearlite is common.

Peritectic

Reaction of a phase that has formed with a liquid of a different composition to form a new solid phase. The new phase may consume all of the liquid to form a totally new solid, typically beta phase in the bronze system.

Peritectoid

An isothermal reaction in which two solid phases in a binary system react to form a new solid phase. A peritectoid reaction occurs in the bronze system, for example, in which at 65% copper a reaction occurs between Cu_3Sn, and the solid solution gamma, producing a new phase, Cu_4Sn at about 580 °C.

Pewter

Ancient pewter is an alloy of lead and tin, much used in Roman times. The poisonous nature of lead has resulted in the replacement of lead with antimony, although antimony is also inadvisable in high amounts for utensils. Common pewter in antiquity may consist of 60–80% tin, 40–20% lead, while modern pewter may be 15–30% copper, 5–10% antimony, and 87–94% tin.

Phase

A homogeneous chemical composition and uniform material, describing one component in a metallic system.

Phase diagram

A diagram with axes of temperature and composition describing the different phases that may occur in an alloy with change in either composition or temperature. A binary phase diagram consists of two metallic components. A ternary system, which is usually more complex, consists of three metals.

Piece-mold
A mold taken from a model that may be assembled in a number of pieces before being used for slushing wax over the mold interior for lost-wax copies of a master model. Such techniques were common in the Renaissance.

Platinum
Metallic element atomic number 78, atomic weight 195.08, mp 1772 °C, specific gravity 21.45. First discovered in South America by Ulloa in 1735, but used by the Indians of Ecuador and Colombia who sintered the metal with gold. Finds are known particularly from La Tolita dating to the early centuries B.C. It can be present in the native state, usually alloyed with some iron. The metal is malleable and ductile. It is used in early scientific instruments since its coefficient of expansion is very similar to soda-lime glass.

Polycrystalline
Consisting of many individual crystalline grains. Most metals are polycrystalline solids.

Polygonal
Many-sided. Some grain shapes may be polygonal.

Prill
In the extraction of copper from primitive smelts, the metal is produced as small droplets or particles in a slaggy matrix. These small metallic particles are called prills and were often extracted by breaking up the smelted product and sorting the metal. In crucible processes, prills are small droplets of metal adhering to the crucible lining.

Pseudomorphic
The replacement in the corrosion process of a material with another that mimics the form of the replaced product. Pseudomorphic replacement of organic materials is common on iron artifacts and can occur on copper alloys and silver-copper alloys as well.

Quenching
The act of quickly cooling a metal or alloy by plunging into cold water or oil.

Quenched structures
Usually nonequilibrium structures or phases that have been made metastable in an alloy by quenching in water or oil. The most common quenched products are martensite in steels and martensite in high-tin bronzes. Quenching may also be used to suppress ordering reactions, especially in gold alloys and some ancient texts refer to this practice to avoid embrittlement.

Repoussé
Working from the back of a metal, often on the slight relief of a chased design on the front. The metal is then displaced by hammering, often on a soft support such as pitch, so as to create raised designs on the front.

Riveting
Joining of metal sheet by small metal pegs passing through and hammered down.

Safídruy
Islamic term for high tin bronzes, often white in color.

Segregation
In alloys usually of three forms: (1) normal segregation, (2) dendritic segregation, and (3) inverse segregation. In normal segregation, the lower melting point metal is concentrated towards the inner region of the cast. In dendritic segregation, fernlike growth occurs from local compositional gradients. In inverse segregation, the lower melting point constituents, such as tin or arsenic in bronzes is concentrated toward the outer cast surfaces.

Shakudo
Japanese term for the deliberate use and manufacture of gold-copper alloys.

Shibuichi
Japanese term for decorative silver-copper alloys often worked and annealed to create decorative surfaces when colored by chemical etching or staining.

Silver
An element of atomic number 47, atomic weight 107.87, mp 960 °C, specific gravity 10.50. One of the noble metals that is not oxidized by heating in air. It is white in color and very ductile and malleable. Silver was usually obtained by cupellation of lead ores, although it may also be extracted directly from silver sulfide deposits. Pure silver is often stated to be 1000 fine and alloys are based on this nomenclature. For example, sterling silver (qv) is 925 fine.

Sinking
A technique with which a vessel can be produced by hammering from the inside. The sheet metal is hammered either on the flat surface of an anvil or more commonly hammered into a shallow concave depression in the anvil. Also called blocking or hollowing.

Slag
A glassy phase or mixture of phases usually to be found in ancient or historic wrought iron or steel. The slag is an important by-product of the smelting of metals. It may be incorporated in copper or iron alloys as a result of incomplete separation or incomplete melting during extraction, as in the bloomery process.

Slag stringers
Small pieces of slag that have become incorporated into the metal and are then strung out as small elongated ribbons as a result of working the metal to shape it.

Slip planes
FCC metals may show slip planes, a fine series of lines in two intersecting directions upon heavy deformation of the metal.

Slush casting
A method of casting in which metal is often spun or agitated in the mold so that a thin shell is formed. More common in ancient and historic metalwork is slush wax work in which wax is slush cast over a piece mold interior before investment.

Soft solders
A term applied to lead-tin alloys used in soldering, usually not of precious metals. The upper limit of the melting range is about 300 °C, and many alloys melt at about 130–180 °C.

Solidus
The line in the phase diagram that separates the pasty stage of the alloy, usually a mixture of solid and liquid, from the completely solid alloy below the temperature of the solidus line. The solidus temperature may be different at different alloy compositions, depending on the type of phase diagram.

Sorbite
A decomposition product of martensite found in steels. It consists of fine particles of cementite in a matrix of ferrite. Sorbitic structures may be rounded cementite not necessarily derived from martensite.

Speculum
A name sometimes applied to Roman or bronze mirrors, containing a high percentage of tin. Historic speculum may contain about 67% copper, 33% tin. Ancient mirrors made use of similar alloys, usually of beta bronze composition and up to about 24% tin.

Spinning
Turning on a lathe followed by depression of metal while in motion.

Stamping
Displacement of metal by a hard die often for assay purposes.

Steel
A malleable alloy of iron and carbon that contains about 0.1–1.9% carbon. The carbon is present as cementite, usually as a component of pearlite. Low-carbon steels contain from 0.09% carbon to 0.2% and are soft. Medium carbon steels contain 0.2–0.4% carbon and high carbon steels more than 0.4%.

Sterling silver
A common coinage binary alloy of 92.5% silver, 7.5% copper.

Strain hardening
A synonym for work hardening.

Strain lines
Same as slip planes. Often seen in FCC metals after heavy working due to slip of planes of atoms past each other.

Striking
A method of making coins and medals. The impression is cut in negative in a very hard material and this die is then placed over the coin blank and given a single heavy blow thus compressing the metal of the blank into the recesses of the die. Before the introduction of steel, bronze coins could only have been struck using stone or bronze dies. Striking may cause stress-related features in the struck metal such as surface cracking or internal defects.

Tempering
Usually applied to steels in which some of the hardness is removed by heating at moderate temperatures, from 450 to 650 °C, depending on the type of tempering required. In ancient metals, tempering, or self-tempering of martensite would have been carried out to reduce the brittleness of the fully quenched steel cutting edges of swords.

Tin
An element of atomic number 50, atomic weight 118.69, mp 231.8 °C, specific gravity (grey) 5.75, (white) 7.31. A soft white lustrous metal obtained almost entirely from the mineral cassiterite, SnO_2. Tin is not affected on exposure to air at ordinary temperatures. At temperatures above 13.2 °C the white tetragonal allotropic form is stable and below this the grey cubic form may exist. Above 170 °C, tin is rhombic in crystal structure. The metal has low tensile strength and hardness but good ductility.

Tinning
The operation of coating a base metal (usually) with tin. The coating may be obtained by hot dipping into molten tin or by flowing the molten tin over the surface of the object.

Troosite
A very fine mixture of pearlite, not resolvable by optical microscopy. Nodular troosite is found in steels not cooled quickly enough to form martensite. On etching in low-carbon steels, troosite appears as a blue etching component in nital.

Tumbaga
The name given in ancient South America to the alloys of copper and gold, of wide range of composition and color.

Tutenag
Copper-zinc-nickel alloy of silvery color imported from China to Europe in 18–19th century A.D.

TTT diagrams
Time-temperature-transformation diagrams. Most useful in considering the nature of the quenched microstructure to be found in steels and high tin bronzes. The quenching rate and composition results in a

differing series of TTT diagrams that are commonly used to investigate transformation effects on components found during quenching of alloys.

Vickers
A hardness scale that uses a diamond having an angle of 136 degrees between the faces. The loading can be used easily for microhardness measurements. It is one of the most useful hardness testing scales.

Weld
A term used to describe a joint made between two metals made by the heating and joining the separate parts with no solder applied. Ancient welds were often made in precious metals, such as gold and silver and in the joining of iron components, especially in the fabrication of wrought iron.

White cast iron
Cast iron with a white fracture due to the presence of the carbon in the cast iron as cementite rather than free graphite.

Widmanstätten
A type of structure that forms when a new solid phase is produced from a parent solid phase as plates or laths along certain crystallographic planes of the original crystals. The structure is associated with many meteoric irons, and with changes upon cooling in worked iron and copper alloys. Most commonly found as an incidental feature of wrought low-carbon steels.

Wootz
Wootz is a kind of steel, made in small crucibles in ancient India and often of hypereutectoid steel with a very low slag content. This cast steel was widely used for the manufacture of sword blades and other quality products.

Wrought
The process of hammering or deforming a metal or alloy, as opposed to casting.

Wrought iron
Iron that has been produced from the bloomery process and has been consolidated by hammering and annealing into a wrought product. Wrought iron usually contains slag stringers that have been elongated and flattened in the process of working from the bloom.

Zinc
Element of atomic number 30, atomic weight 65.38, mp 419.58 °C, specific gravity 7.133. Zinc ores were used for making brass by cementation long before the metal was used in its pure form. The limit of zinc that can enter into solid solution in copper by this process is 28%. The Romans made extensive use of brass and, in India, zinc was being made by distillation in retorts during the 13th century A.D. The metal was not known in Europe until rediscovered in 1746. Zinc is a bluish-white, lustrous metal, brittle at ordinary temperatures but malleable at 100–150 °C.

Bibliography

American Society for Metals
1972–1973
Atlas of Microstructures of Industrial Alloys. In *Metals Handbook.* Vol. 7, 8th ed. Metals Park, Ohio: American Society for Metals.

Allen, I. M., D. Britton, and H. H. Coghlan
1970
Metallurgical Reports on British and Irish Bronze Age Implements and Weapons in the Pitt Rivers Museum. Pitt Rivers Museum Occasional Papers on Technology No. 10. Oxford: Oxford University Press.

Anderson, E. A.
1959
Zinc: the science and technology of the metal, its alloys and compounds. In *The Physical Metallurgy of Zinc.* C. H. Mathewson (ed.). New York: Reinhold Publishing; London: Chapman and Hall.

Bachmann, Hans-Gert
1982
The Identification of Slags from Archaeological Sites. Institute of Archaeology: Occasional Publication No. 6. London: Institute of Archaeology.

Bailey, A. R.
1960
A Textbook of Metallurgy. London: Macmillan.

1967
The structure and strength of metals. Betchworth, Surrey: Annotated Metallographic Specimens.

1972
The role of microstructure in metals. Betchworth, Surrey: Annotated Metallographic Specimens.

Beraha, E.
1977
Color Metallography. Metals Park, Ohio: American Society for Metals.

Brandon, D. G.
1966
Modern Techniques in Metallography. London: Butterworths.

Brown, B. F., H. C. Burnett, W. T. Chase, M. Goodway, J. Kruger, and M. Pourbaix (eds.)
1977
Corrosion and metal artifacts: a dialogue between conservators and archaeologists and corrosion scientists. NBS Special Publication 479. Washington, D.C.: U.S. Department of Commerce.

Bushnell, G. H. S.
1951
The Archaeology of the Santa Elena Peninsula in South-West Ecuador. Cambridge: Cambridge University Press.

Charles, J. A.
1968
The First Sheffield Plate. *Antiquity* 42:278–285.

Charles, J. A. and J. A. Leake
1972
Problems in the Fluorescence Analysis of Cu/Ag Byzantine Trachea and Metallurgical Information from Sections. In *Methods of Chemical and Metallurgical Investigation of Ancient Coinage.* E. T. Hall and D. M. Metcalf (eds.). Royal Numismatic Society Special Publication No. 8. London: Royal Numismatic Society.

Coghlan, H. H.
1975
Notes on the Prehistoric Metallurgy of Copper and Bronze in the Old World. 2nd ed. Pitt Rivers Museum Occasional Papers on Technology No. 4. Oxford: Oxford University Press.

Coghlan, H. H. and R. F. Tylecote
1978
Mediaeval Iron Artefacts from the Newbury Area of Berkshire: Metallurgical Examination. *Journal of the Historical Metallurgy Society* 12:23-29.

Cooke, R. B. S. and S. Aschenbrenner
1975
The occurrence of metallic iron in ancient copper. *Journal of Field Archaeology* 2:251–266.

Corrosion and metal artifacts: a dialogue between conservators and archaeologists and corrosion scientists
1979
B. Floyd Brown, Harry C. Burnett, W. Thomas Chase, Martha Goodway, Jerome Kruger, and Marcel Pourbaix (eds.). NBS Special Publication 479. Washington, D.C.: U.S. Department of Commerce.

Cottrell, A.
1975
An Introduction to Metallurgy. London: Edward Arnold.

Fink, C. G. and A. H. Kopp
1933
Ancient Egyptian Antimony Plating on Copper Objects. *Metropolitan Museums Studies* 4:163–167.

Fink, C. G. and E. P. Polushkin
1936
Microscopic Study of Ancient Bronze and Copper. *Transactions of the American Institute of Mining and Metallurgical Engineers.* Metals Division. 122:90–117.

Ghandour, N.
1981
Elemental and Metallographic Analysis of Objects from Tell Ajjul, Palestine. M.A. Dissertation (unpublished). University of London, Institute of Archaeology.

Goodway, M. and H. C. Conklin
1987
Quenched high-tin bronzes from the Philippines. *Archaeomaterials* 2:1–27.

Hall, E. T. and D. M. Metcalf (eds.)
1972
Methods of Chemical and Metallurgical Investigation of Ancient Coinage. Royal Numismatic Society Special Publication No. 8. London: Royal Numismatic Society.

Hendrickson, R. C.
1967
Applications of Metallurgical Microscopy. New York: Bausch & Lomb.

Hongye, G. and H. Jueming
1983
Research on Han Wei spheroidal-graphite cast iron. *Sundry Trade Journal International* 5:89–94.

Kiessling, R. and N. Lange
1963–1964
Non-metallic inclusions in steel. *Iron and Steel Institute: Special Report No. 90.*

Lechtman, H. N.
1971
Ancient Methods of Gilding Silver: Examples from the Old and New Worlds. In *Science and Archaeology.* R. H. Brill (ed.). Cambridge, Mass: MIT Press. 2–30.

1973
The Gilding of Metals in Pre-Colombian Peru. In *Application of Science in the Examination of Works of Art.* W. J. Young (ed.). Boston: Museum of Fine Arts. 38–52.

Lechtman, H. N., A. Erlij, and E. J. Barry
1982
New perspectives on Moche metallurgy: techniques of gilding copper at Loma Negra Northern Peru. *American Antiquity* 47:3–30.

Lord, J. O.
1949
Alloy Systems. New York: Pitman.

Maryon, H.
1971
Metalwork and Enamelling. New York: Dover Publications. Republished from 1959, 4th edition. London: Chapman and Hall.

Mathewson, C. H.
1915
A Metallographic Description of Some Ancient Peruvian Bronzes from Machu Picchu. *American Journal of Science* (190)240:525–616.

Mayes, P. and L. Butler
1977
Excavations at Sandal Castle 1964–1973. Wakefield Historical Society.

McCrone, W. C. and J. G. Delly
1974
The Particle Atlas. 2nd ed. Volumes I–IV. Michigan: Ann Arbor Science Publication.

Meeks, N. D.
1986
Tin-rich surfaces on bronze—some experimental and archaeological considerations. *Archaeometry* 28:133–162.

Needham, Sir J.
1954
Science and Civilisation in China. Vol. 5, Part II. Cambridge: Cambridge University Press.

Nelson, J. A.
1985
Metallography and Microstructures. "Cast irons." In *Metals Handbook.* Vol. 9, 9th ed. Metals Park, Ohio: American Society for Metals.

Oddy, Andrew W.
1977
The production of gold wire in antiquity: hand making methods before the introduction of the draw plate. *Gold Bulletin* 10:79-87.

1984
Ancient jewellery as a source of technological information: a study of techniques for making wire. In *Fourth International Restorer Seminar: Veszprem* 241–252. Budapest: National Centre of Museums.

O'Neill, H.
1934
The Hardness of Metals and its Measurement. London: Chapman and Hall.

Petzow, G.
1976
Metallographic Etching. Metals Park, Ohio: American Society for Metals.

Petzow, G. and H. E. Exner
1975
Recent Developments in Metallographic Preparation Techniques. *Microstructural Science.* 3:296–306.

Phillips, V. A.
1971
Modern Metallographic Techniques and their Applications. New York: J. Wiley & Sons.

Poluschkin, E. P.
1964
Structural Characteristics of Metals. Amsterdam: Elsevier.

Rajpitak, W. and N. J. Seeley
1979
The Bronze Bowls from Ban Don Ta Phet, Thailand: an enigma of prehistoric metallurgy. *World Archaeology* 11:26–31.

Rajpitak, W.
1983
The development of copper alloy metallurgy in Thailand in the pre-Buddhist period, with special reference to high-tin bronzes. PhD thesis (unpublished). 4 vols. University of London, Institute of Archaeology.

Rhines, F. N., W. E. Bond, and R. A. Rummel
1955
Constitution of ordering alloys of the system gold-copper. *Transactions of the American Society of Metals* 47:578–597.

Rollason, E. C.
1973
Metallurgy for Engineers. London: Edward Arnold.

Samans, Carl H.
1963
Metallic Materials in Engineering. New York: Macmillan.

Samuels, L. E.
1980
Optical Microscopy of Carbon Steels. Metals Park, Ohio: American Society for Metals.

Schweizer, F. and P. Meyers
1978
Authenticity of ancient silver objects: a new approach. *Masca Journal* :9–10.

Scott, D. A.
1980
The conservation and analysis of some ancient copper alloy beads from Colombia. *Studies in Conservation* 25:157–164.

1983
Depletion gilding and surface treatment of gold alloys from the Nariño area of ancient Colombia. *Journal of the Historical Metallurgy Society* 17:99–115.

1986
Gold and silver alloy coatings over copper: an examination of some artefacts from Colombia and Ecuador. *Archaeometry* 28:33–55.

1991
Technological, analytical and microstructural studies of a Renaissance silver basin. *Archeomaterials* 5:21–45.

Slunder, C. J. and W. K. Boyd
1971
Zinc: its corrosion resistance. London: Zinc Development Association.

Smith, C. S.
1960
A History of Metallography. Chicago: University of Chicago Press.

1971
The Technique of the Luristan Smith. In *Science and Archaeology.* R. H. Brill (ed.). Cambridge, Mass: MIT Press. 32–54.

1981
A Search for Structure: Selected Essays on Science, Art and History. Cambridge, Mass: MIT Press.

Thompson, S. C. and A. K. Chatterjee
1954
The age-embrittlement of silver coins. *Studies in Conservation* 1:115–126.

Tylecote, R. F.
1968
The Solid Phase Welding of Metals. London: Edward Arnold.

1976
A History of Metallurgy. London: The Metals Society.

1986
The Prehistory of Metallurgy in the British Isles. London: The Institute of Metals.

1987
The Early History of Metallurgy in Europe. London: Longman.

Tylecote, R. E. and B. J. J. Gilmour
1986
The Metallography of Early Ferrous Edge Tools and Edged Weapons. BAR British Series number 155. Oxford: British Archaeological Report.

Untracht, Oppi
1975
Metal Techniques for Craftsmen. New York: Doubleday.

West, D. R. E.
1982
Temary Equilibrium Diagrams. 2nd ed. London: Chapman and Hall.

Winchell, A. N. and H. Winchell
1964
The Microscopical Characters of Artificial Inorganic Solid Substances: Optical Properties of Artificial Minerals. 3rd ed. New York: Academic Press.

Yakowitz, H.
1970
Some uses of color in metallography. *Applications of Modern Metallographic Techniques.* ASTM STP 480:50–65. Metals Park, Ohio: American Society for Testing and Materials.

INDEX

A

acidified potassium dichromate 72
acidified selenic acid 73
acidified sulfate/chromic oxide 73
acidified thiosulfate/acetate 73
acidified thiourea 73
aggregate carbon 41
alcoholic ferric chloride xvi, 72
alkaline sodium picrate 70
alloys
  annealing 7
  two-phase 14
alpha 14, 15
alpha + beta brass 19
alpha + beta eutectic 12, 14
alpha + delta eutectoid 25
alpha + epsilon phase region 25
alpha brass 19, 20
alpha dendrites 13
alpha solid solution 12
alumina 64
  in polishing 66
ammonia/hydrogen peroxide 72, 73
ammonium persulfate/ potassium cyanide 72
ancient steel 16
anisotropic 39, 49
annealed casting 93
annealing 3, 6, 14
  temperatures 7
  twins 25
aqua dag 63
aqua regia 71, 99, 100
aqueous ammonium persulfate 72
aqueous ferric chloride 72
Araldite XD725 59
archaeological materials 11, 14, 15
arrowhead *88, 114*
ASTM number 51
atomic packing factor 1
austenite 38, 39, 41
  solid solution 16
austenitic grain boundaries 31, 35
austenitic grains 21, 115
austenitic region 17
Australia 106
axe *92*
  fragment *105*
azurite crystals 117

B

Bachmann 50
banded structure 32
Baumann's print solution 70
bead
  French cut-steel 36
  gold necklace *99*
Beaujard's reagent 70
bell 26, *93*
bending 10
Beraha's reagent 70
beta 14, 18
  brass 19
  bronze 26, 28
  needles 28
beta-phase brass 20
beta-phase martensite 95
beta-quenched bronze 28
billet *89*
binary tin bronzes 26
blackheart 39
blade fragment *114*
blast furnace 37
bloom 89
bloomery iron 102, 114
body-centered cubic 1, 49
bowl *94, 98, 112*
  Roman *112*
bracelet *111*
brass 19, 26
  alloy 23
  grain size 53
  jig 63
  medallion xvi
bright-field unpolarized illumination 49
Brinell hardness testing 2, 77
bronze 5, 25
  alloy 23
  annealed 26
  bell 93
  beta-quenched 28
  cold-worked 26
  dagger hilt xvi
  examination of 25
  grain size 53
  high-tin 25
  ingots 28
  low-tin 25
  mirror 28
  sculpture xvi
  system 26
Bronze Age *88, 97*
  sword xx
Buehler
  epoxide resin 54
  Mastertex cloth 55
  wafering machine 63
Bushnell 92
Byzantine *114, 116*

C

cannonball 42, *96*
carbide 37
carbon 23
  alloy 23
  equivalent value 38
  steel 15
carbon content 32
  of ancient objects 16
  of cast iron 37
cast *87, 88, 92, 93, 95, 96, 97, 99, 103, 105, 107, 108, 117, 118, 119*
cast and worked *111, 112*
cast bronze xx
cast bronze incense burner 27
cast iron 16
  cannonball xviii, xix, 42, 96
  etchants 69
  interference etchant 73
  microstructure 40
  scales xvii, 42
  spheroidal graphite 37
  whiteheart 37, 42
cast metals 6
cast, quenched, worked *94, 98*
casting 5
  defects in 24
cathodic graphite flakes xviii
cementation 19
cementite xvi, xix, 23, 32, 37
  free 38
  grain boundary 31
  laths xviii, 42
  needles xix, 13, 35, 36
  networks 70
cements 50
ceremonial axe
  copper 47
Charles and Leake 7
chasing 109
chemoepitaxy 43
chill castings 6
China 19, 27, 37, 38, 42, *93*
  cast iron 39
Chinese cast iron lion xvi
chromic acid/sulfate etchant 74
chromium (VI) oxide 72
close-packed hexagonal 1
coin *86, 97, 101, 117*
  zinc xx
cold-work
  degree of 9
Colombia 23, 46, *90, 95, 99, 107, 115*
color etching
  copper alloys 74
color metallography 73
columnar growth 6
compounds 22
  intermetallic 22
concentrated HCl 71
Cooke and Aschenbrenner 24
cooling 115
cooling rate 14, 17, 23, 24, 25, 31, 32, 39, 51

copper 9, 12, 22, 47, 102
copper alloy 23, *90, 97, 101*
etchants 72
interference etchants 73
copper and tin alloys 25
copper corrosion products xvi
copper globules 47
copper oxide 28
copper sulfide inclusions xvi
copper sulfides 50
copper-arsenic alloy *92*
copper-gold alloy *95, 115*
copper-lead alloy 23
copper-silver alloy 21, *117*
etchants 72
copper-tin alloy 25, *88, 93, 94, 98, 103, 105, 111, 112*
copper-tin phase diagram 18
copper-tin system 16, 26
copper-tin-arsenic alloy *88*
copper-tin-lead alloy *93, 108*
copper-tin-zinc-lead alloy *87*
copper-tin-zinc system xviii
copper-zinc alloy *97, 105,* 107, *113*
copper-zinc system 19
cored bronzes 25
coring xvi, xx, 5, 12, 25, 27, *87*
Cornwall *120*
corrosion 107, 113
colors 49
of gold-copper alloys 46
corrosion crusts 57
corrosion processes 43
metallic fragments 43
corrosion products 43, 44, 57
distribution 49
examination 56
morphology of 49
crab-type graphite 41
crystal fault 2
cuprite 43, 44, 46, 107
cuprite lamellae 90
curing 63

D

daggers 24
blade *116*
handle *94*
damage
due to sampling 58
damping capacity 37
debased silver 21
alloys 7
coin 117
deformation
percentage of 9
deformed grains 8
degree of cold-work 9
delta 15
dendrite arms 13, 25
native copper 103
dendrites 5, 40
alpha 13
ghost 25
growth 5, 25
noncontinuous 86
segregation 5
silver-rich 86
structure 6, 23, 49
dendritic arm spacing 5
measurment 51
depletion
of eutectic phase 14
of the eutectic phase 14
depletion-gilding 46
diamond polishing 44
Diamond Pyramid Number 2, 77
dimethylglyoxime nickel test 71
disc
decorative *90*
discontinuous precipitation 21
dislocation entanglement 3
dislocations 2
dispersion
of lead 27
drawing 6
Dubé 21
ductility 3

E

ear ornament 46, *95, 107*
ear spool *99*
early 20th century *118, 119*
Early Medieval *113*
earring *106*
Eastern Han dynasty 38
Ecuador 47, 90, 92
edge dislocation 2, 3
edge retention 64, 75
edged tools 16
electrochemical replacement plating technique 47
electrolytic polishing 66
electromechanical polishing 66
elongation 41
embedding
small samples 65
emulsion 23
England 35, 42
medieval *100–102, 113, 115*
engraving 109
epitaxial growth 43
Epoxide 75
epoxy 63
epoxy resin 75
epsilon phase 19, 25, 26
epsilon-carbide 35
equi-axed grains xvi
equilibrium 5, 31
defined 5
diagram 11, 25
structure 6
eta and tin 19
eta phase 19, 24, 26
etch pitting 104
etching 67
polished metal 69
etching solutions
for archaeological materials 69
eutectic 14
eutectic phase diagram 12
eutectic point 12, 14
eutectic structures 12
eutectoid
interdendritic 25
pearlite 13
phase 15
point 17
structures 15
transformation 16
-type transformations 15

F

face-centered cubic 1, 7, 49
false-filigree 107
fayalite 50
ferric chloride xvi, 25
ferrite xvii, xix, 21, 24, 31, 32, 41, 42
grain-boundary 21
grain structure 29
grains 35, 104
massed 21
figurine *108*
filligree 95
Fink and Kopp 6
flake graphite 38, 41
France 36
free cementite 38
free ferrite 38
free graphite 37, 40
French cut-steel bead 36

G

gamma iron 24
gamma phase 16
gamma solid solution 16
Ghandour 88
gilded silver 106
gilding 116
glycerol etchant 71
gold 22, *107*
alloys 11
gold alloy
etchants 71
gold foil 57
gold-copper alloy 22, 23, 46, *90, 95, 107*
gold-copper system 23

gold-silver alloy *99*
gold-silver system 11
grain boundaries 20, 21, 26, 28, 32, 46, 49
  austentitic 31
grain boundary cementite 31
grain size
  measurement 51
grain structure
  equi-axial 6
  hexagonal 6
grain boundary ferrite 21
grains
  austenitic 21
graphite xvii, 37, 40
  flakes 38, 42
  free 40
  matrix 38
  nucleation 39
  polygonal 39
  spheroidal 39
gravity segregation 27
Greek Herm xviii, xx
grey cast iron xviii, 37, 38, 96, 118
grinding 24, 26, 54, 65
growth spirals 102

H
hacksaw 61
hammering 6
Han Wei period 37
hardness 2
heat treatment 39
Hengistbury Head 41
Heyn's reagent 70
high-tin alloy 26
high-tin bronze 25, 26
  mirror xix, 28
high-tin leaded bronze xvii, 19, 28
Hilliard's circular intercept method 52
homogeneous bronzes 25
homogeneous solid solution 15
Hongye and Jueming 37, 38, 42
hot-working 7
H_v 2
Hydrogen peroxide/iron (III) chloride 71
hypereutectic 38
hypereutectoid steel 21
hypoeutectic 38
hypoeutectoid steel 21

I
immiscible structures 23
incense burner xvii, *93*
  cast bronze 27
inclusions 101
  cuprite 90
  cuprous oxide 90
  in ancient metals 7
  nonmetallic 49
  sulfide 71
India xix, 19, 26, 35, 36
Indian Wootz ingot xix
Indian zinc coin 9
Indo-Greek *86*
ingot *97, 105, 119*
inkwell *87*
intercept method 51
interdendritic channels 5
interdendritic porosity 47
interdiffusion 26
interference film metallography 73
intermetallic compounds 22
internal oxidation 7
interstitial materials 2
inverse segregation 5
inverted stage metallurgical microscope 56
Iran xviii, xx, 27, *87, 94, 105*
Iranian Iron Age dagger hilt xviii
iron 9, 23, *89, 115*
  etchants 69
  interference etchant 73
iron alloy 23, *100, 101, 102, 114*
iron carbide 38, 39
iron oxide 38
  crust xvi
iron phosphide 37
iron-carbon alloy *96, 104, 116, 118*
iron-carbon phase diagram 16, 17
iron-carbon-phosphorus alloy *119*
iron-iron carbide diagram 40
Islamic 26, *87*
Islamic inkwell xviii, *87*
isotropic 42, 49

J
Japanese sword 29
Japanese swordblade xix
Java xix, 26, 28, *104*
jeweller's saw 61
Jordan *106*

K
kish graphite 38, 42
Klemm's reagent 70
knife *101, 115*
  grain size 31
Knoop 77
Korea 26
kris 36

L
Late Bronze Age *88, 103*
lath martensite 29, 35
lattice structure 1
lead 9, 24
lead alloy
  etchants 71
lead globules 23, 24, 87, 112
lead inclusions 24
lead-copper eutectic 23
leaded copper 23
leaded high-tin bronze 108
leaded zinc brass xvi
leaded tin bronze 27
lead-iron alloy 23
lead-tin alloys 15
leaf gilding 106
Lechtman 22, 47
ledeburite 40, 41
  eutectic 38
  of cast iron 38
  transformed 38
liquidus 24
liquidus line 11
lost wax 93, 95, 107
low-carbon steel 31
low-tin bronzes 25, 27
Luristan *94*
Luristan ceremonial axe xx, 47
Luristan dagger handle xvi

M
magnesium oxide
  in polishg 66
magnetite 50
manganese 37
manufacturing processes 57
martensite 20, 23, 32, 35, 98, 101
martensite needles 35
martensitic 26
  transformation 20, 106
Maryon 6
massed ferrite 21
matte 50
McCrone et al. 50
McCrone low-level microhardness tester 77
medallion *107*
medieval *115*
  Indian zinc coin xx
  knife blade 35
Meeks 27
melts 11
metallic bonds 1
metallic zinc 19
metallographic examination 61
metallography 57
metals
  deformation 1
metastable phase 28
metastable state 21

mirror xvii, 18, 19, 26, *108*
high-tin bronze 28
Javanese 28
Roman 19, 26, 27
modern *105*
molybdate/bifluoride 74
monotectic 23
mottled cast iron 37, 42
mottled iron 38
mounting resins 75

N
nail *102*
native copper *102*
Near East 26
necklace bead *99*
Nelson 39
nickel silver
grain size 53
nital 39, 69, 71
nodular graphite 41
nomograph 51
normal segregation 5
North America
Great Lakes *102*
nose ornament *90*
nose-ring *91*

O
Oberhoffer's reagent 70
optical microscopy 35
ordered regions 22
oxide layers on iron
etchants 72
oxide scale 26

P
Palestine xx, 88
Palmerton's reagent 71
panpipes *115*
Paraloid B72 59
pearlite xvii, xix, 17, 21, 29, 31, 32, 35, 36, 38, 96
lamellae 70
percentage of deformation 9
peritectic
reaction 18, 22, 24
structures 17
transformation 19, 26
peritectoid 22
Petzow and Exner 73
phase 5
defined 5
diagram 11
Phillips 73
phosphorus 37
pickling 86
picral 39, 69, 71
pig iron 37
pigments
examination 56
plasters 50
plastic deformation 1
Plasticine 58
plate *110*
plate martensite 36, 71
pleochroism
color change 49
polarized illumination 49
polarized light 43
polishing 24, 38, 44, 66
electrochemical 63
electrolytic 63
mounted sample 55
polycrystalline 1
polyester 63, 75
polygonal grains 27
porosity 6, 24, 46, 47, 87, 112
of cast metals 6
potassium ferricyanide 72
Pratt Hamilton xvi
pre-etching 74
process anneal 7
proeutectoid cementite 21
proeutectoid ferrite 21
pseudomorphic 43
pseudomorphic replacement
by corrosion products 57
pseudomorphic retention 46

Q
quasi-flake graphite 41
quench ageing 104
quenching 20, 26, 31
with water 23

R
raising 6
rapid cooling 1, 37
recrystallization
temperatures 9
recrystallized grains 8
redeposited copper 47
reflected light microscopy 57
reflected polarized light 39
reflection pleochroism 39, 42
Renaissance *109, 110*
Rhines, Bond, and Rummel 22
Rockwell 77
Rollason 96
Roman xvii, 26, *89, 97, 101, 102, 108, 112, 117*
period 19
coin *97, 117*
figurine *108*
mirror xvii, 27, 28, *108*
wrought iron *89*
Romano-Greek *114*

S
safídruy 26
sample
criteria to be met 61
embedding 63
mounting 63
preparation 58, 63
removal 61
small 64
storage 55
Sandal Castle xix, *96*
saturated thiosulfate solution 73
scalpel 62
Scandiplast 63, 75
Schweizer and Meyers 7, 21
scleroscope 77
Scott 22, 50, 90
screw dislocations 2
segregation 9, 12
inverse 5
normal 5
selenic acid solution 74
sheet fragment *113*
silicon 37, 38, 40
silicon carbide 65
silver 12, 21, *86, 109*
alloys 11
impure 21
silver alloy
etchants 72
silver and gold alloy *106*
silver objects 57
silver-copper alloy 12, 13, 15, 57, *86, 109*
eutectic phase diagram 12
silver-copper phase diagram 21
Sinú *107*
Skandagupta *86*
slag 7, 36
globules 7
inclusions 116
stringers 7, 14, 29, 102, 115
slip 3
bands 9
planes 3
slow cooling 37
of cast iron 41
Smith 7
soft solders 15
solid solubility 11
solid solution anneal 7
solidus 11
sorbite 31
speculum 18, 26
speiss 50
spheroidal graphite 39, 41, 42
cast iron 37
splat cooling 1
stannic oxide 50
steadite xvi, 37, 38, 42, 96
eutectic 42

steel 16, 20
ancient 16
blade *100*
etchants 69
interference etchant 73
prill 35
strain lines 9, 25
stress factor 2
stress-relief anneal 7
stress-strain diagram 1
structure
banded 32
Struers "Autopol" machine 66
subgrain structure 31
sulfide inclusions xvii, xx, 71
sulfur 37
Sumatra 28
superlattice 22
surface detail
of ancient metallic artifacts 44
sword *88*
sword blade 13, 24, *104*

T
taper section 65
temper carbon 41
nodules 39
tempered martensite 31
tempering 29, 35, 101
ternary eutectic 42
steadite xviii
ternary tin bronzes 26
textured effect 9
Thai high-tin bronze vessel xvii
Thailand 26, *93, 94, 98, 111*
thermal history 57
thiosulfate/acetate etchant 74
thiosulfate-acetate xvi, xvii
Thompson and Chatterjee 21
tin xx, 9, 26
alloy *119*
bronze 15, 25
etchants 71
tinned surfaces 26
tinting
copper alloys 74
toggle pin *103*
cast 27
Tower of London 42
troosite 29, 31, 32, 101
tumbaga 22, 90
turning 6
twin lines 8, 102
twin planes 10
in zinc 10
twinned
crystals xvi
grains 8, 27, 90
nonferrous alloys 51
twinning
in CPH metals 9
two-phase alloys 14
two-phased solid 12

U
ultrasonic cleaning 44
untempered martensite 35
Untracht 6

V
Vickers 77
Vickers test 2
Villela's reagent 6, 71, 116

W
wafering blade 61
Warring States period 37
water quenching 23
Western Han 37
white bronze 26
white cast iron 37, 38, 39, 40, 42, 119
whiteheart 39
cast iron 37, 42
Whiteley's method 71
Widmanstätten 20, 106
pearlite 29
side plates 116
structure xvii, 27, 31, 115
transformation 20
Winchell 50
wire
longitudinal sample 58
sampling 58
transverse sample 58
Wootz crucible 35
Wootz steel 13
worked *86, 88, 89, 90, 91, 97, 99, 100, 101, 102, 104, 105, 106, 109, 113, 114, 115*
worked and cast *94*
work-hardening 3, 6
working 5, 6, 14
wrought iron 7, 14, 114
wüstite 89, 102, 114

X
X-ray fluorescence analyzer 57

Y
Yakowitz 73
Young's Modulus 1

Z
zinc 9, 19
alloys
ancient 19
corrosion products xvi
crystals 9
etchants 71
zinc-lead alloy 23

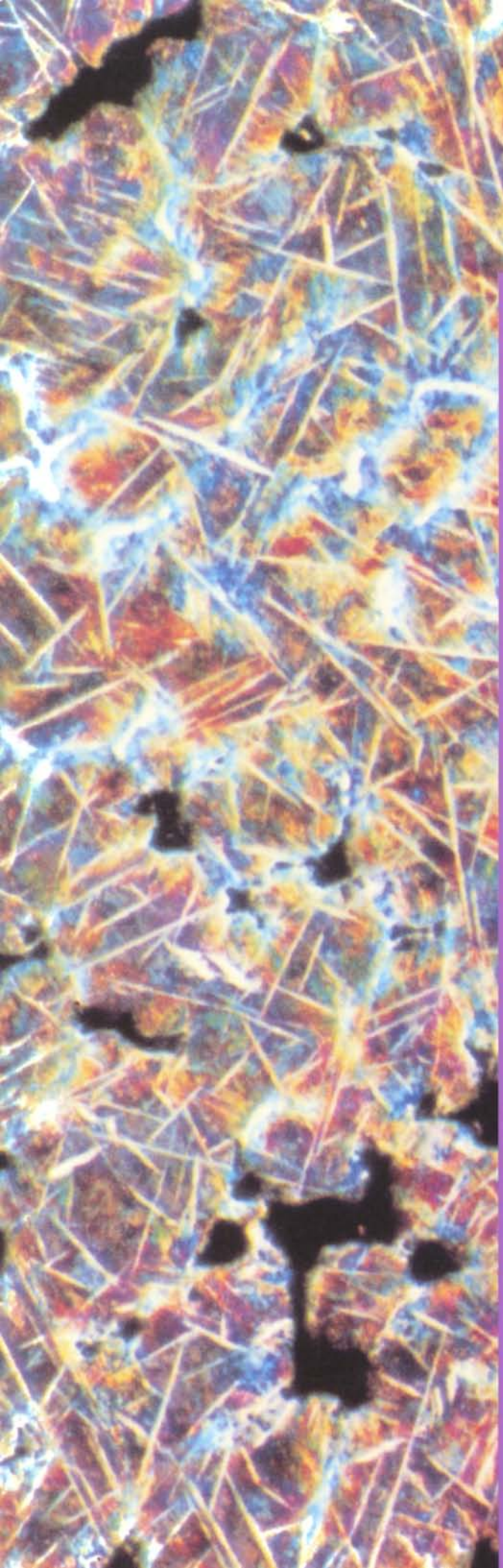

ISBN 0-89236-195-6
Printed in Singapore